CLOSED CYCLE PROPULSION
FOR SMALL UNMANNED AIRCRAFT

By

THOMAS CHADWICK HAYS

Master of Science in Mechanical Engineering

Oklahoma State University

Stillwater Oklahoma

2009

Submitted to the Faculty of the

Graduate College of the

Oklahoma State University

in partial fulfillment of

the requirements for

the Degree of

DOCTOR OF PHILOSOPHY

July, 2015

CLOSED CYCLE PROPULSION

FOR SMALL UNMANNED AIRCRAFT

Dissertation Approved:

Dr. Andrew S. Arena

Dissertation Adviser

Dr. Daniel Fisher

Dr. Jamey D. Jacob

Dr. Richard J. Gaeta

Dr. Russel Rhinehart

There has been no greater contributor to my education at Oklahoma State University than my advisor Dr. Andrew Arena. Working for, and with him on the Dragonfly project and my masters gave me the confidence to challenge continually harder questions as my studies progressed. Not enough can be said for his ability to simplify both engineering problems, and contractual politics. The lessons learned in both areas will guide me for years to come.

I must also thank my parents for their approval of my studies. They have encouraged me during my years at Oklahoma State to go beyond the minimum requirements of the program, and have provided endless support in pursuing that goal.

Name: Thomas Hays

Date of Degree: JULY, 2015

Title of Study: CLOSED CYCLE PROPULSION FOR SMALL UNMANNED AIRCRAFT

Major Field: DOCTORATE OF MECHANICAL AND AEROSPACE ENGINEERING

Abstract:

This study evaluates the merit of closed cycle propulsion systems for use in unmanned systems. The complexity and added weight of closed cycle engines is offset by benefits in high altitude performance, operation in polluted air environments, multi-fuel operation, and potential for flight in low oxygen environments using generic thermal heat sources. Although most closed thermal cycles cannot match the efficiency and power density potential of internal combustion engines (ICE) and turbomachines in aircraft propulsion applications, the addition of design requirements regarding noise output, and operation at high altitude results in IC and CC engine's performance becoming much more comparable. Muffling devices increase backpressure on internal combustion engines thereby reducing power output and efficiency. Multi stage turbo-supercharging for operation at high altitude can in some cases increase efficiency of ICE's, but at the result of significant additional complexity and cost that also reduces practical reliability because of the often intricate mechanisms involved. It is in these scenarios that closed cycle engines offer a comparable performance alternative that may prove to be simpler, cheaper, and more reliable than high altitude or low noise internal combustion or turbomachine propulsion systems.

TABLE OF CONTENTS

LIST OF FIGURES

Figure Page

Introduction

Problem Statement, Scope, and Contributions

This Dissertation summarizes the work performed regarding airborne closed cycle systems to better characterize their performance and design space. Studies were conducted on various types of closed cycle systems for aircraft use, various operating fluids for these systems, and preliminary experiments were conducted to gauge the suitability of components for use in these cycles. Rankine and Brayton cycles with and without regeneration are focused primarily as proceeding research and industrial examples have proven Stirling and Ericsson engines to have unsuitably low power density.

This closed cycle engine study is conducted after an initial investigation into the feasibility of applying passive or active silencing measures to internal combustion engines. This study looked at the underlying physics of noise propagation in space, and determined that due to the strong noise contributors below 4000 Hz. that any passive silencer applied to the intake and exhaust of a small aircraft would be unsuitably large for the overall system. Any device affixed that was sufficiently large enough to direct exhaust noise would be too heavy to allow the aircraft to function. Because of these findings regarding intake and exhaust noise, attempts to muffle existing noise were ceased in favor of investigating a closed cycle engine option to eliminate the need for intake and exhaust entirely.

A.Problem Statements

1. *Determine if closed cycle propulsion systems should be targeted as the next generation of quiet UAV propulsion by modelling and prototyping a low cost demonstration system.*

This portion of the study is to determine which possible closed cycle configurations, operating fluids, and components give closed cycle propulsion systems the greatest benefit for use in unmanned aerial systems. This broad scope's study will assist in properly steering funding into closed cycle engine development, if there is a suitable path at all in comparison to conventional internal combustion engines.

2. *Determine the value of closed cycle propulsion systems in high altitude flight*

Closed cycle engines have the distinct advantage of controlling their operating fluid directly and uninfluenced by the outside atmosphere. While the systems do have to use the external air to combust fuel and reject heat, these processes occur at steady state and should not create significant radiated noise. This study investigates the changes in heat exchange rate that occur as an aircraft ascends from sea level to high altitude.

B.Scope of Research

Figure 1 below shows the relationships between investigated components of this closed cycle engine study. These component investigations are covered in addition to the cycle trade space investigation, and operating fluid investigation for each cycle. While many other sources of research were available for some of these components, virtually none of the background research sources were related to use on aircraft, and even fewer for use as a main source of propulsion. Many of the investigated cycles and components are mainly used for terrestrial power generation or refrigeration systems and as such were designed with much more lax weight requirements. The most important components to system efficiency

are the heater and expander, so these components were the focus of increased computational and experimental work. In addition to work directly on CCE cycle components, computational studies on high altitude heat exchange performance and magnetic drives/gearboxes were conducted.

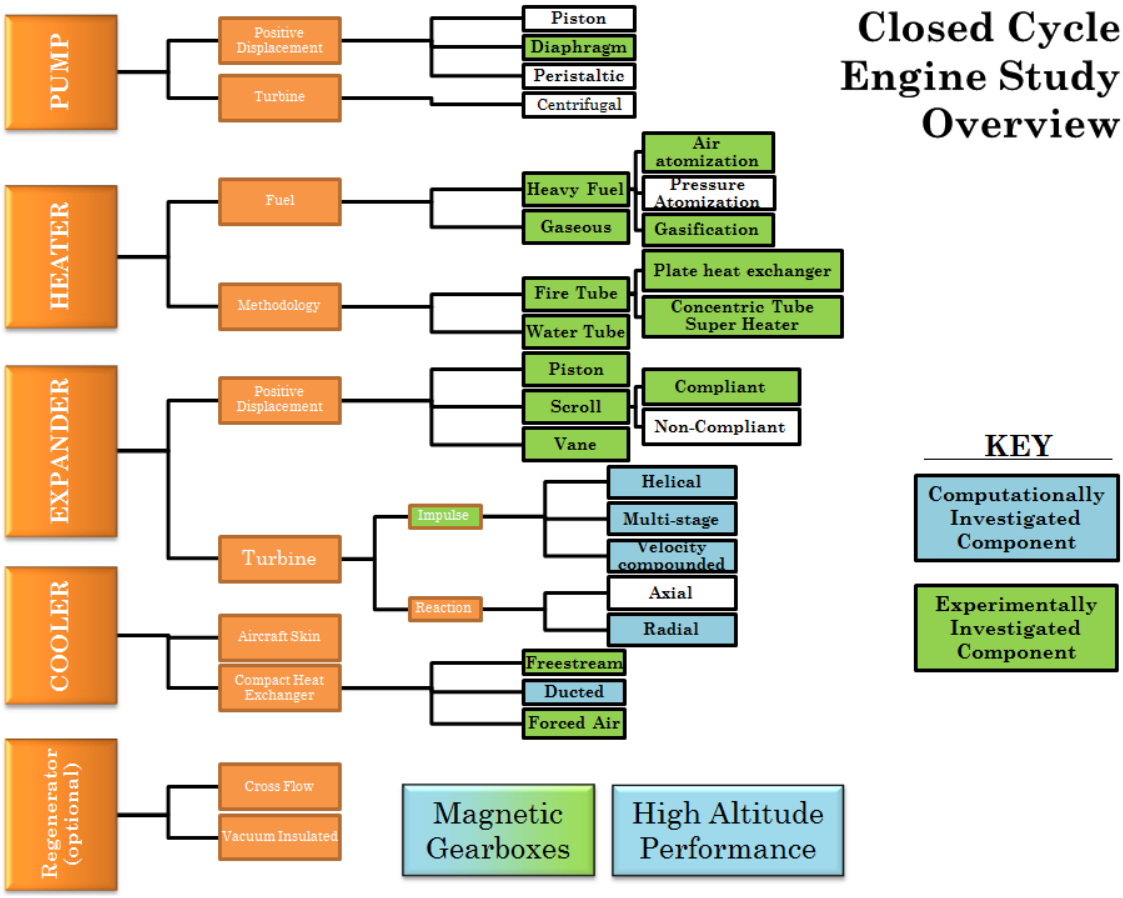

Figure 1 - Diagram of investigated components of Closed Cycle Engines

C.Unique Contributions

This study uniquely contributes SUAV closed cycle propulsion design space analysis and component evaluation. Very little work has been conducted to gauge the suitability of closed cycle engines for use on aircraft. In the early 1900's, when the propulsion question for aircraft had not been conclusively answered, several inventors and engineers attempted to use steam engines for airplanes. In most cases these engines were open cycles, and meant to only propel the craft for short time. Germany and Russia both investigated steam turbine cycles to power long range bombers for some time, but no prototype engines or systems were found. Recent work using Rankine cycles on small cars, and small waste heat

power plants has also been used as foundational work for this study as no better study on airborne closed cycle engines could be found for reference.

The Bessler brothers made the most lasting example with their steam aircraft. While it did include a condenser to economize the use of steam, the aircraft continually vented some of its operating fluid, taking it out of consideration as a truly closed cycle. Even with this venting, the crowd that surrounded its documented public flight was said to remark at how quiet the airplane was. The pilot and ground personnel could shout at one another and communicate as the airplane flew overhead.

Robert McConaghy created the only example that could be found of a small unmanned airplane closed cycle engine. Mr. McConaghy's previous work with stirling engines lead to him developing a small engine capable of producing 20W of power to fly a one meter sailplane. The engine's compressed operating fluid slowly leaked through the propeller shaft seal causing the engine's power to slowly diminish. While several test flights were successful, McConaghy said that the aircraft had barely enough power to turn, and was forced to land in each case by the leakage of operating fluid out of the propeller shaft seal.

With only these few proceeding aircraft based studies to reference, the research area of closed cycle engines for use on aircraft is wide open. This lack of preceding information justifies the broad scope of this study as it must interpret the suitability of long understood cycles and components for use in a new environment.

CHAPTER I

Background and Literature Review

Hays [1] investigated methods of powering small unmanned vehicles and detailed energy density calculations for small engines. Multiple battery chemistries were studied along with fuel cell technologies, internal combustion engines, turbomachinery, and thermoelectric conversion. The evaluation of closed cycle engines builds on this research as a potential technology that retains the energy benefits of combustion, while expanding the capabilities of air breathing engines by flying higher while remaining mostly independent of the atmosphere surrounding the aircraft. and doing so with higher energy density than other available systems.

I. Technical Foundation

A.Low Power Aircraft Design and Flight

Closed cycle aircraft powerplants are expected to have significantly lower power to weight ratios than internal combustion engines and turbomachinery. As a result, an aircraft design capable of flight at high altitude and medium speeds while remaining efficient enough to maneuver on the power of a CCE is required. Powered sailplanes are ideal cantidates for flight using a CCE, an example of which can be found in Figure 2 below showing an 11lb sailplane that cruised on only 50W of electricity.

Figure 2 - Dragonfly 5Kg Airplane Cruised on Less than 60W

The Dragonfly is a plane previously built at Oklahoma State and designed to break several official FAI world aviation endurance and range records in the F5S category (electric aircraft, 5kg limit). To date the airplane has set world records for duration (continuous time aloft) and distance to goal and return. The endurance record set by the Dragonfly team has been recognized as one of "The Most Memorable Aviation Records of 2006" by the National Aeronautic Association NAA. The Dragonfly gets its name from the resemblance of the fuselage shape to the body of a dragonfly.

Pterosoar shown in Figure 3 was another aircraft designed and built at Oklahoma State University. This aircraft continued the design style of dragonfly while adding volume for a compressed hydrogen Proton Exchange Membrane fuel cell. The aircraft set a world record for point and return distance for fuel cell aircraft, cruised on 60 watts with a TOGW of 10.4 lb. The fuel cell's rated capacity of 1000WH allows the aircraft to stay aloft for over 16 hours.

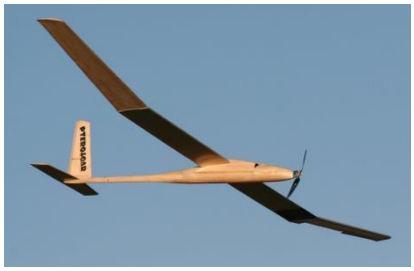

Figure 3 - Pterosoar Fuel Cell Powered Airplane

B.UAV Propulsion system survey

The author [1] conducted a survey of all presently available methods of powering small UAV's. Batteries, Fuel Cells, Combustion engine generators, Metabolic Systems, and Thermoelectric Generation were just some of the systems investigated. From this study a summarizing chart was created that displays all surveyed energy systems for a 200 Watt power system on one chart, shown below in Figure 4. This chart demonstrates that for aircraft to achieve maximum energy density, one must consider the tradeoff between propulsion system efficiency, fuel energy density, pressurized fuel tank weight, and engine weight.

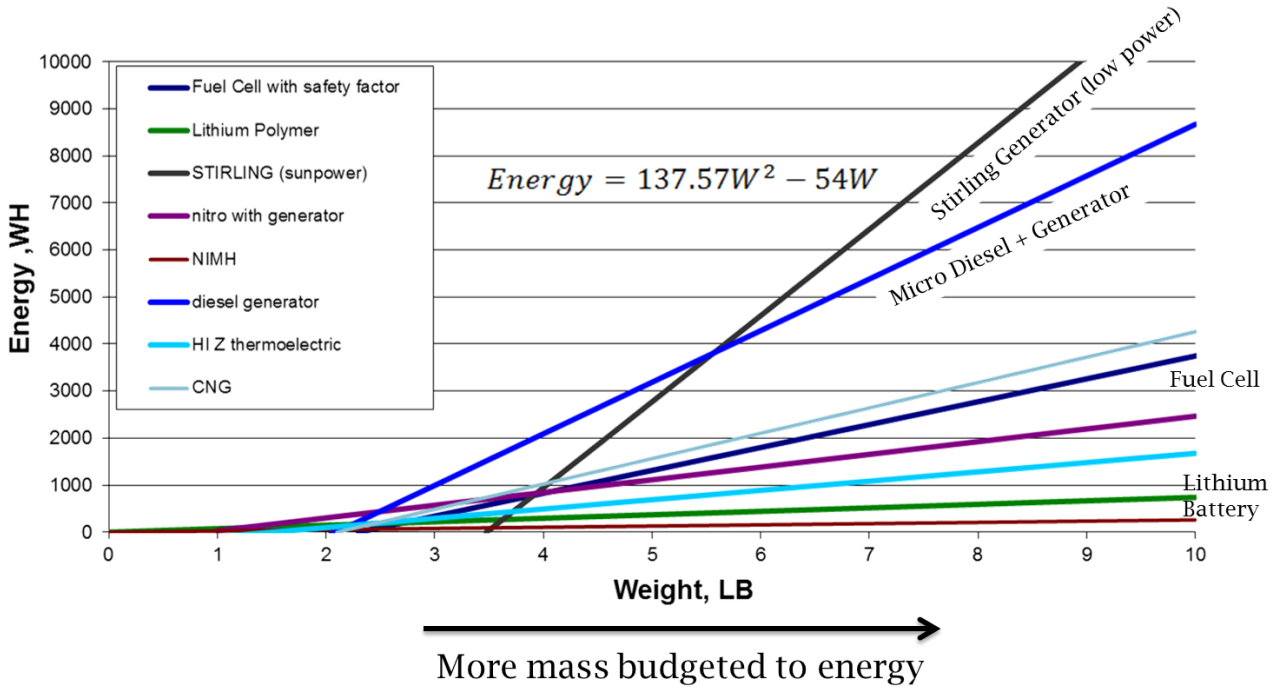

Figure 4 - Product of UAS Energy System Survey

C.Small Internal Combustion Engine Dynamometer

The construction of a small engine dynamometer shown in Figure 5 allows Oklahoma State University to test the power output of small internal combustion engines. Engine tests were conducted with an

electric motor brake dynamometer for constant load tests that confirm true energy densities of 1400 WH/lb of fuel. These tests [1] confirmed that even simple internal combustion engines were capable of delivering higher power density, and higher energy density than even the most advanced fuel cells and batteries.

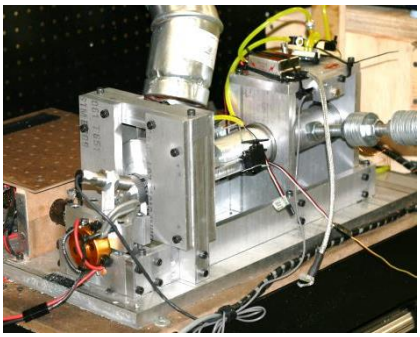

Figure 5 - Small Engine Dynamometer [1]

D.Besler Brothers Aircraft

In 1933 the Besler brothers [2] successfully flew a steam powered airplane shown in Figure 6. The engine used a monotube boiler, reciprocating expander, and a small condenser that was unable to fully condense the cycle's operating forcing the venting of some steam. The aircraft flew successfully, and was quiet enough in flight for the pilot to communicate with observers on the ground from 200 feet in the air.

Figure 6 - Besler Brothers Steam Driven Open Cycle Airplane. [2]

E. Robert McConaghy's Stirling Airplane [3]

In 1986 Robert McConaghy flew a 20W Stirling engine on a small 1Kg airplane shown in Figure 7. While the best flights lasted only 8 minutes and had barely enough power to stay aloft, it is the only flying example of a closed cycle engine this author has located after much research. Most early steam aircraft were open cycle to maximize power to weight, as their designers were interested in achieving flight before worrying about staying aloft for longer periods.

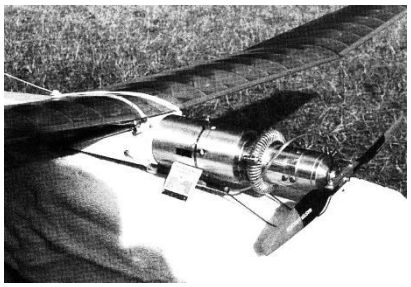

Figure 7 - Robert McConaghy's 1Kg GTOW Stirling Engine Powered Closed Cycle Airplane [3]

Acoustic Directionality Study

Small Unmanned Aircraft are most often utilized to provide a tactical advantage for the warfighter by relaying live video and information providing ground commanders with a better understanding of the tactical situation. First generation aircraft like Raven, Puma, and Tiger shark have flown thousands of these missions and have successfully changed warfare. These small UAV's most often fly against technologically unsophisticated opponents without radar, infra-red, and other modern aircraft detection methods. As our adversaries evolve their own tactics based on their recognition of the power UAV's hold in a battlefield, the easily detectable first generation of UAV's broadcast their presence and allow ones opponent time to react. The optimal tactical solution is an aircraft that can deliver intelligence without its presence being discovered. One's opponent will continue uninformed providing the largest possible boost to friendly objectives.

Kill Chain:

1) Target Identification

2) Force Dispatch to Target

3) Decision and attack order

4) Destruction of Target

If one can remain undetected, the kill chain is never initiated. However, being "undetectable" requires a complete understanding of emissions filtered down to bands corresponding to the sensors that will be used to attempt discovery. Preliminary work is conducted with an equal magnitude discovery criterion (If emitted acoustic amplitude is equal to ambient values at a given frequency, or visual contrast between the vehicle and background exceeding a to be determined threshold.)

The initial study into controlling acoustic propagation is focused on reducing acoustic emissions from small UAV's as reducing visual detection ranges by matching background luminance through diffused lighting camouflage has already been studied in many experiments like those shown in Figure 8, and further advances in visual camouflage must come from research in physics.

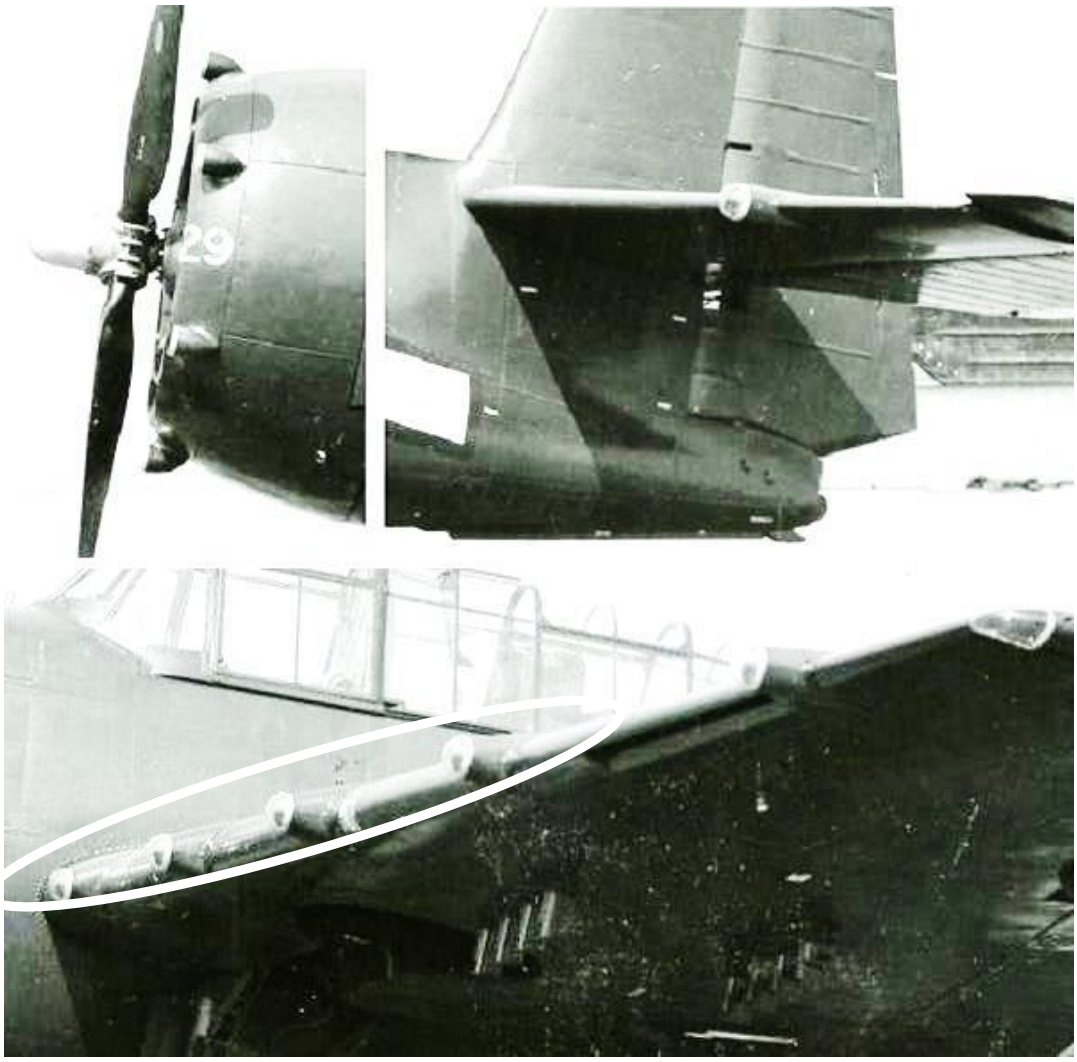

Figure 8 - TBM avenger employing Yehudi lights – U.S. Military source unknown

Mission planning often enhances chances of remaining undetected as one is able to use knowledge of the threat environment to avoid regions of high discovery probability. When flying SUAV's against an unsophisticated opponent every person on the ground is a sensor whose position is unknown. The only way to ensure the SUAV remains undiscovered is to consider the entire ground surface as a distributed sensor network with the capabilities of human eyes and ears. Detection criteria

considers only AGL altitude in detection range calculations from here forward as any consideration of slant ranges to targets neglects the distributed sensor network just discussed.

It is important to note that the sensor network forms a plane beneath the aircraft. Any noise, reflection, or emission that leaves the aircraft and only travels upward cannot be detected by the sensor network regardless of its magnitude.

Propeller noise is the second highest contributor to internal combustion SUAV noise. Numerous studies have been conducted to understand and minimize the sources of propeller noise. The dominant factor is propeller tip speed as it captures compressibility noise effects, and effects from increased pressure differentials across each blade. Having a larger number of propeller blades reduces the pressure fluctuation observed in the far field as the passing of each blade is summed resulting in only a ripple for large numbers of blades.

Aerodynamic noise grows in magnitude with aircraft speed and turbulence level. While it is important to minimize panel vibrations and separated flow regions, this noise source can be minimized by flying slowly to reduce the magnitude of turbulent noise production.

F. Finite Difference Time Derivative Acoustic Propagation Simulation

"Finite Difference Time Derivative" propagation codes are often used to simulate the propagation of acoustic and electromagnetic waves through media. They are simply an Euler simulation to the wave equation, and can be implemented in one, two, or three dimensions. The error associated with the finite difference derivative forces one to use a fine grid to keep the spatial laplacian error acceptable. FDTD methods are quite versatile and particularly well suited for computational solutions. Solutions from FDTD codes are not exact, but are calculated very

quickly in relation to more exact methods (CFD). Complex acoustic simulations can be run in seconds instead of waiting hours or days for a CFD solution. The code can easily support varying properties throughout the domain, the introduction of walls, and attenuation models.

$$\frac{\partial^2 u}{\partial t^2} = c^2 \nabla^2 u$$

Figure 9 - FDTD codes are a simple simulation of the wave equation

Multiple examples of FDTD codes exist on the web but a free to use version for simulation of acoustic propagation in complex environments shown in Figure 10 could not be found so the matlab code "Tiny FDTD" by Nick Clark [4] was used as a starting point.

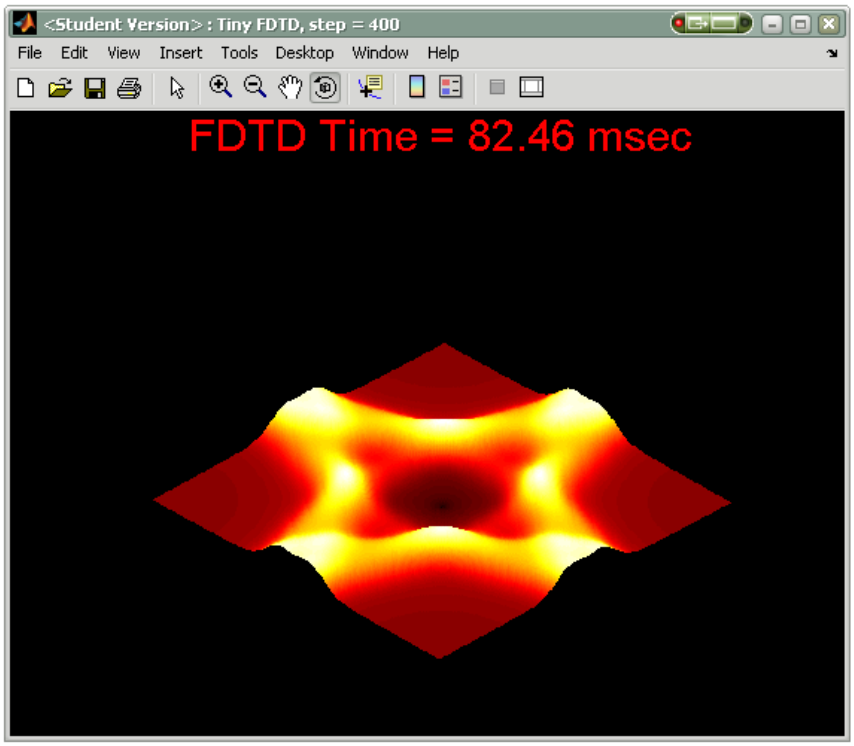

Figure 10 - Tiny FDTD by Nick Clark [4] – default case and output.

Tiny FDTD only simulates a single pulse propagating over a small two dimensional grid with full boundary reflections and no data output. Impressively the entire Tiny FDTD code was written in 25 lines and runs in seconds which is a testament to the methods suitability for computational solutions. The code was modified using the same FDTD core to calculate the sound pressure level as a function of direction around an arbitrary noise source. Further modifications were made to model a reflecting plane near the noise source to simulate the interference of the wing, and splitting of the noise source into multiple emitters to model the behavior of a phased array exhaust system. Phasing delay calculations were included to allow one to focus the noise at an arbitrary angle and distance. This angle can be a function of time, allowing one to maneuver the beam as the simulation progresses. The progression of FDTD code modifications is shown from a single point source to a reflecting scenario through a small slot in Figure 11 through Figure 13.

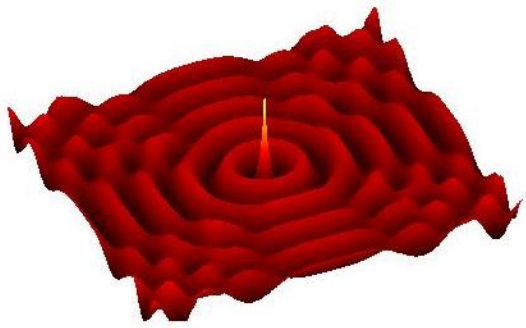

Figure 11 - FDTD Simple Source Propagation with Reflection [4]

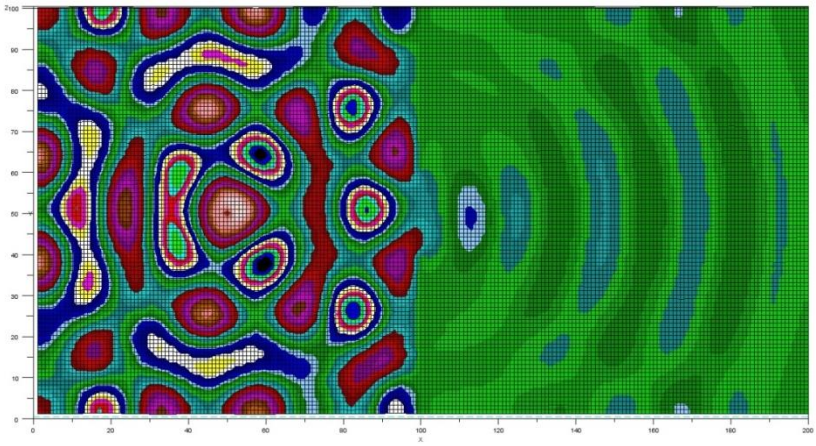

Figure 12 - Tiny FDTD sinusoidal input, reflecting boundaries

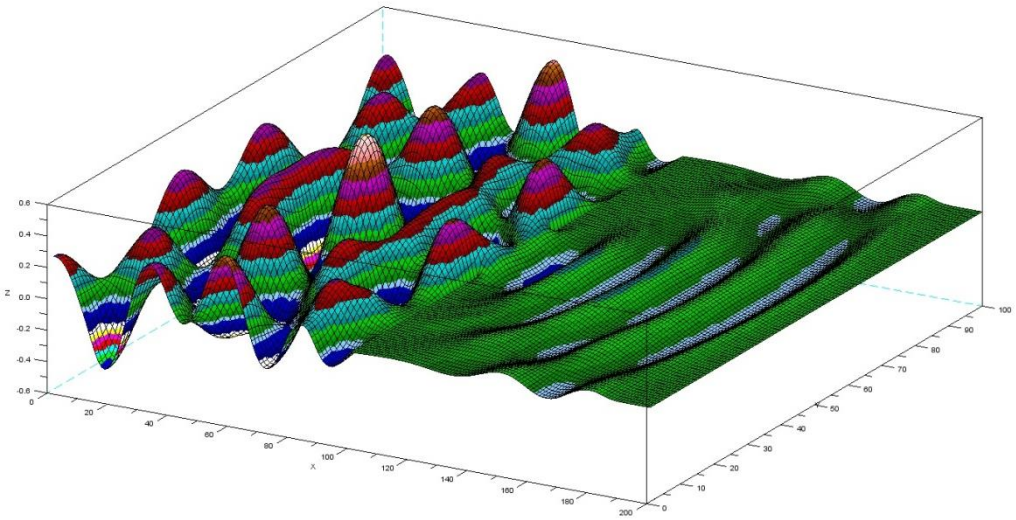

Figure 13 - Single slit simulation with reflecting boundary conditions.

Before the most basic omnidirectional propagation simulation could start, many more fundamental changes were required to the Tiny FDTD code. Firstly, the Tiny FDTD code is a matlab script and to truly allow open use the code was translated into "Scilab", an open source program with

capabilities extremely similar to matlab. The domain size, which had been hard coded, is now controlled by a simple x and y dimensional input. Memory allocation for the program was increased to allow for larger domains. Temporal and spatial grid resolutions are now simple definitions to allow one to easily determine the maximum frequency that can be accurately simulated. Instead of the pressure input following a simple algebraic function, an interpolation routine was implemented to subsample a sound recording. This enables the code to use any recording as a noise source in the model. One test was to use a recording of a DA100 two stroke engine as shown in Figure 14 below. The magnitude of the recording was tuned so that simulation matched that of recorded data taken at 10 feet.

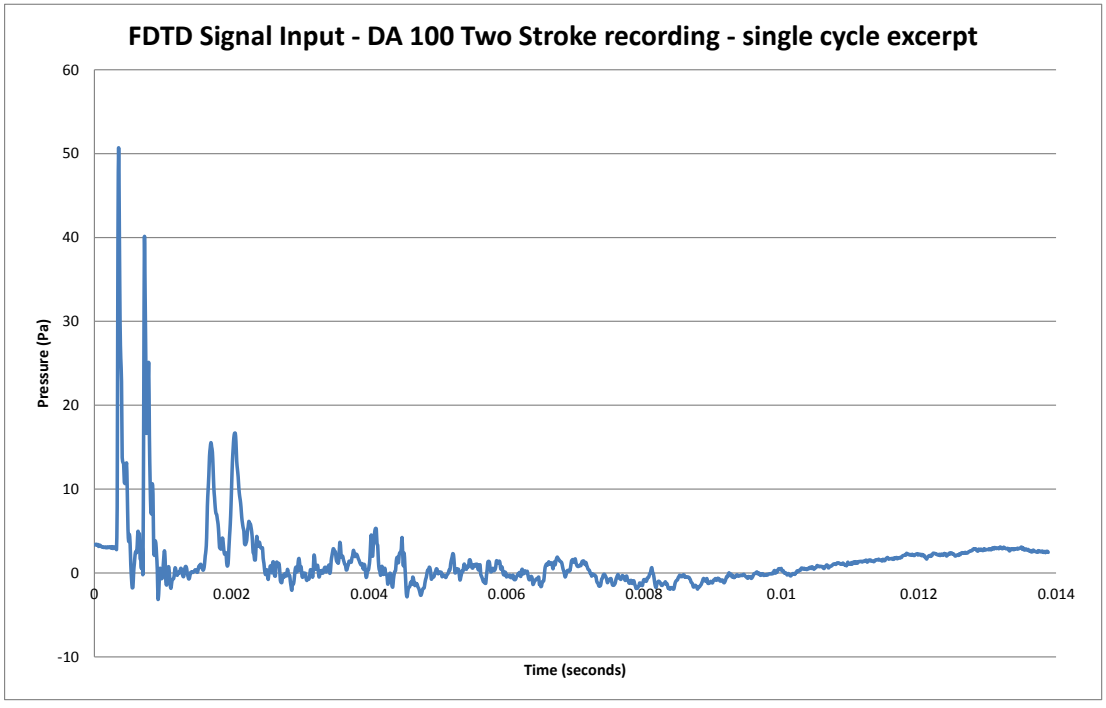

Figure 14 - DA 100 Recording used in FDTD simulation of noise propagation. 96KHz sample

Another essential improvement was a modification of the boundary conditions to eliminate boundary reflections. In the base Tiny FDTD code the boundaries were floating, but reflected all

waves perfectly. This causes the domain to become flooded with reflections soon after the simulation began, and would be useless for measuring propagation patterns as the waves are not free to propagate. A variable length region of forced dissipation was introduced around the boundary to absorb waves as they approached. Second derivative calculations were modified from a fixed to float boundary condition as well. These two changes along the boundary were sufficient to eliminate reflections as shown in Figure 15 and enable free field propagation studies.

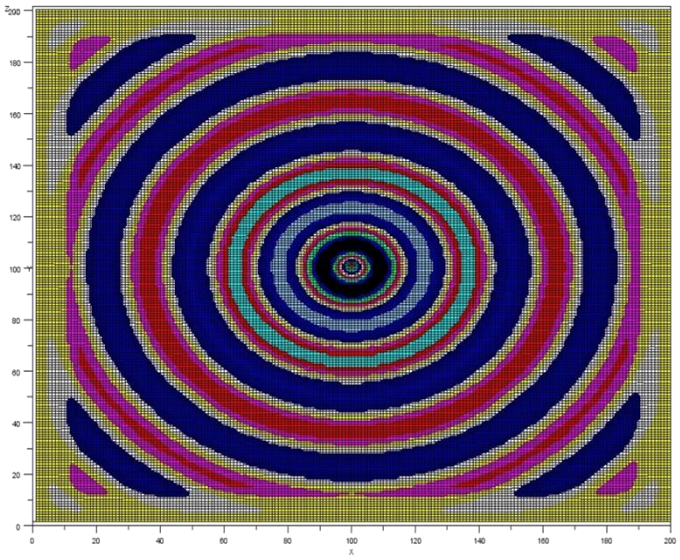

Figure 15 - Modification of boundary conditions eliminates boundary reflections enabling free field propagation studies.

A sampling routine was coded to record the pressure at a specified distance from the noise source in one degree increments at each time step. This recorded data is further parsed into spectral content for each measurement location in a post processing FFT code. Plots of overall sound pressure level (OASPL) and frequency content can be made as a function of direction.

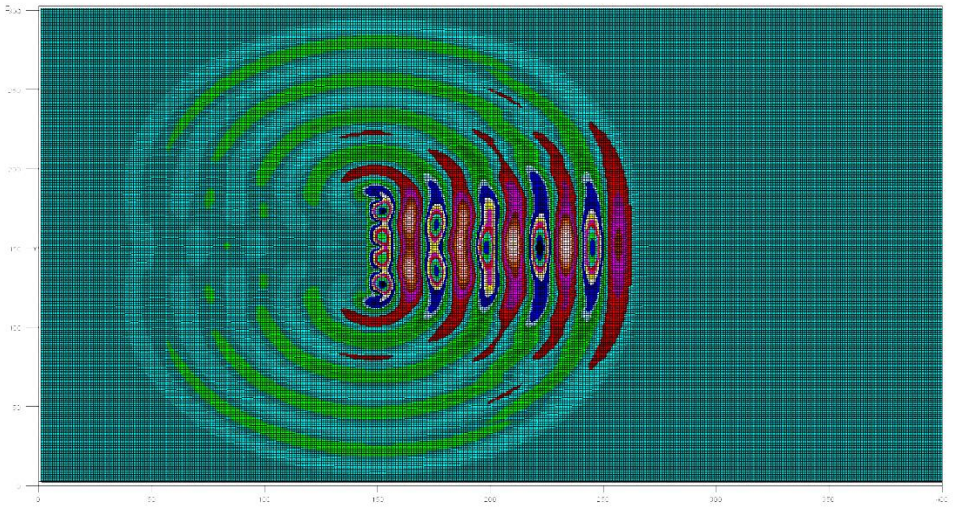

Figure 16 - 5 element broadside array with tone source function.

One of the first cases run for testing of an acoustic array is shown in Figure 16 above. The tone source was duplicated five times in a vertical line, with a wall placed immediately to the left of each source. The magnification of the beam to the right can easily be seen. Also see that what begins as five discreet peaks near the source has turned into a single wave in the far field.

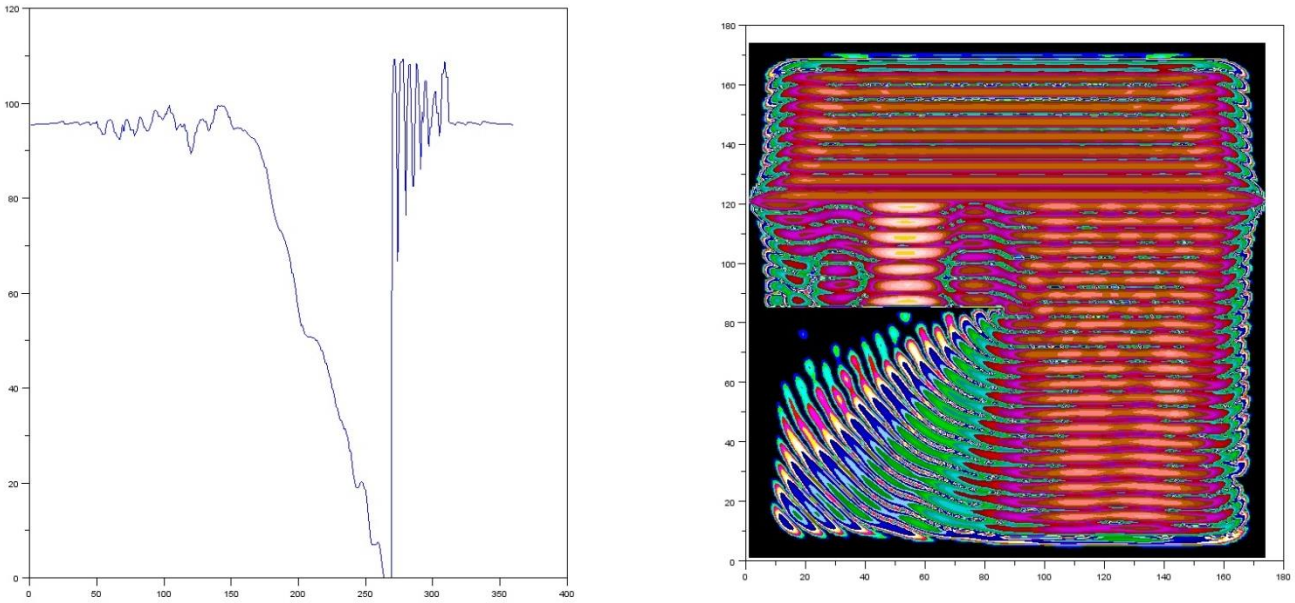

Figure 17 - 500 Hz Diffraction around wall edge from line source (right). Directional magnitude, clockwise with zero degrees being straight up.

The above test case in Figure 17 was run as a study of the diffraction behavior around walls in the FDTD code. A 500 Hz line source was used to create a plane wave that impinges on a half domain span perfectly reflecting wall. OASPL dropped from full magnitude free field propagation to zero dB in only 90 degrees.

Once all modifications were complete to the base FDTD code, a high resolution study was conducted using the DA 100 recording as an input. The domain grid was sized to support waves up to 5760 Hz, beyond which point the nyquist criterion is no longer valid. The directionality study was conducted with omnidirectional free propagation conditions, a two meter wall to reflect the noise upward, and then an exhaust array mounted to the same 2 meter wall. The main interest was the reduction in OASPL 180 degrees away from the exhaust port (straight

down toward ground). The following plots show acoustic intensity as a function of frequency and direction. The code allows one to view the detailed spectrum of the signal in a direction of the users choosing.

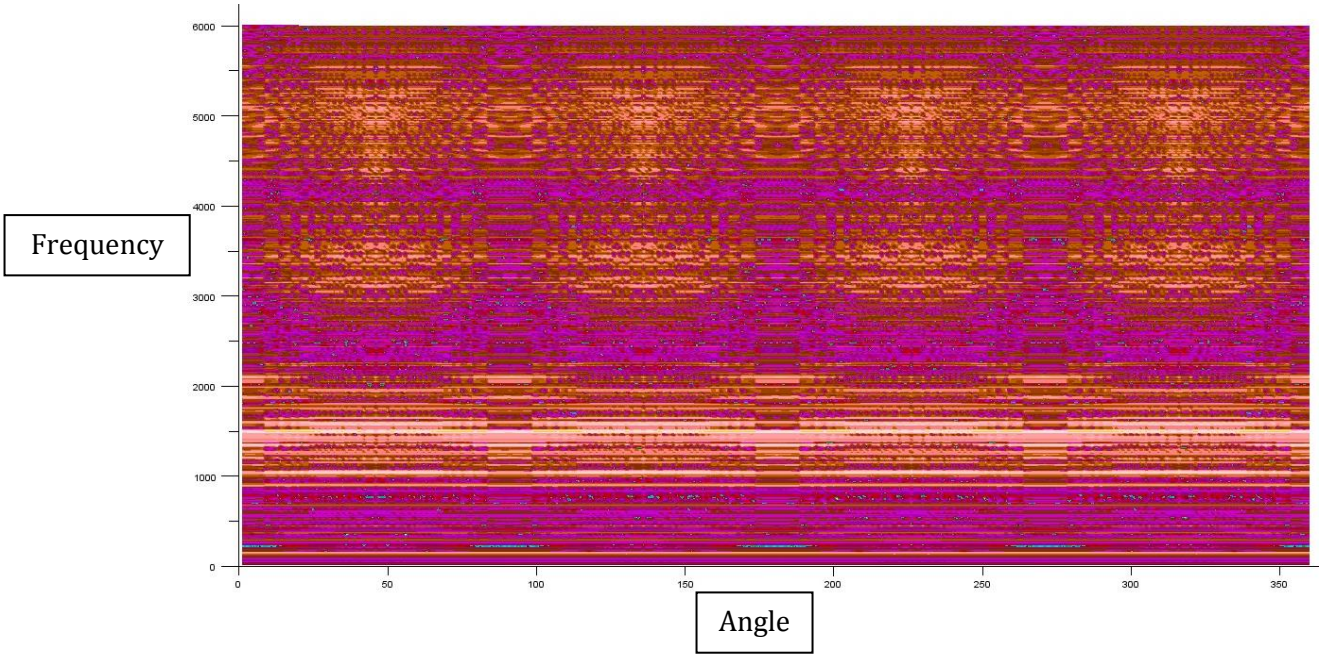

Figure 18 - Omnidirectional test case directional spectrograph

The omnidirectional propagation case shows some artificial directionality. The slight changes in magnitude in Figure 18 are due to the square domain grid. The variation in OASPL is less than 2 Db.

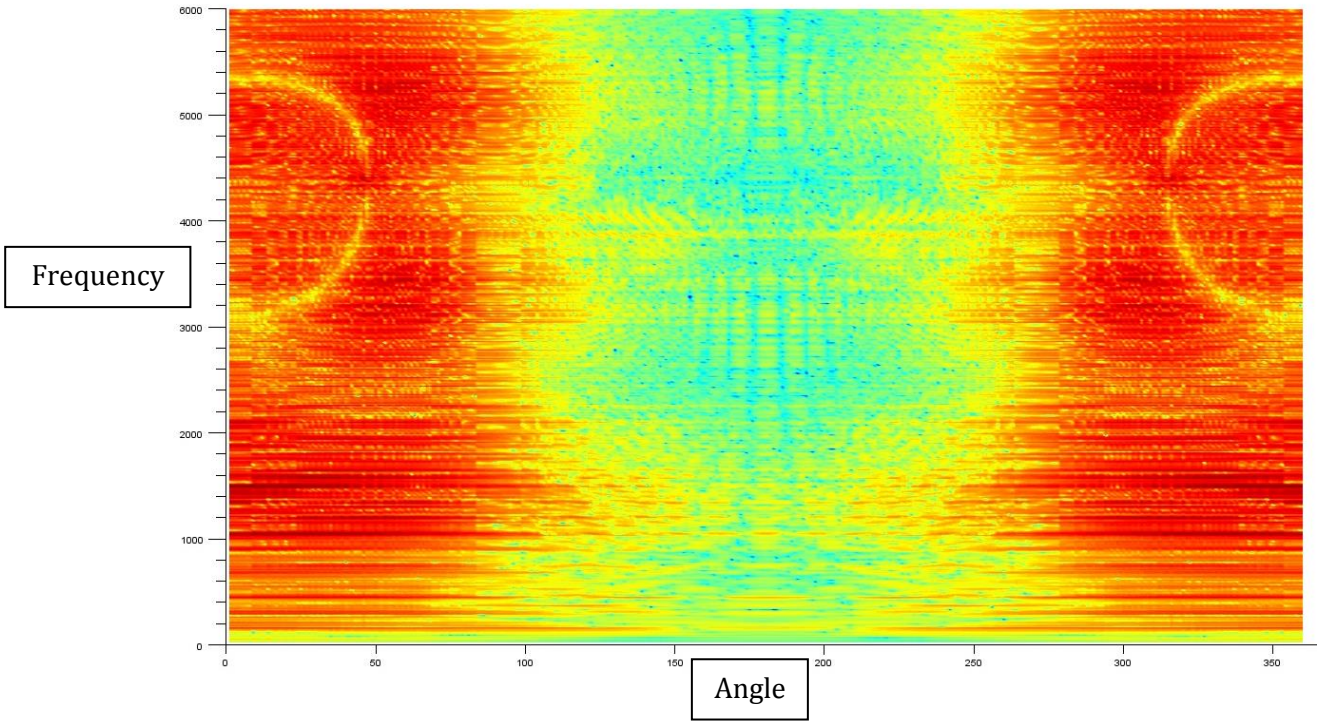

Figure 19 - Wall test case directional spectrograph

The inclusion of a wall in the simulation makes the radiated sound very directional. Regions from 0-90 and 270-360 degrees (straight up) in Figure 19 are increased in magnitude, while the region from 90-270 degrees contain only sound that has diffracted around the wall. It can also be seen that at 180 degrees higher frequencies are more attenuated than those below 1000 Hz. An interesting element in the above chart is the "ring" that is formed from 310 to 50 degrees. It is theorized that this ring is the interference pattern created by the wall ends. This would explain the angular dependency of the interference frequencies.

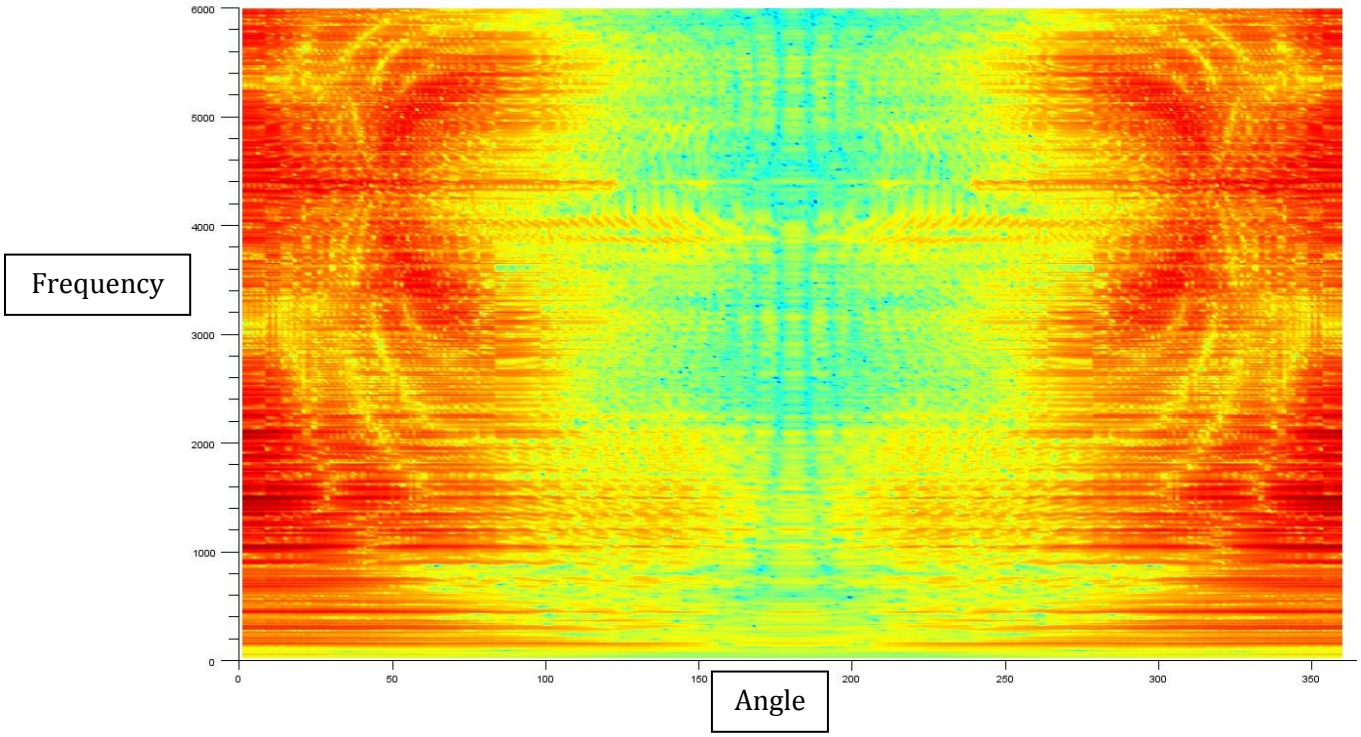

Figure 20 - Wall and array test case directional spectrograph

Lastly, the source was changed to a five element phased array in Figure 20 with the wall left in place. Directionality is marginally better than that of the wall alone, but one can still see that low frequencies show very little directionality, and are not impacted by the addition of the array. One benefit the array does add is extra angular dependent interference frequencies that serve to reduce the OASPL between 300 and 60 degrees. These interference patterns can be seen in the additional yellow (reduced magnitude) rings in the phased array plot when compared to the wall plot.

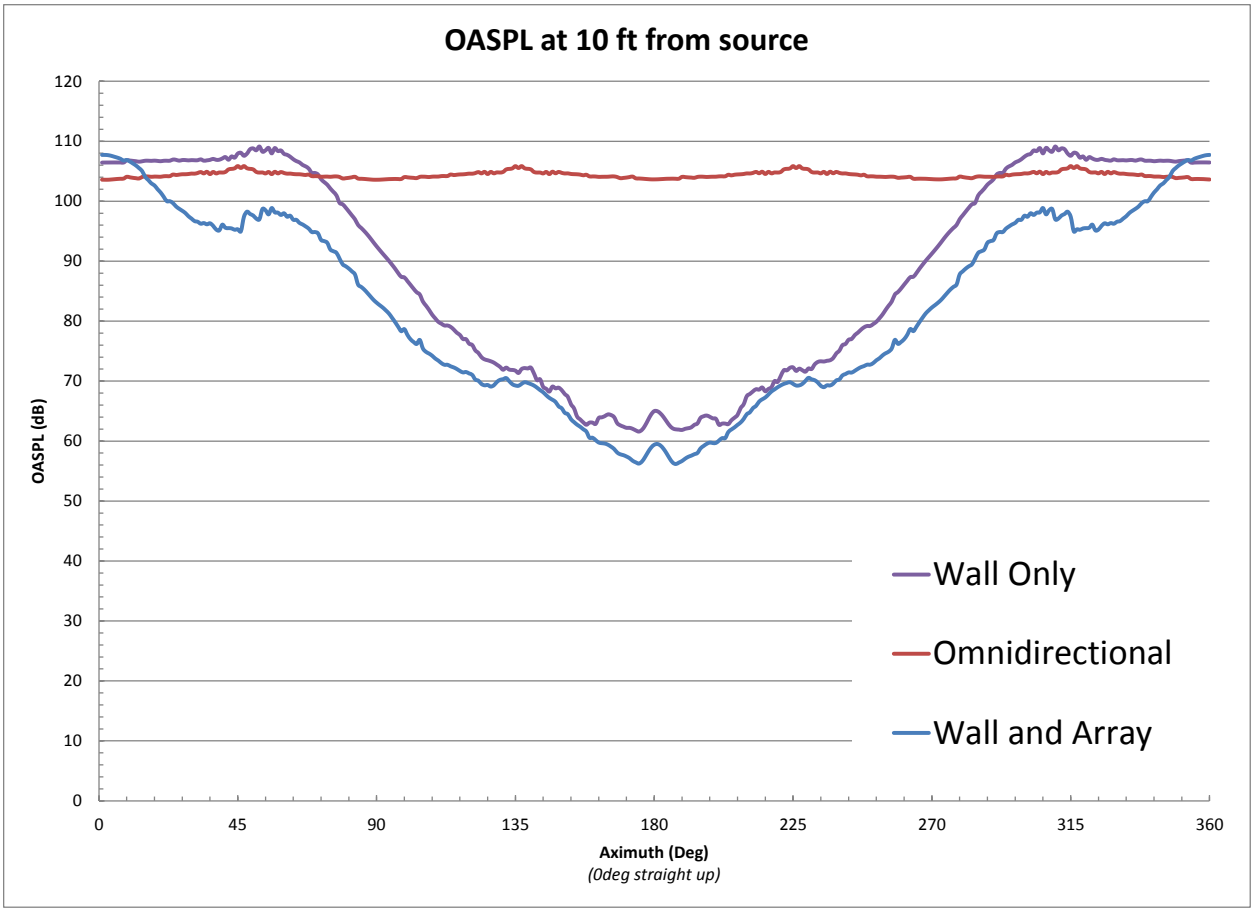

Figure 21 - Azimuthal Variation of OASPL at 10 ft. from Source.

The culmination of all modifications and test cases is shown in Figure 21 - OASPL vs. angle plot showing a -44 dB reduction in radiated noise directly beneath the aircraft. This is a 25,000:1 reduction in SPL.

The omnidirectional case is as expected omnidirectional at 104 dB. The inclusion of a perfectly reflecting wall to crudely simulate the presence of aircraft structure does much to decrease OASPL in the target region (90-270 degrees). While the addition of an acoustic array

does further decrease the OASPL of the wall only directionality by 0-10 dB. All SPL's in the chart above are for 10 ft spacing from the DA 100 noise source.

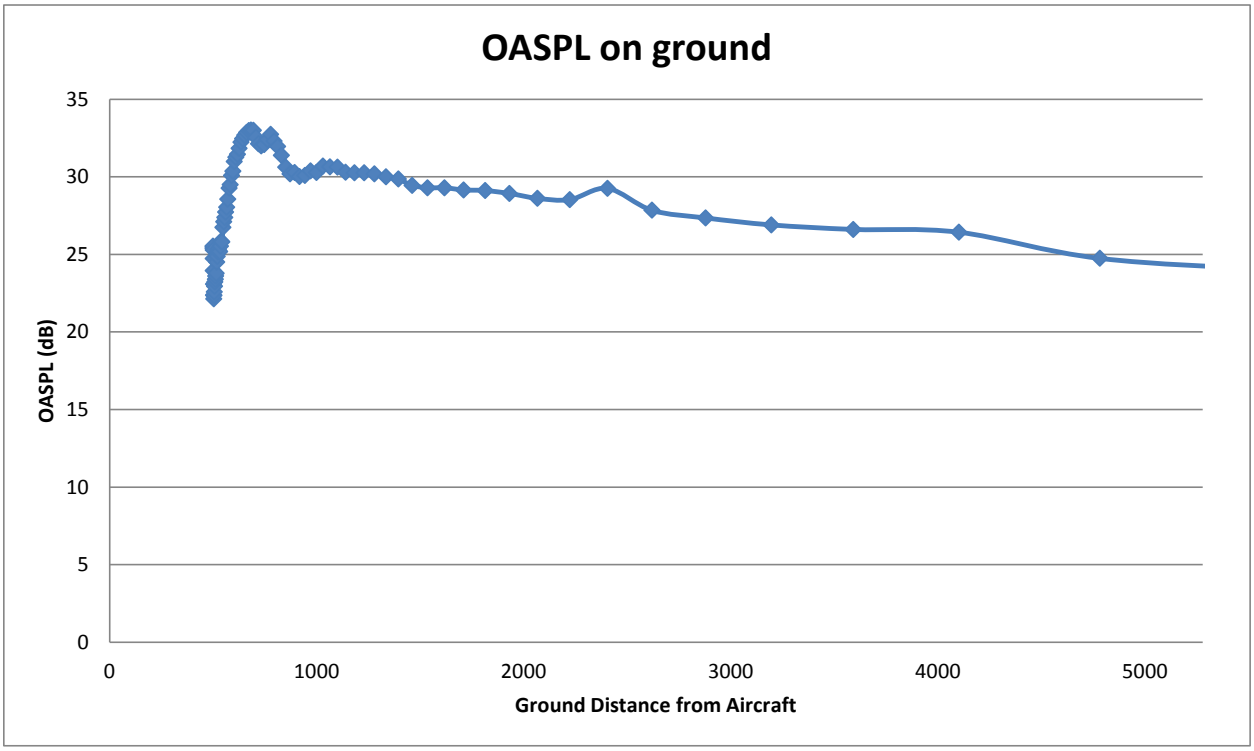

Figure 22 - OASPL on ground for 500 foot AGL flight

Taking the OASPL data from the wall and array, Figure 22 shows the OASPL a person would hear on the ground (neglecting possible 3 dB ground reflection). Note that the loudest point is not located directly underneath the aircraft, and is in fact 40 degrees away from directly down. Beyond this point the dB reduction due to range outpaces the dB increase from the exhaust directionality pattern.

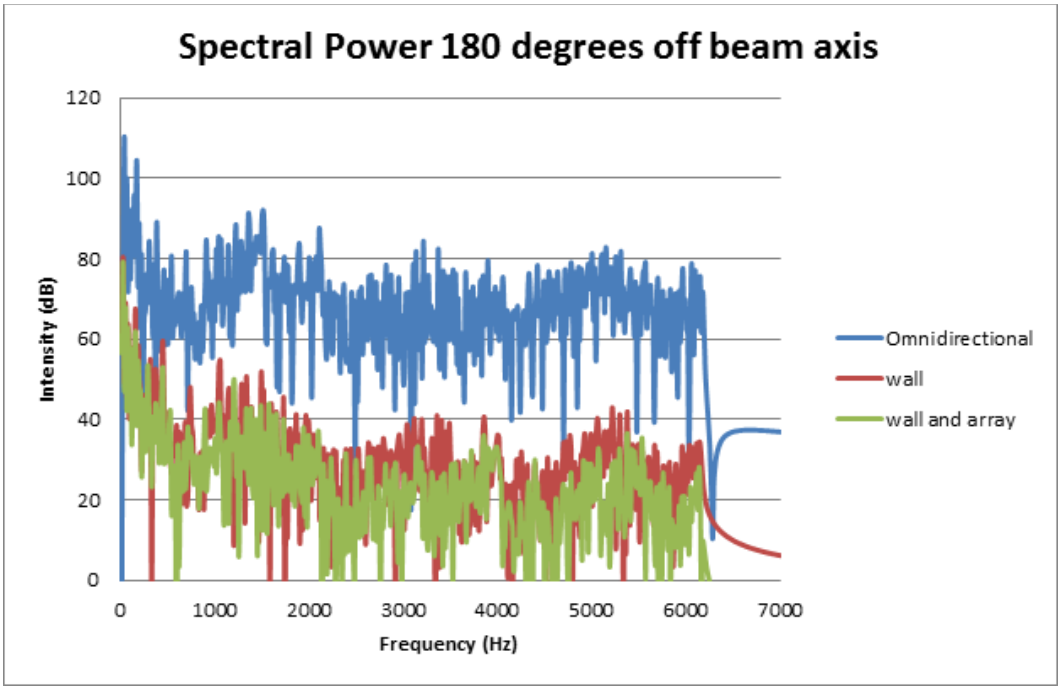

Figure 23 - Spectrum Magnitude in Opposite Direction From Emission

One can quickly see in Figure 23 that the wall significantly reduces higher frequency noise, but is less influential at low frequencies. Just as subwoofer placement in home theater systems is inconsequential because of how well low frequencies disperse in an environment, the low tones of the exhaust are not affected by the presence of a wall or array in Figure 24.

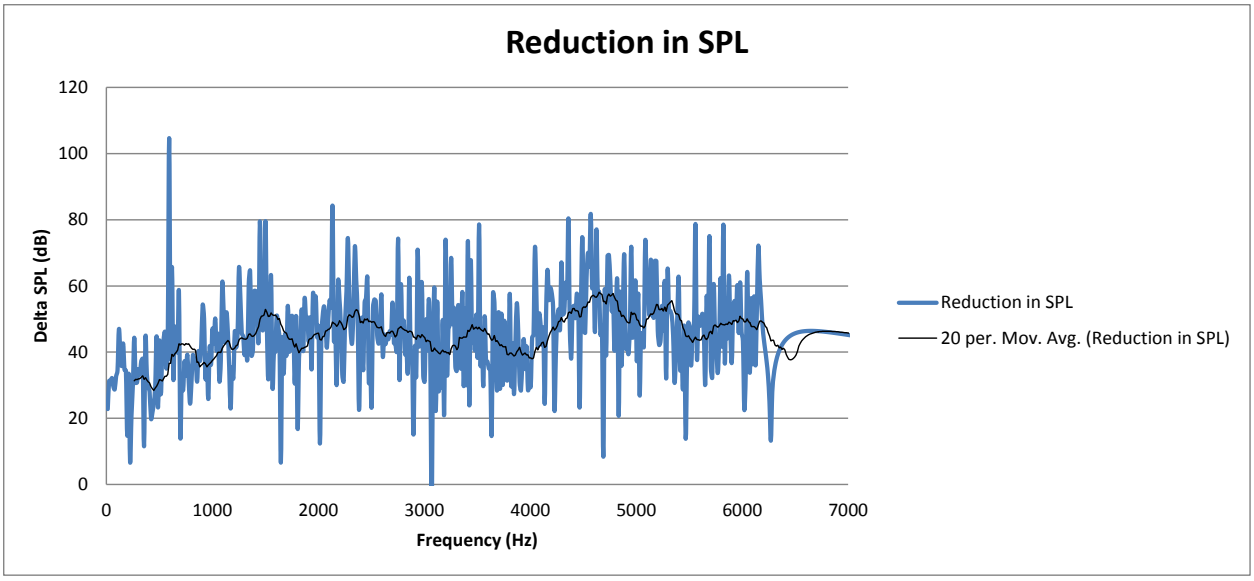

Figure 24 - Phased Array Reduction in SPL

G. Conclusions

After running FDTD simulations to evaluate the potential directionality of a focusing exhaust device, the benefits do not offer a substantial improvement over current state of the art silencing methods, and do not justify construction of a prototype. A directional exhaust system could be applied to the end of a conventional system to improve its ground signature at the expense of added weight and volume. Furthermore since the theory that goes into predicting the emission patterns of such a system has already been thoroughly developed in the antenna community, there is no reason to focus additional research on the development of such equations.

Silencer design is by definition an attempt to correct the unwanted noise of an otherwise desirable power plant. Silencers and directional exhaust devices add weight and complexity only because the original power source is unacceptably loud. In place of trying to correct a high intensity noise source, the next generation of low noise propulsion systems should avoid the

generation of intake and exhaust noise entirely. To eliminate intake and exhaust noise, one could use a closed engine cycle and design it such that mechanical speeds and pipe flow velocities are kept to a minimum. Additionally, acoustic absorption materials can be applied around the closed system just as they are around an IC engine to absorb some of the necessary mechanical and pipe flow noises. Closed cycles have been avoided previously because of the weight penalty associated with having the extra boiler, tubing, and heat exchanger, but as noise requirements for IC powered UAV's continue to drop the increasing silencer weight soon makes the change to a closed cycle engine a draw.

Closed Cycle Engines for Quiet UAV propulsion

Closed cycle engines are well suited for aircraft use in many ways: containing the operating fluid eliminates exhaust and intake noise, their power output does not drop with decreases in outside air density, the cycle BMEP is only limited by fluid operating pressure and can be three to four times higher than IC engines, and the heat exchanger size and weight is decreased proportional to the dynamic pressure of the vehicle. Higher BMEP allows one to trade off engine displacement and operating RPM for equivalent power to an IC engine. In a 600 psi max pressure rankine cycle, one could decrease cylinder displacement to a fourth of an equally rated IC engine and maintain RPM to receive equal power, or decrease RPM to a fourth and maintain engine displacement. When designing a low noise propulsion system one would prefer to slow the rotational speed of the shaft while maintaining power so that mechanical noise and propeller tip speed are both decreased. This higher BMEP lower RPM engine would have a

propeller with lower disk loading and lower tip Mach number than its internal combustion competition.

Disadvantages to using a closed rankine cycle propulsion system include a lower theoretical efficiency than internal combustion engines, heavier base engine weight, more complicated airframe integration due to the heat exchanger, and slower response time to large throttle changes. These factors, specifically the lower efficiency and power density, are the reason internal combustion engines became the only choice for aircraft engines.

In the niche area of quiet SUAS design, the commonly used two stroke engines are very inefficient (as low as 7 to 9 percent) and the additional silencer weight to mask combustion noise significantly lowers the power density of the engine. This opens the quiet SUAS design space as an area that closed cycle engines can be successful. Rankine cycle efficiency is comparable to that of currently used two stroke engines, the volume and configuration requirements of the heat exchanger are comparable to the requirements of internal silencing devices, and the power density after including silencer weight in the IC engine total system weight is comparable, if not better in the Rankine cycle. So each major disadvantage of closed cycle propulsion is at least equivalent to a silenced two stroke engine, with the closed cycle offering significant advantages in OASPL, and performance at altitude.

H. History of Closed Cycle Aircraft Propulsion Research

The idea of using closed cycle engines to power airplane is not new. Several studies on the feasibility of closed cycle engines for aircraft propulsion persisted even into world war two. Articles such

as “New Gas Turbine Projects” from 1943 discussed systems operating on closed cycles with special liquids. These studies were centered around large military aircraft like that shown in Figure 25 , particularly bombers and transports, but more importantly show that closed cycle engines have been considered before for aircraft, but were eclipsed by the more power dense internal combustion air breathing piston engines that became essential to World War Two aircraft.

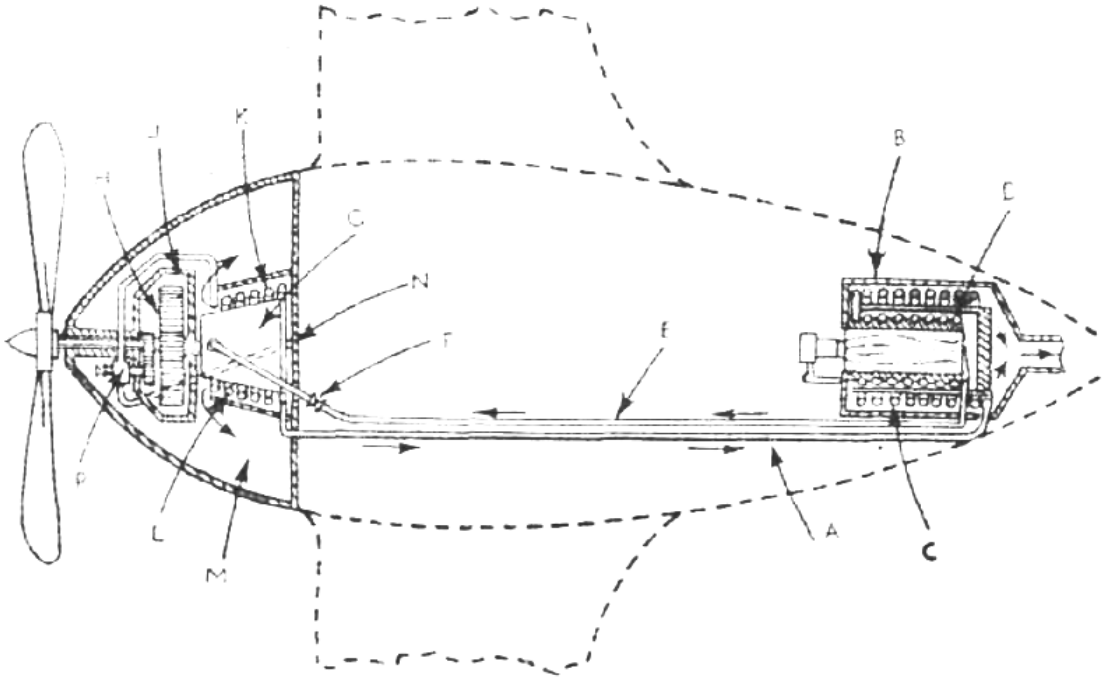

Figure 25 - Diagram of Holmes closed cycle engine from 1943 Flight Global article.

Figure 26 - Compressed Air Engine from Small Model Aircraft [5]

Figure Figure 26 shows a modern Zephyr compressed air engine. This type uses stored pressure in the attached cylinder, but could just as easily be used in a closed cycle configuration. One should note the very small size of the engine in relation to the propeller used.

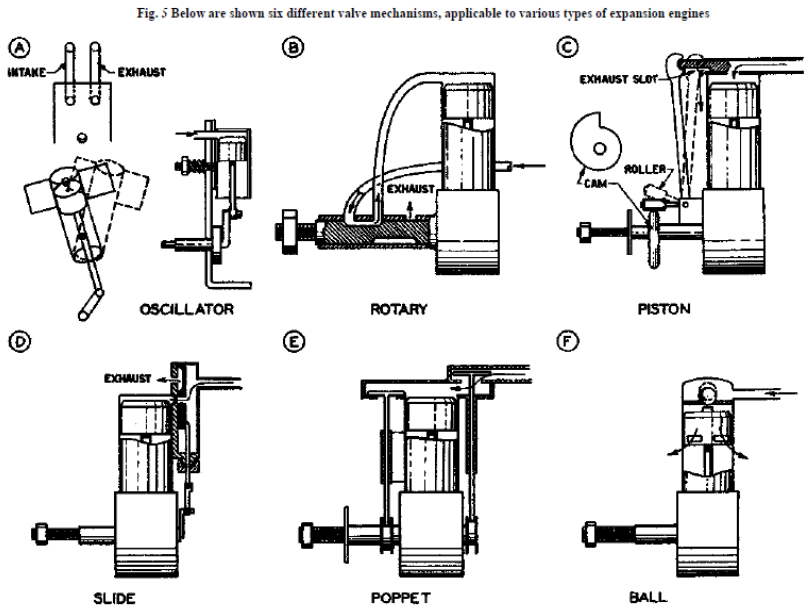

Figure 27 - Notional Layouts of Model Aircraft Engines [6]

Figure 27 is a diagram of 6 different expansion engines featured in June 1948 model airplane news. An excerpt from the Model Airplane News article accompanying the above diagram said: *"The possibilities of steam have never been fully realized. In view of the results obtained with comparatively crude constructions we venture to suggest that if somebody with the time, money and ambition put as much engineering effort into developing a good airplane model steam engine, as has been put into development of present day gasoline engines, the steam engine would give internal combustion a good run for its money."*

Even the NACA conducted a study of the feasibility of closed cycle engines. Without a strong unconventional design requirement, the additional weight of a closed cycle would not buy its way onto an aircraft.

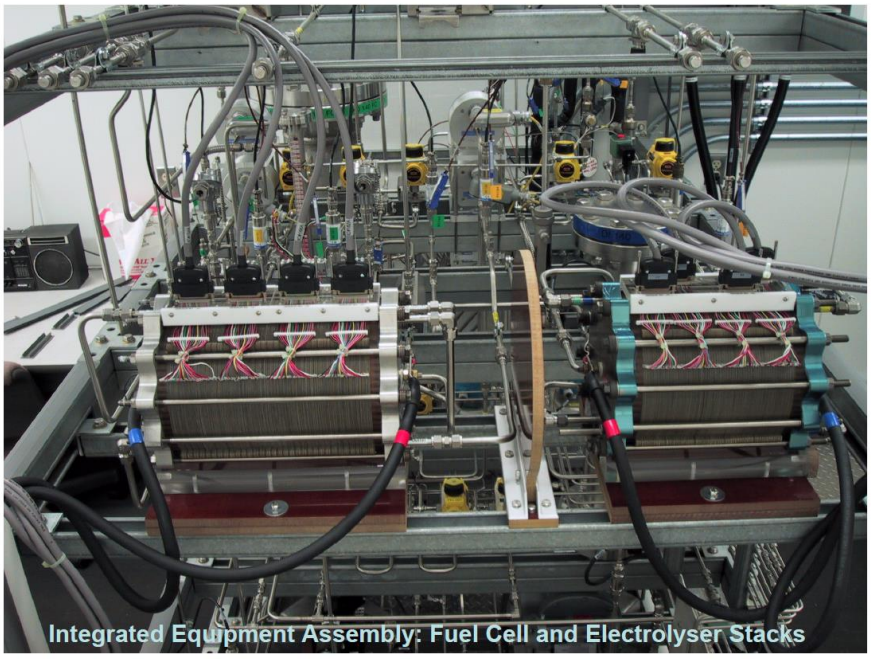

Figure 28 - NASA development of Helios regenerating fuel cell system [7]

Figure 28 shows a Ground test of Helios regenerative fuel cell closed cycle propulsion unit. Thus far a truly closed cycle airplane (other than battery) has not been found, making any successful fully closed rankine cycle airplane a potential world first.

Figure 29 - The Besler brothers pose with their steam engine airplane [2]

The Besler brothers pictures with their steam airplane in Figure 29 made a very quiet airplane. It was said "The 150 Hp engine was so quiet people on the ground could hear the pilot call to them from the air."

While the Besler engine was indeed a rankine cycle, and had a condenser to reduce the amount of water consumed during operation, it was not entirely closed as it vented whatever could not be easily condensed to reduce the size and weight of the condenser. The engine could operate in reverse, granting the aircraft a unique ability to brake on landing, and backup if the pilot chooses.

I. Horsepower

The engine is designed to match power of quiet two stroke system for equal comparison of OASPL. If one supposes the boiler exit pressure to be 600 psi, engine exhaust pressure to be 5 psi, and variable fluid

cutoff, the following chart is an estimate of engine mean effective pressure as a function of the expansion ratio. The maximum MEP occurs at an expansion ratio of 1.0 as shown in Figure 30 in which case the engine is functioning as a hydraulic motor. Although MEP and efficiency are opposed in normal operation, this is not necessarily a bad thing for aircraft operation. Takeoff and heavy maneuvering will suffer from low efficiency, but when the engine is throttled back (by changing the cutoff ratio) for cruising flight efficiency will increase.

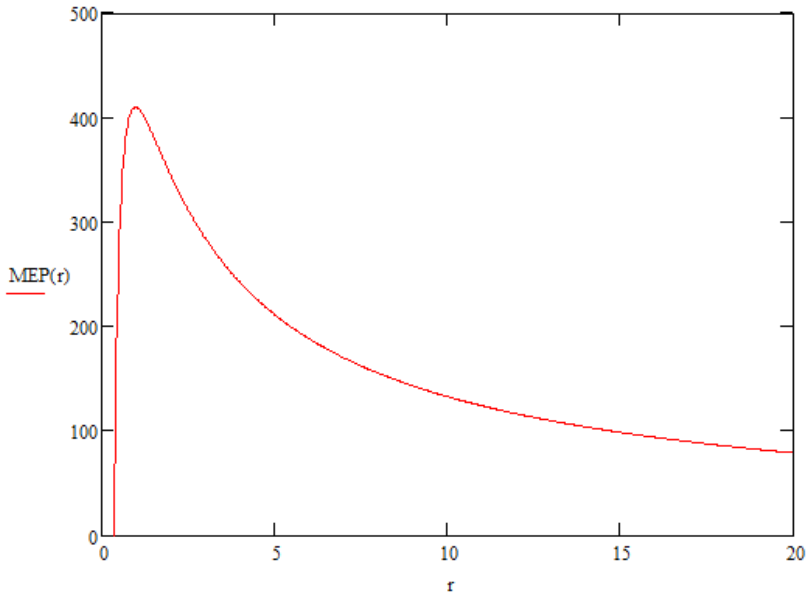

Figure 30 - Variation of Mean Effective Pressure with Crank Radius (inches)

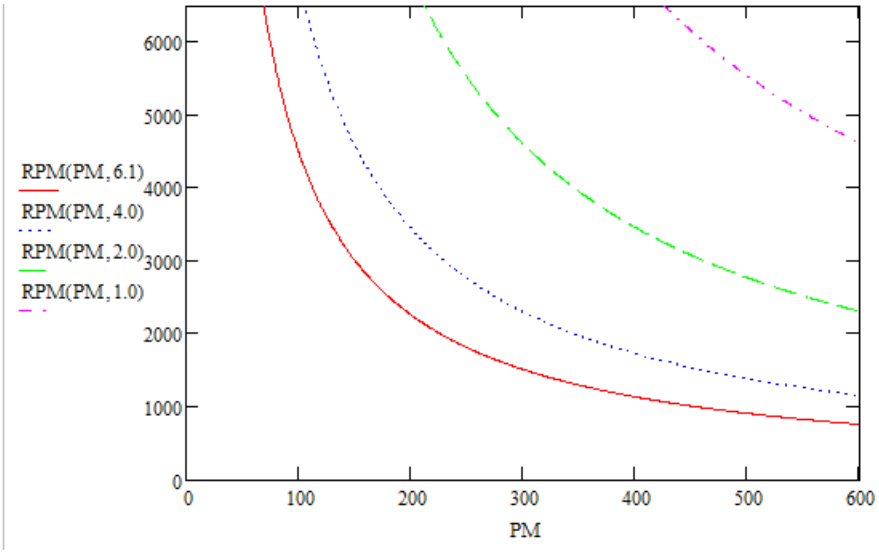

Figure 31 - Variation of Brake Mean Effective Pressure with Engine RPM.

Figure 31 shows the relation between BMEP and RPM required to generate 7 Horsepower. This chart is generic for all engines. The quiet two stroke class engine possesses a BMEP of only 59, while it has already been shown that an expansion engine can have BMEPs in the 300-500 psi range.

J. Noise spectrum

Pipe flow noise prediction equations return extremely low sound pressure levels (SPL) for flow noise. Other strong sources include mechanical noise from the engine, scrubbing noise through the heat exchanger, and burner noise from the boiler. These sources will be measured as time allows. Design decisions will be based on limiting internal turbulence, keeping flow speeds low through use of larger than required diameter pipe, and using thermal and acoustic insulating materials in critical areas. The propeller will most certainly be the dominant noise source, so a small design study was conducted to discover the radiated SPL. The results of that study conducted with Xrotor are included below.

3 Bladed Propeller

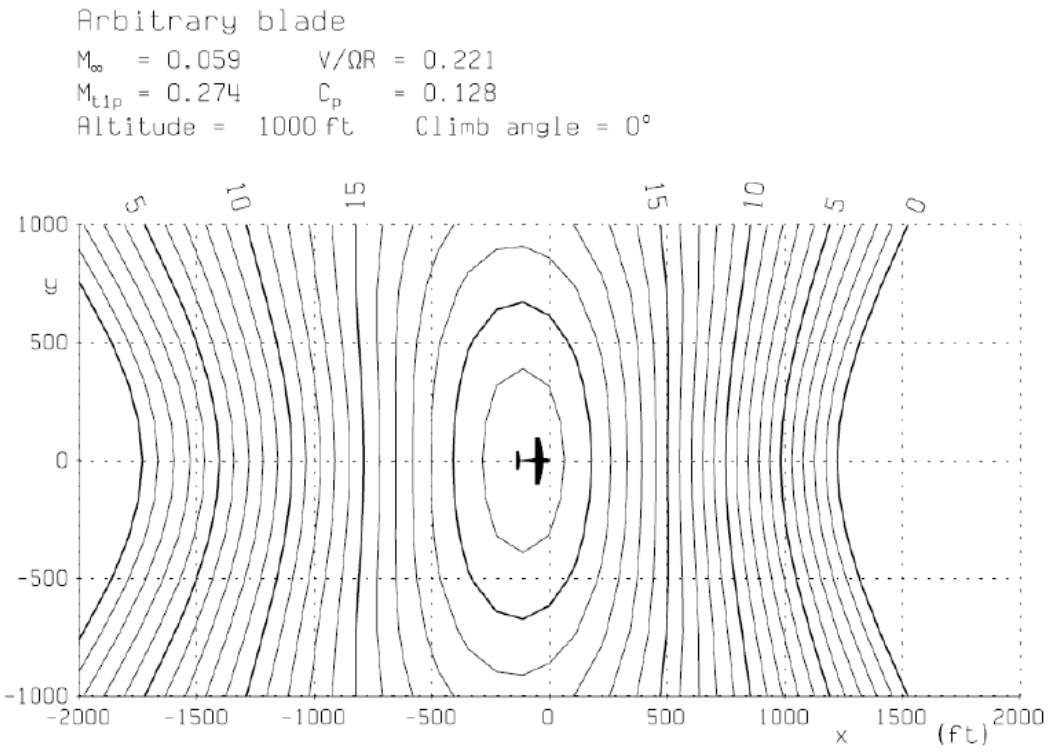

Figure 32 – Notional 3 Bladed Propeller Ground SPL Map as Produced by XRotor

Figure 32 is a plot of ground plane Isobars for Quiet IC engine optimized propeller. The 18" diameter three bladed propeller has a tip speed of Mach 0.27 and cruising altitude of 1000 feet. This serves as a three bladed test case for comparison

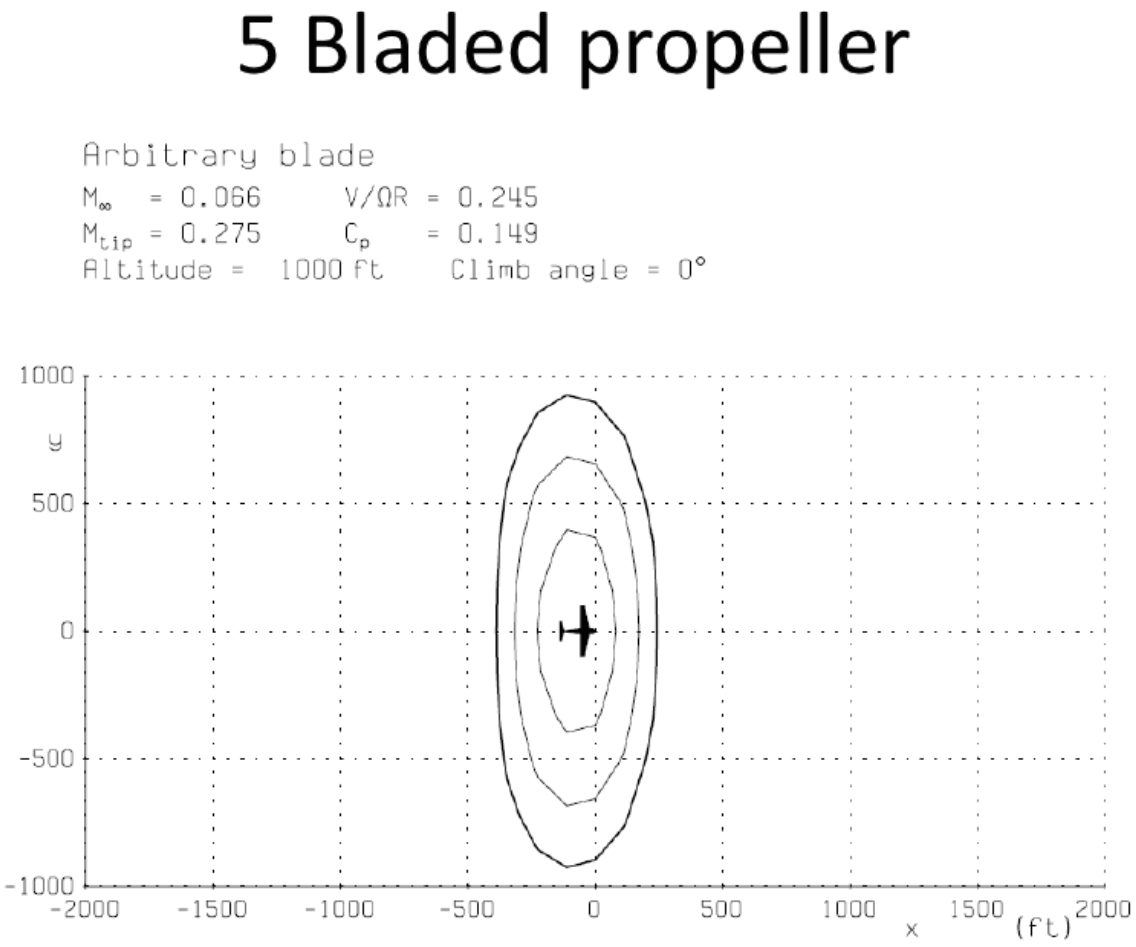

Figure 33 - Notional 5 Bladed Propeller Ground SPL Map as Produced by XRotor

Figure 33 is a plot of ground plane Isobars for Quiet IC engine optimized propeller. The 18" diameter five bladed propeller has a tip speed of Mach 0.27 and cruising altitude of 1000 feet. This data serves as a five bladed test case for comparison. Even with the same diameter, the increase in coefficient of thrust allows this 5 bladed propeller to spin slower with a lower tip Mach number to produce a significantly smaller acoustic footprint than the 3 bladed propeller.

5 Bladed Propeller

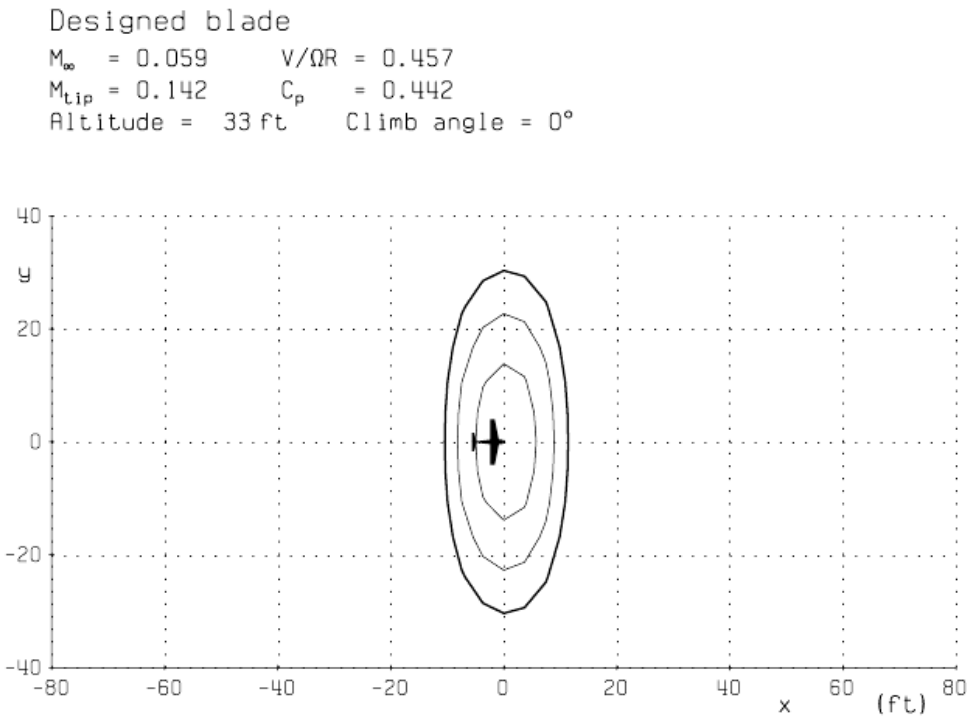

Figure 34 - Larger Diameter 5 Bladed Propeller Ground SPL Map

Figure 34 is a plot of ground plane isobars for a propeller specifically designed for a closed Rankine cycle. The 27" diameter five bladed propeller has a tip speed of Mach 0.14. The higher torque capability of the Rankine engine lowered cruise RPM from 3800 to 1200 for equal power, thrust and speed. Note that this plot is taken at **33 feet** above ground level. Xrotor would not register a ground signature when cruising at 1000 ft. As both IC and CCE propellers register 3 dB on their respective charts, the change in distance for equal SPL means the CCE propeller is theoretically **29 dB quieter** than the already quiet IC prop. The shortcomings of Xrotor are likely over predicting the advantage of this propeller, but the advantages of reducing propeller rotational speed are undisputed.

K. Energy as Function of Weight

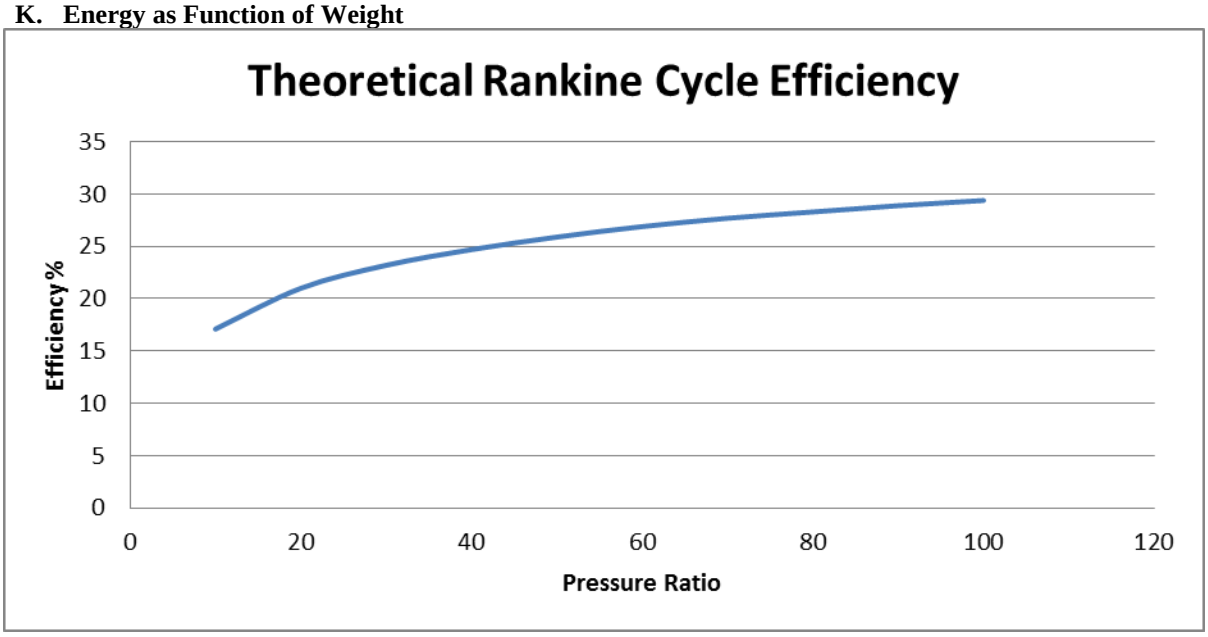

Figure 35 - Variation in Rankine Cycle Efficiency with Overall Cycle Pressure Ratio

Figure 35 represents the isentropic rankine cycle efficiency limit given water as the working fluid, 600 degree boiler exit temperature. Real implementations would see large variation from isentropic conditions, frictional losses, cylinder leakage, etc. A more detailed attempt to predict the isentropic losses will be conducted in the preliminary design phase, but if one supposes even 50% isentropic efficiency, the total cycle efficiency will still be greater than that of the two quiet two stroke engine competition. (But less than that of a properly tuned four stroke UAS propulsion system which can achieve approximately 30% thermodynamic efficiency in the best conditions)

$$WH = Total\ Propulsion\ Weight * \eta * 5680 - 13$$

Where eta will likely be between 6 and 12 percent

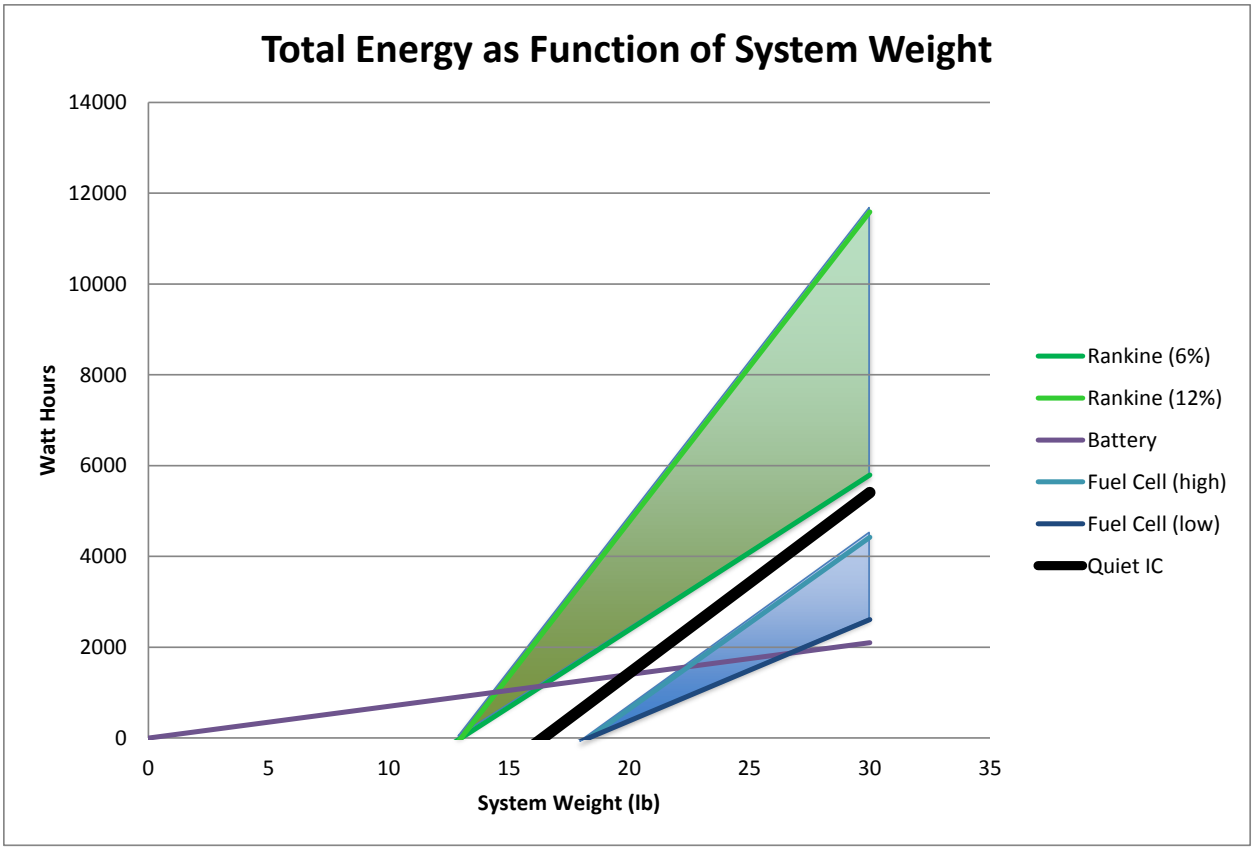

Figure 36 - Placement of Closed Rankine Cycle Systems on Chart of Specific Energy Density of UAV Propulsion Systems

Figure 36 shows that the comparable energy density per pound of fuel, and anticipated slight weight advantage make a closed rankine cycle the most energy dense quiet propulsion system. Fuel cells stacks have a low power density making the system weight necessary for 7 HP peak power, and the energy density of the fuel is low because of the pressure vessel weight. Depending on the efficiency of the end result rankine cycle, the system is at worst comparable to a quiet IC propulsion system.

Theoretical Evaluation of Closed Cycle Suitability

L. Cycle Downselect

Any closed cycle UAV propulsion system must be safe enough for practical use by operators, cheap enough to compete with off the shelf ICE engines, and reasonably standardized so that replacement parts and operating fluid is accessible for repair. These desired system qualities help establish constraints on the operating parameters of any closed cycle system. Other considerations like multi-fuel capability, large temperature differential for heat addition and rejection, and operating fluid freezing temperatures let the systems design constraints become fully bounded. The heat addition temperature is limited by typical heavy fuel flame temperatures ranging form 1200K to 1500K depending on installation and flow conditions. Heat rejection temperatures for low altitude systems are limited by the ambient temperature of air on hot days. For this purpose a 37C day (97F, 310K) was considered as the baseline for heat rejection. Most heat rejection simulations assumed a condenser temperature differential of 40C to make the OPF condensing temperature 350K. Initial operating pressures are desired to be lower than 100 psi for safe handling. Eventual iterations of the system will be designed to handle 300 psi or more to improve the power to weight ratio of the system. The cycle operating fluid assumed temperature and pressure limits are listed below.

Th=500C	Tl=350C	Ph=100	Pl=10

Table 1 - Pressure and Temperature Limits placed on ARC

1. Closed Brayton

Jet engines operate on the open Brayton cycle, but nothing is preventing that cycle from employing two heat exchangers in place of a combustor and exhaust cooler. Open Brayton cycles justifiably dominate high altitude manned aircraft flight because of their high efficiency, tolerance for low air density, and very large power to weight ratios. As these cycles are miniaturized for use in small aircraft the required RPM rises very quickly (blade speed remains relatively constant as diameter is decreased), efficiency drops due to lower compressor pressure ratios and tip leakage, and propulsive

efficiency plummets because of the mismatch between jet efflux velocity and UAV flight speed. Regardless, if this type of system was converted to closed cycle operation within the constraints for prototype CCE's given above, one could expect 19% maximum efficiency, and 224 kj/kg of OPF when run with steam as an operating fluid based on the equation in Figure 37. A closed Brayton cycle will require both a gas compressor and turbine, both of which will be significant weight and volume burdens. Additionally, multiple compressor and turbine stages will likely be required to achieve pressure ratios for respectable overall efficiency. This cycle holds potential for applications requiring high power output, but given the present temperature restrictions is severely hindered in peak thermal efficiency. Figure 37 shows an expression governing the specific power of Brayton cycle engines.

$$\frac{W}{m} = Cp \cdot T_a \cdot \left(\frac{T_c}{T_a} - 2 \cdot \sqrt{\frac{T_c}{T_a}} + 1 \right)$$

Figure 37 - Expression for Power Density of Brayton Cycle WRT Working Fluid Only

2. Rankine

The rankine cycle has seen many historical implementations, with modern variants being used as bottoming cycles for gas turbine powerplants, marine propulsion, and implement power generation. Organic rankine cycles have been a popular research subject of the past decade with many authors investigating their applicability to waste heat recovery, exhaust gas stream heat utilization, and 3rd world power generation applications. The rankine cycle's efficiency is the same as carnot efficiency, but one must be sure to apply the average heat addition and rejection temperatures to the equation instead of only the maximum and minimum reservoir temperatures seen. Depending on the level of superheat, this will lower the efficiency of steam cycles significantly. When constraining this closed cycle to the discussed

prototyping limits, the system would generate 434 kj/kg when operating with steam and exhibit an overall efficiency of 16.6%. When applying more realistic isentropic efficiencies to its components, an efficiency of 11.6% and power density of 307kj/kg can be expected. One significant complication of using a rankine cycle is the low mass flow rates required to remain efficient, yet in the proper power class for small UAV's. A system making 1.0 SHP (746W) and operating at the prototyping pressure and temperature as shown in Figure 38 limits flows only 0.0027 kg/s of operating fluid. While this does show much merit for large aircraft powerplants, making one work on a small scale will be complicated by this low flow rate. The significant advantage of using a rankine cycle is that the compressor can be entirely replaced by a small high pressure electric fluid pump. This is a large weight savings for an airborne cycle, and has the added benefit of enabling self-starting expanders as the small source of power to drive the compressor is decoupled from turbine power output. Figure 38 shows a sample diagram of the thermodynamic cycle involved with a Rankine cycle based engine.

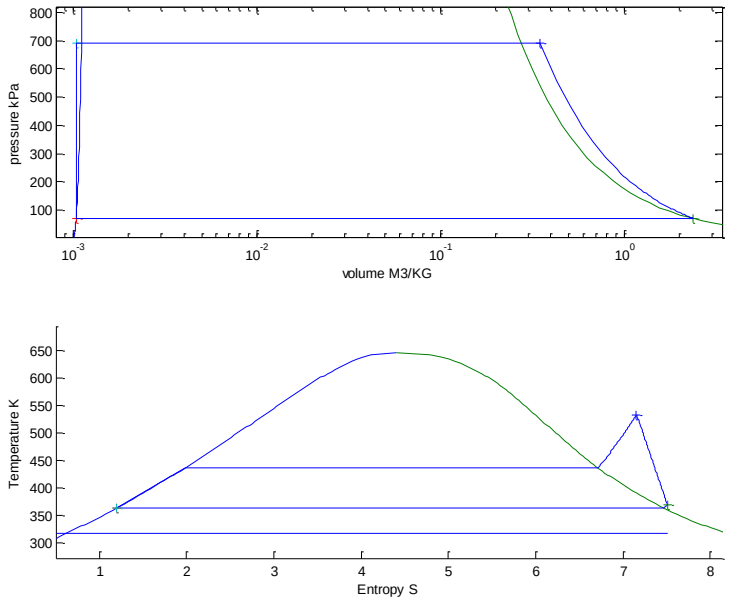

Figure 38 - PV and TS diagrams for airborne Rankine Cycle

3. Stirling

Mcconaghy's [8] flying stirling engine airplane from 1986 demonstrated that stirling engines do produce enough power to successfully fly small scale UAV's. Mcconaghy's 350gram helium stirling engine shown in Figure 39 produced 25 watts of power for 8 minutes using a small propane tank carrying 8 grams of fuel. Test flights showed the aircraft to have little excess power for maneuvering and climbing, and over the course of test flights the crankcase slowly vented the pressurized helium operating fluid causing a further reduction in power. Mcconaghy specifically mentions [8] the difficulties that arose from trying to balance the skotch yoke concentric piston design. Initial attempts to counteract piston vibration with spinning counterweights mounted 90 degrees from the piston rods resulted in large torsional vibrations that shook the engine aircraft in flight. Mcconaghy removed the counterweights entirely and the the axial vibration persist and be transmitted into the airframe. The aircraft was not as severely hampered by this lonigitudinal vibration, and performance was improved through the reduction in weight. This lesson will be carried forward into other CCE designs for small aircraft.

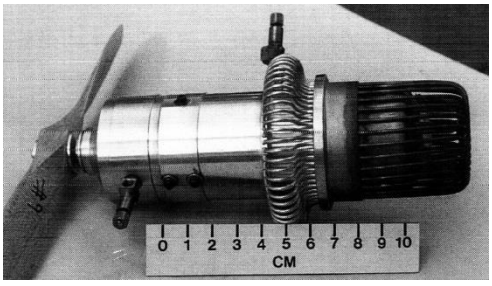

Figure 39 - Rob McConaghy's Pressurized Helium Stirling Engine [3]

When considering the stirling cycle in general terms, Haywood [9] reduces the work output of a stirling cycle to the equation shown in Figure 40.

$$W = -mR\ln\left(\frac{V_2}{V_1}\right)(T_H - T_L)$$

Figure 40 - Equation for Work Produced by Stirling Cycle

This exposes that the net work per cycle is a function of compression ratio, temperature difference, and the operating fluid quantity R*m. The quantity R*m is effected by many factors like volume of the cycle, mean operating pressure of the cycle, gas constant of the fluid used and therefore has a large effect on the overall power to weight ratio of a stirling cycle. Haywood [9] notes that the term m*R indicates one can improve the power output per gram of operating fluid by selecting an OPF with large specific gas constant. This leads one to choose Hydrogen, Helium, or other high specific gas constant operating fluids based on Figure 41.

Gas	Specific gas constant, *R* (J/kgK)
Air	319.3
Ammonia	488.2
Carbon dioxide	188.9
Helium	2077.0
Hydrogen	4124.2
Nitrogen	296.8
Propane	188.6
Steam	461.5

Figure 41 - Large Specific Gas Constants Improve the Power Density of Theoretical Stirling Cycles [9]

Stirling cycle efficiency is expressed algebraeically as equal to carnot efficiency. If heat addition and expansion/compression are truly isothermal and isochoric respectively then the cycle will follow carnot efficiency by definition. In the case of a cycle limited by the desired airborne CCE prototyping pressure and temperature limits listed above, one could expect an optimal efficiency of 26 percent, and power output of 144 kJ/kg of operating fluid. It is worth noting that these calculations do not include the weight of the cycle enclosure, which substantially lowers the power to weight ratio of a stirling cycle as a result of high pressure, difficult seals, and sizeable thermal regenerators.

M. Sensitivity of cycle efficiency to component performance

Understanding the relative importance of component performance in a rankine cycle is important to proper distribution of development time, budget, and weight to these components. A Study was conducted on the baseline component efficiencies as listed in the table below. Each component was then improved by 10% efficiency with the effect on total cycle efficiency noted. The most important concern in capturing as much heat from combustion and regeneration as possible in the boiler, secondly one should make sure this energy is utilized as fully as possible with an efficient expander. Pump power levels are so small to begin with that even a 50% efficient pump hardly has an effect on overall cycle performance. Expansion ratio is primarily influencing overall efficiency from the temperature drop resulting from expansion and the changes that causes to Carnot efficiency. These sensitivities are shown in Figure 42 below.

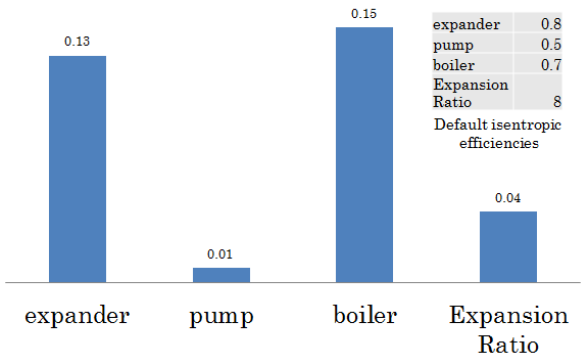

Figure 42 - Influence of Component Isentropic Efficiency on Overall Cycle Efficiency

Robert Mcconaghy's Stirling engine

Figure 43 - Robert Mcconaghy's Son Holding His 1Kg Flying Stirling Engine Airplane [10]

Very few examples of closed cycle engines small and light enough to possibly power small aircraft have been developed with only one found to have been attached to a small glider and flown. Robert Mcconaghy presented at least three papers during the 1986 through 1988 IECEC conferences detailing first the development of his engine design, improvements made to that engine during the following year, and finally an account of short flight tests conducted using his improved power plant. The creation of these engines has gone largely unnoticed, but without other flying examples found predating mcconaghy's, his flights might prove to be the first under power from a closed cycle engine. There is certainly evidence and even video of the Bessler steam airplane, but during flight their steam engine did not condense all of its operating fluid and therefore cannot be considered truly closed cycle. Mcconaghy's development up to his flight of a closed cycle stirling engine using the airplane in Figure

43 is discussed here in overly specific detail as it is the best located example of flying closed cycle propulsion.

N. Design of a stirling engine for model aircraft propulsion

Mcconaghy designed his engine for use on a small aircraft from the beginning, acknowledging the need for high power to weight ratio and a streamlined shape, motivated by low noise and clean exhaust, but foregoing at least for the time the need for long endurance. The initial target power to weight ratio of his engine was 300 to 400 W/kg, which was admittedly much lower than the 6KW/kg power density two stroke RC race engine's were reaching in the same time period. Different physical implementations of the stirling cycle like ringbom, alpha, and beta type engine designs were discussed. Mcconaghy favored fully kinematic engine designs to eliminate the tuning and frequency dependence of free displacers. Mcconaghy included tubular heat exchangers and cylindrical corrugated regenerators in each of his designs based off his previous work designing and fabricating ground based stirling engines. Most components were nickel brazed together which transitions phases between 1790F and 1900F. Most rankine, stirling, and other small scale engines studied made great use of brazing for attachment of parts and reduction of weight. Whether silver solder, copper brazing, or nickel as in the case of Mcconaghy, the technique is quite widespread.

Mcconaghy decided to manufacture a beta type stirling engine with scotch yoke drive, 90 degree offset counterweights (which would eventually prove futile), and in line cylinder and displacer to maximize the use of the available engine envelope on a small aircraft. Additionally, the overall design of the beta type engine simplified heat exchanger design which Mcconaghy viewed as an essential path to creating a sufficiently light engine. Another key to his lightweight and slim engine design was the

incorporation of scotch yoke, 2:1 step up gearbox, and counterweight design all in one mechanism to convert linear piston power into higher frequency rotational motion while also cancelling the axial vibration of the displacer proved quite effective. The counterweights attached to each bevel gear did create a torsional vibration as they spun in opposite directions to avoid exciting an off axis vibration much like the counterweight of a one cylinder engine. Mcconaghy theorized that this torsional vibration of the counterweights would be at least in part offset by the reaction torque of power being applied to the propeller. In practice it was found that the torsional vibration was not sufficiently eliminated and proved problematic for flight. It was better in the end to allow axial vibrations resulting from displacement piston translation to be reacted full force by the airframe.

This first Beta engine was designed to have a buffer space surrounding the crankcase to allow pressurization of the cycle above atmospheric pressure, but the buffer volume proved insufficient as the compression occurring inside prevented the cycle from starting. Mcconaghy decided to vent the volume to the atmosphere to allow the engine to run, but at a reduced output power.

All of Mcconaghy's dynamometer tests were conducted by running a series of propellers on an electric motor, recording the motor reaction torque vs RPM, and then using this data to measure power created by the engine turning the same propeller. This method was used to eliminate the difficulty of measuring power resulting from the lack of flywheel mass on the engine, and the large cyclic variation of torque that results. Mcconaghy notes that the engine was not capable of high speed operation and used this datapoint as an indication of high internal fluid and mechanical friction. The engine never ran above 25 Hz. (1500 RPM).

This first publication concludes in saying the engine design was promising with particular praise of the scotch yoke for durability and efficiency. Many areas for improvement on subsequent engines

were noted such as mechanical friction, weight of heat exchanger, overall compression ratio and mostly improvement of the overall power to weight ratio. The first prototype engine was nowhere close to the 300-400 W/kg target to fly the electric powered model aircraft he was designing it for. Mcconaghy needed a 3 to 4 fold increase in power to reach suitable levels for flight.

O. An Improved Stirling Engine for Model Aircraft Propulsion

Mcconaghy returned the following year with improvements to the same Beta style engine having halved its weight while nearly doubling the power output. The engine in 1987 still used air as the operating fluid at no more than 3 atmospheres of pressure. While the overall engine arrangement was not changed, Mcconaghy rearranged the heat exchangers and based them off small tubes instead of the corrugated layers of aluminum foil. 60 small aluminum tubes were bonded into the crankcase with high temperature cyanoacrylate (superglue) as temperatures in that location rarely exceeded 90C. The placement of these cooling tubes was further enhanced by the propeller slipstream flowing right over their surface. Thirty Inconel heating tubes were used on the hot side. The tubes, hot cylinder and regenerator were all vacuum brazed together to withstand the direct flame impingement. While the engine was operating, the top of the cylinder was protected from the highest flame temperatures with the intention that the Inconel tubes conduct most of the heat transfer into the cycle. Ball bearings were incorporated on all rotating shafts, the bevel gears we machined from unfilled delrin, and the piston seals were modified to require no preloading and therefore reduce drag on the cylinder walls.

Mcconaghy's 1987 engine was able to run for periods of up to 30 minutes while producing 15 watts at 2 Atmospheres of crankcase pressurization. Attempts to run the engine at higher mean crankcase pressures ended up reducing power output, an effect that was traced back to output shaft seal leakage

caused from corrosion. All power tests of the 1986 and 1987 engines ended up being suspect as the propeller calibration curves used to measure output were found to be up to 48% in error.

Overall, an additional year of development reduced engine weight to 360 grams from 725g While power rose from an estimated 7W to 20W bringing the overall power to weight ratio up to 55W/kg. Additional modifications were targeted to improve power output to a theorized 30W minimum required power for flight.

P. Flight Tests of a Stirling Powered Model Aircraft

Mcconaghy used his 1987 engine to achieve marginal flight with a 1.8 meter standard model aircraft glider for a few flights, the longest of which was around 8 minutes of gentle orbiting. After calculating required aircraft power for level flight and for gentle climbs using some fairly non-standard RC equations, Mcconaghy decided that since his engines were not delivering the required power to weight ratio for normal RC flight, he would bring the required power for flight down to meet the power available from his engines. By using a 1.8 meter astroflight glider, and removing the nose of the fuselage to allow his cylindrical engine to be mounted he was able to reach a gross takeoff weight of less than 1 kg which he supposed should take 14.2 Watts of power to fly. Landing gear were removed from the airplane to reduce drag and weight, so a hand launch and recovery in tall grass was required. All of his test flights were conducted without engine speed control.

The engine that flew the glider continually leaked through the problematic output shaft seal during flight. Mcconaghy records that he was able to pressurize the engine case to two atmospheres before launch which helped with power required for climbout and initial flight, but that pressure eventually leaked out and overall power was reduced.

Another flight record of note is that the torsional vibration of the counterbalancing weights proved impractical. The airframe was quite sensitive to this torsional imbalance, so the counterweights were removed altogether to save weight, and transform the principle vibration back to a mainly longitudinal direction that the airframe reacted better to.

Without the ability to maintain elevated crankcase pressure due to shaft seal leakage, the engine power faded during each attempt causing the aircraft to enter a powered descent mode as it did not have power to maintain steady level flight. Mcconaghy concludes his paper with reccomendations for power some 3 to 10 times what was available with his engine for proper flight of the generic 1.8m RC glider.

Q. Conclusions on Mcconaghy Flights:

Robert Mcconaghy's Stirling engine appears to be a superb mechanical and thermodynamic example of an aircraft stirling engine. Aside from being the only stirling engine found to have flown an aircraft, it seems the correct design decisions were made, weight minimized, propeller size optimized, thermodynamics well understood, and yet even in this very well educated and masterfully constructed attempt the stirling cycle failed to provide sufficient power. This anemic result is commonplace in other vehicles and machinery designed to make use of the highly efficient stirling cycle and one of the reasons that this PhD work on closed cycle engines began focused on Rankine cycles. There are many useful construction and part sourcing guides to be gained from Mcconaghy's work. From the small diameter Inconel tubing, to nickel brazing alloy, the author of this modern study of closed cycle aircraft engines could have avoided considerable headache had these solutions been found earlier. Additionally the practical information regarding preferred aircraft vibration modes will be most beneficial when making design compromises in a modern quiet CCE. Mcconaghy's work shown in Figure 44 is very valuable in

directing design of closed cycle engines for flight, but perhaps began with the incorrect cycle for use in small aircraft.

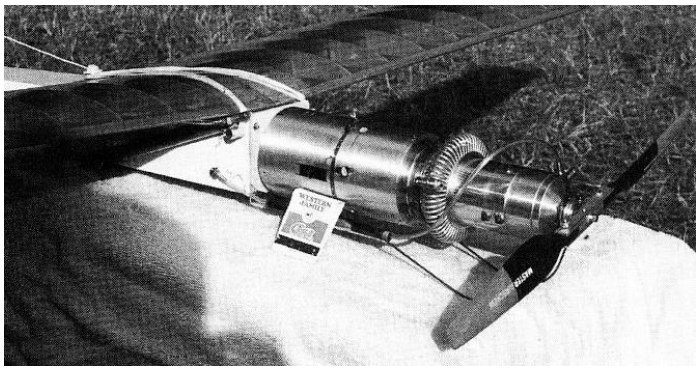

Figure 44 - Robert Mcconaghy's Stirling Powered Model Aircraft [3]

R.Conclusions

After investigating methods of controlling exhaust noise emission, eliminating the intake and exhaust noise entirely was favored over trying to muffle or redirect the emission. Directing the lower frequency content of engine exhaust tones requires too large of a device to fit onto small UAS aircraft given the assumptions of this study. Of the closed cycle systems available, a Rankine cycle is selected as the first prototyping target due to the presence of some historic precedent and organic power generation systems to use as a comparison. Other background research found a single closed cycle aircraft flight by Robert Mcconaghy in 1987 using a small 20W stirling engine. This short 6 minute hand launched flight with a closed cycle engine was the only example found of a closed system being used on a small UAV. The prototype system will start as a Rankine cycle and then depart as required from there.

CHAPTER II

System Simulation Model

Matlab Model of Closed Cycle Systems

Forming a model of the closed thermal system accurate to a design level of accuracy is essential for proper selection of operating temperatures and pressures. While it is simple to predict, and easy to show that increased temperature ratio improves performance, higher temperatures increase material requirements, cost, and as a result effects the ability to successfully develop a prototype system. For testing an evaluation, pressure and temperature were artificially limited to 7 bar (101psi) and 500K (440F) for safety. Even a 100 psi unplanned vent at that temperature is extremely hazardous, but performance of rankine cycles at lower pressure ratios quicly becomes unacceptable, so some risk was necessary to raise efficiency to a point suitable enough for fair evaluation.

While many cycles like otto, diesel, and Brayton are often approximated by using cold gas assumptions, or even some basic variable Cp models, it was known from the beginning that this CCE study would require detailed information on fluids during phase change and supercritical regions. These areas are the most poorly approximated by ideal gas, cold gas, and variable CP models, so a fluids database was sought to make parameter determination easier.

The open source coolprop library was used to provide detailed models of not only water and air, but refrigerants, mixtures of common fluids, and other common gasses. With over 100 fluid options for free, and easy to reference matlab functions, the database was an easy choice to properly study the tradespace of closed cycle airplane engine design. These codes allow for full determination of fluid properties in liquid, transition, gaseous, and supercritical phases. Each type of common thermodynamic chart (and other not so common charts) can be reproduced for any fluid in the coolprop database. Each fluid also has built in domain boundaries so the software does not accidentally deliver poorly fit data from a region that is not validated.

S. Rankine Cycle Model

A rankine cycle model was initially developed to model the selected closed cycle engine prototype cycle. The code allows one to model component inefficiencies through an isentropic efficiency for each stage and component. The code is easily modifiable to account for different expander characteristics such as isothermal, adiabatic, polytropic, isentropic, etc. which makes consideration of these variations in expansion mechanisms possible. Overall the ability to quickly map the performance of a cycle based on corner parameters, the temperature and pressures that create the most stress and cost for the physical prototype, is the primary value of the code. Tradeoffs between operating fluid, maximum pressure, maximum temperature, as well as ambient pressures and temperatures can be included. At varying stages of development the code has incorporated RPM prediction for piston expanders, number of stage estimation for tuboexpanders, and estimates of mass flow rate per HP. Efficiency studies of Rankine cycles properly followed the classical understanding that efficiency improves with both temperature and pressure ratios, with pressure being favored in the domain of small scale systems considered as shown in Figure 45.

Regeneration / feedwater heating was considered for Rankine based cycles, but was found to not be able to drastically increase system efficiency, nor did it effectively modify any underlying physics of the system efficiency profile. Regeneration in Rankine cycles is undermined by most of the heat energy

addition happening at a relatively high constant temperature. If the Rankine cycle is significantly superheated, then all portions of gas after expansion that are still above the temperature of transition in the two phase region can indeed be recycled into the cycle again. Unfortunately this range of enthalpy drop is a small percentage of the total heat flux in and out of the closed cycle, so even in the best 100% efficient case makes very little difference. For large industrial systems, the complexity, weight, and size is worth the additional few percentage points of efficiency, however for small airborne cycles where weight and size are important, the small increase in efficiency is not justified. To quantify these efficiency changes and potential for regeneration P-h charts were used to compare regions of favorable temperature gradient for regeneration for Brayton and Rankine cycles.

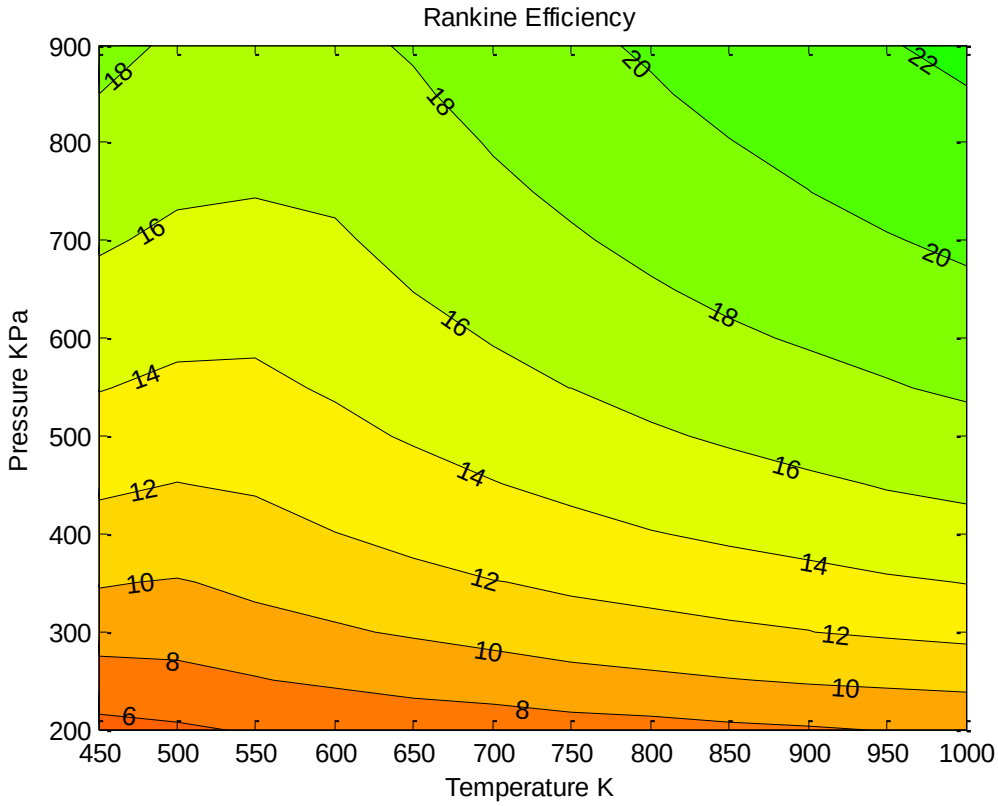

Figure 45 - Variation in Cycle Efficiency with Maximum Pressure and Temperature

T. Brayton Cycle Model

Later during the project, after background research revealed that a regenerator drastically changes the efficiency equations for Brayton cycles, a similar design space study code was developed using cool prop to analyze the efficiency tradeoffs between Rankine, Brayton, and regenerative Brayton cycles. Initially the Brayton cycle was discounted due to its traditional reliance on turbomachinery and the noise that accompanies it, but after more careful consideration and realization that expansion is equivalent regardless of mechanism, the Brayton cycle is very likely a superior option for small scale power production. Just like the Rankine cycle, the Brayton model allows for each component to be modelled through an individually adjustable isentropic efficiency. The cycle also calculates the potential benefit of regeneration and allows one to consider the effects of incomplete heat exchange. Overall the tradeoff between regeneration and natural Brayton cycles was found to have a profound effect on system composition and pressure ratio selection, but in most scenarios the overall system efficiency is extremely sensitive to regenerator performance, which diminishes the real world suitability of such a system. The Brayton cycle study concurred with more simplistic cold gas cycle trends. Classical Brayton cycle efficiency improves rapidly with increasing pressure ratio, thus the reason for modern jet turbine engines have multiple compressor and turbine stages. Regenerative Brayton cycles, at least for cases where regeneration is highly efficient, show that efficiency is both a function of pressure and temperature ratio. Efficiency for regenerative closed Brayton cycles decreases as pressure ratio is increased, but increases with temperature ratio. This is a perfect accommodation of the mechanical constraints placed on a small scale flying closed cycle engine. Small pressure ratios allow a designer to use a single turboexpander stage. Multiple expansion stages are required in high pressure ratio environments due to the constraint of the gas staying subsonic. Small pressure ratios automatically let the operating fluid remain subsonic in the turboexpander. High temperature ratios can become expensive as material and fabrication requirements increase, but even at small temperature ratios, the efficiency of closed Brayton cycles is still very respectable as indicated by Figure 46 and Figure 47.

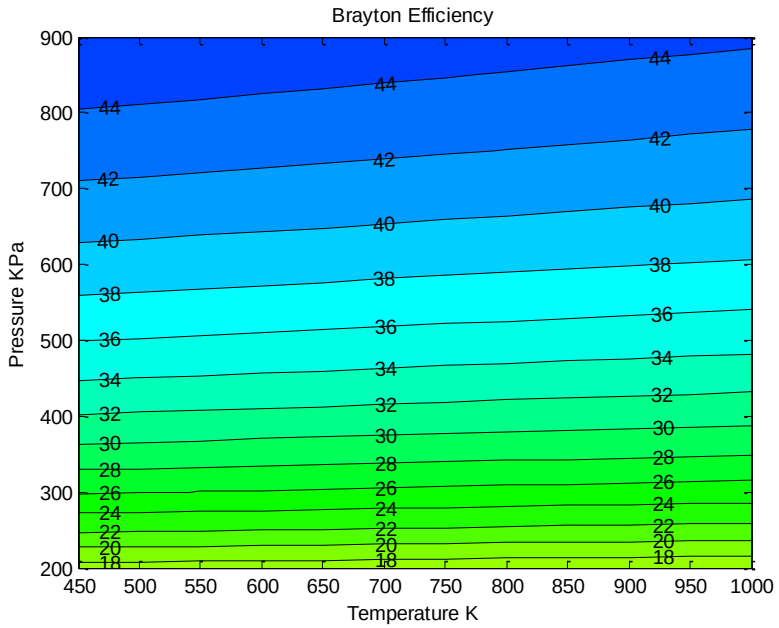

Figure 46 - Closed Brayton Cycle Variation in Efficiency with Maximum Pressure and Temperature

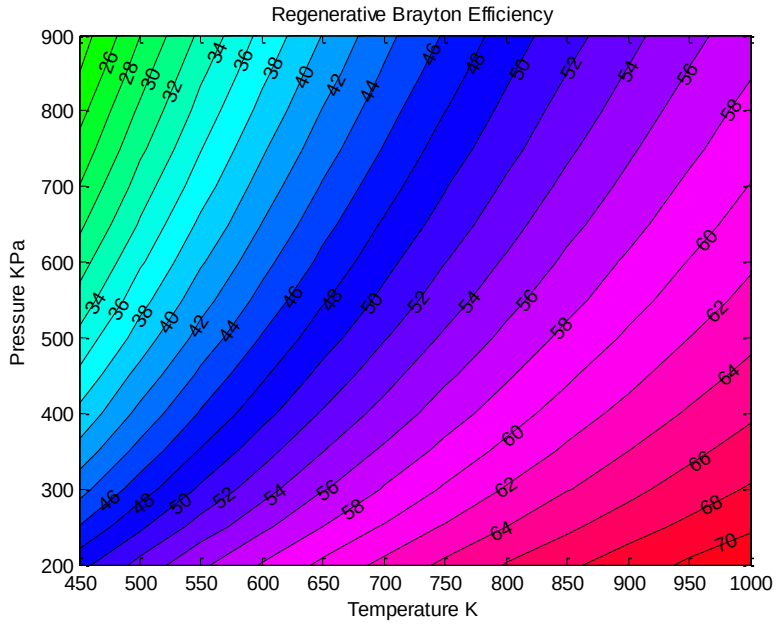

Figure 47 - Regenerative Closed Brayton Cycle Efficiency Variation with Maximum Temperature and Pressure.

Comparison of Cycle efficiency

The best reason to model rankine, Brayton, and regenerative Brayton cycles in matlab using coolprop was to create a simultaneous comparison of possible efficiency and power between each system

type. For a range covering 200 to 900 KPa and 400 to 1000 degree Kelvin with lower pressures remaining atmospheric (but still sealed to the environment) and discharging to a 310 degree kelvin thermal well, the tradeoff between cycles is shown below in Figure 48.

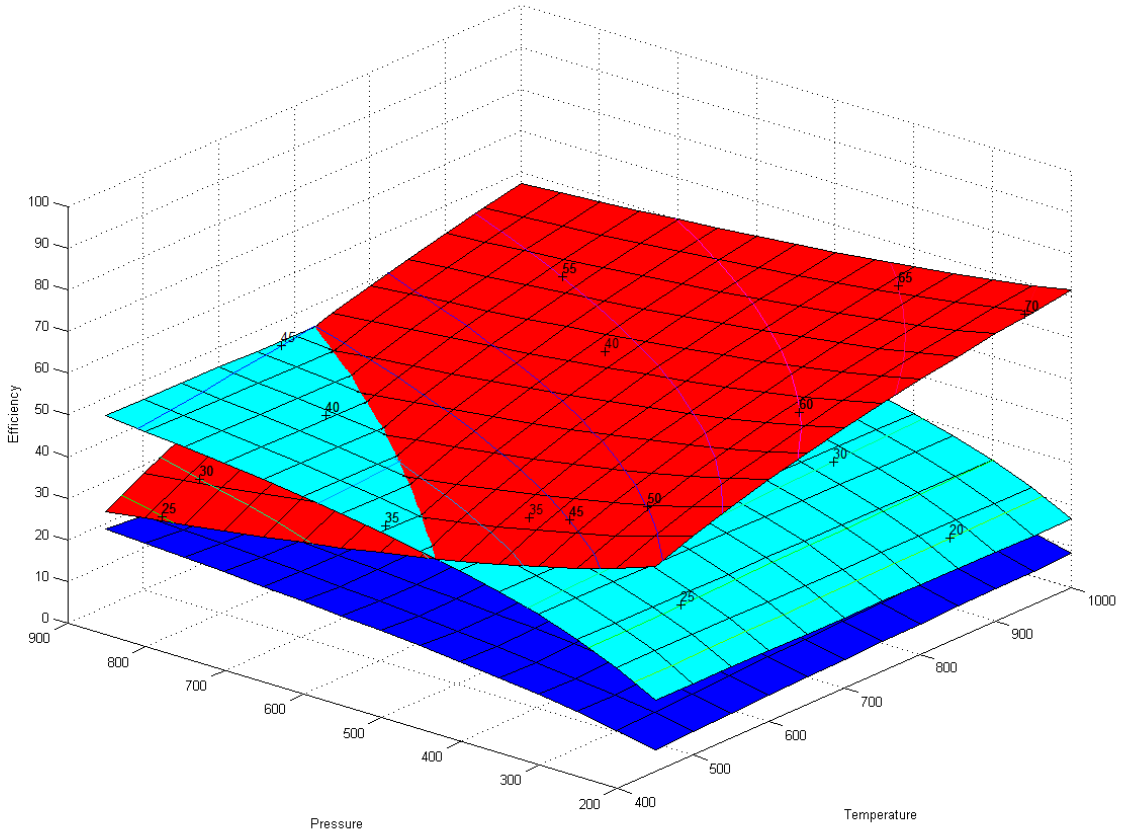

Figure 48 - Regenerative Brayton cycle (red), standard CBC (cyan), Rankine cycle (blue). All closed with perfect component efficiency. 101KPA low pressure. 310K low temp

The obvious, and easy selection is the regenerative Brayton cycle. However, this analysis like the example shown in Figure 49 is conducted for perfectly efficient components. Later charts display the tradeoff's associated with component efficiency. In the system shown, the rankine cycle (blue) is running with water as its operating fluid, while both brayton cycles are using standard air. This plentiful operating fluid is a big benefit as the system could simply pump additional operating fluid into the cycle when

necessary to make up for leaks, or to modify the average pressure (and thus the net power generated). Improved efficiency at low maximum pressures allows the system to use a single stage turboexpander and remain subsonic as the pressure ratio to hit sonic speeds is P/Pt=0.5263. This low ratio does decrease power production, but at the small scale for UAS it is beneficial that the turboexpander can be larger than others considered. Turbomachinery is so power dense that the decrease in specific power is easily accommodated, especially when compared to fuel cells and batteries. While commercial turbofans are made of the highest temperature and strength materials, to maximize the temperature ratio of their open Brayton cycles, cheaper, more common materials like aluminum could meet design requirements for closed regenerative Brayton cycles as overall cycle efficiency (with perfect components) exceeds 55% at 600 degrees Celsius, while aluminum melts at 660C which gives some small margin of safety. Even simple three axis CNC machines could mill turbine blisks capable of withstanding the forces and temperatures called for in a regenerative closed Brayton cycle. This chart shows that in almost every consideration, a Brayton cycle would have been a better choice than the prototype Rankine cycle. Rankine cycles are more dangerous as one not only has to consider the expanding hot gasses under pressure, but also the massive volume of expansion that can take place in boiler explosions. Where a 20 to 30 psi Brayton cycle might expand hot gasses to 2x their contained volume, a venting rankine cycle can expand up to 1600x as liquids stored inside the boiler flash to gas as the vessel loses containment. This safety difference should not be forgotten or considered lightly.

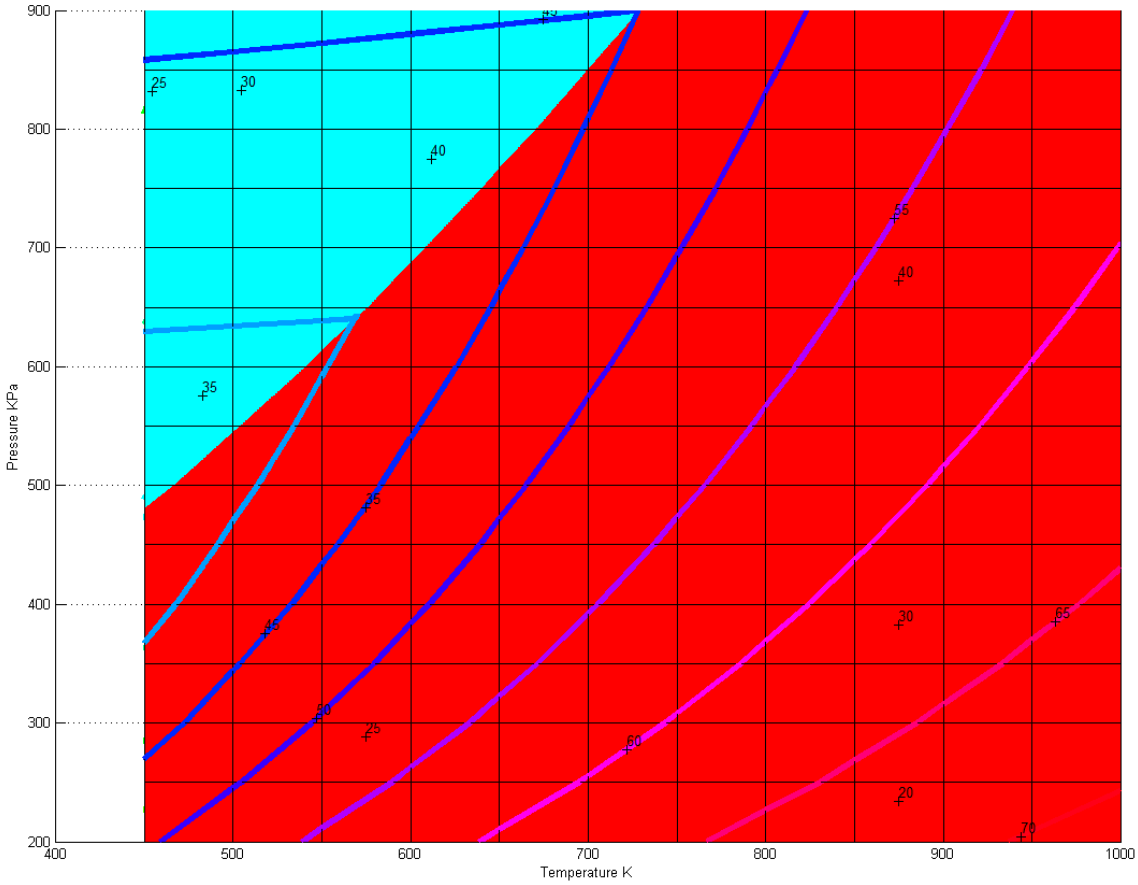

Figure 49 - Contour plot showing optimal efficiency regions for regenerative Brayton cycles and non-regenerative Brayton cycles.

Non-Ideal Component Efficiency

U. 90% of Isentropic

When one takes into account non-ideal component performance of expanders, compressors, and heat exchangers, the overall shape of cycle efficiency plots begins to vary, with effects on which cycle is optimal at different temperature and pressure locations. The one gradient that remains mostly invariant with cycle selection and degradation of component performance, is that on average, cycles become more efficient with increases in maximum temperature, and therefore also temperature ratio, because of the bounding limitation of Carnot. When expander and compressor performance is reduced to 90 percent of isentropic as shown in Figure 50 through Figure 53, the following cycle efficiencies as a function of

maximum temperature and pressure can be expected. Note that these calculations are still conducted with perfect regeneration for the RCBC. It is interesting to note that even with this slight (and still optimistic) reduction in efficiency, the Rankine cycle becomes the most efficient choice for the first time in any part of the domain.

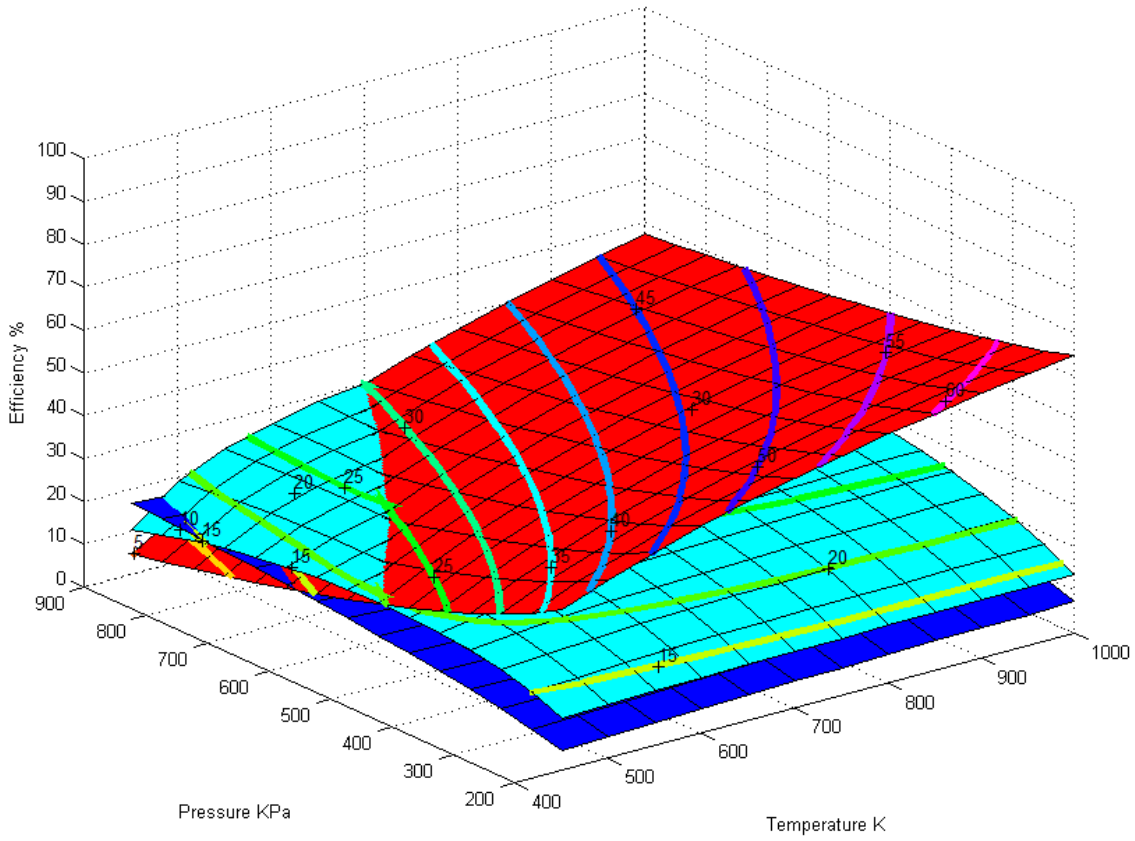

Figure 50 - Regenerative Brayton cycle (red), standard CBC (cyan), Rankine cycle (blue). All closed with 90% component efficiency. 101KPA low pressure. 310K low temp

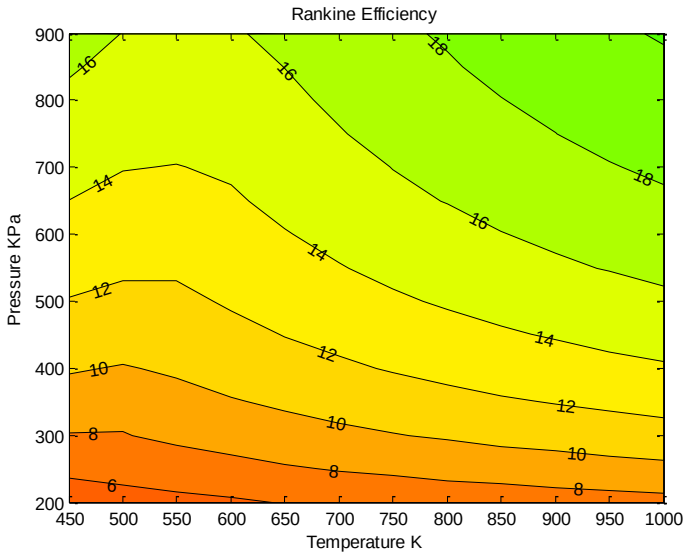

Figure 51 - Rankine Cycle Efficiency with 90% Component Efficiency

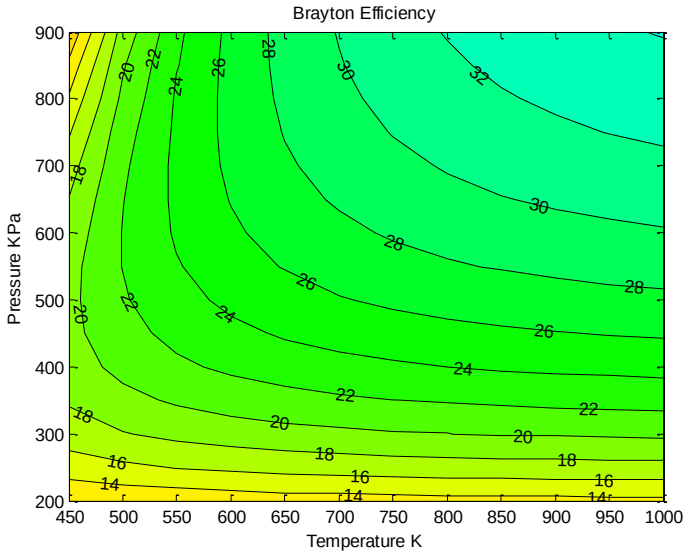

Figure 52 - Brayton Cycle Efficiency with 90% Efficient Components

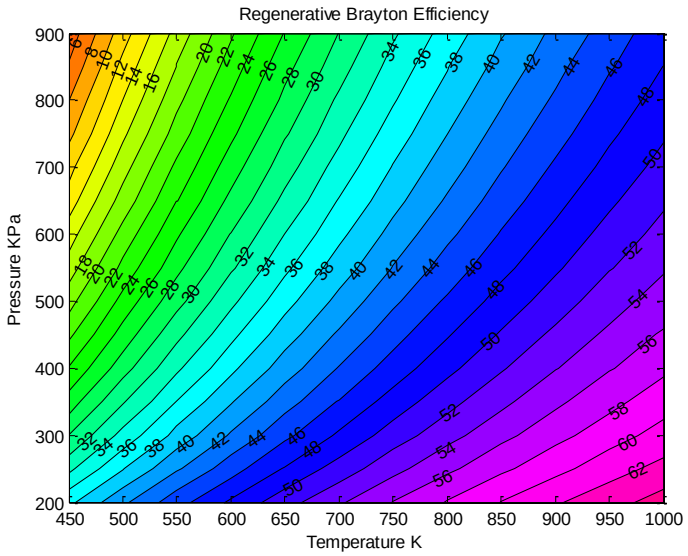

Figure 53 - Regenerative Brayton Cycle Efficiency with 90% Efficient Components

As expander and compressor performance are reduced even further to 80 percent of perfect isentropic performance, the Brayton cycles begin to suffer tremendously. This sensitivity to compressor and expander performance may explain the absence of practical Brayton cycles from KW scale power generation. When all three cycles under consideration are superimposed, the non-recuperated Brayton cycle is no longer the best choice at any maximum pressure or temperature. The Rankine cycle, though exhibiting low efficiency, remains less sensitive to component performance as a result of the very low back work ratio condensing cycles can achieve. In these charts it is important to note that regenerator efficiency is still at 100% for the RCBC.

V. 80% of Isentropic

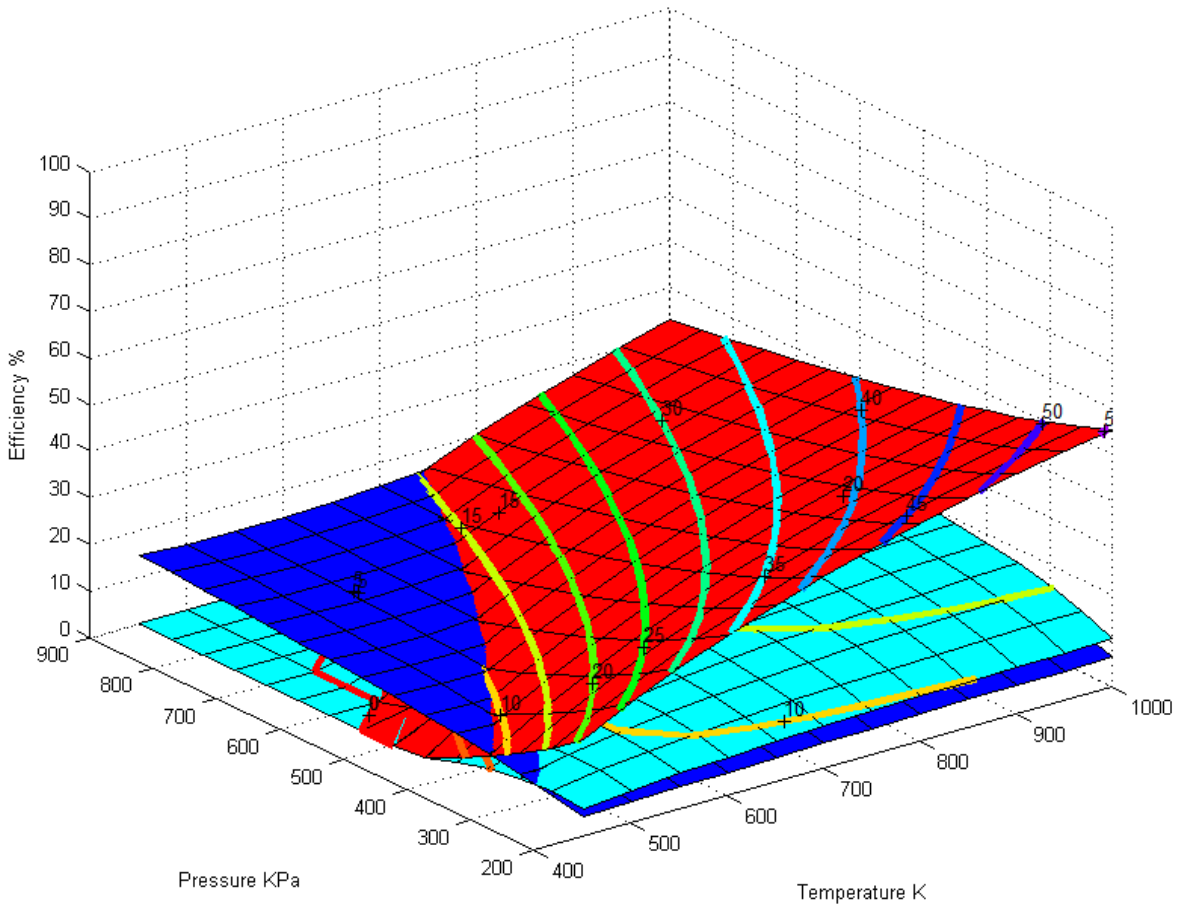

Figure 54 - Regenerative Brayton cycle (red), standard CBC (cyan), Rankine cycle (blue). All closed with 80% component efficiency. 101KPA low pressure. 310K low temp

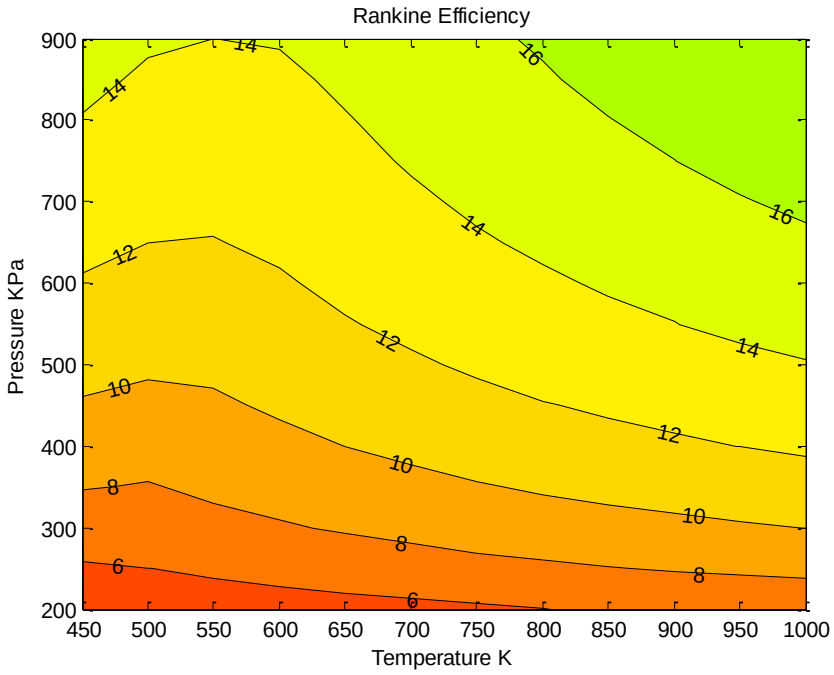

Figure 55 - Rankine Cycle Efficiency with 80% Efficient Components

While the maximum achievable Rankine cycle efficiency has decreased, the form of the plot, and minimum performance has not reached critical levels. Brayton cycle systems have began to exhibit large regions of zero efficiency as shown in Figure 56 and Figure 57. Regions where the cycle cannot produce positive power (even before considering mechanical losses and other sources of imperfection) exist.

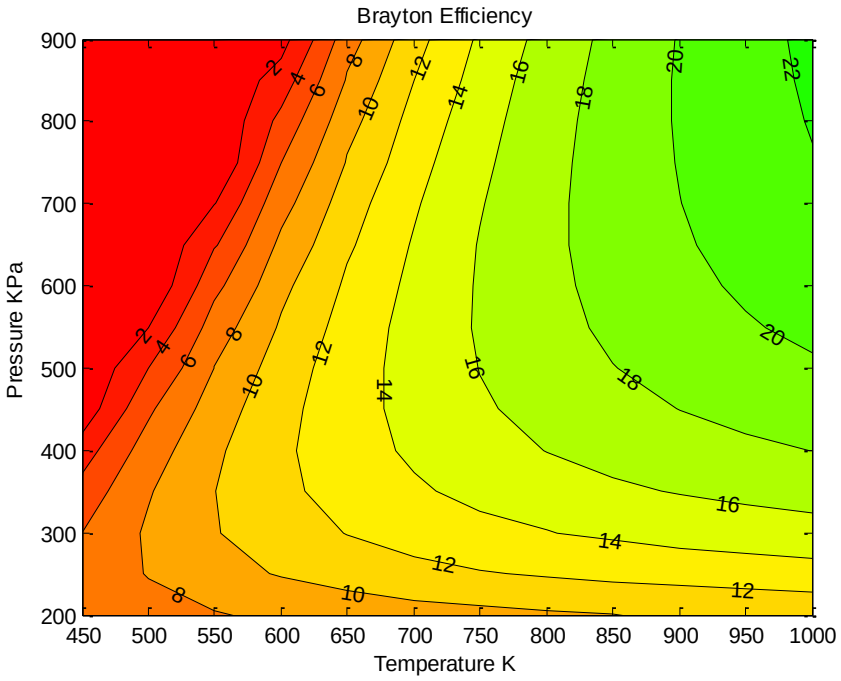

Figure 56 - Brayton Cycle Efficiency with 80% Efficient Components

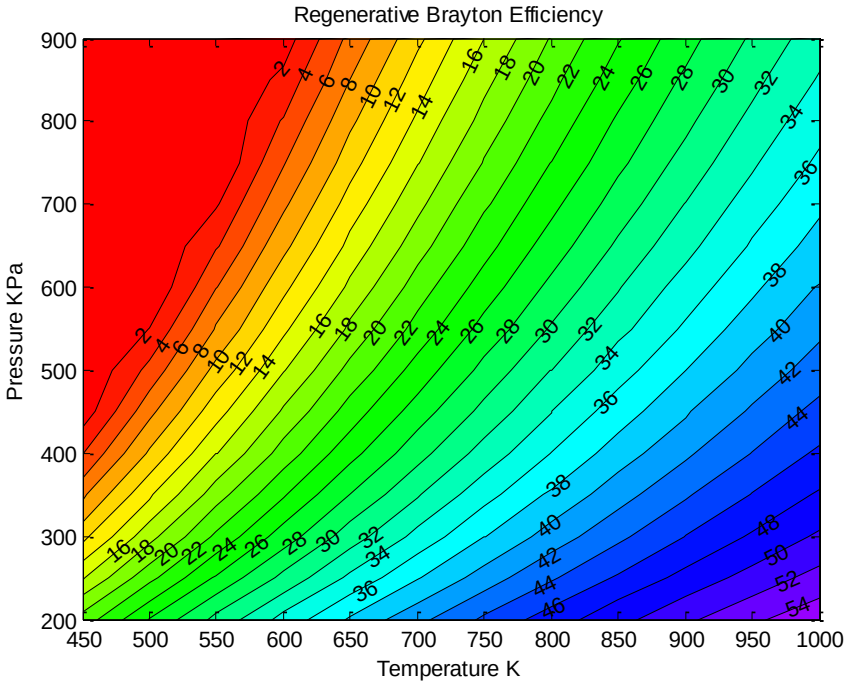

Figure 57 - Regenerative Brayton Cycle Efficiency with 80% Efficient Components.

W. 70% of Isentropic

As component efficiency reaches 70 percent in Figure 58, the cycles are beginning to represent systems that could exist in the real world. Several publications have measured small scale turboexpander, scroll piston performance between 70 and 80 percent isentropic efficiency. The one critical component that has remained untouched during this excursion is the 100% efficient regenerator which is keeping the RCBC performance artificially high at higher temperature ratios in Figure 59 through Figure 61. Though this presently misrepresents reality, changing only one parameter at a time is important for preserving clarity.

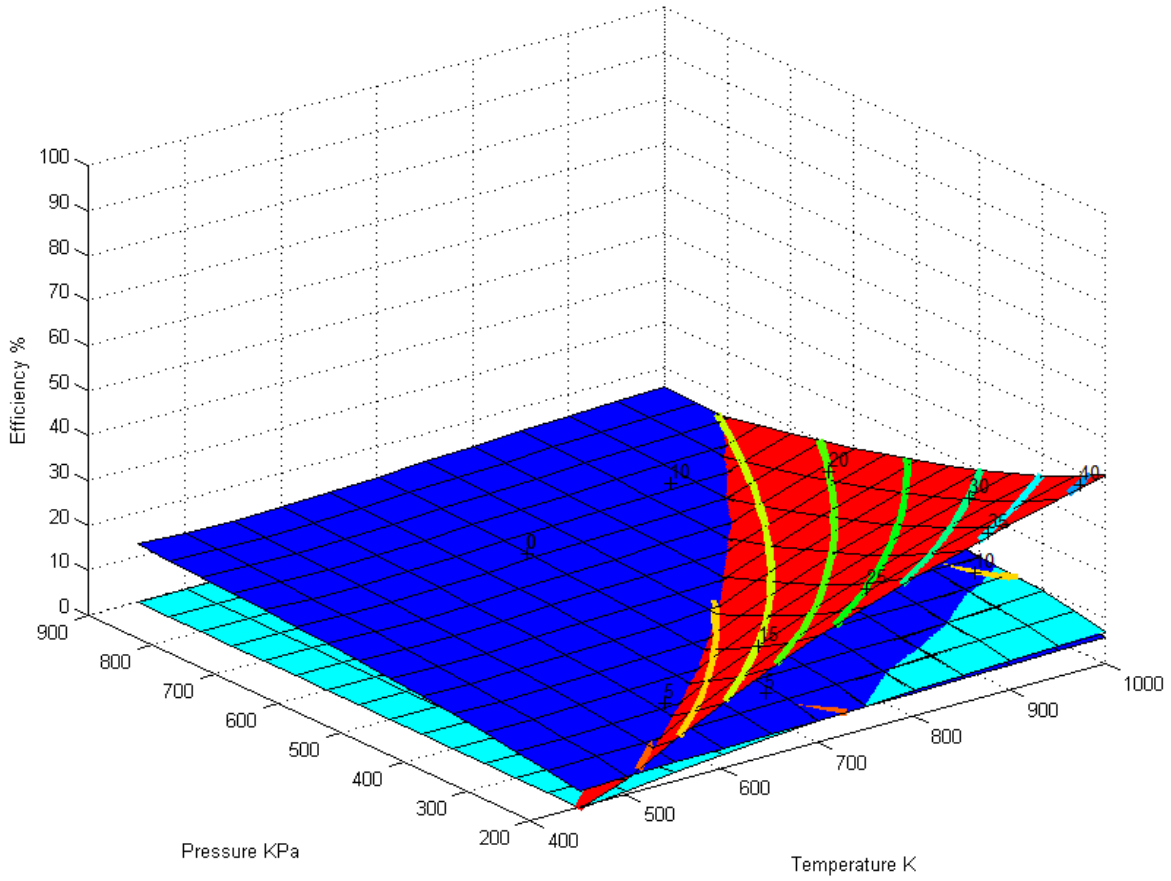

Figure 58 - Regenerative Brayton cycle (red), standard CBC (cyan), Rankine cycle (blue). All closed with 70% component efficiency. 101KPA low pressure. 310K low temp

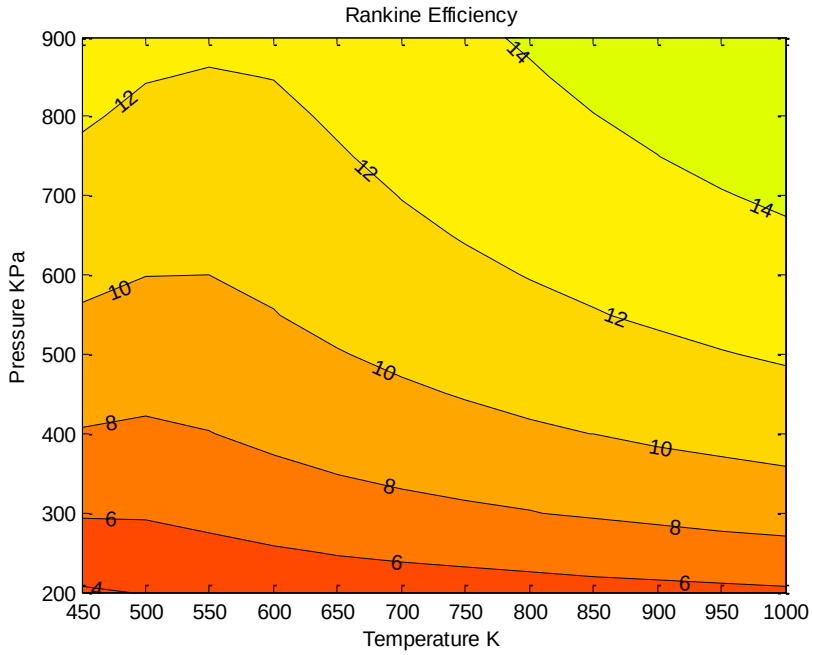

Figure 59 - Rankine Cycle Efficiency with 70% Efficient Components

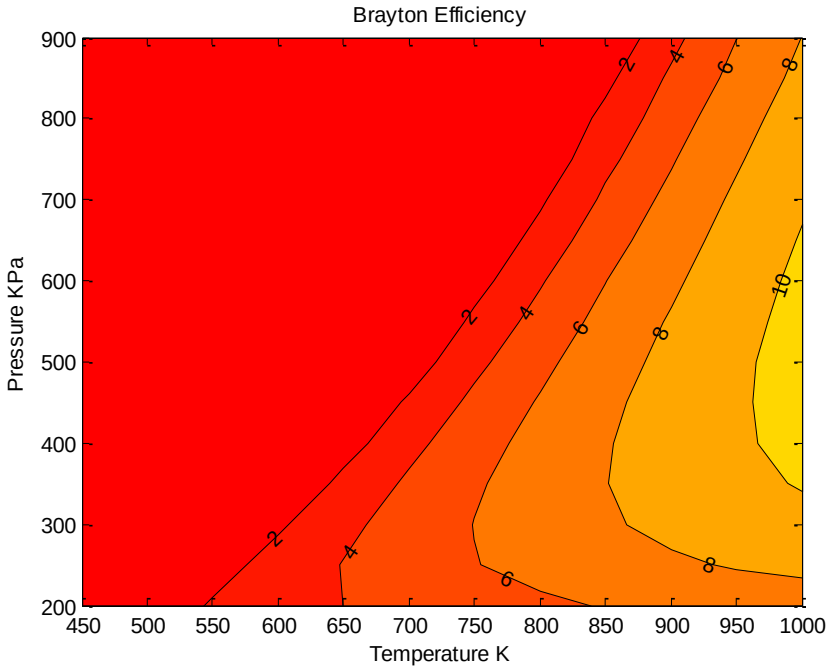

Figure 60 - Brayton Cycle Efficiency with 70% Efficient Components.

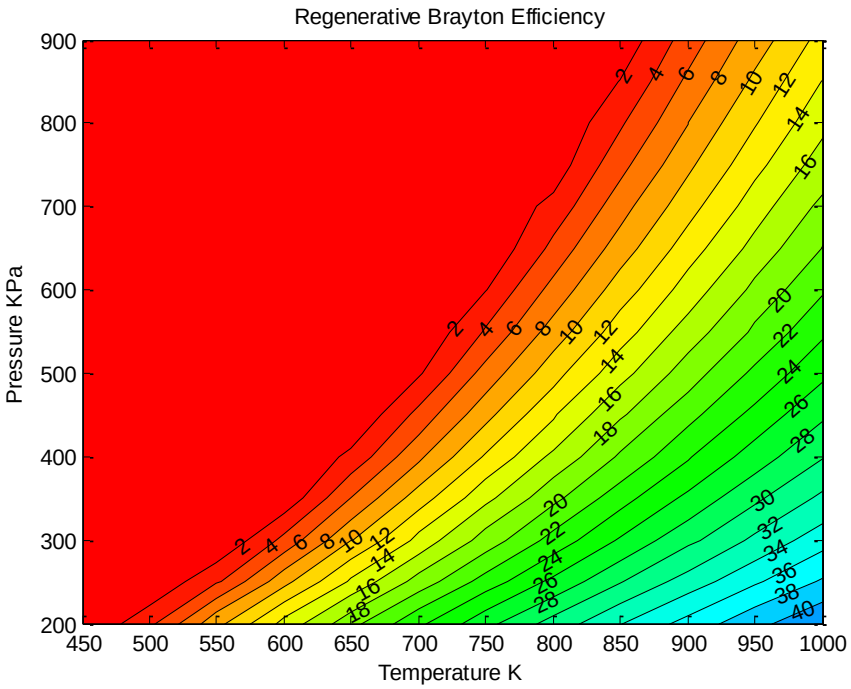

Figure 61 - Regenerative Brayton Cycle Efficiency with 70% Efficient Components

X.70% of Isentropic with Non-Ideal Regenerator

Lastly, regenerator performance was reduced to 90% of maximum heat exchange in Figure 62, while maintaining compressor and expander isentropic efficiency at 70%. These numbers should adequately represent small scale component performance. The superposition of efficiency plots reveals a regenerative Brayton cycle to reach 25% efficiency at high maximum temperature and low maximum pressure, while the second best option remains a Rankine cycle with 15% maximum efficiency at high temperature and high pressure. Other charts calculated for previous comparisons are again repeated in Figure 62 through Figure 65. One should recall the practical danger that is introduced with Rankine cycles using high pressure phase change boilers. Even disregarding the benefit to efficiency, a closed regenerative Brayton cycle is a better decision based on safety considerations for flight crew and vehicle operators. Non-regenerative Brayton cycles at this level of efficiency are moderately representative of efficiencies experienced with model scale jet turbine engines. However, these charts are for thermodynamic efficiency only, and do not include the propulsive efficiency losses those model jet turbine engines experience. With poor thermal performance, and highly mismatched efflux velocities, it

is no wonder small scale turbines are regarded as 'fuel hogs' and remain in the domain of expensive novelties.

If a 27% efficient RCBC engine were realized, this translates into 1533 WH/lb of fuel stored in the system. This makes RCBC engines potentially 22x more energy dense than lithium batteries, and 3x more energy dense than present fuel cells in cases where fuel weight is significantly larger than engine weight.

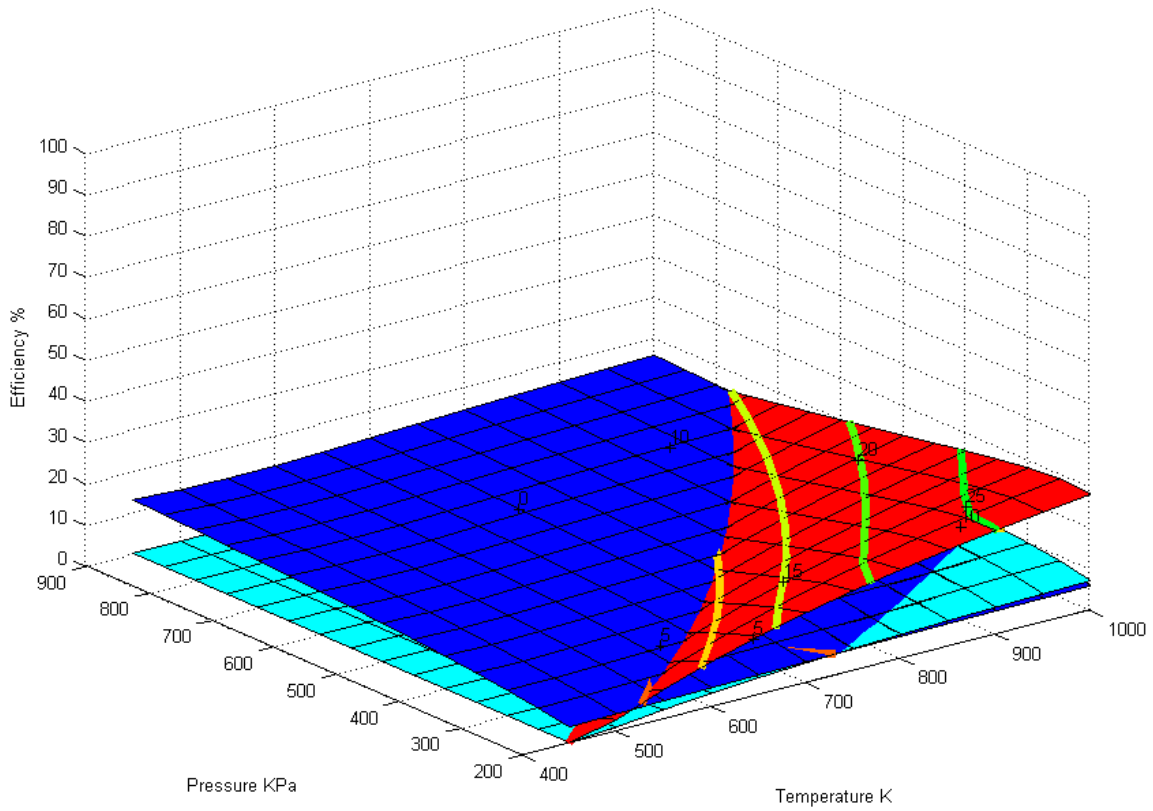

Figure 62 - Regenerative Brayton cycle (red), standard CBC (cyan), Rankine cycle (blue). All closed with 70% component efficiency and 90% Efficient Regenerator. 101KPA low pressure. 310K low temp

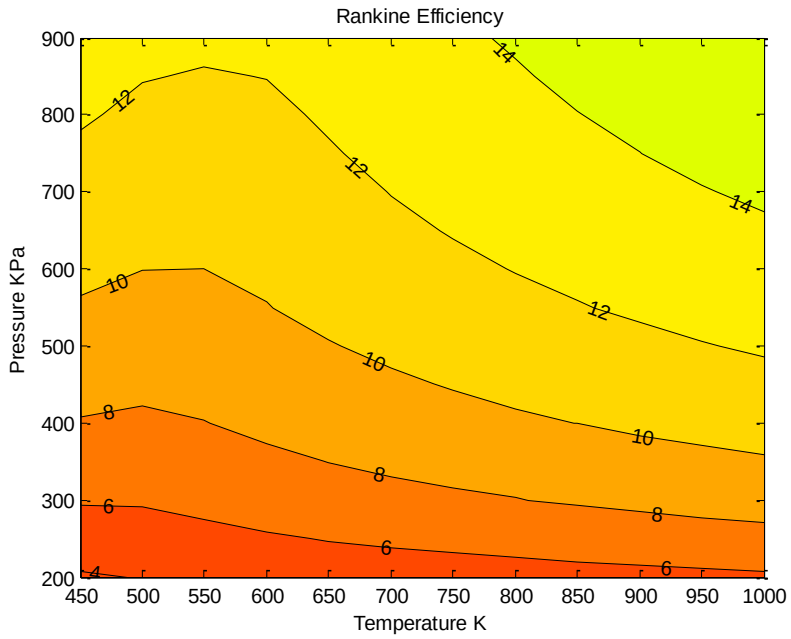

Figure 63 - Rankine Cycle Efficiency with 70% Efficient Components

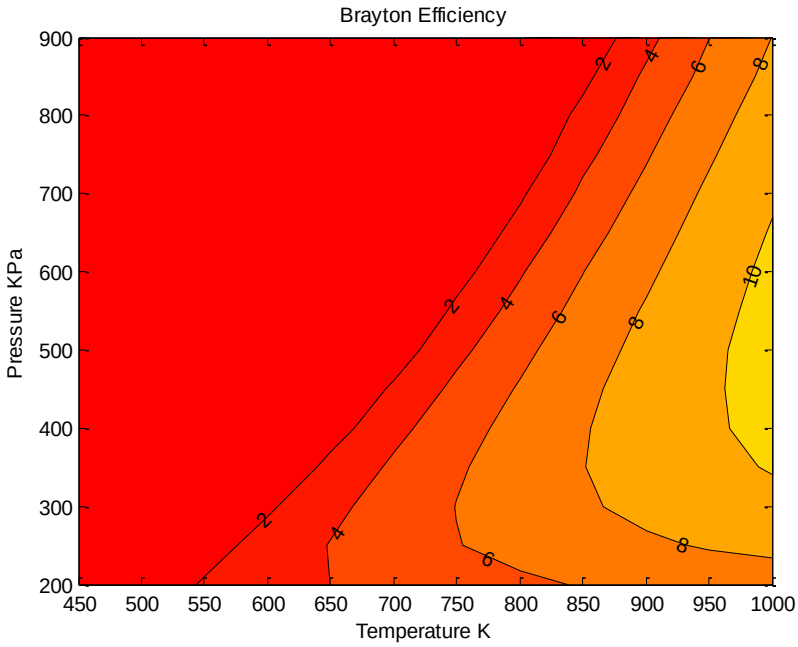

Figure 64 - Brayton Cycle Efficiency with 70% Component Efficiencies'

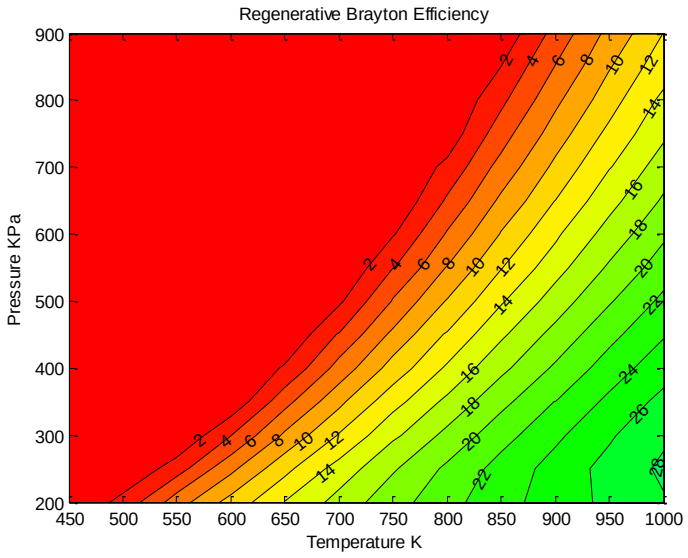

Figure 65 - Regenerative Brayton Cycle with 70% Component Efficiencies and 90% Regeneration efficiency

Closed Cycle Future Growth Potential

After conducting this domain sensitivity analysis of closed cycles and comparing their relative efficiency, the future potential of regenerative closed Brayton cycles far outweighs potential gains available to other systems. In each case considered in this domain, RCBC efficiency always outperforms that of a non-regenerative Brayton cycle, and does it at lower temperatures. While Rankine cycles were overall less sensitive to component performance, and do perform better than RCBC's at higher pressures, (thus pressure ratios as low pressure was held constant in this study). Safety and maximum efficiency potential both favor the RCBC. Additionally, if small scale closed cycle power systems continue to be developed, component efficiency improvements will pay higher dividends for Brayton cycles than Rankine cycles. Poor performance of small scale turbomachinery is the only reason Rankine cycle's find a niche in the plots generated. Once turbo-expanders, regenerators, and compressors are optimized for small flows, there may be no region at all in the domain where Rankine is preferred.

Y.Effects of operating fluid on efficiency

Z. Equivalent Maximum Control Values vs. Equivalent Control Ratios

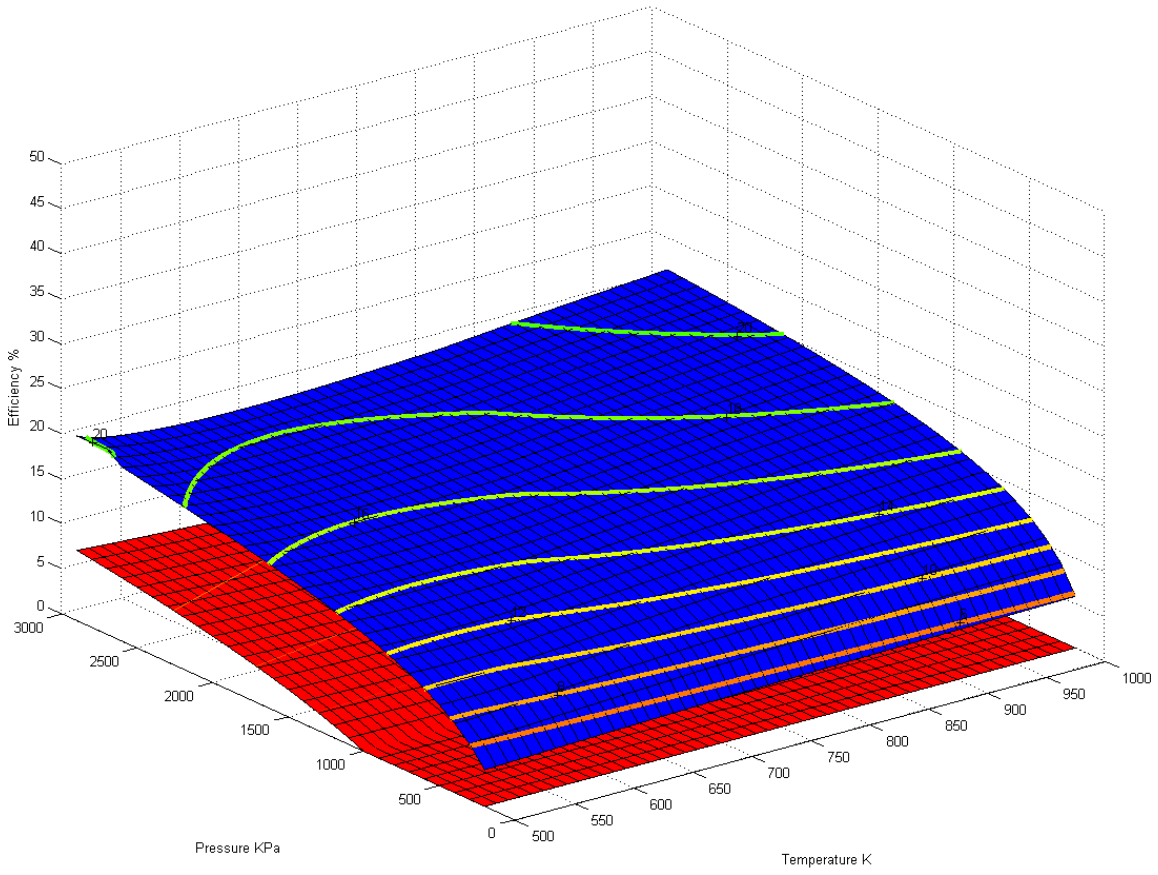

Figure 66 - R134a (red) Compared to Water (blue) at equivalent maximum pressures and temperatures

Figure 66 shows the relative efficiency of water based Rankine cycles and R134a based Rankine cycles when compared in an absolute maximum pressure and temperature sense. Many publications remark that organic Rankine cycles exhibit higher efficiencies than water when fed with low quality (low temperature) heat sources. While this is true when considering equivalent pressure ratio, when one considers material limits or off the shelf component absolute pressure limits, the water based cycle is more efficient in the domain considered. The pressure ratio of the R134a based system is lower for equivalent maximum systems pressures because the lower pressure must be maintained at 1MPA (10 times that of water) so the operating fluid will fully condense back to a liquid state at the design heat

exchange temperature of 310 Kelvin. When one performs the same cycle analysis, but plots the results in a manner comparing equal pressure and temperature ratio, it can be seen that refrigerants do offer an efficiency advantage over water in Figure 67.

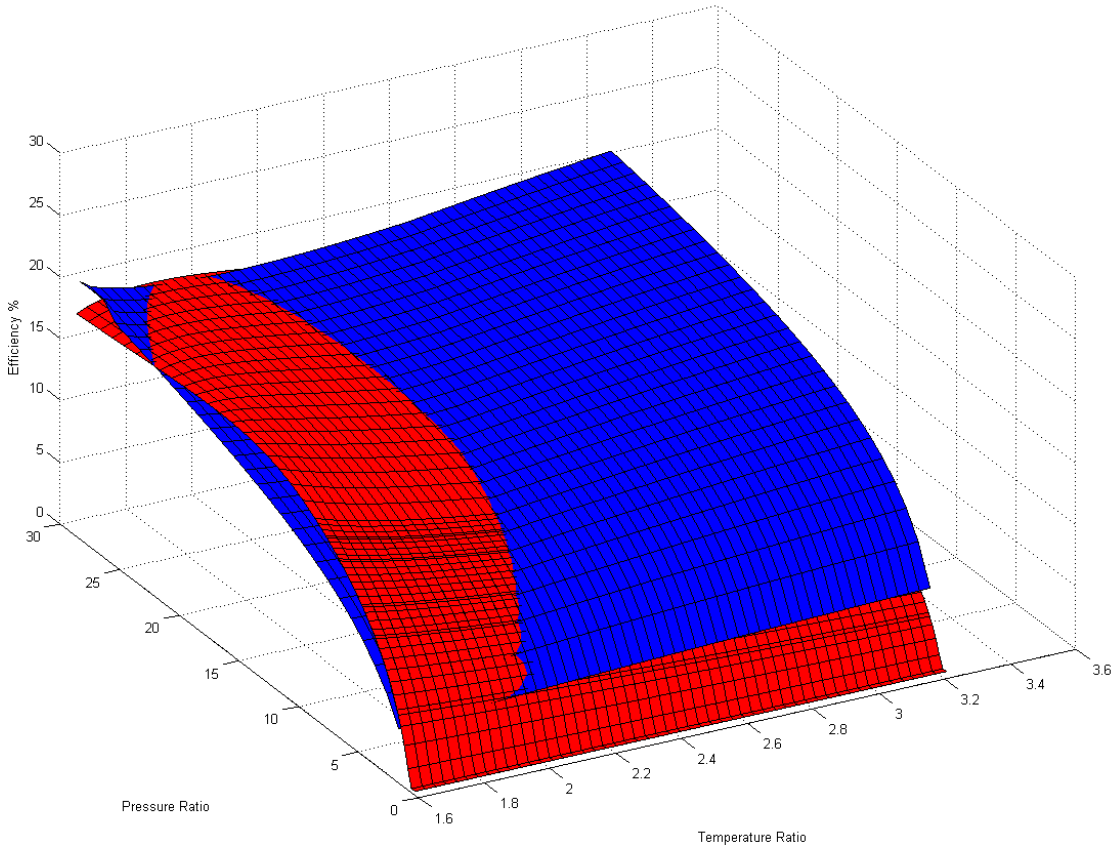

Figure 67 - R134a (red) compared to water (blue) at equivalent temperature and pressure ratios.

When the component isentropic efficiencies are made perfect, the following chart is produced which demonstrates fluid choice independence from component isentropic efficiency. This does not mean that the decision of which fluid to use is independent from ones component design, as the mean operating pressure of a cycle running on R134a will be much higher than that of a water based rankine cycle

discharging heat to a 310K thermal well. Note that the overall efficiencies are higher in Figure 68, but selection regions for each fluid are unchanged.

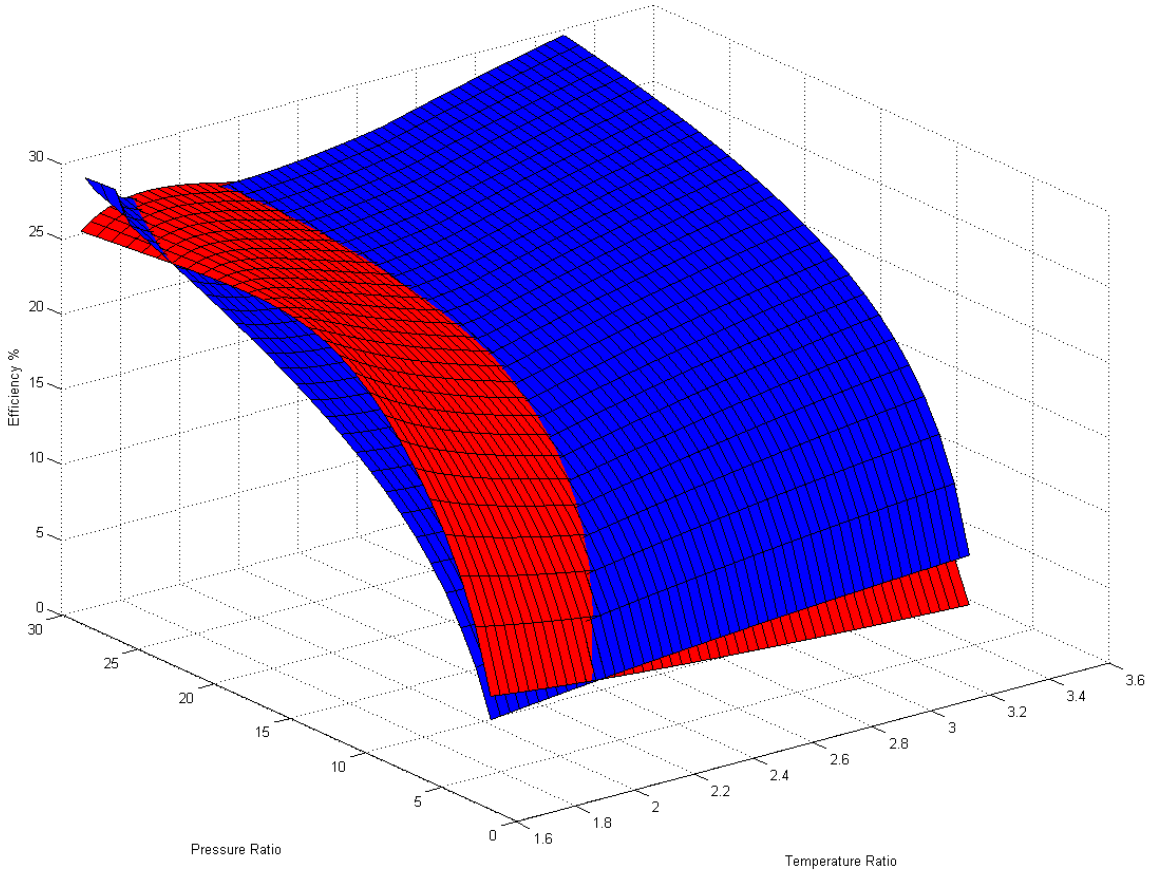

Figure 68 - Rankine Cycle efficiency comparison between R134a and Water with perfect component efficiency

AA. Rankine Cycle Optimal Fluid Selection Comparing Equal Control Ratios

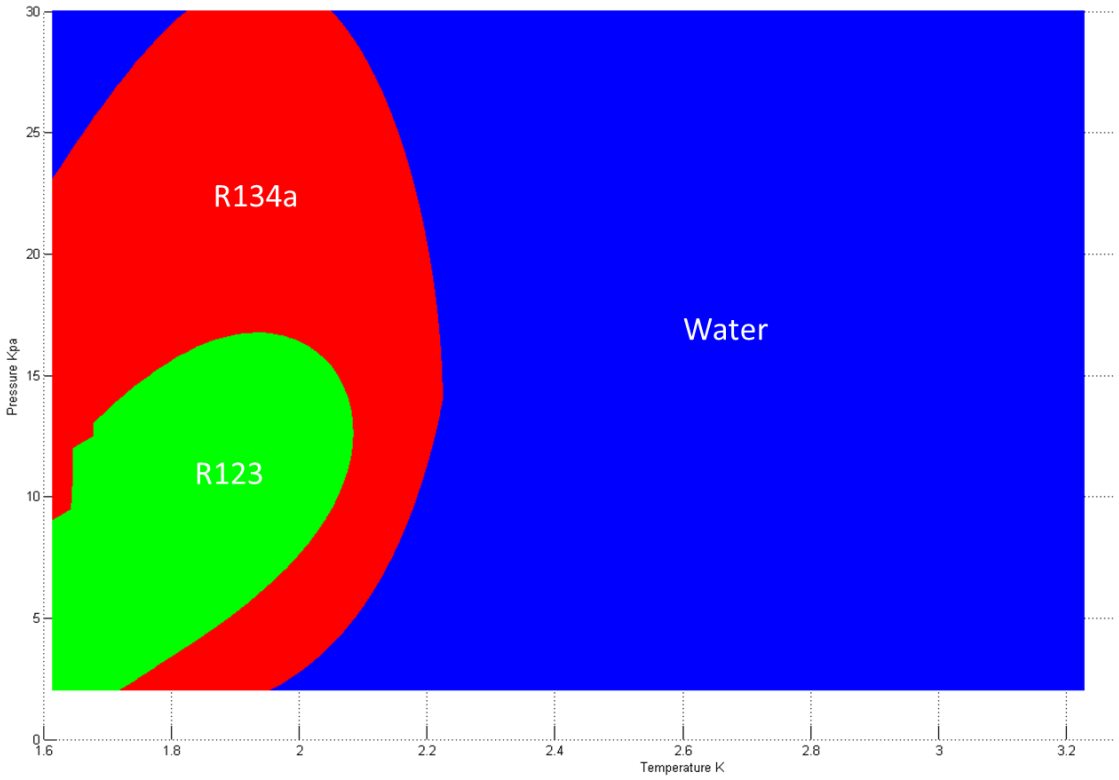

Figure 69 - Comparison of optimal fluids as function of temperature and pressure ratio in a closed Rankine Cycle

When many fluids are compared for optimal efficiency in a Rankine cycle Figure 69 shows which is preferred at differing temperature and pressure ratios. Each fluid starts at saturation pressure corresponding to 310K for studies comparing fluids. As expected and published elsewhere, organic fluids do offer an efficiency advantage over classic steam based Rankine cycles at low temperature ratios. This is in line with organic Rankine cycle's reputation as a good cycle for low quality heat sources. In cases where low cost materials must be used for UAV based closed cycles, one might happen upon a cause for only utilizing low quality heat. However, even a simple propane heat source can produce temperatures above 1700F which is hardly a low quality source, and provides a temperature ratio of roughly 3.9 even on hot days with ambient temperatures approaching 110F. Since it is so simple to create a high temperature (high quality) heat source, one might as well utilize this large available temperature ratio for the benefit of efficiency. The difficult aspect of using high temperature heat sources is not generating the

temperature, but finding materials to make a heat exchanger capable of withstanding simultaneous high temperature and pressure associated with Rankine cycles. It is important to note that in this analysis comparing fluids on equal pressure and temperature ratios, that the absolute pressure experienced by water, R134a, etc. can be very different. It will take a much thicker and heavier apparatus to contain the pressure associated with organic fluids, which when carried by an aircraft may increase induced drag enough to erase any potential efficiency advantage depending on aircraft configuration.

BB. Rankine Cycle Optimal Fluid Selection Comparing Equivalent Control limits

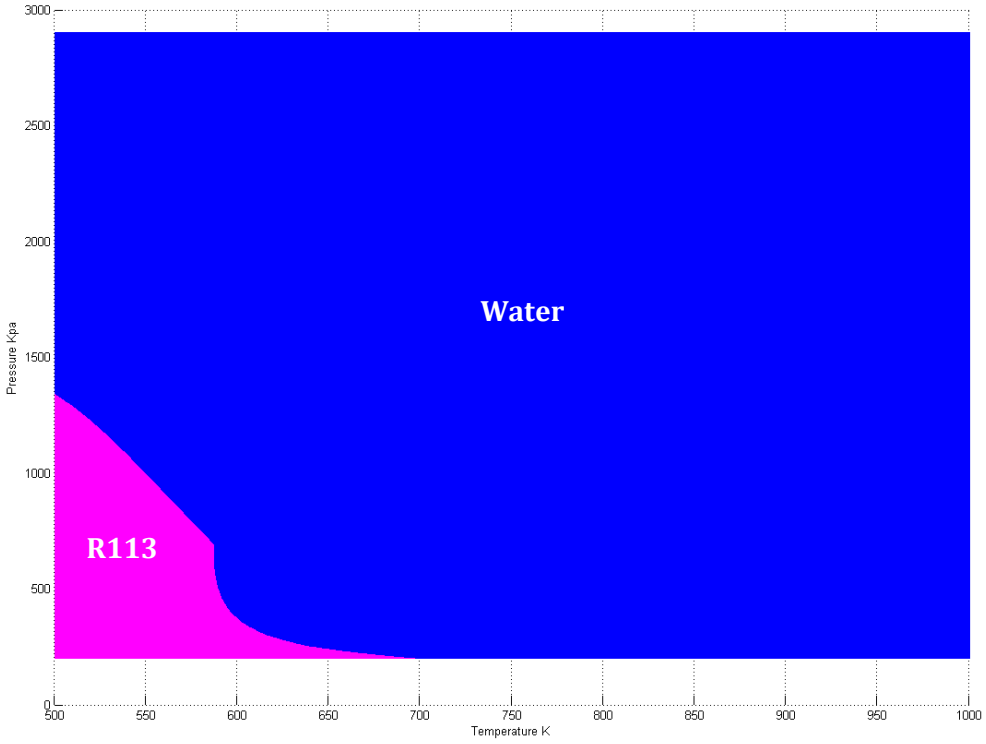

Figure 70 - Comparison of Water, R245fa, R123, and R113 at fixed lower P and T. Chart shows maximum P and T.

When comparing cycles for use in aircraft, conducting efficiency comparisons across absolute temperature and pressure limits is advantageous as the limiting challenge in physical cycle design is invariable limits placed on the system by materials. Pressure vessels, shaft seals, heat exchangers, all have a very limiting maximum temperature and pressure limits that very quickly dominate the design space. Ratio based efficiency and power comparisons are interesting from a thermodynamic perspective,

but absolute limits like those used in Figure 70 are more useful when one is seeking to design a system. When this absolute limit comparison is conducted with a lower pressure corresponding to saturation at 310K and lower temperature of 310K (representing a very hot day 98F) water dominates the region in consideration. Only when one requires pressure and temperature below 1250 Kpa and 600 K does one find R113 advantageous over water. This finding again confirms that ORC's are most useful for low quality heat sources in low power systems.

CC. Brayton Cycle Operating Fluid Comparison of Control Ratios

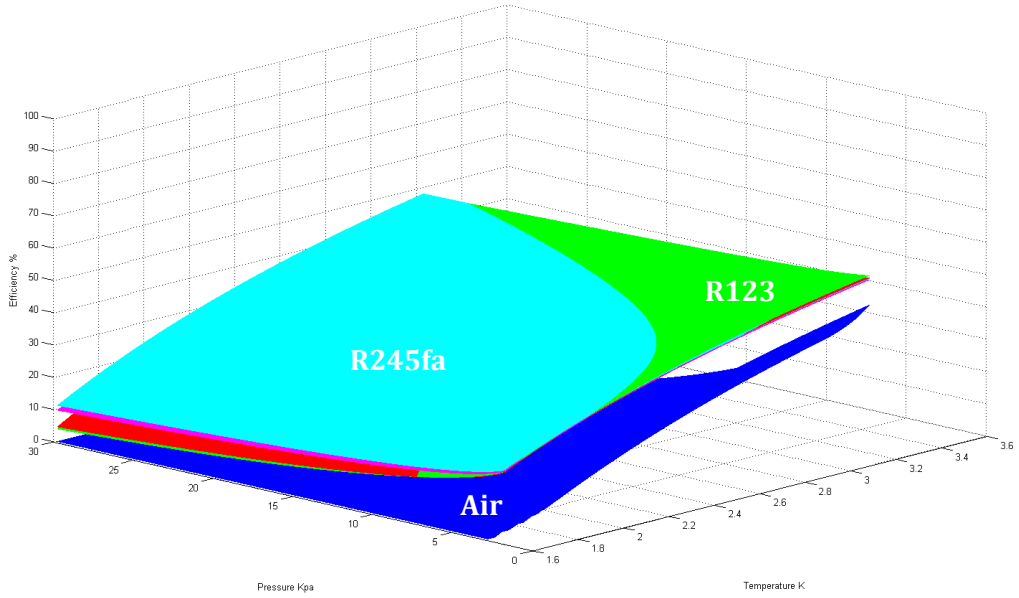

Figure 71 - Brayton Cycle Operating Fluid Comparison Across Equal Pressure Ratios (R245fa, Air, R123)

Comparing Brayton cycles utilizing organic fluids and air, one can see that they are immediately more efficient than their Rankine cycle based counterparts. The results shown in Figure 71 represent analysis conducted with equal pressure and temperature ratios and perfect cycle components and regeneration, a physically unrealizable system. Organic fluids operate extremely well even at low pressure and temperature ratios in a regenerative Brayton cycle. The lowest efficiency experienced by organic fluids at

low pressure in a regenerative Brayton cycle is 20%, which is comparable to the maximum efficiency achieved in this considered domain for a Rankine cycle.

DD. Brayton Cycle Operating Fluid Comparison of Maximum Control Values

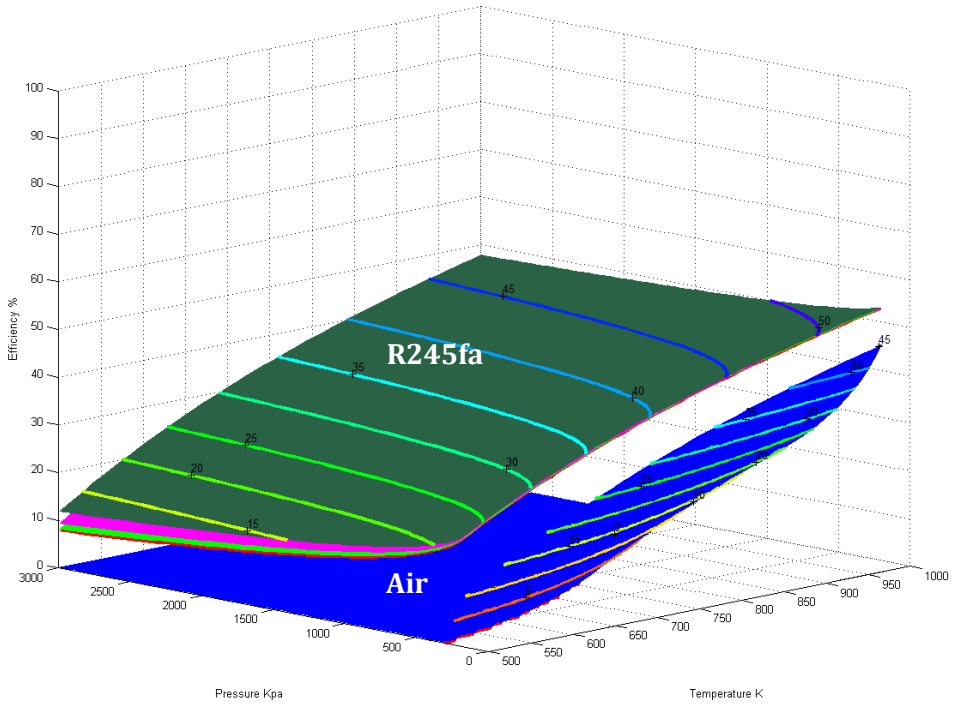

Figure 72 - Brayton Cycle Operating Fluid Comparison Across Different Maximum Temperatures and Pressures

For real systems it is better to compare efficiency and power on an absolute scale of pressure and temperature instead of judging by their ratios as the real material limits manifest themselves in gauge pressure and absolute temperature, not ratios of base values. When efficiency is plotted vs. true pressure and temperature in Figure 72, organic fluids are desirable across the entire domain of regenerative Brayton cycles. This takes away the benefit of being able to "recharge" any leaked air by pumping from the atmosphere when using that fluid, but the efficiency advantages are tremendous, and should not be discounted. One should keep the thermal decomposition temperature of refrigerants in mind when using

them in such high temperature environments. For example, the highest performing refrigerant R245fa is only stable up to 300C (573K) above which temperatures it is prone to pyrolysis and other detrimental effects. If one were to create a regenerative closed Brayton cycle running on air at high temperatures exceeding 1000K, the efficiency difference between refrigerants and air would be small enough at low pressure ratios that one should use air to avoid decomposition and pyrolysis of organic molecules.

EE. Conclusions from Efficiency Comparison

Based on the results of comparing cycles and fluids for maximum efficiency across ratio and absolute basis, the regenerative air based Brayton cycle with the highest possible turbine inlet temperature is the most efficient option, and should be pursued ahead of Rankine cycle based systems. If only low quality heat is available, an organic regenerative Brayton cycle should be used, as it will exceed the efficiency of an air based system while also avoiding complications of organic operating fluid pyrolysis. Brayton cycles avoid many practical problems that Rankine cycles are hindered by, corrosion from liquefied fluids, startup problems caused by rapidly condensing operating fluids on cold surfaces, and very high risk associated with boiling liquid vapor explosions. Brayton cycles are safer in the event of a heater failure as the total energy contained within the cycle at any given point is lower than that of a rankine cycle.

Cycle Power Comparison

FF. Influence of Operating Fluid on Rankine Cycle Specific Power

Operating fluids' differing thermodynamic properties create distinct variations in cycle operating corner parameters, while the effects on cycle efficiency have already been well characterized, it is also important to note the effects of power density on cycle performance as choices are made between operating fluids. Typically, one would seek the highest power density for minimization of system weight, but when designing systems for small UAV's it is important to avoid overly small orifice, turbine, valve, and other

mechanical component dimensions to improve system ruggedness and tolerance for flow contaminants. Additionally, if one were to use a subsonic turboexpander for either a Rankine or Brayton closed cycle propulsion system with extremely high power density, even modest power output requires multiple stages to efficiently capture the total enthalpy drop. Each stage, each flow path bend, increases pressure loss and lowers expander efficiency. Ideally a single turbine stage would fully expand an operating fluid. For high power output, this means that large mass flow and low pressure ratio are desirable. However, steam when expanded adiabatically across low pressure ratios (nominally 1.5-2) also produces a low variation in temperature that limits Carnot efficiency to unacceptable levels. This means that Rankine cycle tuboexpanders designed for efficient operation of SUAV's are relegated to design space including very small mass flow rates, but high enthalpy drop.

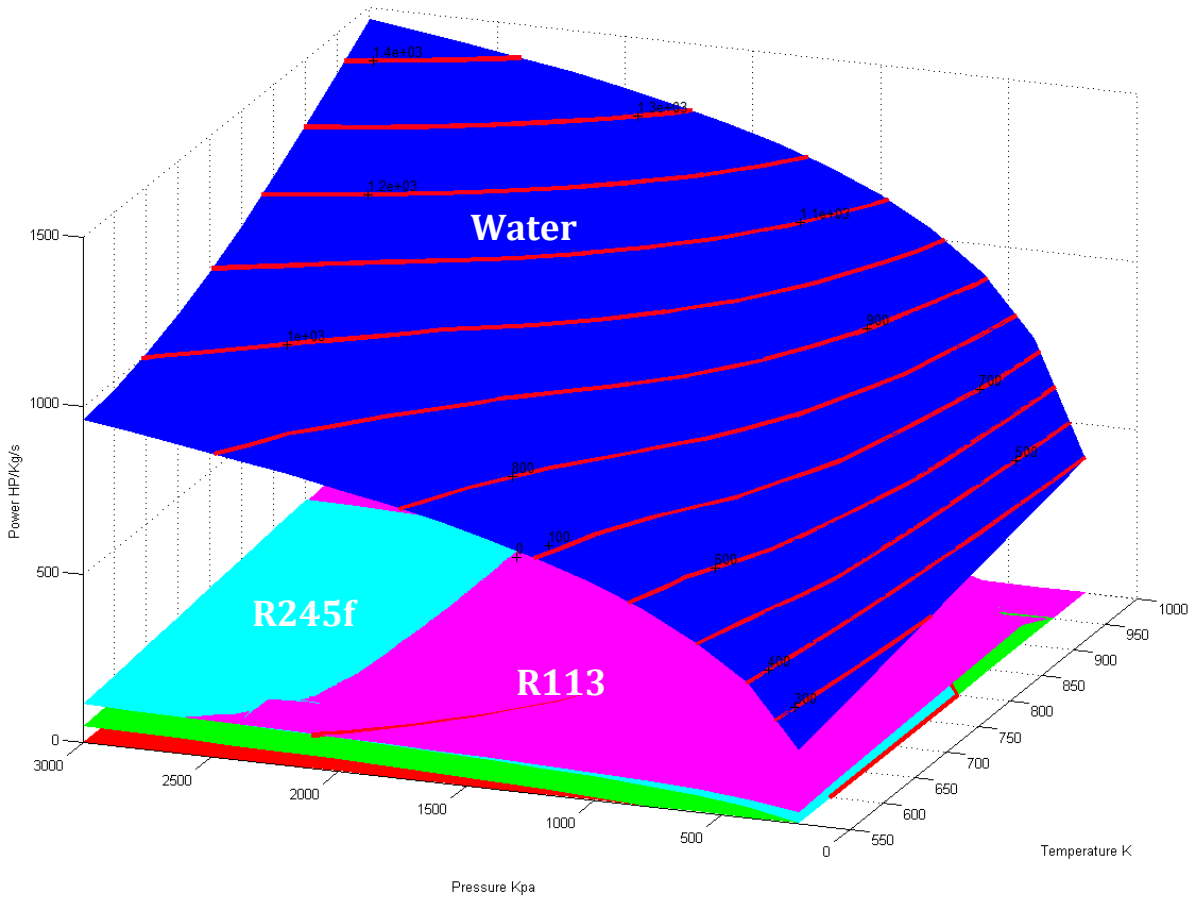

Figure 73 - Rankine Cycle Specific Power Comparison Between Operating Fluids.

Figure 73 above shows that water based Rankine cycles outclass organic Rankine cycles in power density across the entirety of considered pressure and temperature ranges. One should note that this is only per unit mass of operating fluid. As shown elsewhere in this research, organic fluids' higher molecular weight allows smaller expanders for equal power when compared with water. The overall power to weight ratio comparison between an organic system and water based system would be much closer. Additionally, many of the organic Rankine cycles have much higher lower side pressures in the 800 Kpa to 1Mpa range compared to 101Kpa for Water. This results in the organic systems having considerably smaller pressure windows to expand through and create power in the figure above. When the different operating fluids are compared on an equivalent pressure and temperature ratio standard, the chart shown in Figure 74 shows that water offers a more energetic specific power solution than the organic fluids. The specific power for a water based cycle is an order of magnitude larger than that offered by Brayton cycles operating over the same pressure and temperature ranges, though at the sacrifice of efficiency.

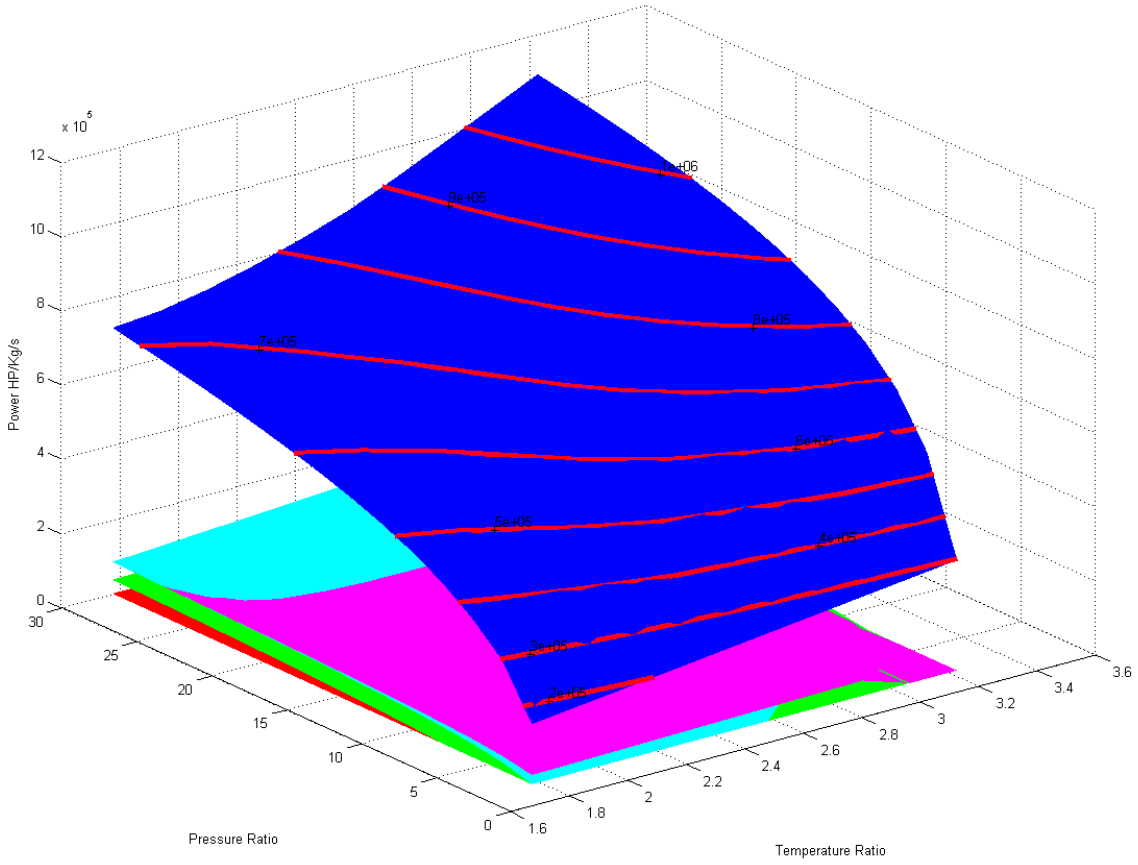

Figure 74 - Rankine Cycle Specific Power Comparison Between Operating Fluids. Equal Control Variable Ratios

GG. Influence of Operating Fluid on Brayton Cycle Specific Power

Most significantly, Brayton cycles offer an order of magnitude lower power density per kilogram of operating fluid flow. While this would be detrimental to any system designed for mains power generation, ship propulsion, jet thrust, etc. it is not a large concern for small scale systems used for SUAV propulsion, as the power density is still plenty large enough to fly small aircraft, and the total system scale is not problematic for SUAV's. Unique problems to SUAV scale closed turbomachine systems include high turbine speed due to small turbine diameter, lower component efficiency resulting from higher leakage percent, and lower Reynolds number. And relatively lower manufacturing tolerances due to smaller components.

When one compares the influence of operating fluids on power density of closed Brayton cycles across equal pressure and temperature ratios, air is the most powerful per KG across the entire domain. But as previously discussed, it is sometimes the lowest power density fluid that is preferable at the small scale so that larger components that are more efficient and easier to manufacture can be used. Additionally, one should remember that this chart is showing power density per Kg of operating fluid and not power density of the overall system. The higher molecular weight of organic fluids helps to improve the true power density of the turboexpander, and will make up for some of the specific power lost to choice of operating fluid. Also, as one considers closed Brayton cycles for larger aircraft in need of hundreds of horsepower, an air, helium, or other light molecular weight gas can increase power density. The total system power density should be maximized, but this is influenced by all previously discussed factors like efficiency, turboexpander losses, fluid choice, and scale.

Figure 75 shows the relative power per kg/s of operating fluid flow of a Brayton cycle operating on air, R245fa, and other common organic fluids. Interestingly, air becomes more powerful per KG as the maximum cycle pressure is lowered. One should not e that this does not mean the system is more powerful at lower pressures, just that it is more powerful per kg of flow. Organic fluids demonstrate a different power trend by increasing in power density with maximum cycle pressure. In this scenario, air's power profile matches the efficiency target region better than that of organic fluids making it compromise less to achieve high specific power and high efficiency simultaneously. The same plot is repeated in Figure 76 in terms of horsepower per kg/s of flow.

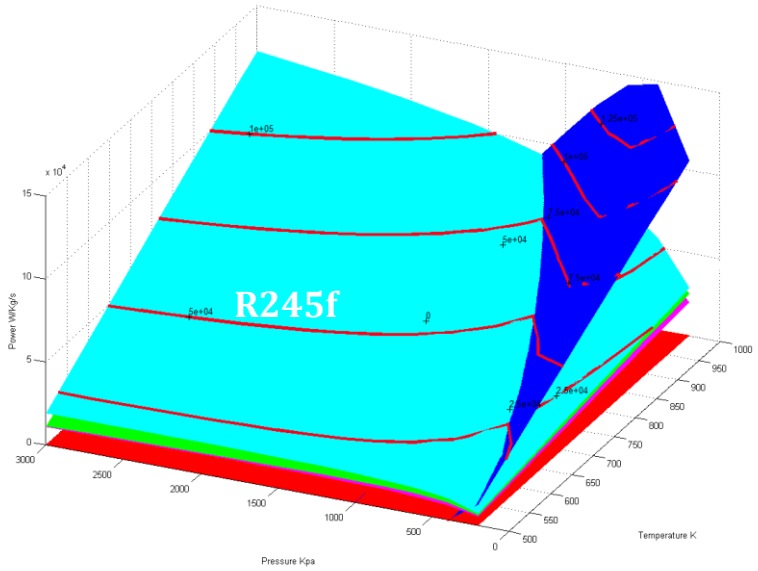

Figure 75 - Specific Power of Regenerative and Standard Brayton Cycle (KW/Kg/s)

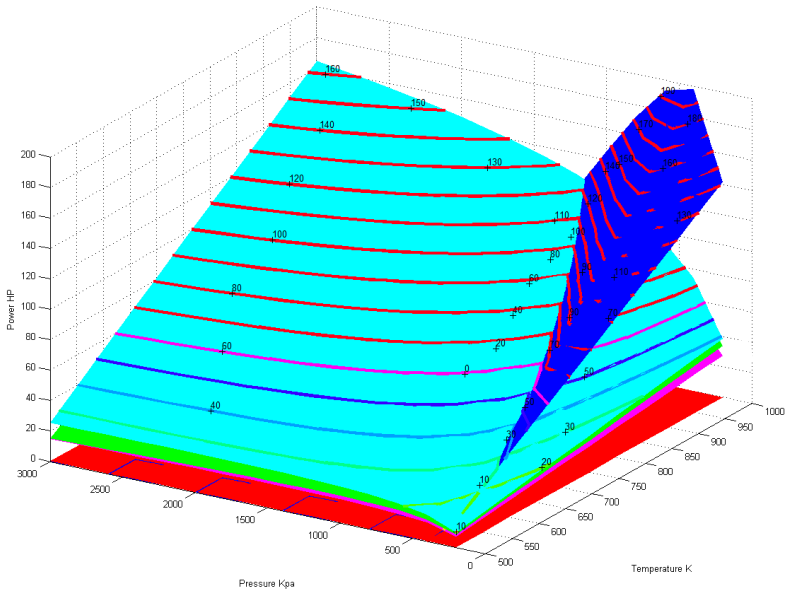

Figure 76 - Power Comparison of Regenerative and Standard Brayton Cycle (HP/kg/s)

Detailed Differential Model of UAS based Closed Rankine Cycle

The previously discussed first order models are useful for detecting changes in efficiency and specific power across a design space of possible pressures and temperatures. The first order models do not however take into account pressure loss through heat exchangers or pipes, heat leakage through all components to the atmosphere, insulation requirements, size of components, heat exchange area requirements, etc. To properly model these losses, a differential model was made such that a specific cycle under a single set of limit conditions could be analyzed. This differential model recorded fluid properties, losses, heat flux, and power generation at each element of the system. Heat exchangers are automatically sized in the code until sufficient heat transfer is achieved for a given operating condition. Alternatively, the heat exchanger size can be fixed to study off design scenarios of the system. The code is not able at present to model the thermal mass of components to show the system warming up, or shutting down which can be a serious complication for cycles requiring phase change like the Rankine cycle. Excessive condensation in expanders can prohibit the cycle from properly starting, or in the worst case, create a hydro-lock condition in a positive displacement system. Adding even a simple thermal mass representation to each component would be a useful progression, though other available codes like thermolib for Matlab already accomplish this task. It would be a more efficient use of resources to use this already developed code featuring a state flow type diagram.

HH. Heat exchanger Model

Heat exchange was modelled by using pipe and flat plate turbulent convection models across constant temperature small elements. Heat exchangers were represented by a grid of heat exchange elements allowing adjustments of the intake air allowed into the exchanger as well as the number of passes that intake air takes over each finned tube. Being able to adjust the volume of intake hot gas (either mixed to lower temperature after combustion, or unmixed to impinge direct flame temperature on the heat exchanger) is critical to properly meter heat addition into the system. Adjustments to the number of passes is essential for making the heat exchanger efficient. Very little of the total heat contained in the

combustion gas intake can be captured in a single pass, so the heat exchanger is essentially built backward in a counterflow arrangement. One knows the maximum temperature allowed by the heat exchangers material, and can set the total input heat flux by modifying intake area, intake gas temperature, and intake gas velocity. From this point, heat exchanger elements are added until a certain percentage of the input heat specified by the user is captured in the operating fluid. This method of calculation basically just adds tube passes until a certain percentage of the required heat is captured. The steps seen in Figure 77 are not a remnant of heat exchange elements, these steps in temperature are created by each pass of the tubes through the heated intake air. Figure 77 also shows the thermal choke point created by the temperature profile of the operating fluid going through phase change in the boiler. This location of narrow temperature differential lowers heat transfer rate in that region and can cause the heat exchanger to grow considerably in size due to that local inefficiency if the pinch point temperature differential is too small.

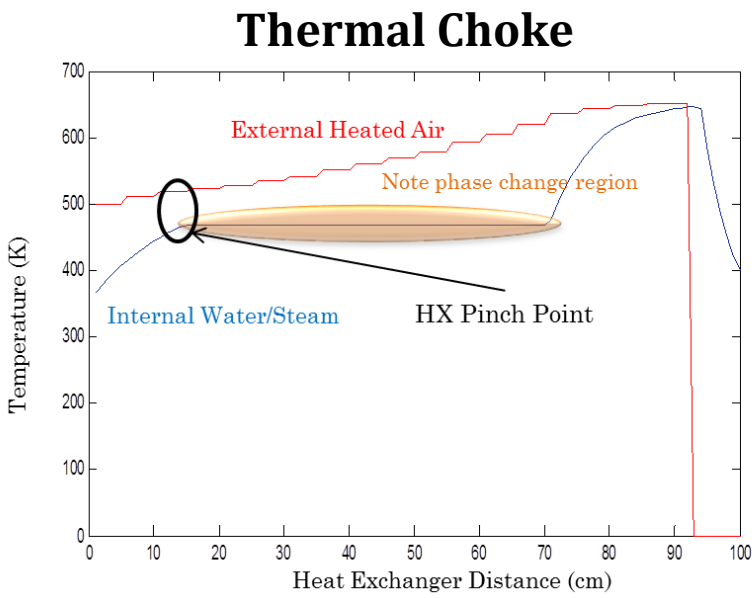

Figure 77 - Heat Exchange with Phase Change in Boiler Model

4. Heat exchange vs cycle position

A very useful property of the differential cycle model is being able to track the net heat transfer rate at each point of the cycle. The region shown in red in Figure 78 is shown in more detail above in Figure 77. The expander region following the red heater is showing the heat energy lost per element of

expansion to work. The condensing heat transfer profile is interesting because of the initial spike of heat transfer from the remainder of superheated gasses creating a region of elevated temperature differential and higher heat exchange rate with the atmosphere. Past this spike, the condensing heat exchange rate is constant, an effect created by the operating fluid maintaining constant temperature during phase change, and use of a single pass heat exchanger that does not require air previously heated by one condenser pass to cool another tube. This preserves optimal heat exchange rate at the expense of requiring a larger area of cooling air which may complicate installation factors and drag of the cooling system. These effects are covered in detail in another portion of this document.

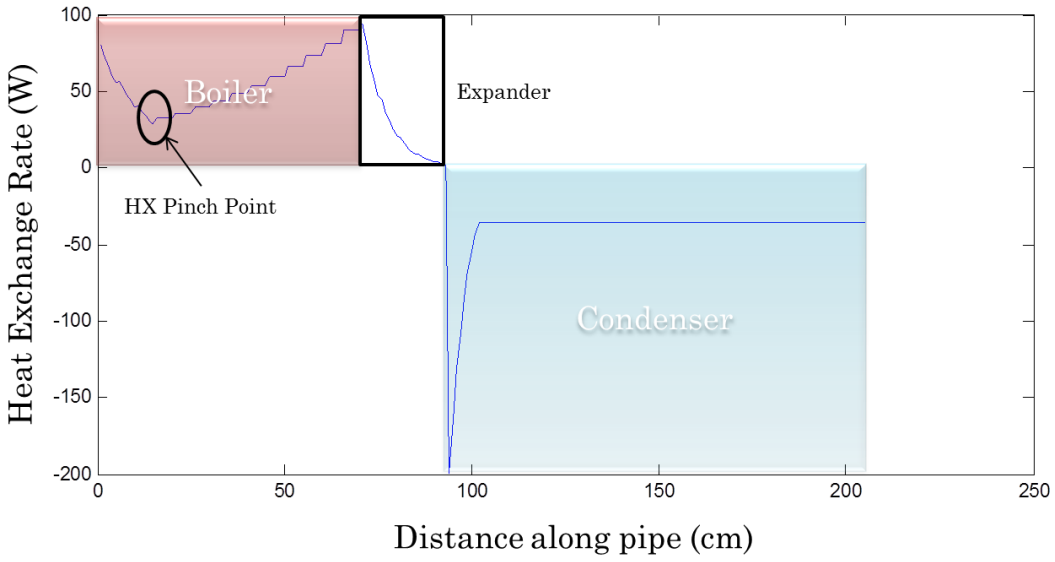

Figure 78 - Heat Transfer in Each Element of Discrete Cycle Model

5. Shortcoming of Heat Exchange Modelling

After the differential heat exchange code was created, and some initial cycle prototypes tested, the heat transfer internal to the pipe directly between fluid elements was found to be a significant contributor to Rankine cycle startup and operation. Though at steady state in areas of steady temperature rise the heat transfer directly between adjacent fluid elements should be small, the rapid temperature change created in regions of condensation and boiling create discrete jumps in temperature that would affect multiple fluid elements in either direction. This intra-fluid heat transfer was not included in the study, and would be especially critical for evolutions of the code seeking to model startup, transients, and

shutdown of closed cycle systems. The importance of this internal heat transfer rate is greater for systems using larger diameter tubing as the area for heat exchange to take place across each fluid element is larger. Small diameter tubing has a higher ratio of external heat exchange area to internal cross sectional area available for intra-fluid element heat exchange.

6. CFD verification of finned tube heat exchanger model

As the interior pipe heat transfer rate is seldom the limiting factor due to high boiling or condensation convection coefficients, the finned pipe exterior heat transfer rate was studied and correlated with heat transfer CFD studies conducted in Solidworks. A single tube and fin 3d model was created in Solidworks, and studied in the built in CFD package. Boundary conditions were set to repeating on top and bottom so that the finned tube became numerically infinite. Hot air was applied in cross flow to allow temperature and convection coefficient profiles to be studied. The flow was considered fully turbulent which resulted in the highest heat transfer rates occurring at the very front of tube fins. Extending the fins farther in the direction of flow does little to increase total heat transfer per unit area, while expanding fins perpendicular to the flow direction will enhance the average convection rate across the finned tube element. The predictions of heat exchange based on flat plate area in each heat exchanger element were scaled to better match the three dimensional effects on heat exchange shown in Solidworks and in Figure 79. This study was essential to adding realism to the heat exchanger model.

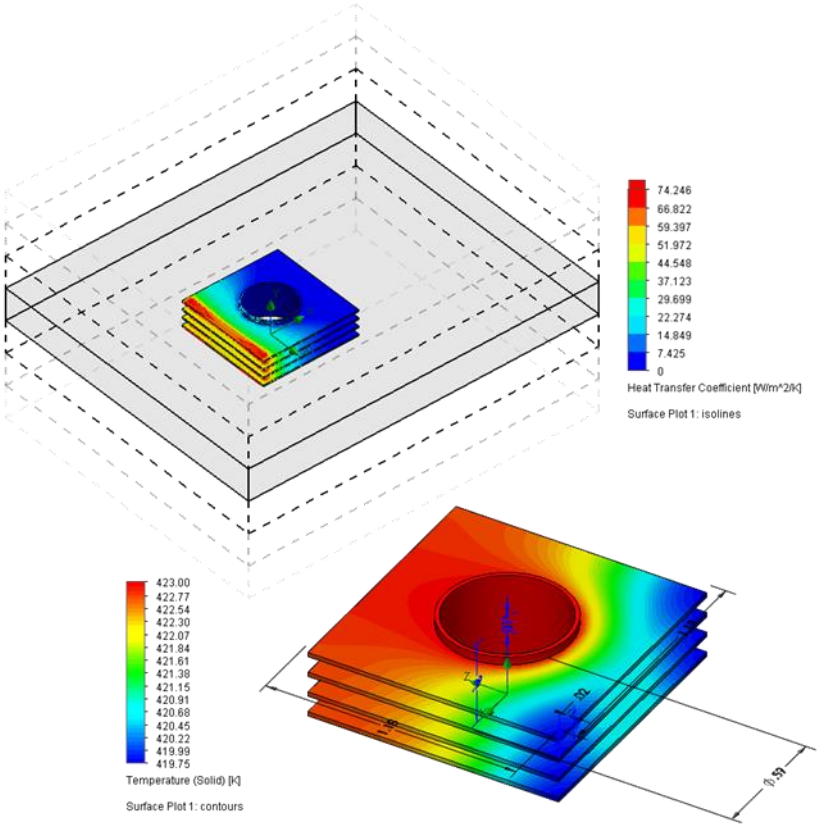

Figure 79 - Example Output of CFD Study of Heat Transfer Rates of Finned Tubing.

7. Effect of Component Efficiencies.

Understanding the relative importance of component performance in a Rankine cycle is important to proper distribution of development time, budget, and weight to these components. A Study was conducted on the baseline component efficiencies as listed in Figure 80. Each component was then improved by 10% efficiency with the effect on total cycle efficiency noted. The most important concern is capturing as much heat from combustion and regeneration as possible in the boiler. Secondly one should make sure this energy is utilized as fully as possible with an efficient expander. Pump power levels are so small that even a 50% efficient pump hardly has an effect on overall cycle performance. Expansion ratio is primarily influencing overall efficiency from the temperature drop resulting from expansion and the changes that causes to Carnot efficiency.

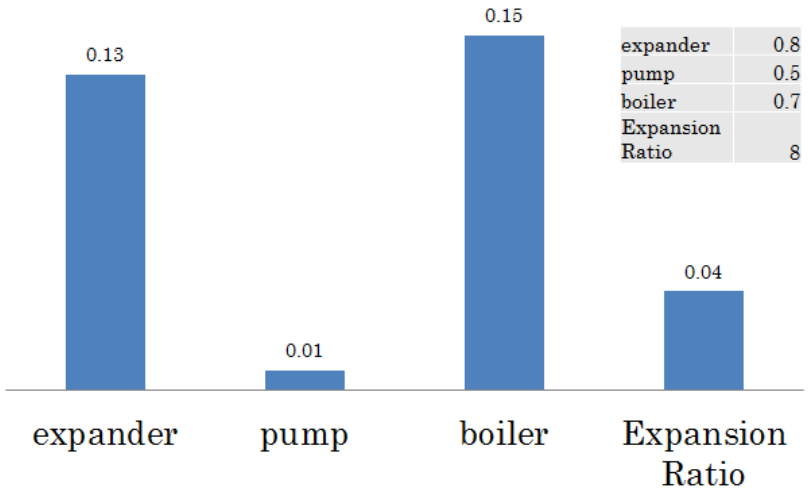

Figure 80 - Cycle Sensitivity to Component Efficiency. ***Influence of Back Work Ratio on Mass Flow Rate***

The larger back work ratio of closed Brayton cycles over that of closed rankine cycles actually offers a practical benefit to manufacturing turboexpanders and compressors for small power systems. The nozzle orifice to accelerate such small mass flows to near sonic speed becomes very small for low power (~1HP) systems. It is on the order of a 2mm square. This makes small turbine design an intricate and high-precision endeavor which undermines the ruggedness and utility of such systems in rough environments. Small flow path leaks become a worrisome percentage of total mass flowrate and a large detriment to component efficiency. Sealing of small turbines like those described here is critical and should use some method of electrical or magnetic coupling to transfer power out of the hermetically sealed vessel so that the system is not reliant on mechanical seals. Rankine cycles exhibit much smaller back work ratios than a similar maximum temperature and pressure brayton cycle as the compression phase occurs when the operating fluid is liquefied. This makes the net specific work of a rankine cycle higher than that of a corresponding brayton cycle and therefore the rankine's mass flow will be considerably lower. The overall problem presented by this is that the choking orifice leading into a rankine cycle turbine, as well as the total output power of the turbine, will be smaller than that of the brayton cycle's. The added power requirement of a brayton turbine to drive a compressor operating on a

compressible fluid makes the nozzle a more reasonable size and trends in the proper direction of alleviating problems arising from leakage, micromachining, and other small scale turbine issues.

For low power design, one should consider positive displacement options like piston, vane, or scroll motors as a substitute for classical turbomachinery found in Brayton cycles as positive displacement options allow for larger pressure drop per stage and demonstrate higher efficiency at very low specific speeds (low mass flow rates with high pressure drop).

Comparison of Closed Cycles and Their Suitability for UAV Propulsion.

From the beginning of experimental work the experimental closed cycle engine was based on a Rankine cycle. This cycle was selected based on comparisons to existing systems of all scales, desire for quiet operation, perceived mechanical simplicity for integration into an aircraft, and existing examples of closed cycle operation. Analysis of competing cycles and background research into the employment of those cycles has continued in parallel with development of the experimental flying Rankine cycle engine. Classical models of cycle performance were created in Matlab using the "Coolprop" fluid property library. These codes allow for quick estimation of cycle performance based on component efficiency, cycle design temperatures and pressures. Performance of pumps, piston expanders, turbo-expanders, heat exchangers, boilers, regenerators and other thermal components and losses are simply incorporated through efficiency losses. Expansion and compression components are modelled by an isentropic efficiency while heat exchangers and boilers are modelled simply by the percentage of transferred energy. Arranging these calculations in the correct sequence allows one to very rapidly judge the sensitivity and relative importance of cycle components. Isentropic efficiencies of comparably scaled components found in literature formed the basis of efficiency calculations for the cycles as well as showing what potential improvements are possible with improved small scale component performance.

Though this research began centered on Rankine cycle development, continued exploration has shown a closed Brayton cycle with regeneration to be of particular merit in the temperature and pressure

scales available to flying Rankine cycles. Brayton cycles were initially discounted because of their requirement for high pressure and temperature ratios to achieve efficient operation. Small scale and model RC turbomachine Brayton cycles are notoriously inefficient in practice achieving 5% or lower nominal efficiency. Disregarding thermal efficiency, their propulsive efficiency alone is extremely low due to the extremely high velocity mismatch between UAS flight speed and jet efflux. Low propulsive efficiency can be solved by using a turboprop type gear reduction and high pressure and temperature ratio requirements can be alleviated by using a regenerator to completely change the governing trend of Brayton cycle efficiency as schematically shown below in Figure 81.

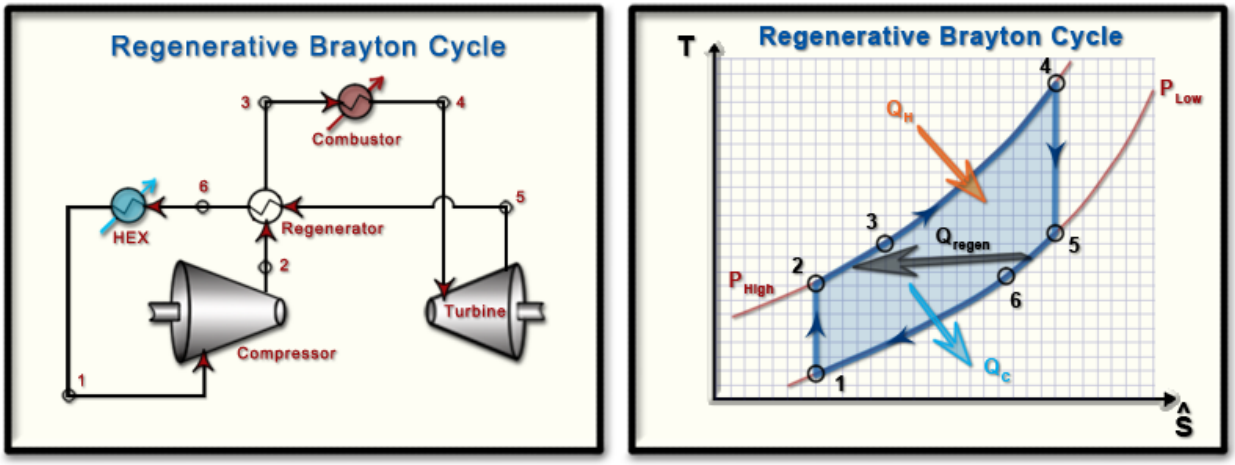

Figure 81 - Regenerative brayton cycle. [11]

II. Regenerative Brayton Cycle Efficiency Equation

Beginning with the base expression for efficiency, note that because of the sign convention regarding work, this does indeed result in subtracting the compressor work required from the work generated in the turbine.

$$\eta = \frac{W_{turb} + W_{comp}}{Q_h}$$

Combining this efficiency expression with the base expressions for heat addition, turbine and compressor work:

$$Q_h = m' \cdot Cp \cdot \left(T_4 - T_3 \right)$$

$$-W_{turb} = m' \cdot Cp \cdot \left(T_5 - T_4 \right)$$

$$-W_{comp} = m' \cdot Cp \cdot \left(T_2 - T_1 \right)$$

The temperature relation permitted by an ideal regenerator creates the foundational change in efficiency by allowing input heat to recirculate the cycle again. This perfect regenerator is modelled by simply equating T3 and T5.

Combining these expressions one reaches:

$$\eta = 1 + \frac{W_{comp}}{W_{turb}} = 1 - \frac{m' \cdot Cp \cdot \left(T_2 - T_1 \right)}{m' \cdot Cp \cdot \left(T_4 - T_5 \right)}$$

Which through assuming constant specific heats simplifies to:

$$\eta = 1 - \frac{T_1 \left(\frac{T_2}{T_1} - 1 \right)}{T_4 \cdot \left(1 - \frac{T_5}{T_4} \right)}$$

One should note that the temperature ratios of the compressor and expander are directly used. Both components are assumed perfectly isentropic in these equations. Because of this assumption the following temperature and pressure relationships are true.

$$\frac{T_2}{T_1} = \left(\frac{P_2}{P_1}\right)^{\frac{\gamma-1}{\gamma}} \qquad \frac{T_5}{T_4} = \left(\frac{P_5}{P_4}\right)^{\frac{\gamma-1}{\gamma}}$$

Which when incorporated into the efficiency equation yields:

$$\eta = 1 - \frac{T_1\left[\left(\frac{P_2}{P_1}\right)^{\frac{\gamma-1}{\gamma}} - 1\right]}{T_4\left[1 - \left(\frac{P_5}{P_4}\right)^{\frac{\gamma-1}{\gamma}}\right]}$$

Which though seemingly complex, simplifies to the following equation given the progression noted in Appendix TTT:

$$\eta = 1 - \frac{T_1}{T_4}\left(\frac{P_2}{P_1}\right)^{\frac{\gamma-1}{\gamma}}$$

This result shows that closed Brayton cycles are most efficient when operated at **low** pressure ratios and high temperature ratios. This result is in opposition to the desired efficient operation of non-regenerative Brayton cycles that rely on high pressure ratio to achieve high efficiency according to the governing equation:

JJ. Comparison of Cold Gas Brayton Cycles With and Without Regeneration

$$\eta_{open} = 1 - \frac{1}{\left(\frac{P_2}{P_1}\right)^{\frac{\gamma - 1}{\gamma}}}$$

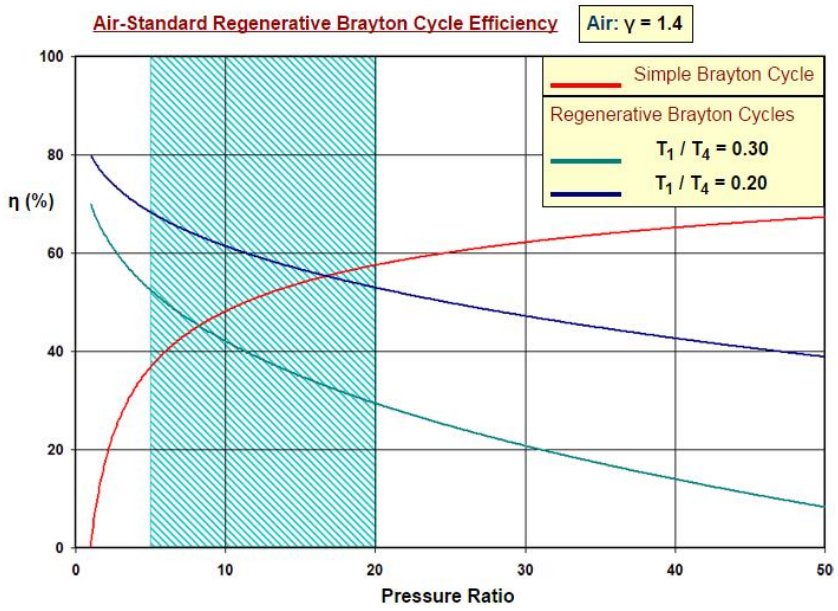

Figure 82 - Brayton cycle efficiency comparison. [11]

This optimality trend seen in Figure 82 matches the practical mechanical constraints that airborne closed cycles are subject to. It is generally lighter to accommodate high temperature design than it is to accommodate high pressure ratios because of the large number of stages (whether axial or radial) required to efficiently capture or create the enthalpy change necessary in high pressure ratio turbomachines.

Influence of Back Work Ratio on Mass Flow Rate

The larger back work ratio of closed Brayton cycles over that of closed Rankine cycles actually offers a practical benefit to manufacturing turboexpanders and compressors for small power systems. The nozzle orifice to accelerate such small mass flows to near sonic speed becomes very small for low power (~1HP) systems. It is on the order of a 2mm square. This makes small turbine design an intricate and high-precision endeavor which undermines the ruggedness and utility of such systems in rough environments. Small flow path leaks become a worrisome percentage of total mass flowrate and a large detriment to component efficiency. Sealing of small turbines like those described here is critical and should use some method of electrical or magnetic coupling to transfer power out of the hermetically sealed vessel so that the system is not reliant on mechanical seals. Rankine cycles exhibit much smaller back work ratios than a similar maximum temperature and pressure Brayton cycle as the compression phase occurs when the operating fluid is liquefied. This makes the net specific work of a Rankine cycle higher than that of a corresponding Brayton cycle and therefore the Rankine's mass flow will be considerably lower. The overall problem presented by this is that the choking orifice leading into a Rankine cycle turbine, as well as the total output power of the turbine, will be smaller than that of the Brayton cycle's. The added power requirement of a Brayton turbine to drive a compressor operating on a compressible fluid makes the nozzle a more reasonable size and trends in the proper direction of alleviating problems arising from leakage, micromachining, and other small scale turbine issues.

For low power design, one should consider positive displacement options like piston, vane, or scroll motors as a substitute for classical turbomachinery found in Brayton cycles as positive displacement options allow for larger pressure drop per stage and demonstrate higher efficiency at very low specific speeds (low mass flow rates with high pressure drop).

Influence of Operating Fluid on turbomachine stage power output.

If one avoids the compressibility losses associated with supersonic turbines, the maximum enthalpy drop per turbomachine stage can be approximated by:

$$m' \cdot \frac{V^2}{2} = m' \cdot \frac{\left(\sqrt{\gamma \cdot R \cdot T}\right)^2}{2} = \frac{m' \cdot \gamma \cdot R \cdot T}{2}$$

Which represents the situation where a perfect nozzle accelerates the flow to mach 1, and the tuboexpander harnesses 100% of that energy into useable power. Steam at temperatures studied during this research exhibits a maximum power per stage of 150KW/Kg which is quite considerable until one notes that mass flow is constrained by total cycle power and for small power systems (like the 1 HP target of this study) the mass flow rates are very small. 2.5 to 5 grams per second is a typical window for 1HP systems depending on the cycle selected and operating parameters. This miniscule flow rate is problematic for low power, yet advantageous for medium power systems in the 50 to 100 HP class that could use closed cycle turbomachines to achieve very power dense engines.

$$\text{Power} = \eta_{\text{isentropic}} \cdot m' \cdot Cp \cdot \left(T_5 - T_4\right)$$

This results in conflicting requirements where one must maximize temperature differential to remain efficient, yet minimize temperature differential to maximize enthalpy drop per stage (by favoring mass flow rate over change in pressure to "make power"). This design conflict can be helped by selecting an operating fluid with lower specific heat at the temperatures considered. Organic fluids like R134a (1.17 KW/KG/K) have lower specific heats than water (2.16 KW/KG/K) which results in a rough increase in mass flow rate of refrigerant based closed Brayton cycles of 3.1x. This means that refrigerant based systems of equal displacement and size can create approximately 1.8 times the power of steam based systems when evaluated at moderate temperature and pressure. It is also worth noting in this basic

comparison, a closed cycle engine using air would offer even higher power than that of R134a but still less than some other refrigerant options. Refrigerants are most beneficial in rankine cycles where their ability to liquefy at higher temperature than air and other gasses is essential. When closed rankine cycles are being considered, refrigerants lose much of their design benefits as phase change is no longer a consideration and other safer and more readily available gasses exhibit similar beneficial physical properties.

If one combines the previous expression with a manipulation of the ideal gas equation it is possible to reduce the feasible enthalpy drop per stage of a subsonic turbomachine to a function of only pressure, volumetric flow rate, and ratio of specific heats. This presentation of the same equation shows in mathematical form why some previous studies (like Mcconaghy) have been able to increase the power output of their closed cycle engines by pressurizing the case even at rest. This raises the average pressure of the entire cycle and improves power output per unit volume with corresponding benefit to engine specific power.

Starting with the ideal gas equation with values entered for water (steam)

$$PV = \frac{m \cdot 1000}{18.01} \cdot 8.314 \cdot T$$

Simplifying and rearranging into rate based mass and volume:

$$\frac{P}{462T} = \frac{m}{V} = \rho$$

Note that prime indicates the time derivative of the corresponding quantity.

$$\frac{P \cdot V'}{462 \cdot T} = m'$$

And then combining this with the previous expression we can see that many of the variables cancel when the ideal gas assumption is made, making the expression for available stage power very apparent. Most interestingly the influence of all gas constants except the ratio of specific heats vanishes. This shows that for equivalent pressure and volumetric flow, a subsonic gas turbine will produce more power when operating on a monatomic gas (gamma = 1.67) compared to a diatomic gas (gamma=1.4). Also interesting to note is that these advantages and comparisons can be made irrespective of temperature. Equations in other states of simplification imply that gasses with higher molecular weights (refrigerants) can offer higher power output, when in actuality it is the ratio of specific heats that most clearly defines maximum power per stage.

$$\frac{\frac{MW \cdot P \cdot V'}{8.314 \cdot T} \cdot \gamma \cdot \frac{8.314}{MW} \cdot T}{2} = \frac{P \cdot V' \cdot \gamma}{2} = \Delta h$$

KK. Conclusion

This chapter considered Rankine and Brayton thermal cycles, effects of regeneration, and multiple operating fluids on each. Airborne Rankine cycles are not significantly assisted by regeneration as tested, and require both high temperature and pressure to function efficiently. Maximum expected efficiencies at the assumed material limits of low cost airborne cycles remained below 18%. Brayton cycles were significantly affected by regeneration. The lack of phase change during heat transfer allows significant regeneration to be employed across a constant thermal gradient, leading to significant efficiency benefits. Keeping a closed Brayton cycle to the same material temperature and pressure limits as the Rankine cycle saw efficiencies up to 27% with realistic components. Furthermore the regenerative Brayton cycle achieves maximum efficiency at low pressure ratios which significantly eases one of the material requirements of the system.

Of all the component efficiencies studied, the heater and expander component efficiencies are the most important. For the regenerative Brayton cycle, the regenerator heat exchanger efficiency is also of paramount importace as the cycle will revert to a low pressure ratio, and therefore low efficiency, conventional Brayton cycle if the regenerator does not perform. As research into closed systems is carried forward, design and experimental focus should be kept on these three components.

Preferred operating fluids varied with assumed pressure ratio and operating temperature. For low temperature heat input to Rankine Cycles, organic cycles operating on refrigerants pose some benefits. For higher temperature ratio Rankine cycles steam remained the most efficient operating fluid covered during this study. Brayton cycles operate at higher efficiency across a larger range of temperatures and pressures when using refrigerants as an operating fluid. They can be operated at low average pressures as there is no need to liquefy the refrigerant during operation, although low pressures will lead to lower density operating fluid and overall lower power density. For simplicity and ability to re-charge the operating fluid during flight, it might remain wise to use standard air as the operating fluid. A small pump onboard could compensate for small leaks, or changes in required cycle power.

The overall recommendation after reviewing all these options is to pursue the development of a regenerative closed Brayton cycle. This cycle retains all the advantages of a Rankine cycle while outperforming in terms of efficiency, material requirements, and reduction of moving parts.

CHAPTER III

Demonstration System

Piston Expander Fabrication

Most instances of mobile Rankine cycles have historically employed reciprocating expanders. Examples like trains, flash steam hydroplanes, and the Bessler brothers airplane all use reciprocating positive displacement expanders to make power. The main advantage being that the steam can be expanded across a large pressure drop in a single step without forcing the power output shaft to spin at turbine-like speeds. Triple expansion reciprocating expanders became more common for large steam engines to prevent condensation on the cylinder walls during single step large expansions. A 100cc two stroke UAV engine was modified to behave as an expander and test run on compressed air as shown in Figure 89. A boxer configuration was selected because they minimize vibration by having each piston act as a mirror of the other. While the engine did function and exhibited little vibration when being driven by an electric motor, the power pulse created a large torque vibration that shook test stands, and would excite any eventual aircraft it would be attached to. These torsional vibration are magnified because both cylinders are pressurized simultaneously. Mcconaghy described similar issues with dynamic balance on his stirling engine. After being unable to completely eliminate mass vibrations in his engine, Mcconaghy modified the system such that vibrations mainly occurred in the longitudinal axis. These vibrations were much easier for his small aircraft to accept, and eliminated the severe torsional oscillation.

LL. Balancing and Vibration of Piston Engines

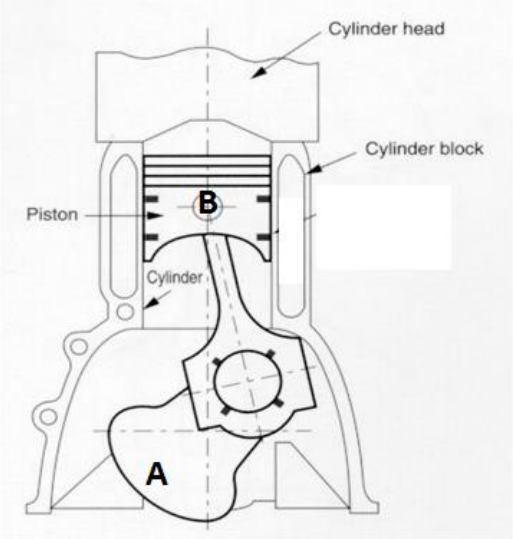

Figure 83 - Piston Mass Diagram [12]

For a standard piston, crank, and counterweight system as shown above in Figure 83 the path of the piston and counterweight centers of gravity in Cartesian coordinates can be expressed by the following equations.

Equation 1 - motion of standard piston, counterweight, and connecting rod system

$$ptax(t) := r \cdot \sin\left(\frac{rpm}{60} \cdot 2 \cdot \pi \cdot t\right)$$

$$ptay(t) := r \cdot \cos\left(\frac{rpm}{60} \cdot 2 \cdot \pi \cdot t\right)$$

$$ptby(t) := ptay(t) + \sqrt{(2 \cdot r)^2 - ptax(t)^2}$$

These component paths can be combined to plot the overall motion and acceleration of the piston system.

$$pathx(t) := \frac{CW \cdot -ptax(t) + P \cdot 0 + CR \cdot \frac{ptax(t)}{2}}{mass}$$

$$pathy(t) := \frac{CW \cdot -ptay(t) + P \cdot ptby(t) + CR \cdot \left(\frac{ptay(t) + ptby(t)}{2} \right)}{mass}$$

For most low cost RC aircraft engines and other simple single cylinder engines, it is not possible to completely eliminate vibration. If one perfectly matches the weight of the reciprocating piston, the vibration along the stroke axis will be mostly negated, but the counterweight produces a vibration perpendicular to this axis that is exactly equal to the magnitude of the non-counterbalanced system. Additionally, the presence of a connecting rod in standard piston engines creates a higher order motion term that makes the actual piston motion slightly non sinusoidal due to the angular offset of the connecting rod as shown in Figure 84. For this reason it is most common to see single cylinder systems use counterweights that are compromised in weight to reduce the axial vibration while not producing excess transverse vibration.

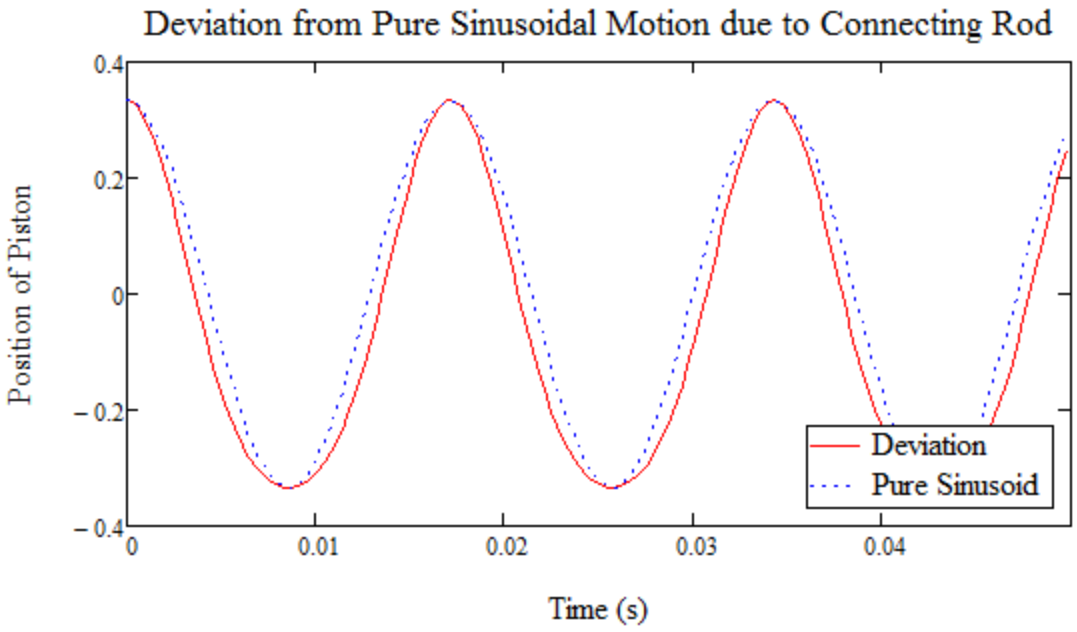

Figure 84 - Deviation of Piston Location from Pure Sinusoidal Motion

The motion of the single piston system center of gravity can be shown in a simple Cartesian plot as shown in Figure 85. A slight acceleration in the stroke direction (Y) can be seen, while the major vibration has been translated perpendicular to the piston stroke axis due to an overly heavy counterweight. Heavier counterweights will further flatten the plot up to the limit where counterweight equals piston and crank weight. Lighter counterweight will create stronger axial variation in the center of gravity motion. In every case and each combination of traditional crankshaft mounter counterweighting, the piston system will continue to make significant vibration. One should also note that this calculation does not take into account the reaction torque created by the power and compression stroke of the engine that creates an additional torsional vibration. All real combinations of this simple piston, counterweight, and connecting rod system from one to five cylinders are not possible to dynamically balance. An inline six cylinder engine can create a perfectly mirrored pair of three cylinders that is capable of simple dynamic balance. This is one reason many high end sports car engines began as V12's. They are simply two inline 6 cylinder engine's connected together to create a smooth running large displacement engine. Some more complicated gear or belt driven counterweights can achieve dynamic balance, but were generally

considered too complicated for integration into this CCE, as any failure in those systems can quickly destroy the engine, or at minimum create a large imbalance.

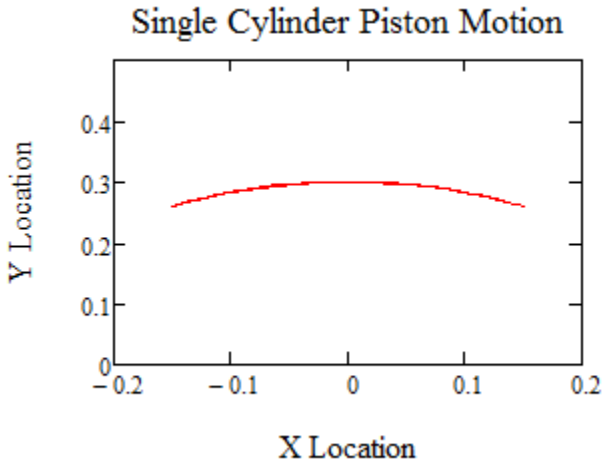

Figure 85 - Motion of single cylinder piston system center of gravity.

8. Scotch Yokes for Minimization of Vibration

A solution to the higher order motion terms introduced by connecting rod driven piston systems is to use a scotch yoke. The scotch yoke uses a more complex sliding motion to translate shaft rotation into linear motion of the piston, but does so in a perfectly sinusoidal fashion. A scotch yoke system generally sees higher stress loads due to the more complex bearing connection between crankshaft and piston, but does allow a simple V twin engine to become perfectly dynamically balanced. The conceptual V twin expansion engine shown in Figure 86 below is perfectly dynamically balanced. It is easiest to envision the scotch yoke V twin as two single cylinder yoke driven pistons connected in a 90 degree phase to one another. In this scenario the piston motion is purely sinusoidal thanks to the scotch yoke, and all vibration of the single piston system would be perpendicular to the stroke axis. When a second single piston engine is attached in proper phase, each system cancels out the lateral acceleration of the other resulting in continuous perfect dynamic balance. The downside to a V twin system is that the power strokes are not perfectly balanced, nor are they evenly spaced since the cylinders are only 90 degrees apart. This leaves the designer to address the torque ripple resulting from power and compression strokes.

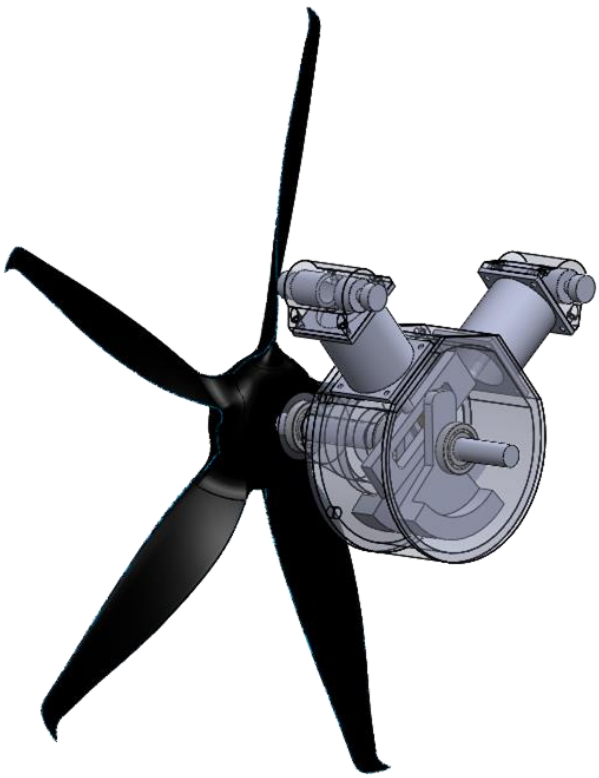

Figure 86 - Dynamically Balanced V Twin Scotch Yoke Piston Engine

MM. Components

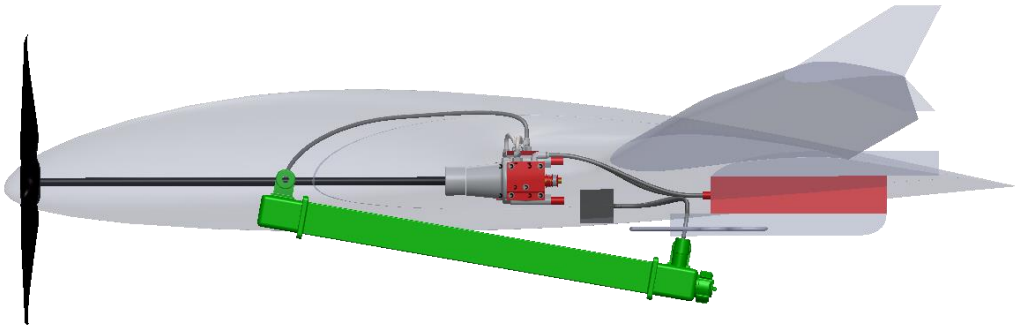

Figure 87 - One Notional Installation of Rankine Cycle Components in a small UAS

Of the components making up the finished piston expansion engine, the piston sleeves, cylinder heads, belt drive system, power takeoff, and mounting extensions were all machined by hand at Oklahoma State

University by the Author. As Shown Below in Figure 88 and Figure 89 these components significantly changed the look, weight, and complexity of the source DA 100 engine which is shown installed with other parts in Figure 87 above. Belt tensioners were 3d printed in Oklahoma State's 3D Printing lab. 3D Printing these components allowed two design iterations in the same afternoon.

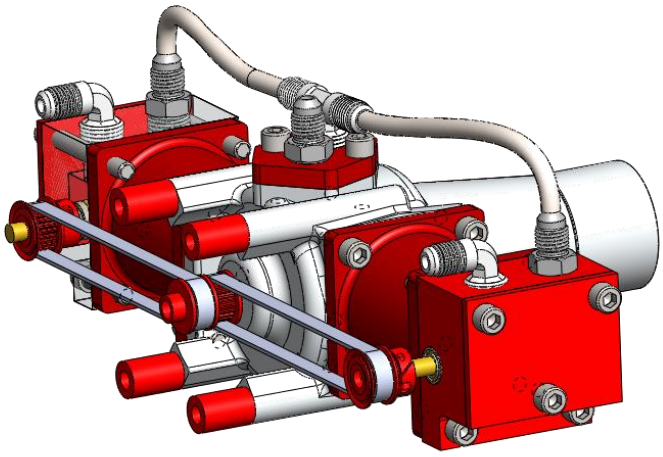

Figure 88 - Solidworks Model of Engine Modifications

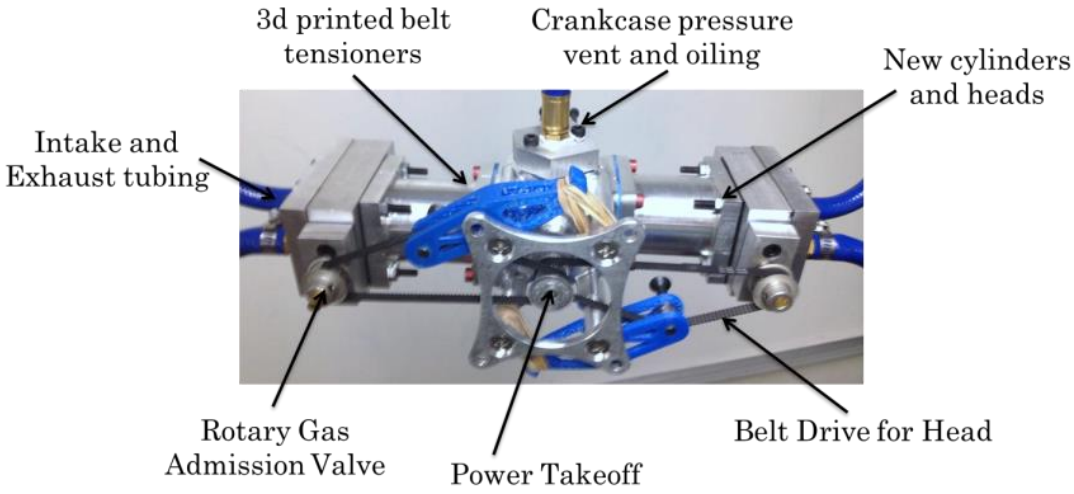

Figure 89 - Annotated layout of ICE conversion to expander

9. Custom Cylinders

The stock DA 100 piston cylinders featured ported cylinder walls, which are a common feature in most scales of two stroke piston engines. These fixed ports allow the piston location to dictate admission and exhaustion of fuel air mix and combustion products. In a closed cycle system the expander is placed after heat addition, unlike a typical 2 stroke internal combustion engine where the heat addition happens near TDC after the fluid has been compressed. This means that a passive admission and exhaust system cannot possibly work for an expansion only engine. Some simple piston steam expanders work by using a pin protruding from the top of the piston to force open a valve when the piston expander system is near top dead center. This method produces a characteristic "ping" noise as the pin impacts the ball bearing valve each revolution making it a less-than-quiet option. Custom cylinders were fabricated to a diametric accuracy of +- 0.002in to work with the stock DA 100 pistons. Cylinder height was shimmed properly with gaskets to account for the dome in the stock pistons. These basic piston sleeves allow all of the gas admission and exhaust control to happen in the cylinder head, and will not suffer from loss of power caused by residual gasses being recompressed during the upstroke following compression. The stock cylinders were made of 100% aluminum, which in retrospect was a poor choice due to its higher coefficient of friction than other materials like ductile iron, brass, or some steel alloys. The main motivation in picking aluminum was similarity to the DA 100 cylinders and light weight. It is important to note that the DA 100 cylinders are lined with hardened sleeves to modify the piston/cylinder wall boundary condition.

10. Rotary Valves

A rotary valve system was created to eliminate the need for complicated cams, followers, and the translation of motion they require to work properly. A cylindrical rotating valve can turn at the same speed and in the same vector direction as the engine output shaft and still properly control gas admission and exhaustion by properly placing ports on the cylinder to control phasing. Unfortunately the first prototype's cylindrical valves were manufactured with the phase angles reversed, causing the engine to only function properly in reverse. This system was still capable of being evaluated for leakage, friction,

and overall suitability to be carried forward. Unfortunately in all of these areas the gas control system was found lacking. The rotary valves in particular exhibited higher than anticipated friction and created a loud squeak after operating for only a few minutes. The rotary valves were made of Brass to lower their coefficient of friction against the aluminum housings, and machined to close tolerance, then lapped to a near air-tight fit. The accuracy of the valves in their rotation sleeves was rather remarkable, as inserting them into their sleeves created an air bearing resulting from the compressed gasses below the valves. For a few minutes it acted as a piston system where the rotary valve could literally bounce on the air column with little friction whatsoever. However once the system was running, this same low friction environment did not last and evidence of minor wear was quickly noticeable. Additionally, even at these best practice tolerances, the rotary valves still leaked a noticeable amount of air through the system when tested with air pressure alone. The valve system did function (in reverse), but was never tested reliably enough to warrant further pursuit.

11. Power Takeoff Shaft

A mechanical power takeoff shaft was added to the DA 100 to allow the main crank to drive the rolling cylinder valve. A small hole was drilled in the back plate to allow the PTO shaft to pass through. The high hardness of the heat treated crankshaft proved problematic when trying to drill and press the precision steel PTO shaft into the existing hole in the back of the crankcase. The drill bit used was damaged by the crankshaft instead of the crankshaft being drilled by the bit. The press fit was reversed by machining a piece of ductile iron in to the shaft size available in the stock crankshaft. This reduced the bending strength of the PTO shaft but was the only reasonable way to proceed without annealing the crankshaft. The PTO is loaded equally in both directions, so the system should be reliable even with a softer metal shaft.

12. Belt Tensioner

The belt tensioner went through two 3d printed design iterations, and eventually proved reasonably successful in allowing rapid modification of the rotary valve timing. The initial design placed 0.5 inch outer diameter bearings in contact with the smooth side of the tensioning belt, but the bearing

were cantilevered out from the tensioning arm axis of contact with the motor frame. While functional, this design tended to twist when impulsively loaded due to friction in the rotary valve system. Thus, the belt tensioners were redesigned to place the bearings in line with the axis of contact with the motor frame, and the 3d printed material supported the bearing axis from both sides. While a bit more difficult to install and modify belt tension, this system proved very effective and quick to implement thanks to 3d printing. Unfortunately, when the engine encountered moments of increased rotary bearing friction, the belt tension would momentarily spike, causing the belt tensioners to actuate and allow the timing belts to slip. With gas admission occurring across only 5 to 10 degrees of engine angle, a slip of even one tooth on the timing belt severely affected engine operation. Tension could be increased on the belt to reduce the possibility of skipping, but this added tension would also create a stronger side loading in the rotary valve head thus increasing the frictional losses causing the root problem. Ideally the rotary valve could simultaneously seal the system air tight and support side loads, but at the available level of manufacturing accuracy, the valve both leaked and seized. Redesign of the rotary valve system allowing for separation of load bearing and sealing components would allow the rotary valve system to work much more successfully. In practice, once the belt skipped, the engine usually stopped running and required recalibration of valve phasing.

13. Crankcase Vent

The conversion of a DA 100 offered the potential to use the back side of the piston to transform the engine into a double acting type. While cylinder heads control gas admission into the normal top side of the piston, because the engine's cylinders are in phase with one another, the crankcase can also act as a power generating expander by admitting high pressure gas into it when the pistons are near bottom dead center. This could be used to have the engine become a double expander, or to simply double the power output over the same expansion ratio. For the initial prototype engine, the prospect of pressurizing the crankcase was not utilized, and instead it was passively connected to the low pressure side of the system. Simply sealing the crankcase would turn it into a pneumatic spring and make the system much more difficult to turn over. Venting the crankcase allows the engine to turn freely while letting some of the

lubricant traveling in the low pressure side gas stream to find its way into the crankcase to lubricate the crank, connecting rod, and piston bearings. The prospect of a double acting engine would alleviate some of the engine's self-starting deficiencies, but not completely. When the engine is stopped near top or bottom dead center, neither side gas admission would likely allow the engine to start up properly, and there is nothing preventing the engine from starting backward. Overall the mechanical complexity and lack of a self-starting mode made the piston expander a lacking design choice.

NN. Testing

The converted DA 100 piston expander was tested on Oklahoma State's medium engine dynamometer to evaluate its base performance as shown in Figure 90. During testing several fundamental problems became evident that lead to different expander options being pursued. The belt tensioners proved inadequate to hold the belt and admission barrel valve in proper phase during peaks of engine friction. The engine exhibited very large vibration when mounted to the rotary dynamometer mount which in turn excited many subsidiary vibrations in the dynamometer apparatus similar to what the engine would do to an airframe. These vibrations are seen in the output measurements shown in Figure 91 The engine required a manual start at every attempted starting phase angle, and produced only limited power and RPM even when fed with high pressure shop air. Lubrication was also a complicating factor as the engine would displace the lubricant applied to its cylinder heads in a matter of minutes and start squeaking loudly. A dedicated lubrication system for the cylinder heads and crankcase would be difficult to integrate alongside the closed loop of operating fluid. Avoiding physical contact entirely would be preferable, yet impossible for positive displacement expanders. Any addition of lubrication to the system operating fluid would decrease performance, and further decrease system power to weight ratio by requiring additional mechanical systems.

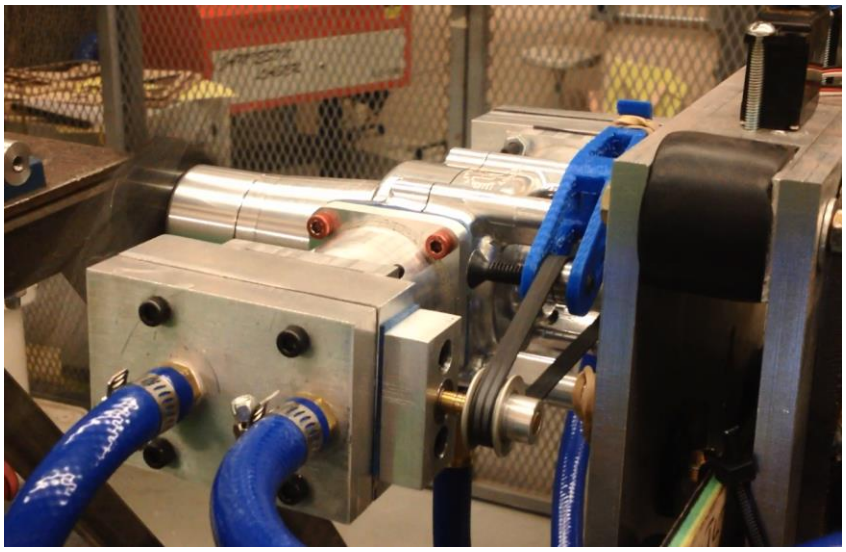

Figure 90 - Modified DA 100 piston expander mounted on dynamometer

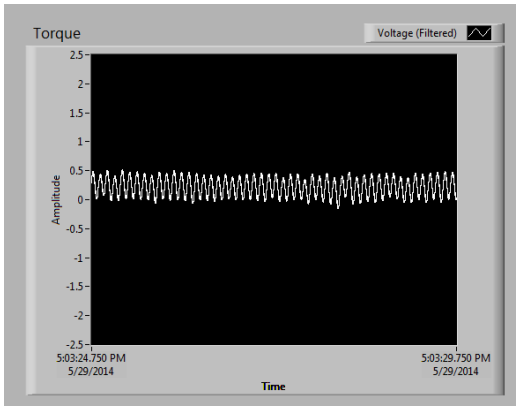

Figure 91 - Example of piston expander vibration.

OO. Acoustic Testing

The converted DA 100 engine was tested in Oklahoma State's anechoic chamber to characterize the base noise of the system. The engine was run on compressed air in a blow down non steady state condition. Pressurized air was fed into the anechoic chamber and exhaust piped back out of the chamber so that any exhaust note would be insulated from the receiving microphones. The engine had to be hand started, so an operator also had to be present in the anechoic chamber during these acoustic tests. The engine was tested with a Mejlik 17 inch 3 bladed propeller mounted as a load to prevent overspeeding.

When one observes the trend of the data, the primary noise peaks are visible from 1000 to 4000 Hz which is unfortunately the prime region of sensitivity to the human ear. When one looks at Figure 92

the narrowband noise spectrum remains below 40 phons when measured at 5 feet. While this seems promising, it is important to note that the engine was only spinning at 1000 RPM due to mechanical and pneumatic losses in the test setup. Faster engine operation closer to the cruise RPM would show much higher sound pressure levels. This data is very useful in characterizing the spectrum of noise of the engine, and what components are creating these noise sources. The acoustic test showed that the barrel valve and its bearings along with a loose crankshaft bearing created the majority of mechanical noise.

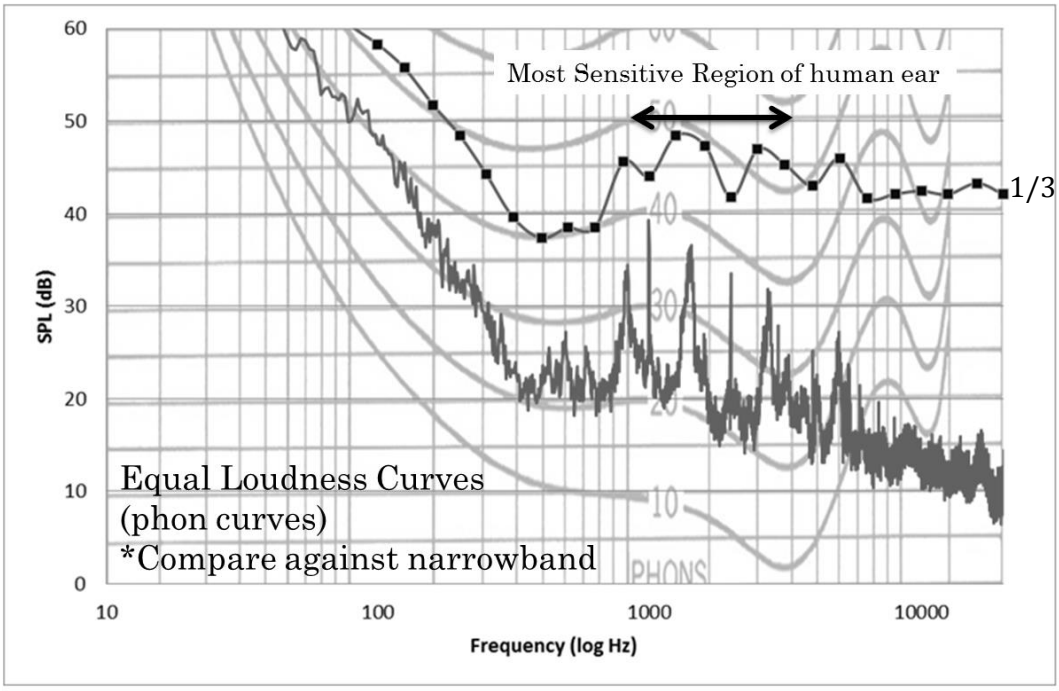

Figure 92 - 1000 RPM piston expander noise spectrum

Vane Expander

Vane motors are similar in concept yet mechanically simpler than radial engines. Both types avoid vibration because nearly every component rotates around a constant center. Torsional vibration as a result of torque ripple is still a factor, and adding more divisions to an air rotor, or more cylinders to a radial engine helps to mitigate torque ripple. Vane expanders would be an ideal option for airborne closed rankine cycles were it not for their reported overall low efficiency shown in Figure 93 and other publications [13]. Large areas of mechanical contact and imperfect sealing were reported by Davidson and Robertson as causes for large isentropic losses. Davidson [13] estimated the expansion efficiency of a multi-vane air motor to be 19.8% at 500 rpm and 30.2% at 1000 RPM.

Leakage and friction between the sizeable rotating assembly and expander casing are listed as reasons for such low isentropic efficiency. Robertson et. Al. also reported in 1977 that their test of a vane expander exhibited low isentropic expansion efficiency ranging from 10% to 21% in tests. This was also attributed to leakage and friction losses.

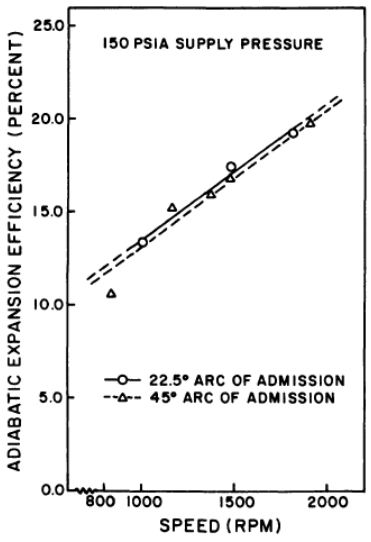

Figure 93 - Robinson et. al. studied the adiabatic expansion efficiency of vane motors

PP. Testing

A simple vane motor shown in Figure 94 was purchased for evaluation in Oklahoma State's acoustic chamber and medium dynamometer. When tested on the dynamometer this vane motor operated exceedingly smoothly with minimal torque ripple and virtually no transmitted vibration into the dynamometer. This vane motor was tested directly after the piston expander, so the difference between the two was even more pronounced and lead to an easier decision to abandon the piston expander development path in favor of an expansion methodology more suitable for low noise and isolated applications. While quiet and smooth running, the vane expander suffers from low efficiency due to large internal leakage, low expansion ratio, and large areas of surface on surface contact that increase frictional losses. Testing of this overweight off the shelf vane motor did prove the value of fundamental dynamic balance and steady torque application.

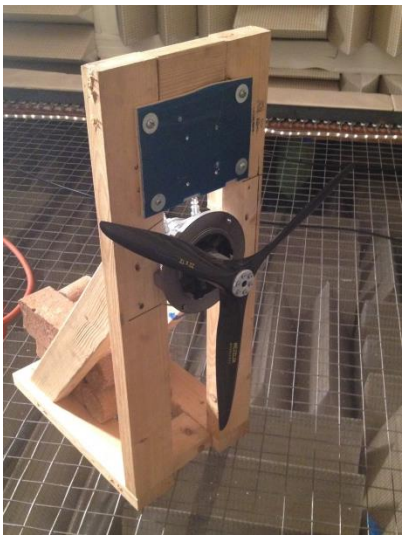

Figure 94 - Vane motor mounted for acoustic testing

14. Acoustic Testing

The vane motor was tested in Oklahoma State's anechoic chamber to evaluate its noise characteristics against the other piston based expander option. The narrowband and 1/3 octave measurements are shown in Figure 95 The vane motor was easier to test as it is a completely self-starting system requiring only the application of pressure into the high pressure side. This meant that the test apparatus could be left alone in the anechoic chamber without requiring an operator in the chamber to start the system. With the application of the same maximum pressure air onto the vane expander it spun the attached Mejlik 17 inch 3 bladed propeller at 1700 RPM vs. the piston expander's 1000 RPM output. This difference is a result of the piston expanders internal losses resulting in lower power output combined with the piston expander's lower admission ratio. Overall in testing the vane motor was considerably quieter, with much of the low frequency noise absent in the vane motor test, and still remaining under 40 phons at 170% of the RPM of the piston expander. This 170% increase in RPM is a significant change in power output as the power required to turn a propeller grows with the cube of RPM holding all else constant.

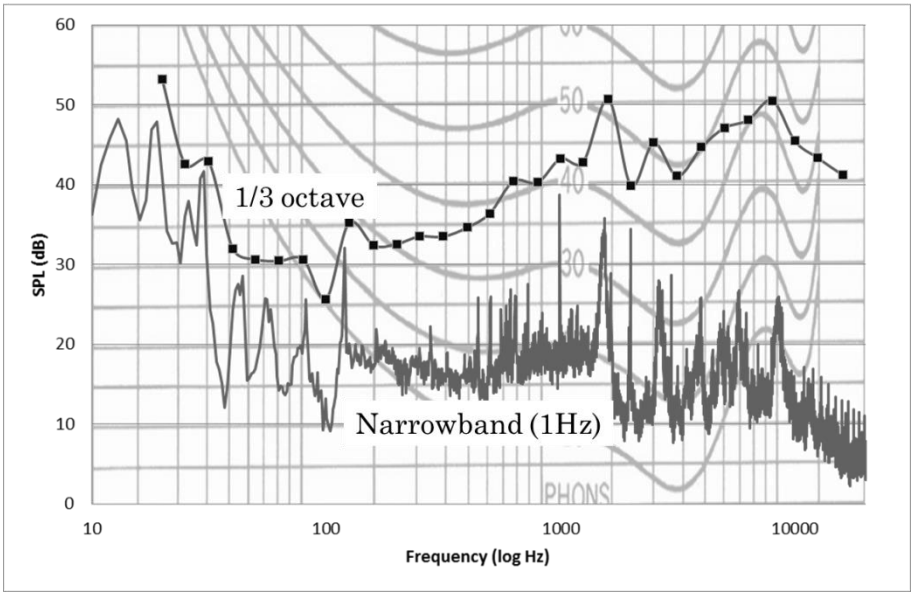

Figure 95 - 1700 RPM vane motor noise spectrum

Scroll and Gerotor Expanders

Gerotor positive displacement pumps are an attractive and dynamically balanceable option for ACC expanders, however in reported tests [14] their efficiency is nearly always eclipsed by scroll expanders. Mathias tested both gerotors and scroll expanders in an Organic Rankine Cycle system and found the performance of gerotors to range from 45% to 66% isentropic efficiency while scroll expanders consistently tested between 50% and 75% isentropically efficient. Scroll expanders exhibited respectable efficiency at a broad range of pressure ratios as shown, making them suitable for partial load operation without large drops in efficiency. The chart below from Lemort's study shows scroll expander isentropic efficiencies at different RPM and expansion ratios in Figure 96 and Figure 97. The system shows consistent efficiency. One should note that efficiency drops at low rpm because of the increased portion of gas leaking around seals.

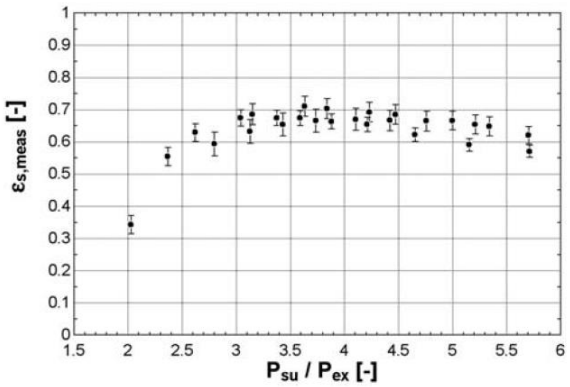

Figure 96 - Isentropic effectiveness versus pressure ratio [15]

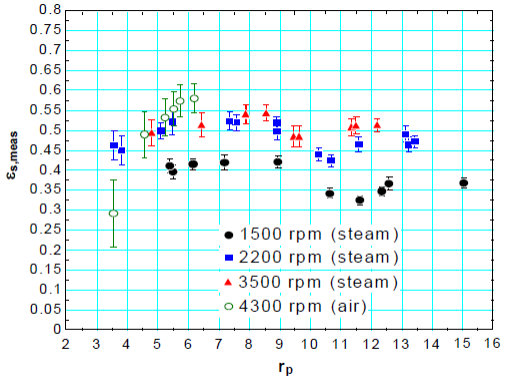

(a)

Figure 97 - Scroll Expander isentropic efficiency as function of expansion ratio (Lemort)

Other studies like Zanelli in 1994 reported 60% to 65% efficiency from 90% to 170% of the scroll's designed pressure ratio. Peterson et. Al. reported volumetric efficiency between 70 and 85%. And Mathias et. Al. tested scroll expanders with multiple fluids and operating conditions and found the isentropic efficiency ranged from 50 to 83 percent. These studies for small scale stationary ORC applications show scroll expanders to be a versatile and efficient positive displacement expander

QQ. Modifications

Figure 98 - One Way "Check" Valve that was removed from the TRSA Compressor to Allow it to Function as an Expander

Figure 99 - Primary Orbiting Scroll Component (shown without sealing gasket)

A stock TRSA12 scroll compressor for automotive air conditioning systems was purchased and modified to act as a scroll expander by removing the one way valve shown in Figure 98. Modifications consisted of removing the unnecessary belt drive and electromagnetic clutch from the primary shaft, opening the expander and removing the one way valve that would otherwise prevent the scroll from operating in expansion mode, and ultimately saw the replacement of the spherical ball bearings with ceramic to prevent rapid corrosion in the presence of water. The primary scroll is pictured in Figure 99 covered in

shipping oil. The scroll compressors were shipped with generous amounts of PAG (polyalkylene glycol) oil in the system that must be cleared, as this oil can react with water to form a mildly acidic solution that can lead to pitting and enhanced corrosion of components.

RR. Testing

A brief evaluation of the scroll compressor was conducted with compressed air before adding the expander to the closed loop system. When run on shop air at up to 120 psi, the scroll compressor reached an RPM of 3600 to 4000 RPM which is much higher than either the vane motor of piston expander was capable of reaching. The scroll compressor did exhibit some vibration even when mounted firmly to a thick steel welding table. This vibration is a result of the low cost automotive compressor being dynamically imbalanced. Unlike the piston expander, there is no fundamental reason this scroll compressor could not be dynamically balanced. The mechanical solution for perfect dynamic balance is straightforward and easy to implement, but likely for reasons of cost savings and total compressor volume was omitted from the cheap automotive compressor. A purposefully designed scroll expander for aircraft applications could be designed to be perfectly dynamically balanced.

SS. Corrosion

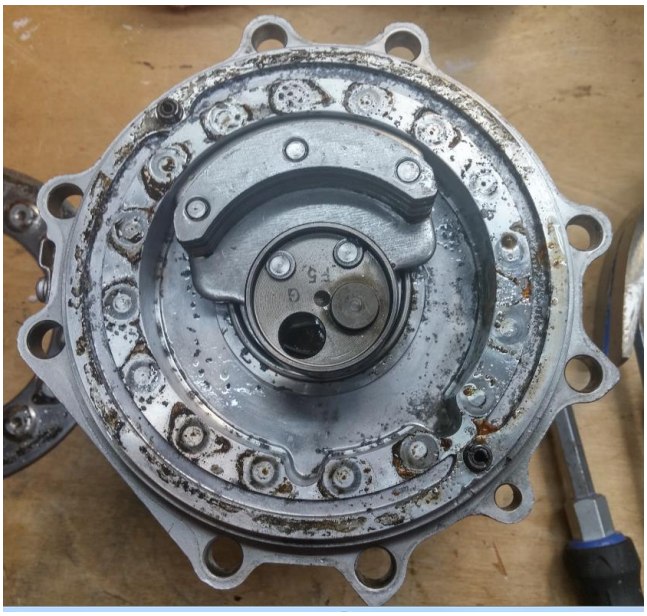

Figure 100 - Corrosion of Internal Components One Week After Initial Tests.

When the scroll compressor was first run with steam, the system suffered rapid and very detrimental corrosion of internal bearing surfaces shown in Figure 100 to the point that one week after testing the scroll expander would no longer rotate. From this failure it was learned that the PAG oil mixing with water enhanced pitting and corrosion of metal parts. Additionally, as the scroll compressor was disassembled part by part it became evident that no attempt had been made to limit galvanic corrosion in the system as many different types of metal were found in direct contact with one another in the system. Aluminum, Steel, Iron, and Magnesium were all found in different components of the scroll expander. A purposefully designed aircraft scroll expander should be made from the same type of metal throughout, with proper galvanic insulation between components using plastics and other materials where appropriate. This corrosion results from using a cheap modified scroll compressor in place of a purposefully designed aircraft scroll expander. Overall due to the time and design effort saved from using a modified off the shelf component, it is still worthwhile for this prototype to use the automotive scroll compressor, but if the prototype system proves even moderately successful, design effort should be devoted to creating a better suited mechanism for expansion.

Turbine

If one were to drive a propeller with the power generated from a Brayton cycle the propulsive efficiency would massively improve. For quiet systems this leaves the problem of transforming the high-rpm output of a turbomachine Brayton cycle into higher torque low RPM power suitable for a propeller. Mechanical systems offer reasonable transmission efficiency, but classical straight tooth gear systems cannot be considered quiet. Some more modern mechanical drives employing constant contact helical gears, harmonic drive reduction, and other high-ratio gear systems might offer reduced noise production, however mechanical transmission through gear meshing would remain.

TT. Magnetic Gearboxes for Turbine Speed Reduction

The growing use of neodymium magnets in common technologies has yielded the creation of magnetic gearboxes which offer many potential advantages for efficient turbomachine speed reduction. While many magnetic gear systems simply use the opposing magnetic fields as gear “teeth” that mesh in a

very traditional sense without contact, an even more compact and useful method of reducing speed with magnetic gears exists by employing a material with high permeability to modify the field attached to the power input shaft and transform it into a field that spins an output shaft consisting of a higher number of magnetic poles at a much slower speed. These systems have demonstrated high efficiency operation, low mechanical vibration, and without physical contact, they eliminate the noise generated through physical gear meshing. Limitations of magnetic gearboxes include the demagnetization temperature limit of the magnets themselves (samarium cobalt offers higher temperature limits than neodymium if required), as well as the "slip" torque point at which magnetic fields are forced past one another. The slipping torque when used properly could offer advantages like limiting torque feedback into the turbomachine in the event of a prop strike or other failure.

Two distinct varieties of electromagnetic gearboxes exist; designs that use a ferrous gate to transform the magnetic field between input and output shaft to establish a large gear ratio as shown in Figure 101, and those designs that use magnets as direct replacements for traditional gear teeth, but without contact as shown in Figure 102. These magnetic teeth can also easily act as non-contact couplers that function just as well through non-conductive divisions in pressure vessels. It is important to control the materials present around these moving high power magnets not only for reasons of safety, but also for the sake of efficiency. If a large magnetic coupler were designed with an aluminum wall hermetically sealing the input from output, the rotating magnetic field would encounter a drag force due to the eddy currents generated in the conductive aluminum wall. With sufficient power input, the internal resistance of the aluminum wall would heat the material enough to weaken or melt the aluminum to the point of failure. Because of these detrimental eddy currents, a non-conductive dividing plane made of plastic, ceramic, etc. should be utilized to achieve similar isolation without magnetic drag and heating.

Aside from the benefits of contactless efficient operation, magnetic gearboxes are also capable of duplicating more complex mechanical gear sets like crown, bevel, worm, and perpendicular helical sets.

The utility of magnetic materials in gearboxes is just now being realized after the advent of strong rare earth magnets.

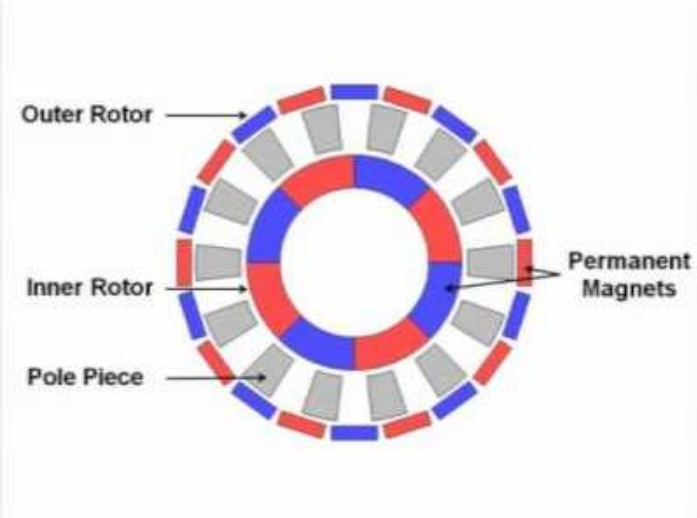

Figure 101 - concentric magnetic gearbox using ferrous comb to transform field between input and output [16]

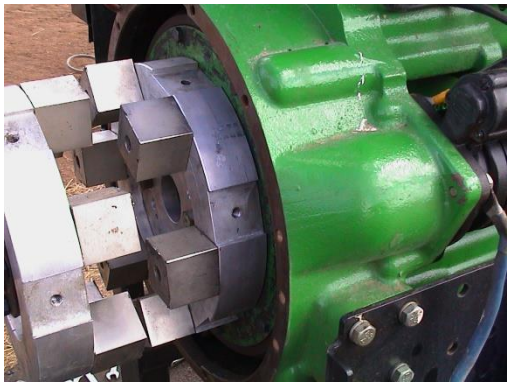

Figure 102 -Large contactless magnetic coupler using magnets in place of gear teeth. [17]

UU. Turbine Expander Design Overview

A low rpm high power gas turbine expander would be ideal for airborne closed cycle applications, the the optimal blade speeds for impulse and reaction turbines make small diameter turbines impractical. Optimal impulase blade speeds are half the incoming gas velocity, meaning that a 6 inch diameter impulse turbine disk spinning at optimal blade speed on steam would reach 30,000 RPM and ideally generate 420 watts of power. If one remains limited to subsonic turbine operation the maximum steam pressure ratio per stage is 0.6 causing the turbine to use 4 to 5 stages to capture energy across the full system pressure drop as supported by Figure 103. Preliminary turbine CAD models for the notional 1HP UAV ARC turbine predicted weights near 10 lbs resulting in quite poor power density even before accounting for viscous and leakage losses. Additionally, use of a high RPM turbine will generate significant bearing mechanical noise which negates one of the main advantages of closed cycle propulsion.

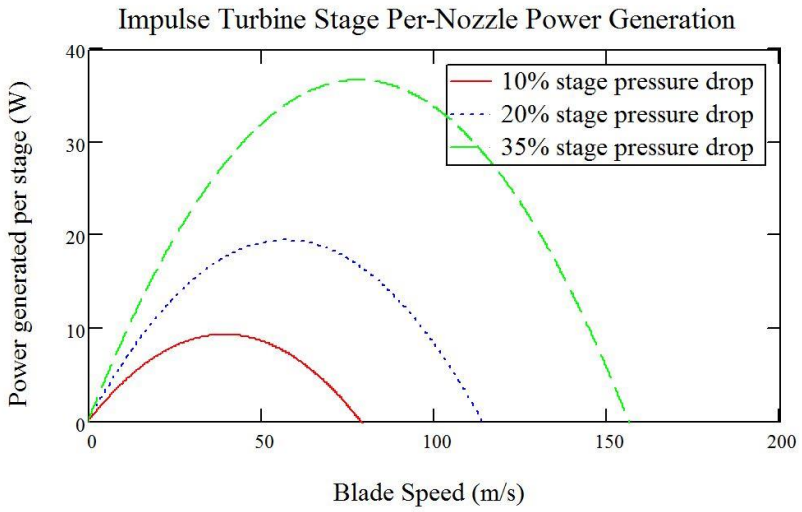

Figure 103 - Impulse Turbine Power Generation

15. Impulse

Turbine expanders for larger ACC applications should not be neglected. If the aircraft can fit large diameter turbine disks, the shaft output RPM drops tremendously eliminating noise and the need for a gearbox. The blade passing frequency remains high, but the poor transmission coefficient between air and the turbine case would help a designer limit noise propogation into the atmosphere. Turbines are the most power dense option for ACC engines. Pini et. Al. published about their design for a 6 stage pancake reaction turbine shown in Figure 104 for a stationary ORC. This 1.3 Megawatt (1743 HP) 4.6 ft diameter turbine used 10 bar inlet pressure at 3000 rpm and reached an isentropic efficiency of 89%.

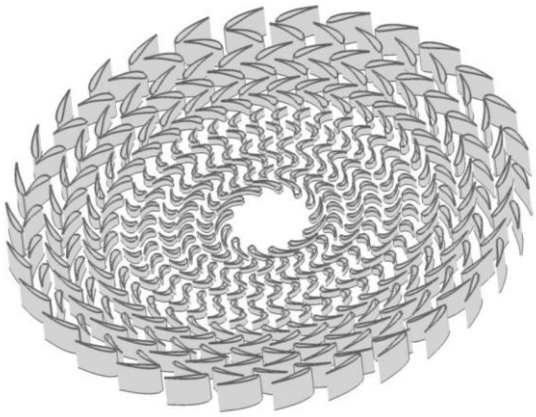

Figure 104 - Pini et. al. designed 1.3 MW pancake turbine [18]

Velocity compounded impulse turbines, re-entry turbines, regenerative turbines, and other methods were investigated to lower the output speed for small diameter turboexpanders. Of all these methods the velocity compounded and regenerative turbines offered the best combination of enthalpy drop and output shaft speed, yet both are reported to exhibit low effieincy due to viscous losses. Folding of the flow stream across many vanes to reduce output shaft velocity inherently produces viscous losses that rob the turbine of efficiency. In the case of a regenerative turbine, the helical flowpath around the rotor periphery results in the stream continually shedding power to viscosity. Multistage velocity compounded impulse turbines can achieve large enthalpy drop and low shaft speed, but are mechanically large and quite heavy.

16. Impulse turbine

17. Velocity Compounded Impulse

While the base impulse turbine uses one row of nozzles to accelerate the flow to near Mach 1, and a second to harvest this converted momentum, a multi stage velocity compounded impulse turbine uses many stages to slow the gas flow from each nozzle acceleration down to useable speeds. One should note that many expansions (nozzles) will still be required to fully expand the operating fluid across even modest pressure ratios while maintaining subsonic operation. For a turbine operating with air, each stage can only support a pressure ratio of 1.89 before the flow becomes supersonic and losses due to shocking ruin the performance of the turbine. This approach means that the output shaft speed of the turbine follows an inverse relationship with the number of stages in the expansion. As high output shaft speed is the primary detriment of small turbine engines, this technique for lowering that speed is attractive yet undermined by the contorted flow path and additional losses it requires. Especially in systems discussed in this study with low mass flow rate and high enthalpy drop, a velocity compounded turbine would weigh considerably more than most other options due to the large mechanism involved.

18. Center Exit

This style of turbine is advantageous in that each stage of the turbine can efficiently capture nearly all of the accelerated gas flow by forcing it to exit at the center of the turbine disk as shown in Figure 105. The relation between input and output angular momentum expressed in the Euler turbine equation makes it readily apparent how forcing a flow to exit at the center of the turbine disk and in a plane perpendicular to the axis of rotation can lead to high turbine efficiency. Additionally, if the center exit turbine is made to expand the gas as it passes through the stage, that momentum can also be imparted into the turbine.

Figure 105 - Typical Automotive High Flow Center Exit Turbomachine made by GS Industries in India

19. Helical and Re-entry Turbines

Helical turbines as depicted in Figure 106 offer perhaps the most mass efficient method of expanding small mass flows across large pressure differentials. The fundamental premise of a helical turbine is that the operating fluid is injected perpendicular with the turbine disk and in-plane with the turbine output shaft. The periphery of the helical turbine acts as rotor blades, while the inside of the turbine housing acts as stators. The operating fluid flows in a helical path around the turbine disk forming a toroid of spinning fluid. This allows the operating fluid to undergo multiple sequential expansions while also keeping total turbine rotational speeds low. The turbine free speed can be determined by the pitch of the operating fluid helix and velocity the fluid is accelerated to. While this turbine arrangement should prove advantageous over multistage impulse turbines, the helical turbine will still lose efficiency to large lengths of viscous losses magnified by the local acceleration of the operating fluid in the helix.

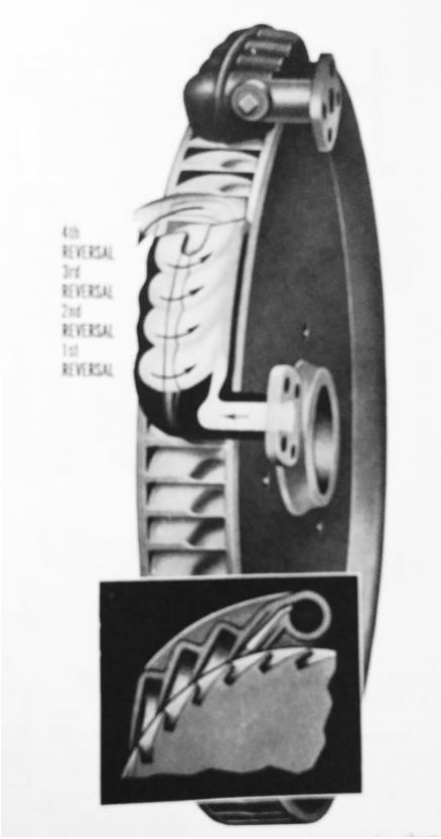

Figure 106 - Diagram of helical turbine [19]

Re-entry turbines are similar to helical turbines in that a single blade disk will serve to expand the same operating fluid multiple times by utilizing the turbine case stator blades to reverse the flow. Re-entry turbine flow paths are generally two dimensional implementations of helical turbines and are much less space efficient as a result as evident in Figure 107. Optimal turbine speeds are similar to those of basic impulse turbines (half of inlet velocity) so there are no major RPM advantages for small aircraft re-entry turbines. Because re-entry allows multiple expansions on a single disk, it can offer a weight reduction to the system.

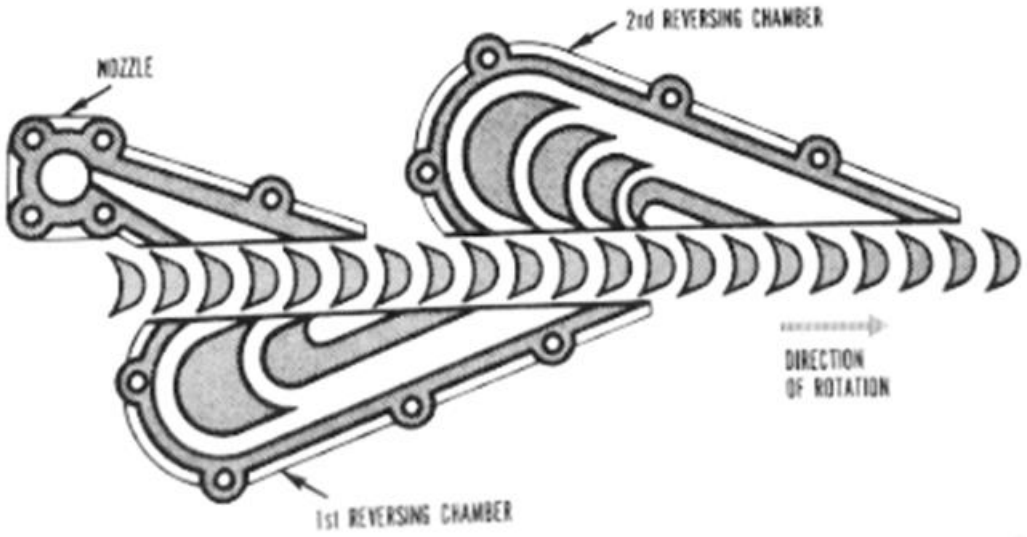

Figure 107 - Re-entry turbine schematic from [19]

There are few examples of helical turbines available for study in literature on in service. The helical and re-entry turbines that are described in use are found in steam ships that use them for auxiliary power. They are labelled as less efficient, and have fallen out of favor as more modern ship systems are using electrical power distribution in place of steam.

VV. Optimal Speed

Each type of turbine exhibits an optimal blade speed that can be expressed as a fraction of the incoming fluid velocity into the turbine after acceleration through a nozzle. Ideally all of this velocity would be purely tangential with respect to the rotational axis, but the nozzle must admit fluid at some measurable angle or no net flow could pass through the turbine stage. This real peripheral velocity is marked as cos(a) where alpha is the deviation away from pure peripheral velocity. Figure 108 shows the optimal turbine speeds expressed in this ratio. While these speeds may represent the mathematical optimal, in many cases the efficiency of turbine stages does not decrease precipitously away from these optimal speeds. The off design performance is much more configuration dependent.

$$\frac{V_b}{V_1} = \frac{\cos(\alpha)}{2}$$ Simple Impulse

$$\frac{V_b}{V_1} = \frac{\cos(\alpha)}{2 \cdot n}$$ n Stage Velocity Compounded

$$\frac{V_b}{V_1} = \cos(\alpha)$$ Reaction

Figure 108 - Optimal turbine speeds for common turbine types

Aside from the optimal blade velocity it is important to understand how much power each type of turbine can produce when at its peak condition. Figure 109 shows the work resulting from each stage of common turbine types. One might observe the stage multiplier in the numerator and see this as an opportunity to magnify the power output of a velocity compounded stage, but the reduction in the square of blade speed undermines the work gained back through additional compounding.

$$w = \frac{2 \cdot V_b^{\,2}}{g_c}$$ Simple Impulse

$$w = \frac{2 \cdot n \cdot V_b^{\,2}}{g_c}$$ n Stage Velocity Compounded

$$w = \frac{V_b^{\,2}}{g_c}$$ Reaction

Figure 109 - Work capability at optimal speed for common turbine types

WW. Turbine Efficiency Relationship to Blade Speed

Use of the basic compressible flow relationships from Equation 2 can show that turbines are highly dependent on blade speed for efficient operation. The inherent nature of subsonic turbine speed

only being bound by the sonic speed of the operating fluid means that understanding the theoretical relationship between turbine speed and efficiency.

$$P(Pt,M,\gamma) := \frac{Pt}{\left(1+\frac{\gamma-1}{2}\cdot M^2\right)^{\frac{\gamma}{\gamma-1}}}$$

$$T(Tt,M,\gamma) := \frac{Tt}{1+\frac{\gamma-1}{2}\cdot M^2}$$

$$a(\gamma,T) := \sqrt{\gamma\cdot\frac{8314}{MW}\cdot T}$$

$$V(M,\gamma,Tt) := M\cdot a(\gamma,T(Tt,M,\gamma))$$

$$\rho(\gamma,Pt,Tt,M) := \frac{P(Pt,M,\gamma)}{\frac{8314}{MW}\cdot T(Tt,M,\gamma)}$$

Equation 2 - Common Compressible Flow Relationships

When Figure 110 is compared to Figure 112 one can see the influence that operating fluids of differing molecular weight can have on sonic speed and compressible characteristics when looking at the problem in dimensional units. Figure 111 and Figure 113 demonstrate the similar difference between density and velocity vs. Mach number. For this example the total pressure of both fluids was kept at 100 psi and total temperature at 500K. Steam with a molecular weight of 18.02 g/mol has a significantly higher speed of sound than R123 with a molecular weight of 152.93. Again, the designers preference will be determined by the design objective. If one wishes to make the turbine quiet, cheap, and long lasting then slow speeds will be advantageous to permit use of cheaper bearing types. If the design objective is to maximize the power density of the turbine system, high speed operation is superior in capturing more enthalpy per stage. This is a result of enthalpy drop being proportional to the square of change in velocity. Most turbine systems are bound by sonic velocity as a result of the shock losses incurred if

velocities are increased to supersonic. If one were to desire the maximum power density from a small turbine, hydrogen offers the most advantageous molecular weight to maximize the speed of sound and resulting enthalpy drop per unit mass.

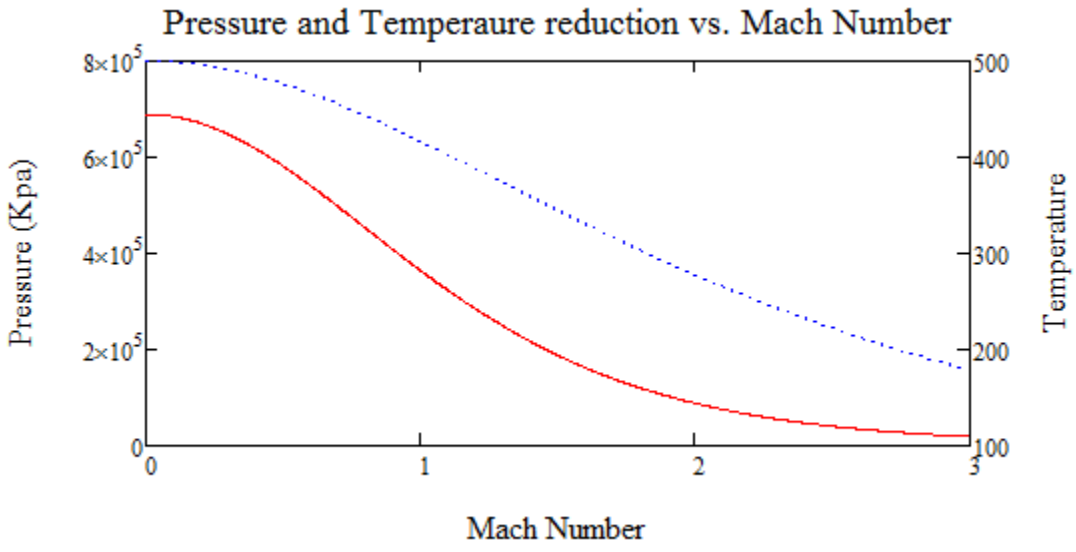

Figure 110 – R123 Pressure and Temperature Reduction vs. Mach number. Total pressure 100 psi, total temperature 500K

For this prototype system that is being designed with low cost and low noise in mind, a heavy molecular weight fluid exhibiting a smaller sonic speed would be advantageous to choke the flow and minimize turbine speed. The drawback of this compromise for low turbine speeds is that multiple stages will be required to efficiently harvest the desired dV. One could substitute significantly higher mass flow to make up for the specific power loss resulting from lower flow velocity, but the mass flow of the turbine is dictated by the overall cycle power output to be extremely small in the case of Rankine cycles. Typically this mass flow for a 1HP UAV based system is on the order of 0.003 kg/s for steam based Rankine cycles. Lowering the power output of the turbine without decreasing the inlet mass flow is the definition of decreasing efficiency, while raising the mass flow of the system to allow a single stage to fulfil power demands will simply result in an increase in power required to heat that fluid to input enthalpy. It is most useful to view the balance of power, turbine speed, and efficiency on a per unit mass (specific) basis to demonstrate the constraint of low mass flow rate.

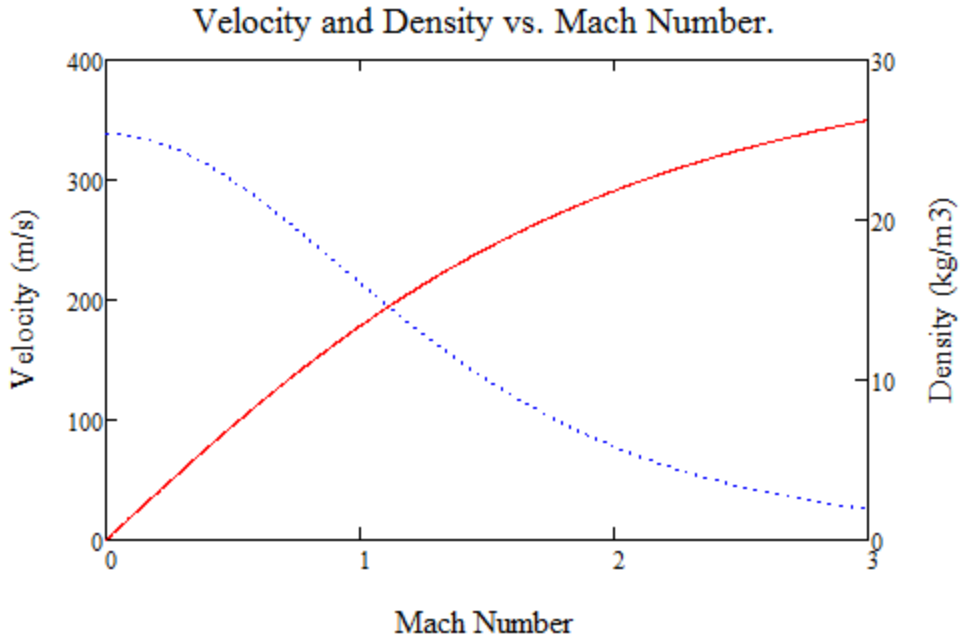

Figure 111 – R123 Velocity and Density vs. Mach Number. Total Pressure 100 psi, Total Temperature 500K

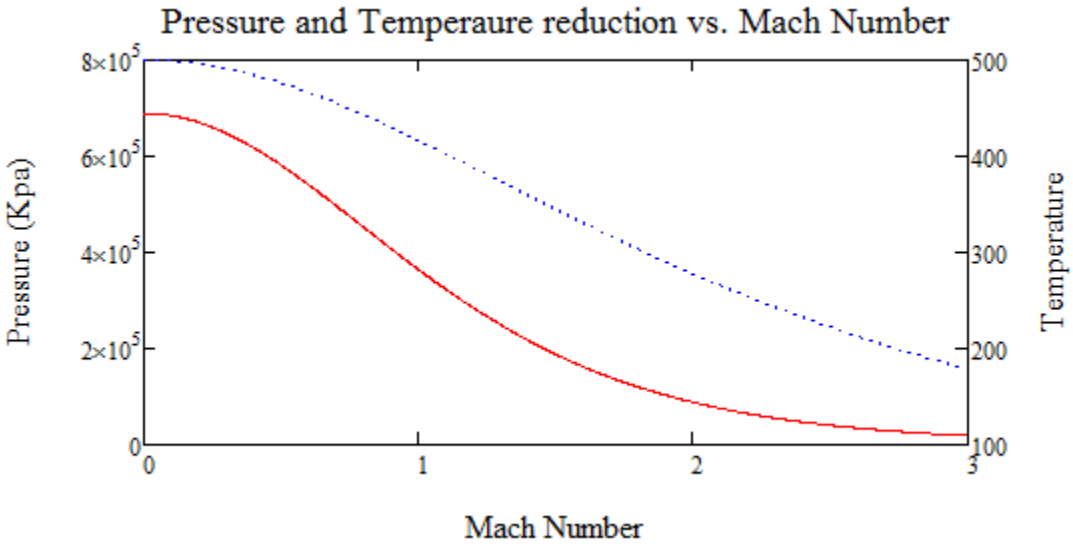

Figure 112 - Steam Pressure and Temperature Reduction vs. Mach number. Total pressure 100 psi, total temperature 500K

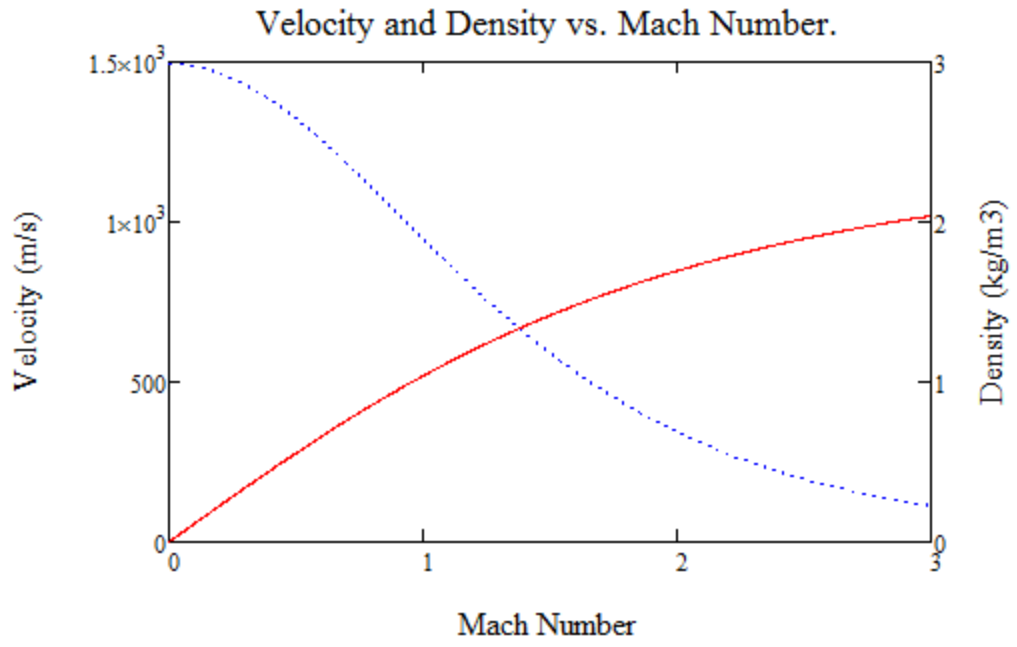

Figure 113 – Stream Velocity and Density vs. Mach Number. Total Pressure 100 psi, Total Temperature 500K

All of this common knowledge buildup is required to show the power generated by a single stage and the efficiency changes that occur in off design conditions. The power generated per stage is shown in Figure 114 which also as a result demonstrates the relative efficiency as a function of blade velocity RW for impulse turbines. It has been discussed that the optimal blade speed for impulse turbines is half of the inlet velocity so that the fluid is brought to a near rest after passing through the impulse stage. This represents the scenario where the turbine is able to harvest the most kinetic energy from the flow. It is no surprise then that cases where the inlet nozzle generates less kinetic energy (lower pressure ratio) do not generate as much total power. It is useful to note that in these cases, the slower incoming gas speed does allow for slower optimal blade speeds which will help to make the turbine quieter and more affordable. Unfortunately the enthalpy drop per stage at low velocity is prohibitively low, even at optimal conditions only generating ~80 Watts and therefore requiring 10 stages to generate the design power of 1HP. Higher Mach number nozzles generate up to 300 watts per stage, but do so at the expense of required blade speed. If one were to consider velocity compounded impulse turbines in a similar chart, the power levels

would drop according to the viscous losses incurred, and the velocity scale would be halved for each stage of velocity compounding.

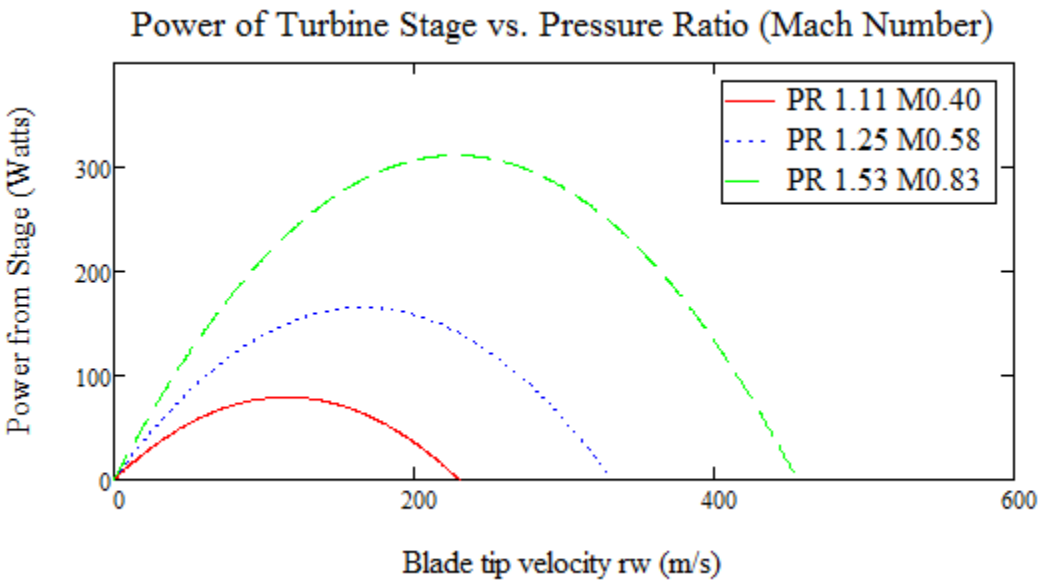

Figure 114 - Power of Impulse Turbine Stage vs. Pressure Ratio (Mach Number) (Steam)

Considering only the term rw disassociates the designer from the true implications of making a small diameter turbine for use in small UAV's. If one were to make a turbine the size of a typical RC electric motor, approximately 5cm in diameter, the required speed of the Mach 0.8 stage shown above in Figure 114 would be 118,000 RPM. At this speed and diameter the peripheral blades would experience 392,000 times the force of gravity, which poses a significant load on the turbine blisk. To assist in considerations of the relationship and design tradeoffs between radius, blade speed, and required RPM, the conversion is visualized in Figure 115 below.

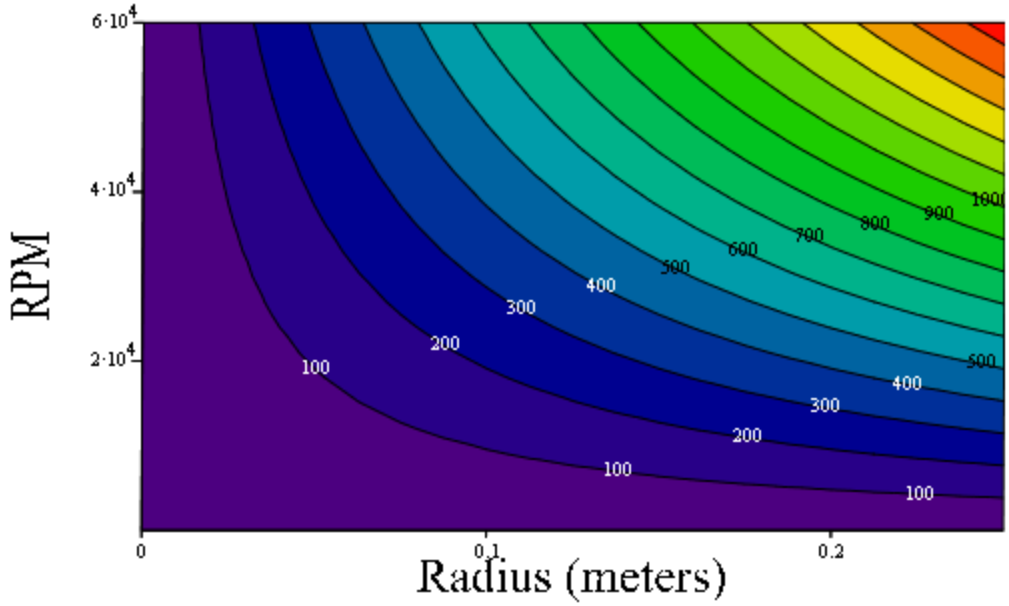

Figure 115 - Reference for Governing Parameter rw vs. RPM and Turbine Radius

XX. Design Strategies for Reduction of Optimal Speed

Aside from the schematic changes allowed by the turbine types discussed previously, one is only left velocity and mass flow as methods of changing the optimal speed of a turbine. Optimal speed is typically expressed as a fraction of inlet velocity, so a drastic reduction in inlet velocity will also directly result in a drastic reduction in the optimal blade speed. However since enthalpy drop per stage is proportional to the square of the fluid inlet velocity, the slower fluid does not create as much power per unit mass. If one were to design an overall system with low pressure and high mass flow in mind, a small turbine spinning at acceptable speeds (less than 20,000 RPM) could be made. Small Rankine cycles require high pressure ratios to remain efficient, and thus require multiple expansions and low mass flow to create power suitable for SUAV's. However, small regenerative closed Brayton cycles become more efficient at low pressure ratios and higher mass flow than Rankine cycles. A RCBC paired with a "large" mass flow center exit turbine could generate similar power levels to a closed Rankine cycle and with better efficiency and lower BLEVE (boiling liquid expanding vapor explosion) risk.

Boiler Design

For the Rankine cycle based demonstration system, the boiler is by far the most hazardous component. Even though the power input to the boiler is modest at approximately 10KW for 746W output (1HP), the hazard arises from the amount of energy stored in the boiler system during operation and not the flux of energy through it. A failing boiler containing 1 liter (mass 1 kg) of water at 100 psi (6.895 bar saturated at 164.34 C) and evacuating instantly (expanding adiabatically and isentropically) to atmospheric pressure would discharge 326 KJ of energy. For comparison, this BLEVE explosion is equivalent to one third of a classical 8"x1.25" stick of dynamite which makes it an extremely serious safety hazard. If the pressure vessel were to rupture, this water would flash to steam 0.667 kg/m^3 and occupy a volume 5.4 times that of the former vessel nearly instantaneously. The shock wave and hot gasses generated from this event would be the main hazards.

While safety of the boiler design is important, one must not overlook the overall efficiency of the boiler as any losses incurred during heat input scale the overall system efficiency accordingly. Boiler efficiency is defined as the ratio of heat rise in the operating fluid over the heat input to the system. If the boiler is insulated well, and losses through its walls can be safely neglected, this efficiency can be practically measured by gauging the exhaust gas temperature alone. In a perfectly operating crossflow boiler/heater, the exhaust gasses would be cooled to atmospheric temperature. The heat exchanger design that most closely approximates this is quite large as most of the heat transfer would have to occur over a very narrow temperature margin within. Therefore the practical goal is to minimize the temperature difference between exhaust gasses and ambient while keeping the heat exchanger within size and weight constraints. This goal of minimizing the exhaust gas temperature differential grants another advantage to organic fluid based systems. Since most refrigerants boil below ambient temperature at atmospheric pressure, power cycles employing them as an operating fluid can be pressurized such that the operating fluid's lowest encountered temperature corresponds exactly to ambient temperature plus the heat exchange delta. Steam based systems will always waste at least the bottom 100C of combustion heat above ambient. One might suggest that the condenser could subcool the condensate to ambient

temperature to allow this boiler heat to be captured, but this just moves the unnecessary loss from the boiler side to the condenser, resulting in the same overall problem.

Boilers can be classified into two main groups based on which containment vessel is inside the other called either Watertube or Firetube boilers. While both accomplish the same task, they do so with very different benefits to boiler weight, efficiency, and safety during pressurized failure.

YY. Combustion Efficiency

While combustion optimization and efficiency is not the main focus of this paper, it is important to note the differences observed between air atomized heavy fuel combustion and gaseous propane based combustion. Initially, an air blown atomizer for heavy fuels was used as it allows direct control of fuel to air ratio by the planned onboard digital engine controller. The system could easily modulate air pump power to control the amount of excess air supplied to the system and therefore control combustion efficiency and flame temperature. However, in practice the air driven nozzle selected from a diesel fueled space heater proved extremely heavy and loud. The motor driven vane air pump was much louder than the combustion occurring in the middle of the heating coil. Additionally as shown in Figure 116 the combustion process produced significant soot that covered the heating coils and leads to decreased heat transfer with buildup. This example of soot on the heating coils is after only 20 minutes of run time. It is interesting to note the two distinct types of soot visible. In the center one finds glossy smooth coating that resulted from direct flame impingement. The surrounding coil shows a dull matte finish, indicative that this region experiences lower temperatures.

Figure 116 - Soot Formation from Heavy Fuel Firing of Coil Boiler.

As a result of this soot formation, loud air compressor, and heavy components the attempt to utilize a heavy fuel burner for the prototype system was transferred to follow on work, and a much cleaner propane burner was used. This type of combustion is much easier to control, safer to operate, and lighter weight for prototype system installation. The propane based burner is not optimal for real system use as the tank weight associated with the propane burner is wasted. The eventual project goal would be to initialize heavy fuel vaporization through electric heating, establish a gaseous mix of air and fuel, combust this mix much like the propane heating system presently used, and then as the system comes up to temperature transition the gasification of heavy fuel away from electric heating, and let the flame provide the heat necessary for vaporization. This type of system is employed in high speed hydroplane steam engines. The drawback of such a self-heating system is that it is possible to overheat the fuel during the gasification stage causing pyrolysis and eventual blockage of the fuel tubing. With proper modulation of heat around this gasification stage, this pyrolysis effect can be avoided.

ZZ. Firetube

Fire tube boilers are very obviously named because the combustion gasses pass through smaller tubes inside of a larger water filled pressure vessel. Because of the multiple parallel constant temperature (due to water phase change) narrow channels the combustion gas must flow through, fire tube boilers make efficient heat capture relatively simple to calculate and implement. Unfortunately, since these combustion tubes must pass into, be contained within, and then exhaust from a larger water filled pressure vessel capable of withstanding the highest cycle temperatures and pressures the overall system is rarely lightweight or safe. This safety and weight concern arises because high aspect ratio pressure vessels (tubes) are naturally more weight efficient than low aspect ratio vessels (pills). Additionally, the presence of welded, brazed, or otherwise connected pass-throughs for combustion gas in the pressure vessel creates stress concentrations that further raise the necessary weight to safely use a fire tube boiler. For mass insensitive applications like trains, power plants, or boat steam generators, fire tube boilers are most often used in practice. But for airborne applications, the large pool of operating fluid and need for a complex, high strength pressure vessel exposed to damage and with minimal protection against BLEVE makes fire tube boilers a concerning option

AAA. Water tube

Water tube boilers offer an inherent safety benefit in that if the pressure side becomes ruptured, the sudden vaporization of steam is controlled by the choked pipe flow and kept to safe discharge levels. In some designs, the evacuated steam in a failed water tube boiler is used to extinguish the flame and turn off the boiler system in the case of a pressure tube rupture. While starting with a water tube boiler in the prototype airborne Rankine cycle, difficulty was encountered in coiling tubing close enough to encounter all the combustion gasses or finding finned tubing that could withstand the heat of combustion products available inside the budget of this prototype. The simple water tube boiler created for testing consisted of 1/4” stainless steel tubing coiled into a 5” diameter helix inside of a sheet metal flame can. While this system was adequate to generate steam when a high heat kerosene flame was placed in its core, there was never any chance of the system being efficient. The hottest portion of the flame passed directly through the open center of the coil without impinging on water tubes at any time. During evaluation this simple

coil and air driven kerosene burner exhibited many negative traits. Fuel pooling, large soot generation, flame emission from the back, low efficiency, high noise from the kerosene nozzle air pump, heavy weight (5 lbs.) of the kerosene nozzle air pump, etc. This test boiler was abandoned due to noise and fire hazard in favor of a propane fired boiler for testing and evaluation. Implementation of a heavy fuel burner was detached from the project into a follow on work item to keep design and testing efforts centered on core cycle development. Use of a propane flame will be quieter, safer, and cleaner than the attempted heavy fuel burner. A second water tube boiler is being constructed to work with propane. This boiler will use $1/8^{th}$ inch stainless tubing as water tubes to allow for a more easily compacted tubing core. The larger ¼ inch tubing is adequate in size to choke expansion in case of a tube failure, and allow sufficient heat transfer, but was too difficult to bend into small diameter coils which limited heat capture in the absence of fins attached to the coils.

Condenser Design

The key energy savings of a Rankine cycle comes from being able to recompress the operating fluid easily by doing so in an incompressible state. This minimizes the work required to elevate pressures back to expander admission levels so heat can be added back to the fluid and the cycle continues flowing in the same direction. Since the gasses coming out of the expander are usually far from completely condensed (though some condensate may have formed if the expansion ended in the two phase region of the fluid) a cooling heat exchanger is necessary to turn this vapor mix into cooler condensate. A finned tube liquid to gas heat exchanger makes the most sense for use here as the internal heat transfer rate will not be restrictive as a result of extremely high heat transfer that occurs as a result of condensing mechanics (sometimes greater than 12,000 W/m^2) The limiting heat transfer condition will exist in transferring the heat of the expander emissions into the air charge passing through the compact fins. Later chapters discuss in detail the best methods of installing these cooling systems into aircraft. Many different styles of heat exchanger are available for use in the condenser. For the prototype system, there were many more off the shelf components available to use in this lower pressure and temperature

environment. The most readily available finned heat exchangers are automotive replacement parts: oil coolers, motorcycle radiators, CART radiators, turbo intercoolers, etc. Figure 117 from [20] details common automotive heat exchangers, their compactness, operating pressure, temperature, and average cooling performance. The design choices are opened up because the condensing heat exchanger should never see much in excess of atmospheric pressure. In environments that provide ample cooling flow, condensing vapor will very likely result in a negative gauge pressure in the condenser caused by the rapid reduction in volume of condensing vapor emitted from the expander. This serves to increase expander power and cycle efficiency. One drawback to pulling a negative gauge pressure in the condenser is that the system may start to admit foreign fluids through any leaks that exist or develop in the system. If the whole cycle is continually over pressurized, the operating fluid will remain pure as any leaks will only emit fluid. When the cycle involves both positive and negative gauge pressures one runs the risk of air, water, or other contaminants working their way into the system. As the prototype system is not meant for proving long term operational reliability, these concerns are minimal, but should be considered when designing a successor system meant for applied use.

Heat Exchanger	Compactness m^2/m^3	Performance kW/m^3K	Operating Pressure bar	Operating Temp, °C	Mass kg
Radiator	1000-1500	30-200	1.6-2.5	80-125	1.5-5.0
Condenser	950-1300	20-100	15-23	75-100	1.2-4.0
Heater	1800-2800	65-130	1.6-2.5	80-125	0.5-1.2
Evaporator	900-1000	40-80	3-3.8	3-7	1.2-3.5
Oil Cooler	500-1500	40-600	3-10	120-150	0.3-1.5
Charge Air Cooler	600-900	20-60	2-3.5	120-200	0.6-3.5

Figure 117 - Automotive Heat Exchanger Parameters

The prototype system uses an automotive heater core as the primary condenser. This was selected because of the high surface area to volume ratio (compactness), low cost, and presence of reservoirs to allow for easy attachment of other pressure relief valves and gauges. A variable pressure relief valve was mounted that allows for the pressure limit to be set between 0 and 100 psi to hopefully

avoid ruining the condenser through a possible pressure spike even though the circumstance in which that could happen is not readily apparent.

BBB. Conclusions

Many components for Rankine cycle operation were prototyped. Most construction and evaluation efforts were centered on heater and expander components as they control system efficiency more than any other component. Rapid movement between computation and experimental evaluation allowed the boiler and expander design to evolve rapidly, yet in admittedly low depth. Further study will benefit from these surface level experiments of each component type. In the absence of significant funding and sophisticated fabrication options, guidelines for fabrication of boilers from $1/8^{th}$ inch stainless tubing were given along with instructions for modifying automotive scroll compressors into scroll expanders through removal of a one way valve inside the compressor. In the end, all prototyping efforts were found lacking in some dimension and creation of custom components is recommended for further progress in closed cycle engine development.

CHAPTER IV

Integration of Closed Cycle Engine Into Airframes

Low Drag cooling installation for small UAV's

CCC. Practical benefits of compact heat exchangers for heat rejection

Closed cycle engines, regardless of the specific cycle in use, will be required to reject more heat than the equivalent open cycle engine that is able to discharge some waste heat through its own hot exhaust stream. Internal combustion engines are typically capable of discharging 30 to 40 percent of their input heat through exhaust, with the remainder either leaving through the engine's cooling system or converted to useful power. Turbomachine open cycles can typically discharge all of their waste heat into the operating fluid passing through the device. Because closed cycle aircraft engines will be burdened with this extra cooling requirement, finding a method of discharging this heat to the atmosphere with minimum drag is essential to making a closed cycle propulsion system viable.

The issue of heat rejection in unmanned aircraft is similar to challenges faced by early manned aircraft designers. As engines became more powerful than direct finned cylinder air cooling could keep cool, engineers began to look for other methods of improving heat transfer without increasing drag. Early methods used a simple liquid cooling loop with radiators placed directly into the airstream as exemplified by the Freidrichschafen G.III in Figure 118.

Figure 118 - Freidrichschafen G. III showing common front mounted radiators. [21]

Though effective, the radiators proved a dominant source of drag. Other attempts at more efficient radiator installations included "lobster pot" shown in Figure 119 radiators formed into more aerodynamic shapes, but still directly exposed to the air.

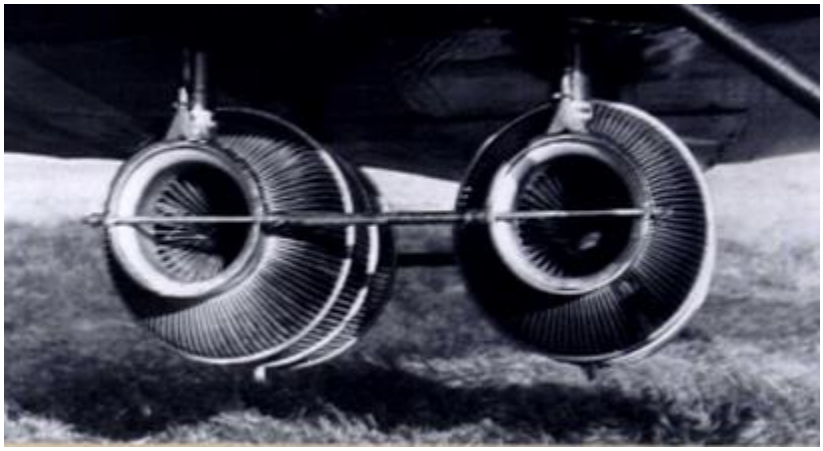

Figure 119 - "Lobster Pot" radiators slung under an early 20th century airplane – Navy-Wright NW2

Some aircraft designed specifically for speed used wing surfaces as smooth heat exchangers as shown in the RC3-2. The gold colored portions of the wings in Figure 120 are in fact copper heat exchangers dissipating engine heat.

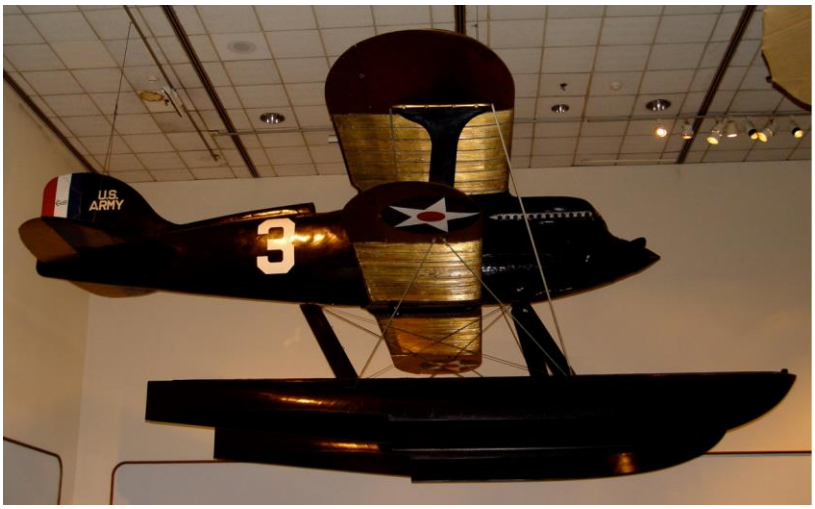

Figure 120 - Copper wings used to radiate engine heat without a standalone radiator. [22]

The eventual design standard for heat dissipation can be seen in the P51 (Figure 121), spitfire, Me109, and many other world war two liquid cooled aircraft. High performance WWII airplanes began using ducted radiators as shown in the schematic of Figure 122 to lower cooling drag, and as described by F.W. Meredith [23] could in some cases even use this waste heat to generate positive thrust from the waste heat stream.

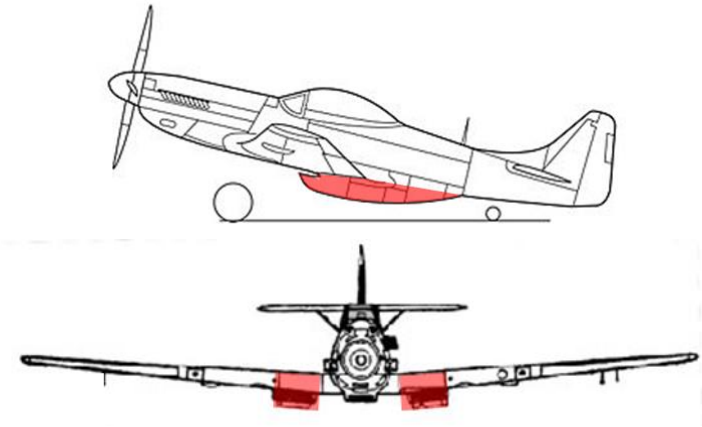

Figure 121 - Location of radiator and ducting in P51 and ME109.

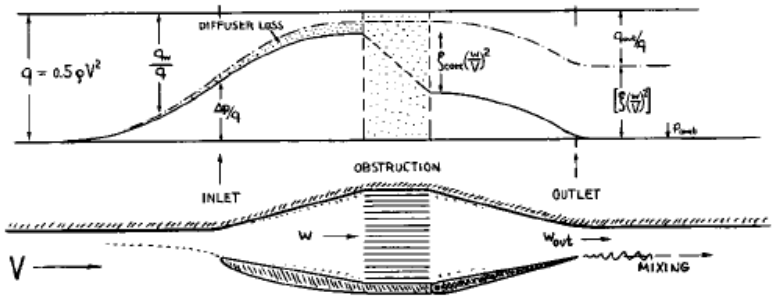

Figure 122 - Schematic of typical radiator ducting in aircraft for low drag installation

DDD. Area Requirements

If one were to attempt to dissipate the waste heat of a 1HP closed cycle engine through the skin of a UAS alone it would require some 3.5 m^2 per horsepower (with obvious variations accounting for speed, temperature differential, etc.) of propulsion. Conversely this same amount of heat can be dissipated through a ducted compact exchanger with a frontal area of only 0.05 meters. A notional comparison of required area is shown Figure 123 where the red outlined area indicates the surface area required for heat dissipation, and the small green square shows the relative size of a compact exchanger. While a skin heat exchanger would not introduce new sources of profile drag, the materials required for efficient heat conduction (copper, graphite, aluminum) are prohibitively heavy for SUAS use. Additionally, distributing the waste heat evenly from the engine to all surfaces of the airplane becomes another complex, and heavy feature. Aircraft disassembly, wing breaks, service ports, all become much more complicated when used doubly for heat exchange.

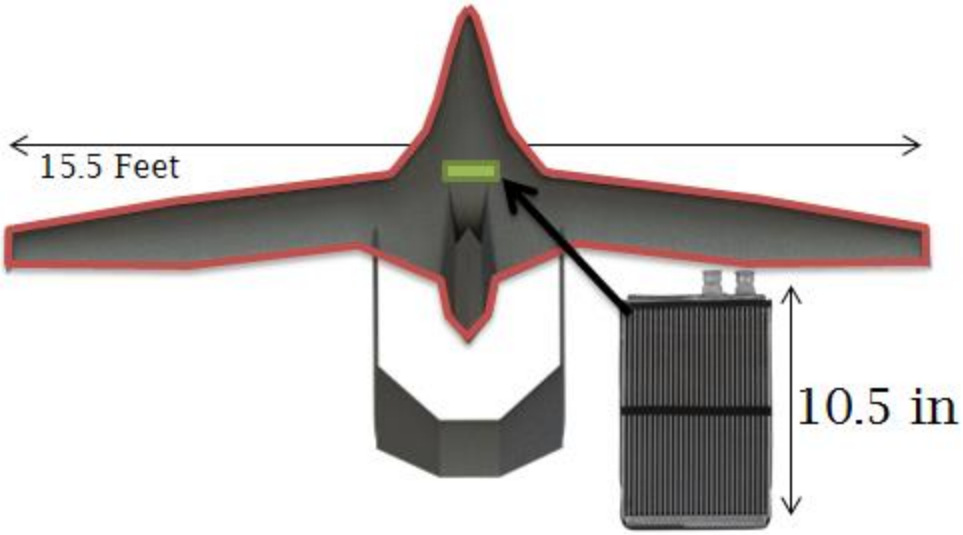

Figure 123 - Notional area requried for skin based cooling compared to compact heat exchange

A tradeoff exists in cooling system design, where the faster an aircraft flies, the less drag generating area is required to keep the engine cool and operating. Again for the notional 1HP system, chart Figure 124 demonstrates the tradeoff of speed and area. As expected, when velocity is small, cooling area requirements grow with a 1/x trend. This means that when the aircraft is running on the ground, special equipment carried either onboard or with external supply must temporarily keep air flowing over the exchangers or the engine will not be in a condition ready to provide maximum power at takeoff. Similarly, high speed flight is not an unbounded solution to cooling because an increase past the UAS's best endurance or range airspeed would sacrifice overall aerodynamic efficiency and raise power requirements thus creating a self-reinforcing loop.

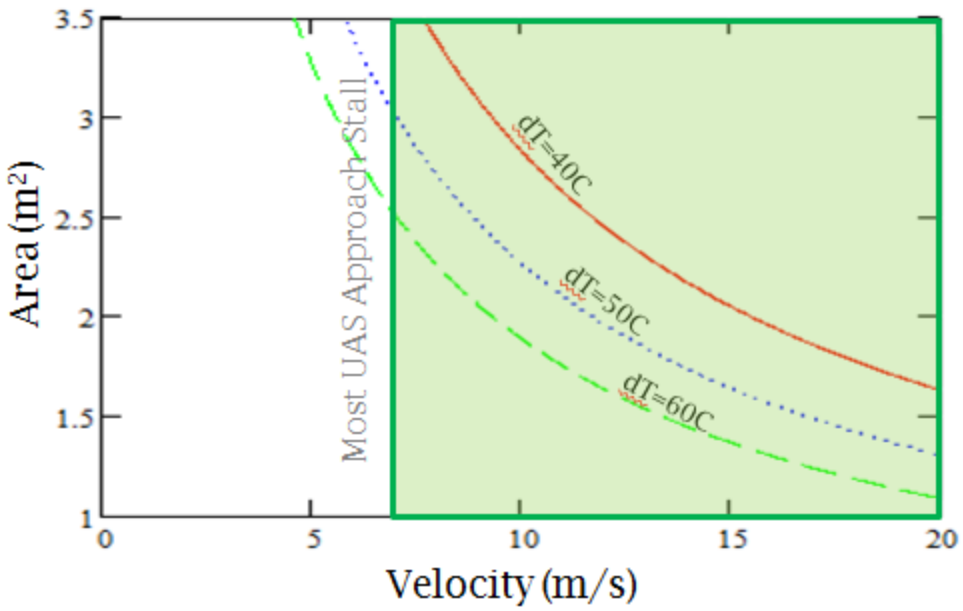

Figure 124 - Cooling area required based on heat transfer temperature differential and transfer surface area

EEE. Cooling power requirements

To model this power dependent source of drag, and additional term was introduced to the basic aircraft drag model. This additional term combines Nusselt number convective heat transfer models, newtons law of cooling, and a representative heat exchanger coefficient of drag per unit area of heat exchange surface. Unsurprisingly, the dominant influences on drag from heat exchange are shaft power required, cycle efficiency, temperature differential, thermal conductivity of the air, and velocity of the airflow over the heat exchanger. Of these governing parameters, the designer can strongly control the temperature differential of heat exchange by modifying the cycle expansion ratio or operating fluid inlet temperature, and also the velocity of airflow over the heat exchanger through use of a diffuser on the incoming air stream. Of these two options, using a diffuser is the more independent and less complicated solution.

$$P_{flow} = \frac{1}{2}\cdot\rho\cdot Vx^3\cdot\left[CDo\cdot S + CDr\cdot\frac{P_{flow}\cdot L^{\frac{1}{5}}}{\eta_{cce}\cdot(TL - Tamb)\cdot 0.037\cdot\left(\frac{Vx}{\upsilon\cdot Ve2Vi}\right)^{\frac{4}{5}}\cdot Pr^{\frac{1}{3}}\cdot k} + \frac{CL^2}{\pi\cdot e\cdot AR}\right]$$

By using a diffuser (as modelled with the Ve2Vi term in the equation), the drag of a ducted heat exchanger can be reduced to near zero, and does not significantly influence performance of a properly designed system. If the duct is improperly set, or does not sufficiently slow the flow past the high drag radiator, significant losses will slow the aircraft down. While the example in Figure 125 shows the utility of proper ducting, it does not include compressibility effects, heating of the fluid by the radiator, and is dependent on airframe parameters to determine the tradeoff between power required for cooling and power required for propulsion. In this combined circumstance of cooling and propulsion power requirements, the analysis of suitability could be skewed by considering a glider type platform in place of a less efficient aircraft. A formulation of cooling power requirements that is independent from airframe parameters is more desirable.

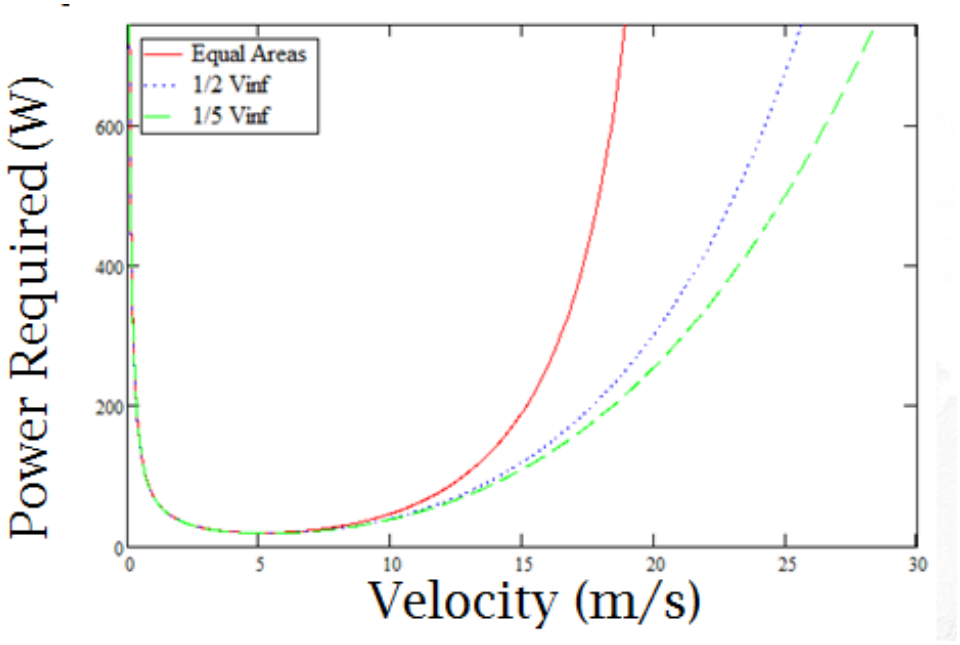

Figure 125 - Comparison of different cooling installations as a function of velocity

FFF. Cooling power loss per watt

Isolating the power required to push a heat exchanger from the power requirements of the rest of the aircraft allows one to independently judge the performance of heat exchanger installation. The plot in Figure 126 shows the portion of power produced by the closed cycle engine that is required only to overcome the drag of the heat exchanger. This example does not take any ducting into account, so Vx in the chart is the velocity seen across the actual heat exchange element. If any ducting occurs before and/or after the heat exchanger this velocity should be modified accordingly. Another method of reading this chart is to consider it the number of watts consumed to create a watt of useable power. At the point where 1 watt is necessary to discharge the heat associated with making that watt, the aircraft cannot possibly fly as there is no energy left to overcome profile drag, induced drag, rolling friction if on the ground, etc.

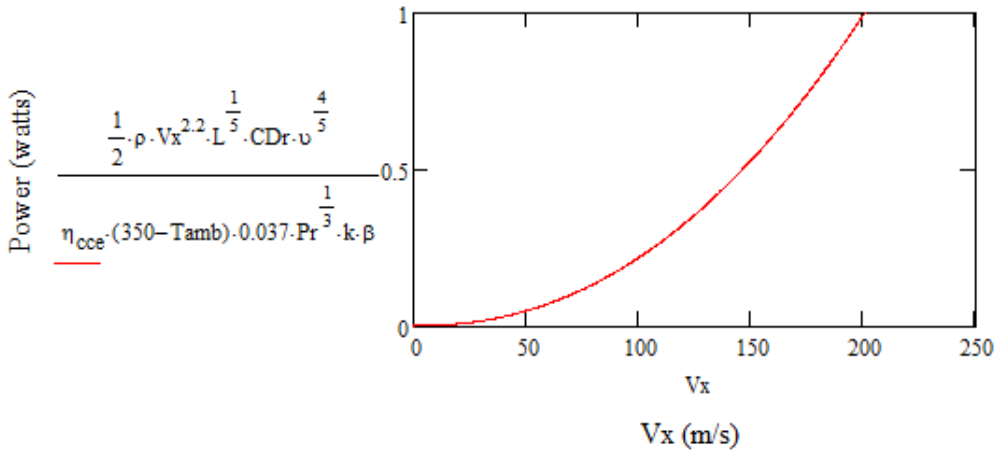

Figure 126 - Power required for cooling per watt of power generation

Cooling duct model

GGG. Incompressible example

Without surprise the most effective variable in reducing cooling drag is to reduce the velocity across the heat exchanger. In incompressible scenarios this is simply the inverse ratio of areas of the duct. 9 times the area would produce 1/9th the velocity of the inlet. As with most cooling ducts in aircraft, the exhaust port controls mass flow as a result of pressure matching while the inlet can see varied operational states depending on the flow effects occurring in the duct behind it. This is why mass flow controls for ducting should be placed at the exit of the duct as they are on the P51.

Proper ducting of cooling air as laid out in Figure 127 is achieved by diffusing the incoming air charge at point 1 sufficiently to reduce radiator drag at location 2 and have sufficient energy to accelerate the flow back to flight speed at point 3. The area of the nozzle exit at station 3 should be sized such that pressure in the nozzle returns to that of freestream. If the pressure built through diffusion is insufficient to overcome the pressure loss from the finned exchanger and accelerate the flow back to freestream velocity, then a net momentum loss will occur. Except at the slowest of design flight speeds, the energy of incoming air is generally sufficient to overcome the pressure drop of the heat exchanger given proper diffusion.

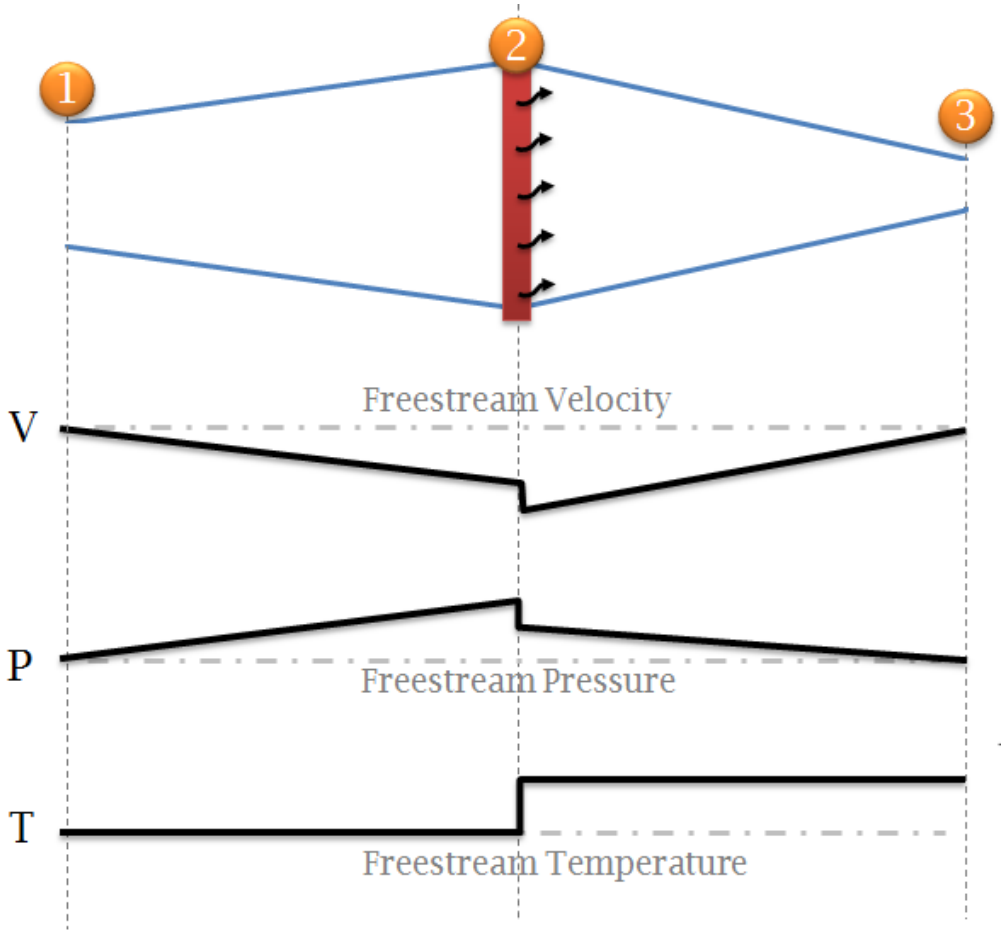

Figure 127 - Schematic representation of flow channels in compressible heat exchange example

20. Compressible example

When the influence of compressibility is taken into account, proper ducting of a heat exchanger with significant thermal load can indeed produce a positive net thrust. As mentioned previously, H. W. Meredith discussed this effect in the years preceding world war two which lead to inclusion of the advanced ducting technique on many fighter aircraft of the era.

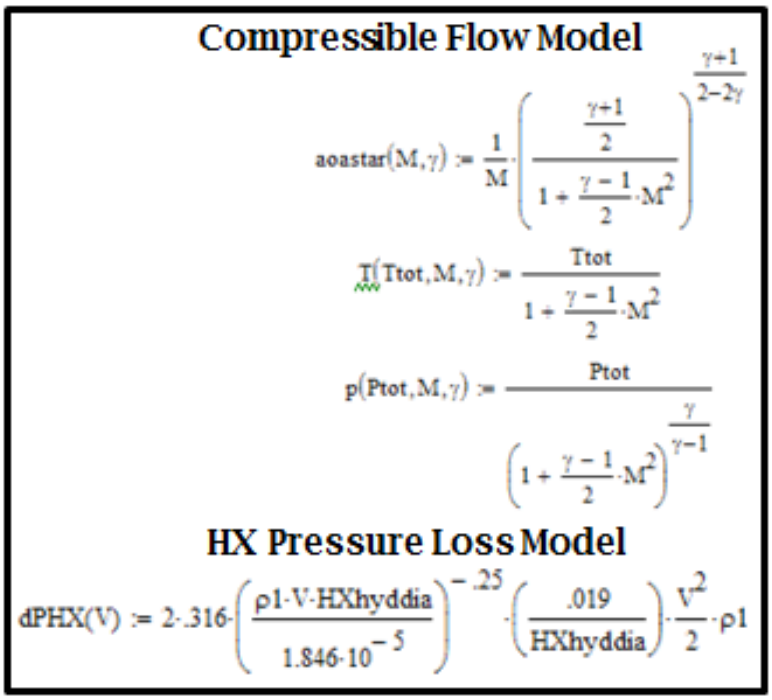

Figure 128 - Primary equations of compressible flow used in model

A model shown in Figure 128 for temperature, velocity, and pressure was developed for ducted heat exchangers using only the classical compressible flow 1D equations. The two major design variables for this system are heat exchanger area (A2), and the ratio of inlet to heat exchanger area (A1/A2). The ratio nozzle exit area to heat exchanger area (A3/A2) is determined automatically to make the nozzle exit pressure match atmospheric pressure. Pressure matching is naturally enforced at the exit both physically and in the code so that any positive or negative velocity mismatch can be bookkept as thrust or drag. The code creates plots of overall coefficient of drag (based on radiator area) and horsepower consumed by the flow momentum loss of heat exchange. Figure 129 shows that through proper selection of diffuser ratio one can actually achieve a net thrust by harnessing some of the heat added to the ducted airstream to expand the gas, and increase the velocity as it is ducted out the exit. This benefit normally occurs at A1/A2 ratios of less than 0.35 which roughly corresponds to that found on the P51. The thrust produced per unit of heat is quite low, so this method should not be considered in this form as a primary source of

propulsion. It is in essence a low pressure Brayton cycle with a heating element in place of a standard combustion chamber.

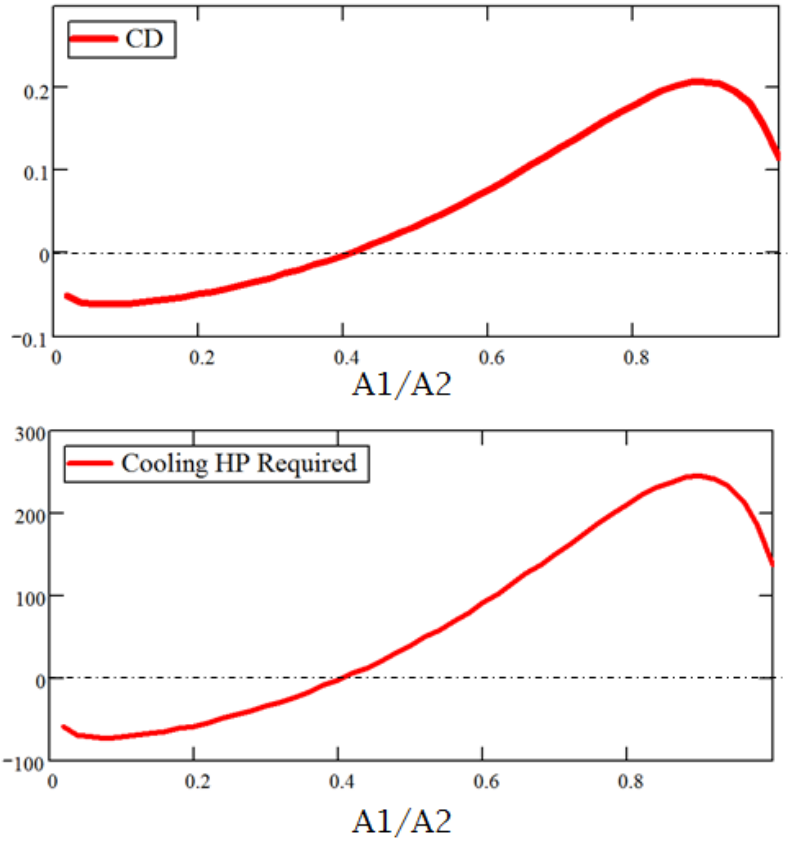

Figure 129 - Drag incurred due to cooling at compressible Mach numbers

Being able to optimize the flow through 1the cooling duct is essential to minimizing cooling drag at all operating conditions. Given the method of calculation employed in this study, one might think that actuation of both intake and nozzle are necessary to minimize drag across all segments of flight, but only the exit nozzle must be actuated to preserve most function. Proper convergence after heat exchange is what determines the re-acceleration of the flow to hopefully freestream levels. The nozzle primarily serves to convert the remaining duct gauge pressure back into kinetic energy to minimize drag. If the flow is insufficiently expanded with a large nozzle opening, the duct mass flow rate will increase due to the surplus motive pressure from the diffuser and drag will increase as this extra mass will undergo an

unnecessarily large momentum loss because of the inadequate nozzle. If the nozzle opening is too small at the exit, mass flow is restricted, air will "spill" out of the duct inlet, cooling rate will suffer, and in extreme cases can severely limit engine power capability through decreased condenser performance. A simple PID control system with static pressure sensors located just inside and outside of the nozzle exit would be able to properly modulate the nozzle exit height to maintain proper flow. In some cases like takeoff and maneuvering where absolute engine power is more important than overall engine efficiency, it may be desirable to have the duct full open during that whole phase. This system can thankfully be actuated with a single servo, and will be mechanically simple. The implementation of this method on the P51 is shown in schematic form in Figure 130 below

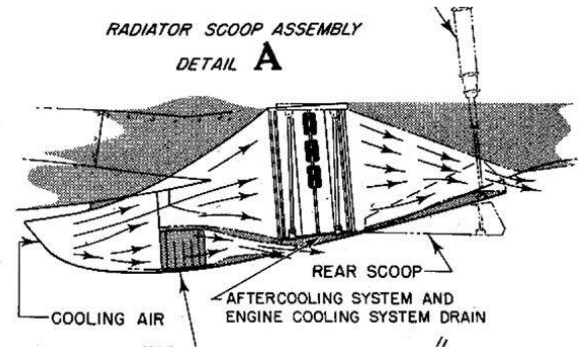

Figure 130 - Installation of radiator in P51 Mustang [24]

HHH. Notional installation example in CFD.

To confirm the validity of the various methods of calculation discussed, a computational fluid dynamic based simulation of a notional cooling duct installation was conducted. Additionally this study allows judgement of the duct performance in the presence of other bodies affecting the flow field. A two dimensional cross section of a notional flying wing or lifting body UAV shown in Figure 131 was used as a baseline, with the duct areas properly implemented on a skewed centerline to decrease total installation height and bias the required volume internally to the fuselage. The study was conducted at sea level standard temperature and pressure, farfield velocity at 15 meters per second, A1 A2 and A3 were 0.038, 0.125, and 0.037 m^2 respectively.

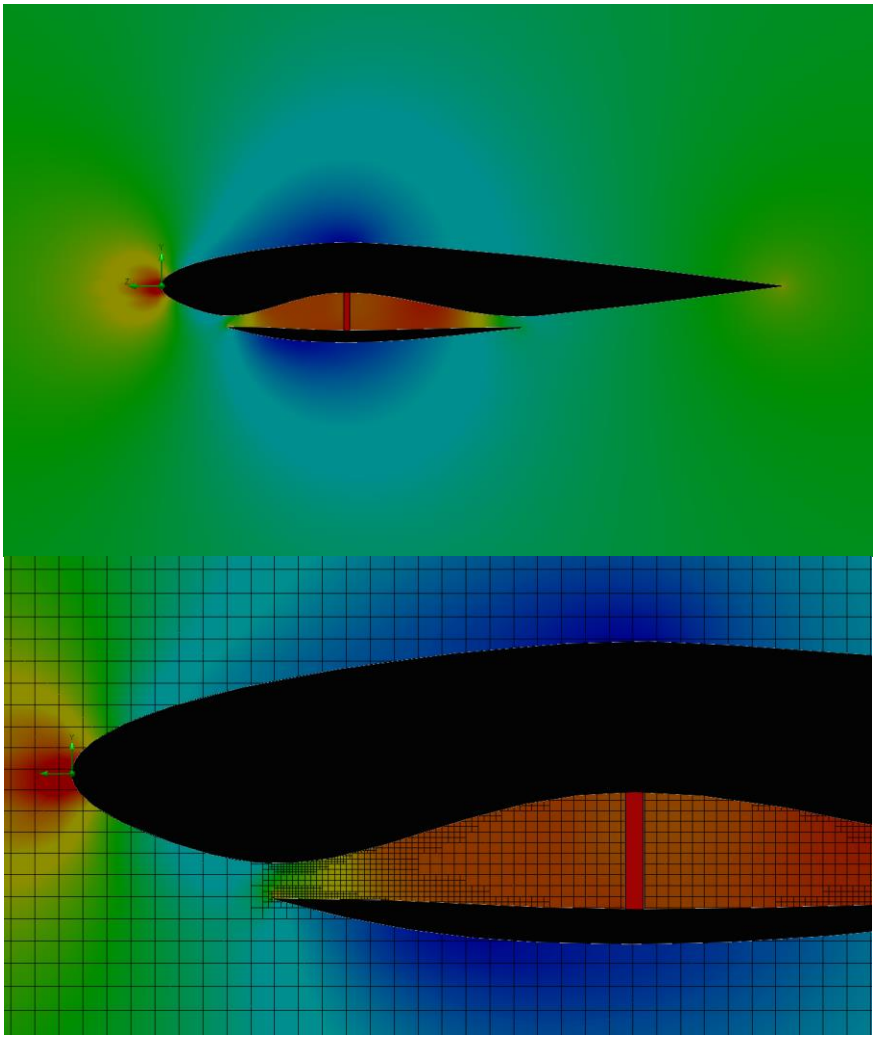

Figure 131 - CFD cooling verification case and grid refinement

The CFD grid was locally refined in regions found to have high pressure gradients and narrow passageways. The red region in the simulation indicates the porous media model standing in for the heat exchanger. This body allowed flow only in the axial direction, and created additional area restriction as the real heat exchanger would.

The pressure and velocity plots show in Figure 132 show trends along the curved dashed centerline of the duct. In the plots, black chevrons indicate the calculated pressure and velocity at the heat exchanger. Both plots show a sharp drop right as the permeable media is encountered. This pressure

drop and velocity increase (note negative reference) occurs as the flow passes through the additional restriction imposed by the unidirectional media. The duct successfully diffuses the flow to predicted speeds and returns it to both freestream pressure and velocity which indicates that the area ratios calculated by the simple algorithm can indeed be used for low drag installation of heat exchangers in UAV's.

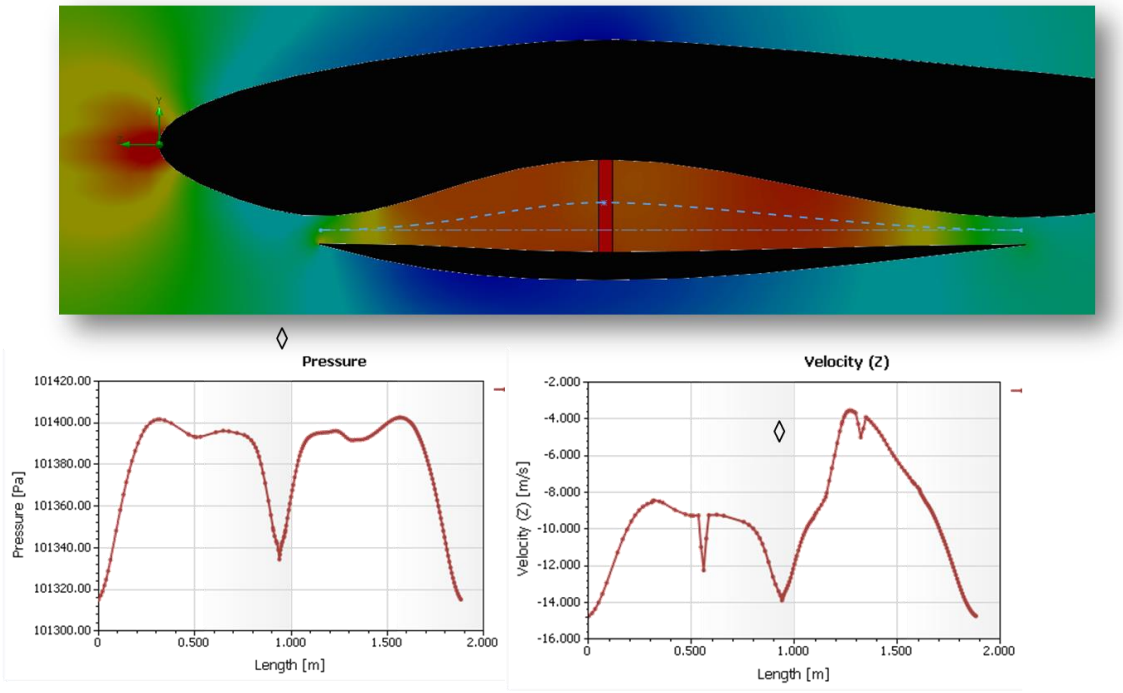

Figure 132 - Resulting pressure and velocity plots from CFD study

III.
Conclusions on UAV heat transfer

Integrating heat exchangers into UAV airframes is not a constraining task according to drag, power requirement, or cooling capability. Integration is further eased by the general ease with which UAV's can integrate more internal volume. This propulsion system is designed to remain subsonic at low to moderate Reynolds numbers which allows for even bulbous fuselages and containers to exhibit acceptable drag on an airframe. CFD studies conducted to validate installation drag and underlying assumptions about flow through and around an installed cooler did confirm calculations. Building on the

techniques employed by early 20th century aircraft allows one to efficiently integrate cooling systems and avoid very penalizing drag from improper integration.

Temperature of Exhaust Flow

Closed cycles can control to some degree the temperature of exhaust gasses leaving the aircraft by modulating the flow of air past the condensing heat exchanger. The previous sections have shown how changes to this air flow rate can have significant implications on the drag of cooling installation, and similarly the amount of airflow has strong control on the exhaust temperature of the air stream leaving the system. This exhaust temperature can be constrained in different ways depending on aircraft design parameters. Designs requiring the lightest engine weight and most compact power system without constraint on the exhaust temperature will likely use a higher temperature differential across the condenser and lower cooling air mass flow rate to minimize the size and weight of the cooling equipment, but as a result will exhaust air at higher temperatures. Systems where low exhaust gas and surrounding surface temperatures are desired are able to uniquely accomplish this objective by enlarging the cooling radiator which allows it to operate over a larger temperature differential at the sacrifice of size and weight. Again, by increasing the mass flow of cooling air the exhaust stream does not accrue as much heat per unit mass and experiences lower temperature rise as shown in Figure 133.

When one compares the trends shown between exhaust temperature and cooling power required, their desired area ratios conflict. One should note that at very low mass flow rates (indicated by small intake areas) the indicated exhaust temperature is extremely high as a result of the model being based on full transfer of the cooling heat flux to the exhaust stream. While this is unrealistic if condenser temperature is constrained to a specific delta T, it does indicate the effect low cooling flow has on the lower cycle temperature. Such low cooling mass flow rates would force the lower temperature of the fluid higher and higher until the system is unable to turn the low side operating fluid back into a liquid to be compressed. In this example shown in Figure 133 an intake area of 0.025 square meters avoids the worst temperature penalties, is just past the knee of the curve in exhaust temperature, and minimizes drag

associated cooling power losses shown in Figure 134. Only in circumstances seeking minimum temperature exhaust would one push the intake area size higher.

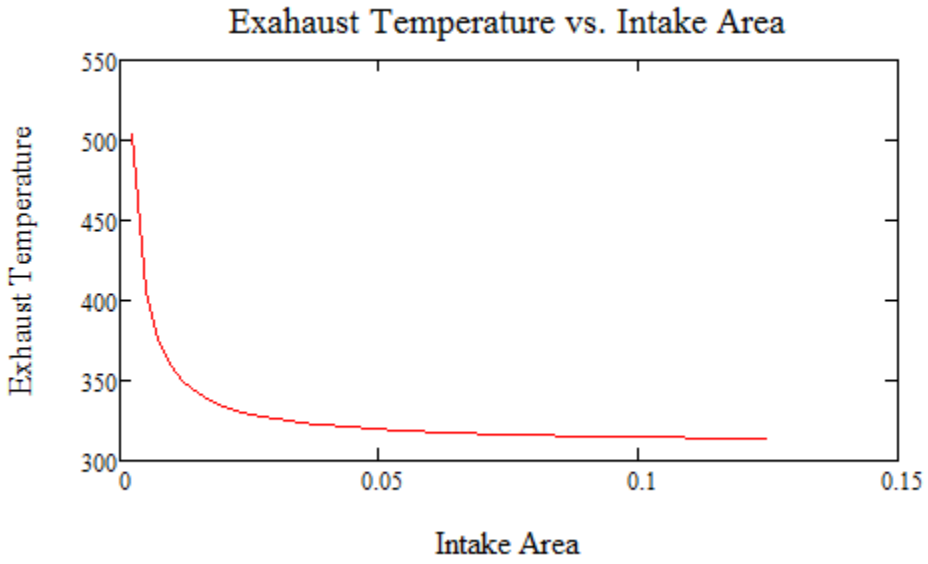

Figure 133 - Exhaust Temperature vs. Intake Area

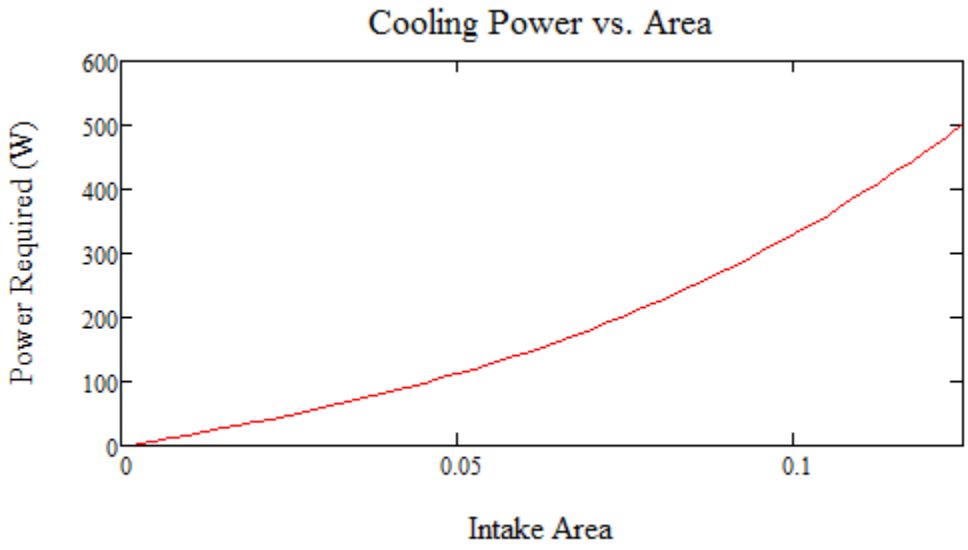

Figure 134 - Cooling Power Required vs. Area

Conclusion

After creating a one dimensional subsonic compressible model for gas flow through a ducted heat exchanger, the overall drag of a properly designed condenser was found to be near zero for small UAS applications. While higher subsonic Mach number operation was found capable of producting thrust from the waste heat of aircraft engines, the typically low incompressible Mach numbers of small UAV's does not facilitate the same thrust generating physics. It is still beneficial to find that through proper duct design, the installation can be made to exhibit near zero drag force on the airframe at low speed. Proper diffusion and nuzzling of the flow allows the designer to account for pressure drop across the heat exchanger. If any controls are placed on the duct, they would be best placed on the exhaust side of the system, as the nozzle exit dimensions govern the flow through the system.

CHAPTER V

Closed Cycle Engines at High Altitude

II. Closed Cycle Benefits in High Altitude Flight

JJJ.Power Lapse of CCE vs. ICE with altitude

CCE carries its operating fluid around with it. Airplane maintains constant dynamic pressure so while density drops, heat exchange performance drops much slower. If a CCE aircraft is flown to maintain constant dynamic pressure as it ascends the additional heat transfer due to reduced ambient temperature causes the available power to increase up to 35,000 ft as shown in Figure 135 using the standard atmospheric model, and not reduce back to sea level power conditions until 52,000 ft. The main constraint to high altitude operation of a CCE is keeping the OPF from freezing, and sustaining combustion in the thin atmosphere. Proper OPF selection can remove risk from the freezing constraint, while proper combustor design and testing will solve the second.

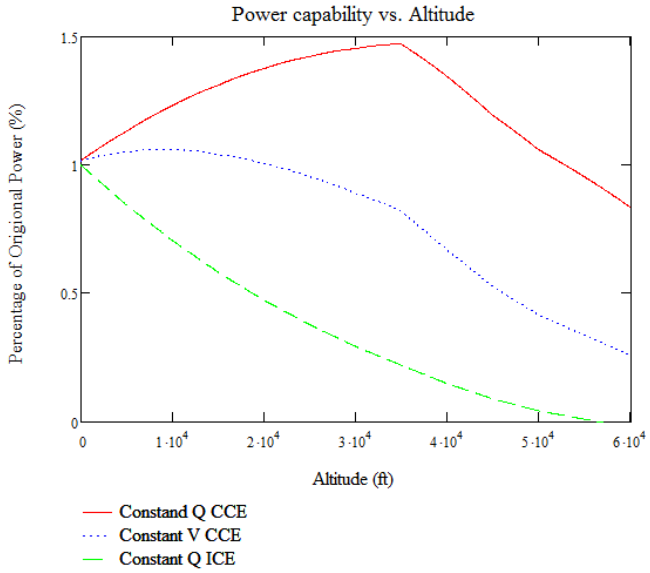

Figure 135 - Heat Rejection Capability vs. Altitude

KKK. Use of Organic Operating Fluids at high altitude

Organic operating fluids (R134a etc..) Can hadle colder temperatures without freezing, allowing one to operate with a colder average heat rejection temperature and improve cycle efficiency at high altitude. The drawbacks to refrigerants is these systems need to operate at higher average pressures than a water based cycle to keep heat rejection temperatures above ambient at sea level. Operation with refrigerants at high altitude however poses fewer problems as atmospheric temperatures remain much lower than the cycle's heat rejection temperature. Using refrigerants can increase the specific power of CCE expanders, and improve boiler efficiency by being able to utilize lower hot side temperatures. The best result of using organic operating fluids at high altitude is holding the heat addition temperature high, being able to expand the gas to lower temperatures while maintaining sufficient heat rejection, and maximizing the temperature differential to maximize cycle effieincy. One also has the alternative of holding the expansion ratio constant, and rejecting more heat due to the suddenly decreased ambient temperatures. When coupled with a variable pitch propeller this would allow the engine to produce more power as it gained altitude as the same hardware could reject more heat.

Figure 136 below show two cycles with water and R134a operating at the same maximum temperature, expansion ratio, and volumetric flow rate on the same chart. One should note the temperature of R134a after expansion is well below the ambient design temperature of 310C (100F) which would prevent this cycle from rejecting heat entirely. The heat rejection temperature of the steam cycle is very near the supercritical temperature of R134a nearly forcing any rankine cycle hoping to reject heat to the atmosphere at sea level function at neat supercritical levels.

21. Freezing point of Operating Fluid

One must maintain the operating fluid above freezing if flying at high altitude, and be aware of risks associated with icing of the heat exchanger. When only considering methods of optimizing efficiency of a closed cycle it might seem advantageous to make use of the additional temperature ratio available between heat source and sink at high altitude. However, if one is using steam, the external temperatures can reach -70F at altitudes between 10,000 and 20,000 feet in the Tropopause layer of the atmosphere and the operating fluid may freeze inside the system. A particularly troubling side of freezing water in pipes is that the expansion may rupture a pipe or seal in the system and result in the loss of operating fluid if the system ever comes back up to temperature. Also, if the operating fluid is changed to a refrigerant to accommodate low temperatures at altitude, one has to seriously consider the potential for ice buildup on the outside of the heat exchanger due to atmospheric moisture. Both internal and external icing can be avoided by operating the system at the same lower temperature point and utilizing the increased temperature differential across the condenser to make more power. This method may be acceptable if the mission is accepting of dash speeds at altitude and does not require maximum range (which seldom occurs at maximum power). Refrigerants would be best used in any system designed for high altitude flight, as even transient changes in throttle could result in a water based system freezing and failing mission requirements. If a water based CCE were flying at altitude and executed a descent, the near idle throttle setting would cause a drop in condenser temperatures that may induce freezing inside the

system and result in an engine failure until it might thaw at lower altitudes. Throttling a high altitude system by changing propeller pitch to a less efficient setting, or even a mechanical shaft brake at altitude may be preferable even though it is much less efficient. Especially in the case of the mechanical brake, the resulting heat could be used to keep the system in an operable temperature range. Figure 136 below shows both organic and water based cycle diagrams on the same PV and TS charts. The potential for organic operating fluids to operate at lower heat rejection temperatures is immediately evident. Even if Ice does form on the outside of an organic system's condenser, the cycle should self-regulate back to a temperature that will melt the ice at the sacrifice of efficiency. Utilizing a semi-infinitely renewable block of ice to reject heat is not the worst state for a closed cycle system to be in.

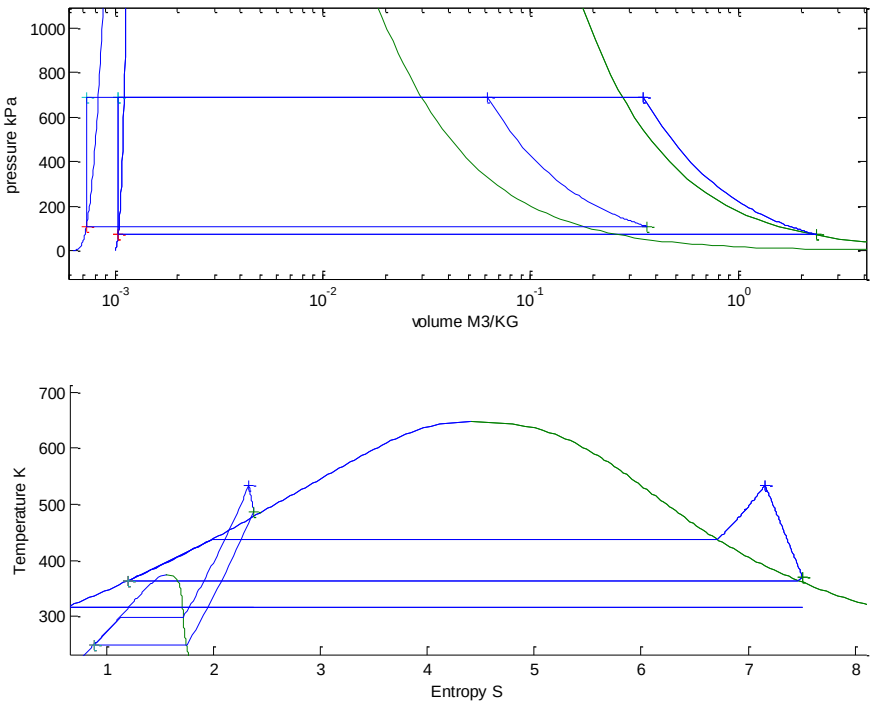

Figure 136 - Comparison of Water and Organic Fluid Cycles

LLL. Martian Applications

The environmental independence that closed cycle engines offer means that as long as heat transfer in and out of the system is preserved, it can provide power in exactly the same manner on Mars as

it can in the atmosphere of earth with a change to an oxygen free heat source. This could mean solar reflectors, nuclear heat, or some type of chemical reaction can keep the system running off world. Further integration of non-contact turbomachinery and other long-life mechanisms would offer a very robust system for exploration. The power profile shown for a Martian atmosphere is shown in Figure 137. This atmospheric model does not include corrections for temperature lapse that some more sophisticated models include, yet it still shows a similar and expected trend to the earth atmosphere flight scenario. The closed cycle system flying at constant Q can maintain necessary heat rejection to very high altitudes, in fact being able to create more power as the aircraft ascends, making it an excellent candidate for flying long durations above the weather. As with other Martian aircraft concepts, Mach number will likely become a strong constraint.

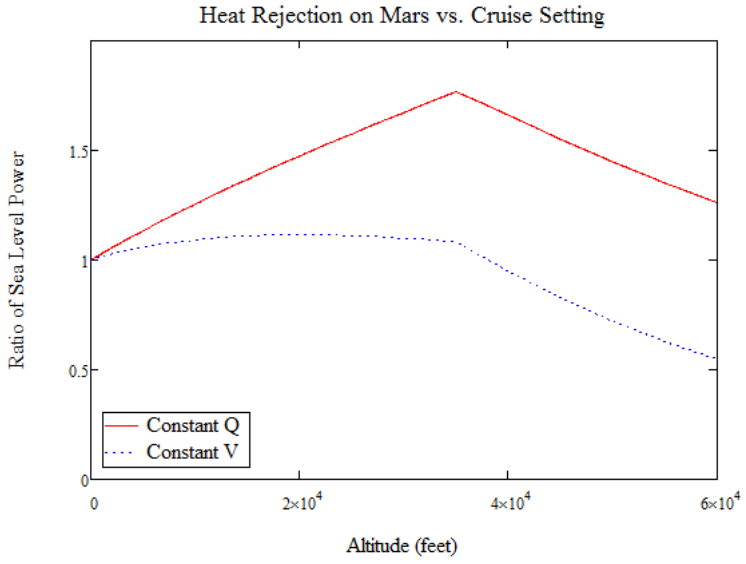

Figure 137 - Mars Atmosphere Heat Rejection Capability vs. Altitude

MMM.Radioactive Heat Sources

Since heat flux is the only true requirement for a closed cycle engine, it is possible to consider applications in environments that do not allow for conventional air breathing cycles. Submarines and space probes are some of the most justified in using closed power generation systems. Submarines have the luxury of being able to accommodate massively heavy power plants and being surrounded by an

excellent heat rejection medium. They also serve as an excellent example of quiet operation of closed cycle systems as the primary design principle of submarines is to remain protected by their silence. Space probes like Voyager shown in Figure 138 use closed power systems in a more challenging environment. Typical radioactive thermoelectric generators like on voyager, Cassini, Mars Curiosity and other long duration probes are extremely inefficient, but use such an energy dense fuel that the overall system can function for decades if not longer. The primary challenge in these space based CCE's is that all heat rejection must be performed in a relative vacuum. Radiation heat transfer is the most powerful method available, so the spacecraft end up using large surfaces to radiate waste heat away from the craft. Interestingly, two spacecraft have been launched with full fledged nuclear reactors, the soviet RORSAT and American SNAP-10A. The difference between these full reactors and a simple RTG is that a full reactor system employed a closed cycle power generator as well instead of only a solid state thermoelectric converter.

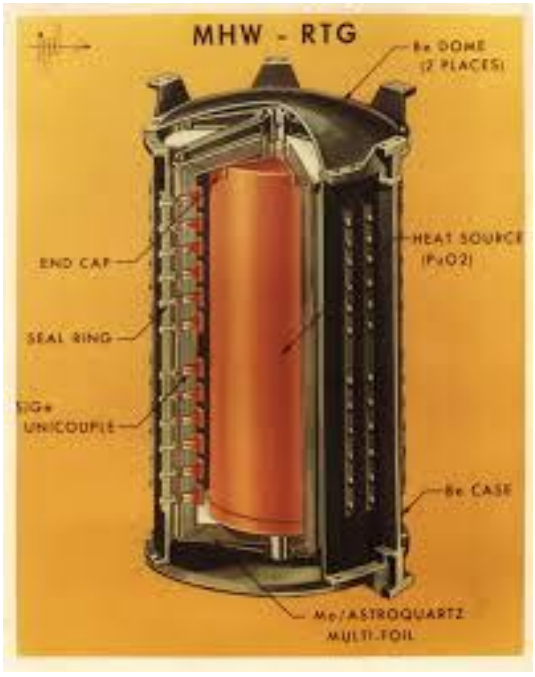

Figure 138 - Voyager's radioactive thermoelectric generator [25]

NASA has investigated closed cycle systems for space applications. Sunpower stirling's closed cycle stirling engine was developed for the purpose of powering space probes through long endurance missions.

This engine used planar springs in place of sliding bearings, and avoided other sources of friction and wear to make a system that could last for years completely isolated in the vacuum of space. The system operated at much higher efficiency than present RTG systems (14% in some load cases compared to RTG's best of 2%).

The most feasible radioactive heat source for closed cycle power production has been, and will likely continue to be Plutonium 238. This material can generate 0.54 watts of heat per gram and most usefully exhibits low levels of dangerous radiation that can be contained with as little as 2.5mm of lead. This means that a closed cycle power system need not even become radioactive in its whole. The dangerous radiation could be completely contained within the heater of a closed cycle engine, and any eventual irradiation of the operating fluid would remain contained within the system. As little as 1.4 kg of Pu238 could generate 1HP of input heat for use in a closed cycle system. For a more realistic example, NASA's multi mission radioactive thermoelectric generator under development can generate 2000W of heat, and 110W of useful power while only using 4.8kg of Plutonium Dioxide. This RTG by those numbers is only 5.5% efficient. A small closed brayton cycle according to the studies conducted with this research could obtain two to five times that much power from the same input heat. Alternatively NASA could shrink it's valuable Pu238 resource allocation for these missions to prolong the supply and reduce cost of probe power systems.

NNN. High Altitude Combustion

The issue facing closed cycle engines with operation at high altitude is different than that faced by internal combustion systems. Flying high has always required some manner of compression either through turbo or supercharging the intake air of an internal combustion engine. In these engines the displacement is very much fixed, so as their operating fluid drops in density, the power generated by heating that reduced mass of fluid drops considerably as well. Closed cycle engines have the benefit of maintaining operating fluid pressure in all conditions as the system is theoretically perfectly sealed. This

reduces the problem of heat input at high altitude for closed cycles to simply maintaining sufficient mass flow to achieve efficient combustion and provide sufficient heating to the boiler. While operating at high altitude will certainly require a larger combustor and heat exchanger, this system does not have to remain in use during all phases of flight. It would indeed be a disadvantage to use the full flow volume of the heater at low altitude. Ideally the inlet and exit of the combustor would be variable either continuously or discretely. This change to combustor is all that is required to accommodate high altitude flight. For most general purposes the mass fraction of oxygen at high altitude remains the same, only mixing and ignition become more difficult due to low temperature and pressure. Closed cycle engines can overcome this design challenge much easier and with less mass compromise than internal combustion systems that have to dedicate additional turbomachinery or increase their displacement. Figure 139 below shows the range of combustion that many common fuels are capable of burning. Within this useable range, there will exist an optimally stoichiometric balance of air and fuel. Regardless of altitude, as long as these proportions are maintained and suitably mixed, combustion can continue uninterrupted.

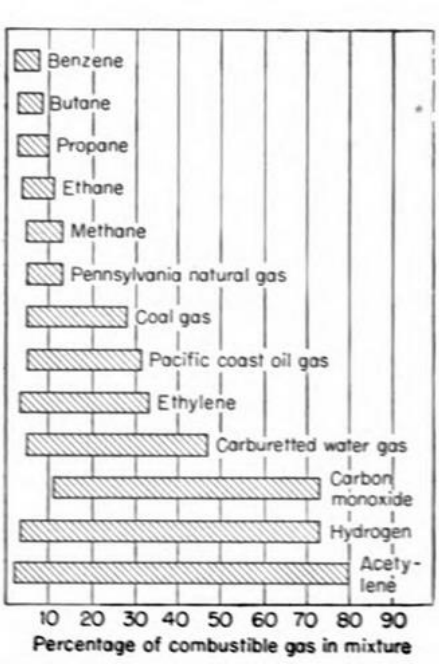

Figure 139 - Range of possible combustion for various common fuels

Conclusions

The finding of heat rejection increasing with altitude is a significant advantage for closed cycle systems. Much of the weight disadvantage created by carrying heat exchangers and discrete compressors is negated when a comparable internal combustion system must carry a supercharger, turbocharger, or some other method of maintaining operating fluid density to avoid power loss. Additionally, these compression systems heat up the IC engine's operating fluid and often require their own discrete heat exchangers to operate properly. While the heat rejection side is studied sufficiently here, the heat addition remains a design problem to be solved. Oxygen is still present at altitude, but at a distinctly lower density than sea level. A burner system that does not precompress the combustion air would be required to be very large in size to capture enough mass flow for proper combustion. Fuels that are capable of burning at lower air to fuel mass ratios might be beneficial for increasing the ceiling even further given a burner with fixed geometry. Even without an acoustic advantage, the high altitude performance of closed cycle systems justifies their use in many missions.

CHAPTER VI

Conclusions and Recommendations

OOO. Properly Designed Closed Cycle Engines offer Acoustic Advantages over the Present Generation of Quiet Aircraft Engines.

During testing of different expander options, the primary noise source has been mechanical noise transmitted from inside the mechanism through other metal components. The piston engine experienced squeaking form the rotary valve, the scroll compressor emitted a scratching sound sourced from the scrolls orbiting one another, and the vane motors emitted similar noises as the vanes moved over one another. In all of these cases adding lubrication helped the noise problem and reduced friction as expected, but then the systems in question must include systems for proper oiling and separation of oil. Performing these tasks and keeping the oil evenly distributed has been difficult in air conditioning systems for some time, and is further compounded in airborne systems where the additional weight and performance loss due to oil and its associated metal equipment make an already heavy propulsion option prohibitive for use. In all of these test cases, the noise of fluid passing through the expander in question was a small contributor. It is also important to note that in these expanders, no attempt to smooth flow paths or make corners turn softly had been made. The flow path was very contorted, narrow, and experienced right hand turns, yet the flow contribution to noise outside of the expander was not

significant. This acoustic insulation is supported by calculating the transmission coefficient between air and steel. As long as the pipelines are kept from resonating, the total transmission between flow to the outside environment can be made negligible. Furthermore, in the case of a steady flow turbine or other rotary expander, since the flow does not experienced pulsating backpressure from a positive displacement expander, opportunities to resonate fluid spaces or create physical vibrations of piping are minimized. In many places, a free expansion turbine based closed cycle engine makes logical sense.

PPP. Closed Brayton Cycles are Recommended as the Preferred Research Path

While Rankine cycles can offer efficiencies nearing 20 percent at high pressure, the danger involved with storing even moderate amounts of saturated steam in a UAS is prohibitive. Most UAS systems are operated in close quarters by people that may not be completely aware of the danger of BLEVE explosions. In the cast of the prototype fire tube expander made during this study the energy contained within it would be equivalent to 1/3 a stick of TNT. Using a closed Brayton cycle is preferable from a safety standpoint because the fluid contained within is not going to undergo a phase change if the containment vessel ruptures. The difference in expansion energy between the high pressure side of a Rankine and Brayton cycle is significant. Rankine cycles, and other cycles involving phase change of the operating fluid, will also suffer from a more complicated startup procedure. Especially in cases where the operating fluid must be contained without venting. Until the entire Rankine system is brought up to temperature, the cold thermal mass of the expander, piping, condenser, etc. will nearly instantly condense the operating fluid. This liquid forming inside the system can lead to hydrolock in positive displacement expanders. Startup of single fluid phase systems is vastly preferred as the operating fluid should never liquefy inside the system.

Additionally, when a regenerator is added to the Brayton based closed cycle system the preferred pressure ratio is inverted. Where normal Brayton cycles achieve optimal efficiency at high pressure ratios and use many stages of compression to achieve this, efficient regeneration modifies the cycle such that the lowest possible pressure ratio is desirable. One might think that this low pressure ratio would decrease turbine power output, but when compared to a turbine based Rankine system the opposite is true. For SUAS scale Rankine turbines, the flow delivers energy at very high pressure and low flow rate. Visualizing this as a steam injection needle is a proper analogy. Each individual turbine stage is not limited in power because of pressure available, but because of the small mass flow rate (that cannot be increased without lowering system efficiency). The flow becomes choked at Mach 1 long before the total desirable pressure drop is met. This is the key difference between Rankine cycle turbines and RCBC turbines. Rankine turbines require multiple expansions to capture the fluid's enthalpy drop efficiently, while a RCBC due to its large back work ratio and low pressure ratio can utilize a single turbine stage to expand a larger mass flow rate of operating fluid and generate much more power per stage. The real discussion here is one of turbine admission percent. Rankine based turbines will admit over 0% to 1% of the circumference, while Brayton cycle turbines might admit 100%. There is a studied and measureable efficiency benefit to increasing the admission of turbines, so having higher admission is generally always better.

Due to improved safety for engine researchers and field operators, reduced turbine weight, improved stage efficiency, improved overall efficiency potential, better specific power, and suitability for turboexpansion coupled to magnetic power transmission, the Regenerative Closed Brayton Cycle is a preferred option to Rankine cycle based engines going forward.

QQQ. Effective UAS Closed Cycle Engines will Require Custom Part Fabrication

This study attempted at times to adapt scroll compressors, air vane cutoff tools, and two stroke piston engines to become suitable options for closed cycle expanders. When work continues on this subject, the researcher should secure the proper budget and time to create custom components made for use on aircraft. Requirements specific to airborne CCE's would include oil free operation, air cooling where required, and minimization of weight of operating fluid and component packaging. Few off the shelf items were found to be suitable for use in prototyping closed cycle engines. The typical resource of adapting hobby industry products for use in more outlandish research is not possible with such a unique and previously uninvestigated system.

RRR. Closed Cycle Engines Offer Significant Advantages for High Altitude Flight

The single most powerful advantage of closed cycles is that their power can increase with altitude. A hermetically sealed system can retain sea level operating fluid density throughout its flight envelope. One could also engineer a simple reservoir system such that injecting or absorbing excess operating fluid from the primary loop can raise or lower the median cycle density, and therefore control system power. It would become a pressure operated throttle. Isolation from particulates, weather, and independence from the atmosphere surrounding the aircraft makes the closed cycle engine a very reliable power source for long duration missions. High altitude flight characteristics have not been verified in this study beyond calculated heat flux models, but the finding of improved heat rejection with altitude is invariant with changes to assumed thermal parameters.

SSS. Magnetic Coupling and Gearing Enables Hermetically Sealed Closed Cycle Engines

As exemplified by Robert McConaghy's stirling engine, operating fluid leaks can drastically reduce system power for closed cycle engines. Shaft seals, valves, pipe threads, and other mechanical sealing

locations pose risk of venting operating fluid to the atmosphere. In the case of cycles using air as the operating fluid a leak is not necessarily mission-ending as the system could include a pump to re-pressurize the cycle at low energy cost from ambient air. However if the cycle requires a refrigerant at an average pressure many times that of the surrounding atmosphere, a leak will cause large power loss and a forced landing. Magnetic coupling eliminates the need to pass a physical shaft through the CCE casing. By using a rotating magnetic field to either generate electricity or drive a coupled set of external magnets the system can be sealed as solidly as possible. While belt drives can offer similar acoustic properties as magnetic gearboxes, they do not offer the potential for hermetically sealing the engine system.

Recommended Research / Program Path

22. Turbine Bearing Prototyping

Construction technique of a non-contact turbine bearing can be developed without the need for any other thermal system involvement. An air hose driven simple turbine can be driven to test the experimental bearing for suitability. Fluid bearing design methods and magnetic bearing circuitry have both been created and documented for straightforward reproduction. Being able to create custom integrated non-contact high speed bearings will be essential for turbine integration.

23. Regenerator Efficiency Testing

As regenerative Brayton cycles are the recommended path forward, it is important to understand the performance of the regenerator as it is the single most significant component in controlling system performance. Though thermal models are quite accurate for calculating heat transfer, the regenerator is

such an important part of system performance it would be wise for the investigator to test its capability before proceeding with further investment.

24. Starter/Generator Design

If one chooses to use a shaft driven compressor design with the suggested regenerative closed Brayton cycle, it will require external power to get the system up to speed. Integrating high temperature samarium cobalt magnets into the rotating turbomachine will allow a FADEC controller to apply or harvest torque from the engine depending on the needs and status of the system. Shaft position measurements and coil timing are all within the capabilities of modern speed controllers. The same magnets that are used to start the system will be suitable to extract useful electricity from it. This method will encounter efficiency losses not present in a shaft driven design, but the aforementioned sealing advantages make it an extremely attractive option for engine reliability.

25. Electric Drive vs. Magnetic Gearbox Design Decision

One can either extract power from a hermetically sealed turbine by generating electricity, or passing a magnetic field through the casing. Integrating a generator into the turbomachine is a common method of handling large speed and torque mismatch in systems that can also benefit from excellent sealing. In the case of pancake turbines built for aircraft, it allows the turbine to be oriented in any position regardless of the power output location. Magnetic gearboxes for the most part remain coaxial with the turbine, but escape the efficiency losses of changing energy from mechanical to electrical and back again.

CHAPTER VII

Future Work

TTT. Moving Mesh CFD Turbine Analysis

The analysis of turbomachinery with computational fluid dynamics requires methods of computing the effects of relative motion between stator and rotor blades of the turbomachine. Additionally, since most turbomachines are radially symmetric (each blade is identical) a code that can use pie shaped domains with symmetric boundary conditions in combination with moving meshes would be ideal. The CFD package integrated with this studies primary CAD modelling package, Solidworks 2014, is not capable of true moving mesh or radial symmetry. But the next release of Solidworks' integrated CFD package includes both of these features which will make it ideal for rapid computational optimization of small turbines. The present release of Solidworks 2014 does include some rotating mesh tools, but these methods require that the flow be uniform at each radial station at the boundary between rotating domains. Turbines will inherently create fluid property fluctuations across the cylinder shaped boundary, and as such are not compatible with this rotating mesh method. As shown in Figure 140 below which depicts a failed CFD experiment with rotating meshes, Solidworks attempts to create constant fluid conditions at the boundary of the rotating region. In the figure the rotating region was the central blue vane section, while the outer red region remains stationary. The solution diverged and failed because this geometry will naturally produce property variations in each vane volume and especially high gradients around

the vane tip. Solidworks' rotating mesh method cannot handle this semi-periodic boundary condition so the solution failed.

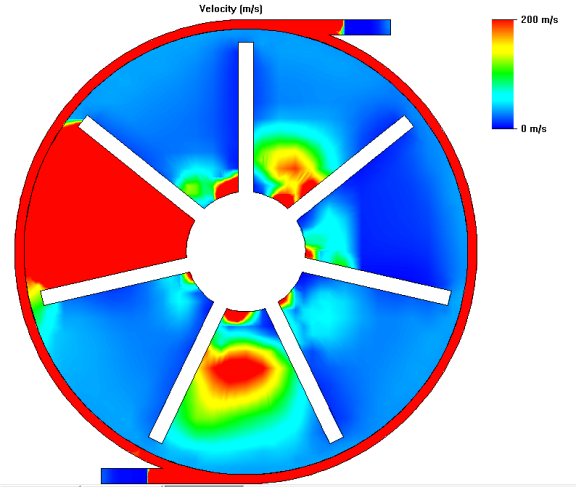

Figure 140 - Erroneous CFD results obtained from uniform boundary condition of rotating mesh

Introduction of true moving mesh methods into the simulation as shown in Figure 141 below will allow proper analysis of many turbomachines that were previously not possible. CFD is an essential part of optimizing turbomachinery as simpler algebraic methods similar to those used for propeller analysis become prohibitively complex when accounting for the more complex boundaries and imperfectly periodic blade conditions. The essential advancements and optimizations of small scale turbines required for enhanced closed cycle engine performance require the use of CFD.

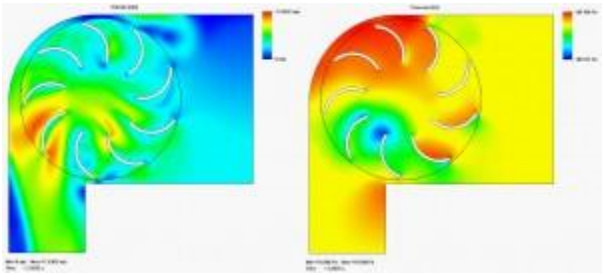

Figure 141 - Solidworks 2015 CFD Simulation utilizing moving mesh methodology. [cadimensions.com]

UUU. Integrated Brushless Motor/Generator

A challenge of using turbomachines in power generation has always been the design problem of how to extract power from the pressurized turbine casing. Early stationary power producing turbines used stuffing boxes with various materials compacted against the turbine shaft to act as a pressure seal to allow mechanical extraction of power from the high pressure turbine casing.

Figure 142 - Large Scale Power Generation Turbine Shaft Seal. [26]

Later advancements have seen fluid bearings, labrynth seals (Figure 142), and other more sophisticated methods used to create a mechanical pressure seal with longer life and higher pressure ratings. The problem of efficient mechanical sealing is made more difficult in small scale turbomachinery

as the shaft speed (and therefore seal speed) is much higher than grid scale power producing turbines. Megawatt class turbines may only spin between 3000 and 8000 RPM, while a 1HP class turbine because of how turbine physics scale will most likely spin at speeds above 100,000 RPM. Additionally, the torque output of a small UAS turbine is extremely low, so even a light drag on the high speed turbine will cause a significant portion of the output torque to be wasted. One very promising solution is to use rare earth magnets to either directly generate power, or couple an output shaft directly through the wall of the turbine housing. Transmitting power through a solid wall in this method will allow for the most difficult sealing problem in the entire closed cycle system to be avoided. Stationary and very effective gasket seals may be used to completely isolate the turbine from external influence. When using magnetic force trasmission, the turbine housing should be made of a non-ferrous and non-conductive material to avoid eddy current drag created by the moving magnetic field through the turbine housing. One drawback of using simple magnetic coupling is that the output shaft speed is still very high and will require gearing, a noisy, heavy, and potentially expensive stage. However, it is possible to integrate a gearing mechanism into the magnetic gearbox itself. Several publications have detailed the creation of magnetic gearboxes. While these prototypes are outside of the weight class necessary for UAV's, the demonstrated principles are effectively shown to work and remain efficient. In the case of turbine power transmission the high speed rotor shown below in Figure 143 would be attached directly to (or integrated inside of) the high speed turbine. The stationary pole pieces made of low reluctance materials would be embedded in the non-conductive turbine housing, while the propeller would be mounted on the low speed rotor. This allows for simultaneous transmission of power through a solid sealed wall, speed reduction of power, and mounting of a "low" speed propeller on the front. The number of rotor and stator poles can be manipulated to create gearboxes of widely varying ratio. One other advantage of this type of gearbox is

the torque limiting nature of magnetic gears. In mechanical gearboxes if the torque limit and safety factor are exceeded, the system will most likely encounter an unrecoverable mechanical failure. With magnetic gearboxes, above their torque rating they will simple slip. The system efficiency will drop precipitously, but as soon as torque loads reduce below the system rating again the gearbox will resume normal function. This will be very useful in preventing damage to high speed turbine components in the case of a prop strike on landing (common for UAV's) or other mishap with the attached propeller.

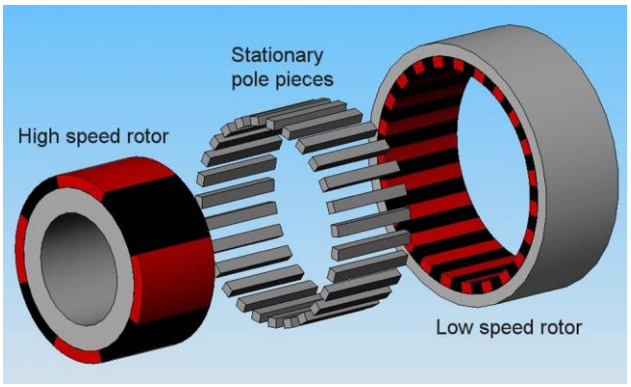

Figure 143 - Schematic View of Magnetic Gearbox [27]

The alternate method of extracting power from the turbine is to use the magnetic high speed rotor to directly generate electricity. While this method will likely be at a disadvantage in efficiency when compared to direct mechanical power transmission from the turbine, it does allow one to efficiently integrate the required electricity generation system for the UAS into the default engine system. This also allows the UAV propulsion system to become more universal in application. The UAS CCE instantly became a general purpose power producer for small loads that occur often in UAV field operations. The airplane could very well become the primary tool for recharging the system ground station during preparation.

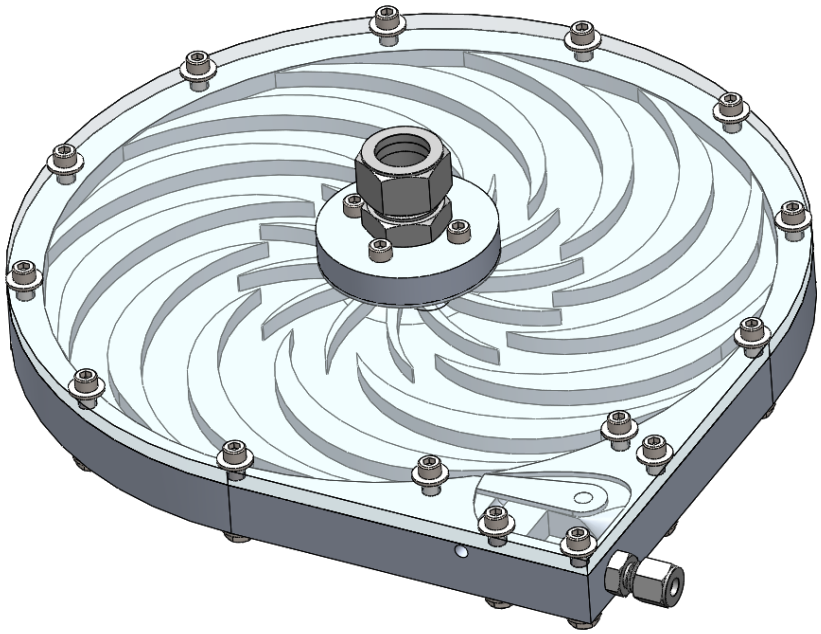

Figure 144 - Notional pancake turbine with integrated starter/generator

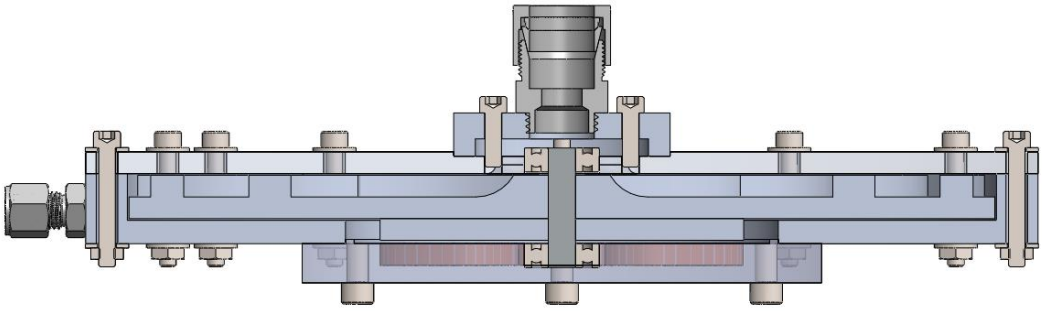

Figure 145 - Cross Section of Turbine with Integrated Starter/Generator (coils shown in red)

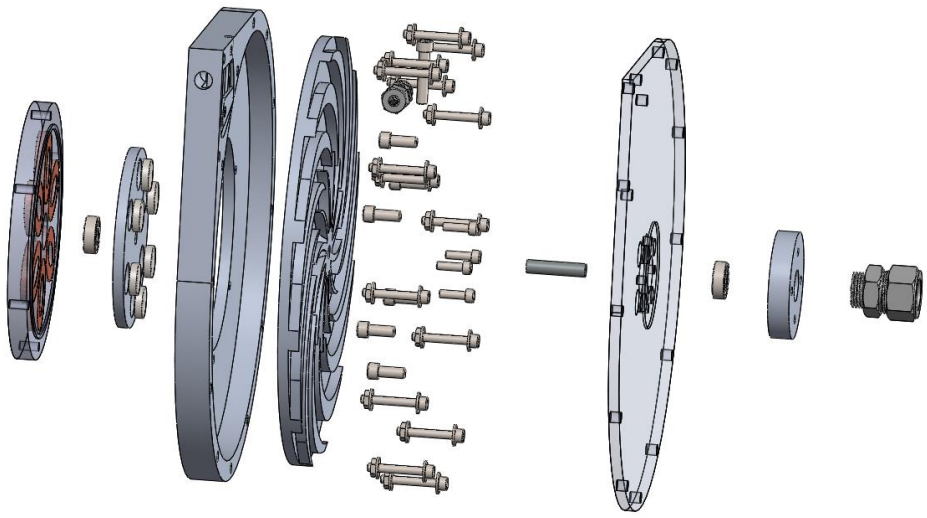

Figure 146 - Exploded view of Turbine with Integrated Starter/Generator

Every closed cycle engine discussed in this study will require an alternator/generator to be attached for payload and electronic power to be practical. It only makes sense to integrate this starter/generator into the turbine blisk itself. Additionally when considering the scaling effects of turbine diameter, it will likely be advantageous to use a larger diameter turbine than is practical to axially align within a fuselage (as would be required with a direct magnetic gearbox). The thermal conditions inside the turbine pose challenges for rare earth magnets as the most common type, neodymium, will demagnetize at even modest turbine temperatures. This means either relocating the magnets a modest distance away from the hottest regions (as done in Figure 144 through Figure 146), and/or using Samarium Cobalt rare earth magnets which combine a useful combination of high strength and high temperature capabilities. Using an integrated turbine starter/generator would allow one to use a pancake turbine with its axis mounted vertically in the fuselage so that a blended body type aircraft could accommodate turbines of very large diameter. A conventional brushless motor could utilize a portion of the output power for propulsion just

as easily as payloads, avionics, or battery systems could utilize the energy. While likely imposing a modest efficiency disadvantage resulting from power generation, rectification, and conversion back to three phase for the motor, this arrangement could make up that efficiency loss through advantages of a larger diameter turbine.

VVV. Regenerator Efficiency Optimization

Regenerative Brayton cycles are the most logical option for further closed cycle development, but these cycles are heavily dependent on the efficiency of regeneration to be viable at all. Regenerator efficiency is defined as the ratio of heat transferred from the turbine exit flow to the compressor exit flow divided by the total heat lost by the turbine exit flow in the regenerator. This component will reach optimal efficiency when thermal leaks are minimized. Notional methods for minimizing these leaks include housing the regenerator inside of an evacuated container to maximize thermal isolation, and insulate the mechanical connections between the vacuum housing and fluid entrance/exit to minimize thermal leakage at that interface.

WWW. High Temperature Metal 3D Printed Components

Figure 147 - Selective Laser Sintering 3D Printed Heat Exchanger featuring complex heat exchange paths not possible with subtractive manufacturing. [28]

Direct Metal Laser Sintering 3D printers will be extremely useful in creating boilers/heaters tolerant of direct flame impingement like that shown in Figure 147. While using stainless steel tubing is sufficient for an early prototype, 3d printing of complex shapes meant to maximize convective heat transfer between the products of combustion and boiler/heater material will significantly reduce system mass by increasing the average temperature of heat transfer into the system, and maximizing the surface area to volume, and surface area to weight ratio of the boiler/heater system. Significant improvement in heat transfer rates through use of 3d printed heat exchanges has been demonstrated in literature by integrating complex shaped microchannel directly into the heater structure. Being able to produce such complex shapes from a material tolerant of the chemical and thermal environment will significantly improve heater performance.

Evaluation of Methodology

XXX. Mistakes

26. Need for a Self-Starting Piston Engine

The necessity of a self-starting engine option was discounted during this study when first considering piston expander options. The prototype boxer two cylinder engine has identical self-starting problems as a single cylinder engine since both pistons fire at the same time. The minimum number of cylinders necessary to allow for self-starting at any crank angle is three, each with 60 degree inclination to the other. Additionally, the natural drag torque on the engine at zero RPM was too high to allow an "air driven restart" where the flow passing over the propeller generates a starting torque to turn the engine over. This was never tested, but the drag incurred by driving the rotary valve heads and other engine systems was significant enough to determine an air restart is unlikely.

27. Rotary Valves

While rotary valves may work better with a few more iterations and CNC precision machining, they were a source of squeaking, leakage, and mechanical drag in the engine system. Poppet valves are favored in other piston expander options (as well as four cylinder engines) for a reason; their sealing capacity increased with cylinder pressure as the higher pressure forces them even harder into the valve seat. Even though the rotary valves were made from brass, they exhibited significant friction, and the smoothness of their operation varied as soon as 5 minutes into engine testing, often requiring a teardown and recalibration of the valve system after each test. This quickly made testing a prohibitively tedious task and other expander options were sought.

Scroll expanders, vane motors, rotary piston engines (with more than 3 cylinders), and turbines should all be easy enough to self start, with turbines being the easiest system to operate intermittently.

28. Startup Condensation

Most all analysis of the engine cycles centered around steady state operation and did not consider start-up scenarios. While the assumption that a Rankine cycle is straightforward to start up was true, the amount of condensation generated during startup was not accounted for with the first piston and scroll expander systems. Significant amounts of steam will condense on the inside of the expander during startup because the thermal mass of the expander must be brought up to steam temperature before the fluid can travel through the system without condensing. Because condensing heat transfer rates are extremely high (~20,000 $W/m^2/K$) virtually all of the steam at startup is instantly condensed into water. This condensation has specifically negative consequences when considering positive displacement expanders that could enter hydro-lock or fail structurally. Piston expanders have little recourse against condensation besides modifying the valve timing to hold the exhaust continuously open. The piston expander prototyped during this study would likely enter hydro lock at every startup of the steam system as it had no method to vent the condensate. Scroll expanders can be created as either compliant or non-compliant scrolls. The compliant variety is able to pivot slightly to allow the passage of incompressible oils and liquids through the system. These systems allow for small quantities of liquid only and should not be relied upon for passage of 100% liquid. This condensation at startup is another advantage for turbomachine based expanders since they are not positive displacement, the condensate can follow the same fluid path that the eventual gas can follow out of the system. One special consideration of turbomachines is that the condensate does not become trapped at some point of the rotating machinery due to centripetal acceleration. If the fluid does become trapped, it should in time reach a temperature that will turn it back into a vapor and allow the system to function normally, assuming that the presence of this fluid did crash the rotor as a result of imbalance.

29. Belt Driven Heads

While the timing belts and pulleys used to drive the piston expander rotary valves were a worthwhile and functional solution, the belt tensioners used did not provide sufficient tension to prevent frequent belt skipping and timing adjustments. In a system where the head valves rotated more freely, the rubber band driven tensioners may have been sufficient, but during each test of the piston expander, the valves invariably built up rotational friction until enough load was created in the belt system for a tooth to skip position and lose timing accuracy.

30. Coil Boiler

While the coil boiler is an inferior heat exchange option when compared with traditional fine-tube heat exchangers, the coil heat exchanger is one of the only simple to manufacture options that can tolerate direct flame impingement and the high pressures associated with Rankine cycle operation. Many finned heat exchangers use aluminum fins and aluminum brazing to seal pipe connections and thermally connect fins to the fluid tubing. If these common heat exchangers were exposed to flame temperatures up to 1900F, all aluminum surfaces would melt near 1200F. The presence of liquid operating fluid should keep the pipe and brazed connections in tact as long as the system is operating properly, but if an aluminum boiler ever encounters a state where liquid is not available to immediately sweep away the excess heat from the metal walls, the boiler will rupture and create a BLEVE explosion. The safety risk of these BLEVE explosions is why aluminum heat exchangers were avoided for the high temperature and high pressure side of the closed cycle system.

Stainless steel monotube boilers are much safer when operating at high temperature and pressure. The ¼ inch and 1/8 inch diameter tubing used in this study were both capable of withstanding over 3,000 psi of pressure and temperatures up to 2550F. While it is important to remember that material strength is

reduced at higher temperatures, there was still plenty of margin for stainless steel tubing. In the circumstance that the monotube boiler did experience a failure, the relatively small flow channel will immediately choke the flow of high pressure gas expanding from the boiler. This limits the mass flow rate out of the boiler system and creates a hot jet of steam instead of a steam explosion. While this jet can still be harmful, it will likely be contained by the ceramic insulation placed over the boiler and does not pose anywhere near the safety risk that a larger fire tube boiler does.

31. Corrosion of Automotive Scroll Compressor

After initial tests of the scroll expander with steam, the system was left resting for approximately one week. During this time the inside of the scroll expander corroded significantly as shown in Figure 148. This rapid corrosion was likely a result of normal galvanic corrosion in the presence of water that was exacerbated by the PAG oil shipped with the compressor combining with water to form a mild acid. This formation of acid is common with PAG oils mixing with water, and should be avoided if possible by flushing the shipping oil out of the compressor before running it on steam. Additionally, the compressor was designed with multiple dissimilar metals in contact with one another promoting galvanic corrosion. If a scroll expander were to be used for an aircraft closed cycle engine, the scroll should be made compliant, and preferably non-conductive materials. At minimum the materials selected for the scroll should be as similar as possible, even to include any required nuts, bolts, and washers.

Figure 148 - Scroll compressor corrosion one week after short test run.

32. Tubing Bender

Initially ¼ inch diameter stainless steel tubing was used to create a heating coil. This tubing was sourced from automotive brake line stock and is more than capable of withstanding typical prototype temperature and pressures. While this tubing was used to make a coil 4.5 inches in diameter, making smaller bends in the tubing proved difficult. Even with the assistance of a tubing bender like that shown in Figure 149, the ¼ inch tubing's minimum radius of curvature was too large for many engine applications. Later in the project 1/8th inch outer diameter tubing was used to reduce the minimum radius of curvature to useable levels. This smaller tube has much better space utilization and does not increase the mass of the heat exchanger significantly, though a longer length of tubing is required to the lower surface area per foot of length. One detriment to using smaller tubing is that the small flow channel will restrict mass flow rate and increase pressure drop through the boiler system. Since the heat flowing into the boiler is generating pressure, this loss will be masked, but if the flow in the small diameter boiler tube ever becomes choked, system performance could be severely limited. If flow restriction will be a problem for future systems, creating multiple parallel channels will alleviate much of the flow losses

while retaining the ease of working with smaller diameter tubing. 1/8th inch tubing is malleable enough to be formed into shape by hand with minimal risk of collapsing the flow channel inside.

Figure 149 - Tubing bender tool used to turn stainless tube

33. Propane Flow Rate

During initial experimentation, the assumption that a propane torch was delivering more than sufficient heat to power the prototype boiler was proven wrong when the torch was left sitting on a gram scale while burning fuel. The fuel expenditure was one tenth the heat level required for proper heating of the boiler. The flame holder and orifice of the propane torch were removed and replaced with hardware store fittings and flexible hose that terminated in a brass screw on flare cap. Several caps were purchased with varying micro-hole sizes drilled in each. Through trial and error, a proper hole size was found to burn the required amount of fuel. The method of gauging heat input by weighing fuel burned vs. time on a gram scale proved very effective and should have been performed earlier in the study. Future investigators should not hesitate to create or purchase alternate burner orifices to meter propane effectively. The needle valve still allowed precise control of flame size and output heat, just with the maximum flow rate properly scaled for the system's requirements.

YYY. Successes

34. Thermal Imaging of System

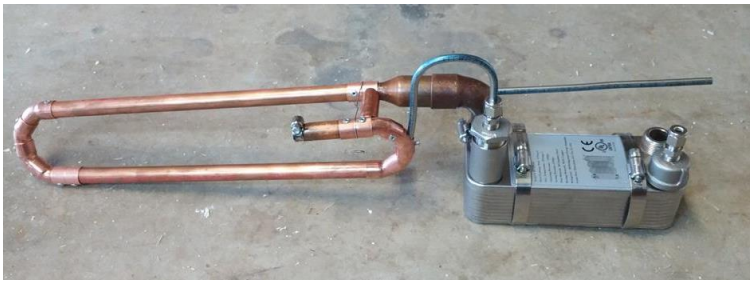

Figure 150 - Internal piping of the second boiler prototype contained within insulation

A Flir thermal imaging camera was used to evaluate the leakage of heat from a second prototype of the boiler system for the airplane shown in Figure 150. This was the first system to be insulated with one inch thick inhalation safe ceramic insulation to improve heat retention. The system was heated with a standard propane torch. As can be seen in the visual and infrared spectrum comparison below in Figure 151 the insulation was extremely effective at preventing thermal loss to the environment. The hottest region of the thermal image is the small section of exposed copper tubing the torch fits to. Another warm region of heat escape can be seen beneath the top "glove" of insulation placed over the ¼ inch tubing as it passed from the plate heat exchanger to the superheating pipe. The gap between that glove and the rest of the insulation was not sealed to allow easy removal of the insulation for inspection. While this thermal imaging test was not essential for evaluation of the system, it proved the immediate value of a thermal camera system in discovering areas of leaking heat in closed cycle engines. Thermal cameras should continue to be used in closed cycle engine development for this purpose especially when one considers the plummeting cost of smart phone mounted bolometers.

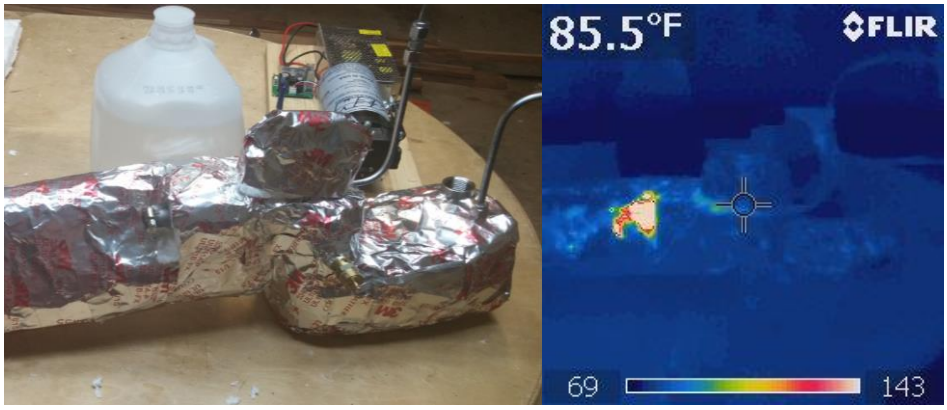

Figure 151 - Comparison of Visual and LWIR spectrum of insulated heat exchanger.

One other test was conducted to measure the effectiveness of 1 inch thick lung safe ceramic insulating mat. In the images shown below in Figure 152 the bare propane torch thermal image can be seen in the top left (with temperatures very quickly above the maximum measureable by the thermal camera). The top right image shows the same propane torch and flame with the insulated copper pipe placed over it. The insulated region of the pipe exhibited a near ambient surface temperature which indicates little heat will be lost from this region. This ceramic mat insulation is safe, cheap, and easily applied around thermal systems. It is an excellent candidate for further use in closed cycle engine experimentation.

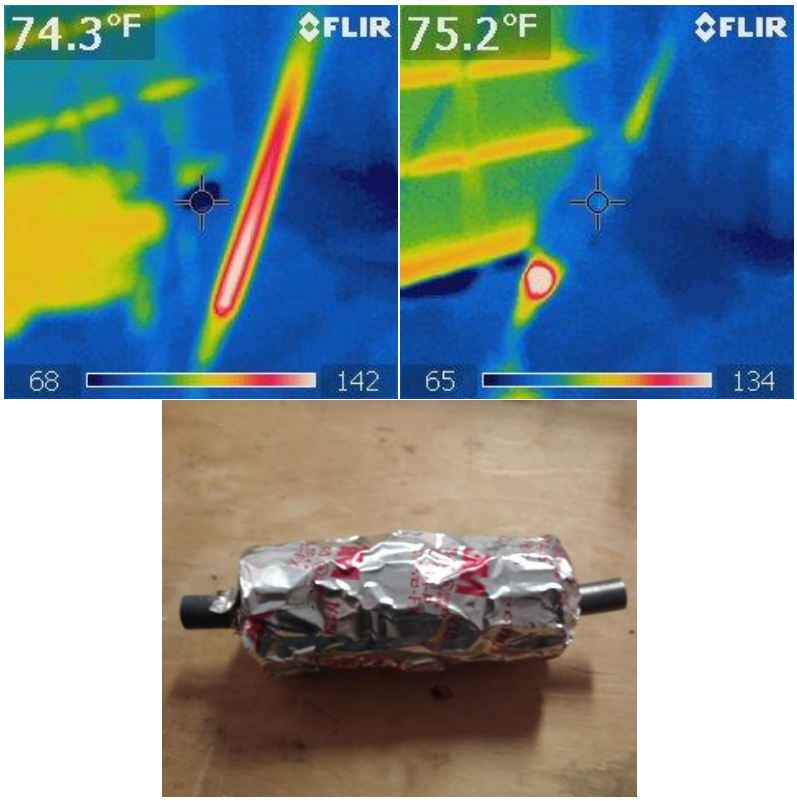

Figure 152- Effectiveness test of inhalation safe ceramic insulation with propane torch flame

35. Ceramic Bearings

As a result of corrosion problems encountered with the scroll expander, non-metallic bearing options were sought to upgrade the scroll expander to a state suitable for operating in a wet environment that lead to rapid corrosion in the multi-metal scroll design. Ceramic bearings exhibit lower friction, eliminate corrosion concerns between the bearing balls and race (through corrosion may still occur if a hybrid ceramic bearing is mounted in a dissimilar retainer), and can reach higher speeds than traditional steel bearings. Figure 153 shows a simple hybrid ceramic skateboard bearing that is suitable for moderate speed turbine applications. Current micro turbine research has well exceeded the capabilities of these small bearings and continued to develop higher speed turbines using fluid or magnetic options. Speeds in excess of 250,000 rpm are not uncommon for these contactless bearing types. If a closed cycle turbine based engine is to remain cost effective, the system should be made to function with simple and robust bearings.

Figure 153 - Low Cost Ceramic Skate Board Bearings suitable for High Speed Corrosion Resistant Operation

The steel bearings found inside of the scroll compressor rapidly corroded after the first steam based test as shown in Figure 154 below. These bearings were removed and the races cleaned as best as

possible with solvent and steel brushes to remove the residue left by corrosion. These bearings were then replaced with ceramic balls of the same type shown in Figure 155 to eliminate the conductive path between the steel thrust plates in the scroll compressor. During operation this thrust bearing carries considerable load as the entire back plate of the orbiting scroll is pressed against this bearing with the average scroll pressure. Proper tensioning and smooth operation of the thrust bearing is fundamental to efficient scroll operation. Ceramic bearings in place of steel will mostly eliminate the possibility of serious corrosion in the bearing's race.

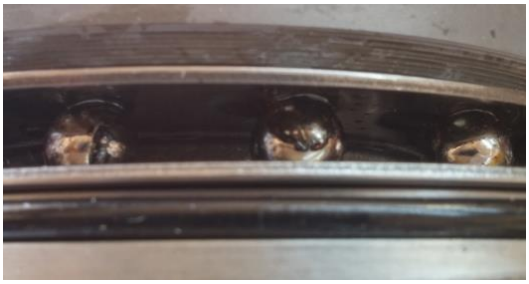

Figure 154 - Corrosion shown on steel thrust bearing inside of scroll expander.

Figure 155 - Ceramic ball bearings to replace Stock Steel Bearings in Scroll Expander

36. Ceramic Insulation

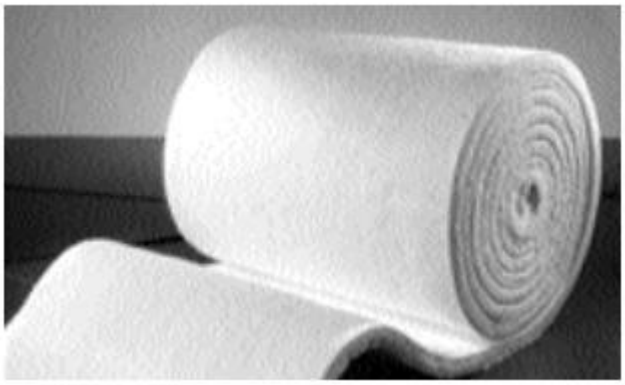

Figure 156 - Lung-safe CMS ceramic blanket insulation

A low cost lightweight thermal insulation was required to prevent heat loss from the closed cycle system. Typical cotton or fiberglass wool insulation was easily accessible, but would have posed a considerable fire risk. Even home insulation types manufactured to be fire resistant could possibly burn at the continued elevated temperatures experienced near a propane flame. Ceramic mat insulation depicted in Figure 156 as used in furnaces, wood burning heaters, and other high temperature home appliances was sourced to insulate the boiler, expander, and other high side elements where heat retention is paramount. Lung safe CMS insulation was used because it retained all the essential temperature and flame tolerance requirements while simplifying safety during use. The ceramic material produces many fine particulates as it is flexed and cut during application. Using a lung-safe variety of ceramic wool reduced the risk of chronic effects of using the material.

Simple tests were conducted with the ceramic insulation to make sure it would not become more of a fire hazard than it helps to prevent. Small sections of material were exposed to direct flame and did not catch fire. The material did reach its melting point and changed irrevocably, but did not continue to burn or show signs of sustaining flame. This is useful in the insulation of closed cycle systems, because and high temperature leaks from the boiler flame shield will somewhat cauterize the insulation

surrounding it and reduce the magnitude of the thermal leak automatically. In most circumstances the ceramic insulation is expected to work within its material limits. The insulation is covered with aluminum HVAC tape to maintain the wrap's structure and make the systems easier to handle without encountering large amounts of ceramic particulate residue on the experimenters hands.

37. Stainless Steel Tubing

Two diameters of stainless steel automotive brake line were used during the study, ¼ inch and 1/8 inch. As previously discussed, the ¼ inch tubing was overly difficult to shape into compact heat exchange coils. Additionally, the relatively large radius required meant that simply turning the tubing requires significant space that often could not be contained within heating pipes. Another advantage of using smaller diameter tube is that the larger thickness to diameter ratio meant that it could be more easily formed without requiring a mandrel to prevent buckling of the tubing. A mandrel failure while bending copper tubing can be seen below in Figure 157, while a successful bend of 1/8 inch diameter tubing around a common 1.5" diameter wooden dowel is shown in Figure 158.

Figure 157 - Buckled copper tubing during attempt to make superheating coil.

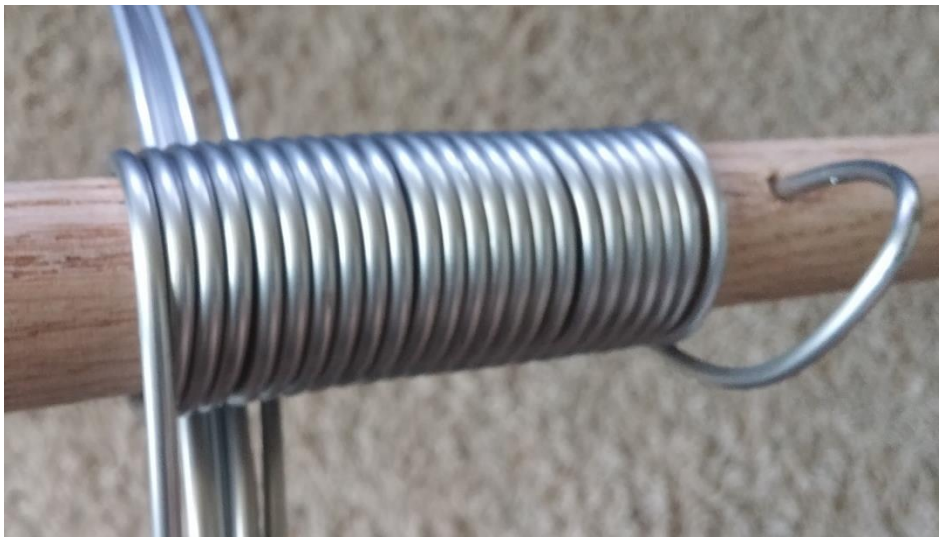

Figure 158 - 1/8 inch Stainless tubing bent around 1.5" diameter dowel without need for mandrel to prevent buckling

The downside of using smaller diameter tubing with proportionally thicker walls is that the weight of the cooling system will increase and maximum flow rate through a monotube boiler will be limited by the speed of sound through the pipe and other increased pressure losses. Theoretically, smaller diameter tubing can create lighter weight systems when thinned to the theoretical limit, however practical

manufacturing capability cannot produce adequately thin walls, so in practice the weight benefit of using smaller diameter tubing will stop once the minimum manufacturable thickness is reached.

38. Superheater Made of Copper Fittings

In some cases a future experimenter might wish to make a superheater to increase the gas temperature beyond the saturation temperature reached in the boiler. A particularly easy method of surrounding a stainless tube with combustion gasses before entry to the main boiler was created with ¼ inch brake line and a series of 45 degree copper fittings. These 45 degree fittings shown in Figure 159 were used so they could be slid over a straight section of tubing without the need to bend the pipe which would prohibit the straight sections of tubing. Figure 160 shows this same series of copper tubing and fittings after the internal tubing was bent into proper shape. Using 90 degree fittings would have made construction considerably more difficult. While the author acknowledges this is far from the most efficient superheater, it is one that can be easily created on a low budget and withstand high temperatures and pressures seen in the internal pipe. The copper tubing is never pressurized as it only serves as a flame barrier between the stainless tube and ceramic insulation. Copper fittings were joined with stainless rivits to solidify the assembly.

Figure 159 - Simple superheater created from copper pipe around stainless pressurized tubing

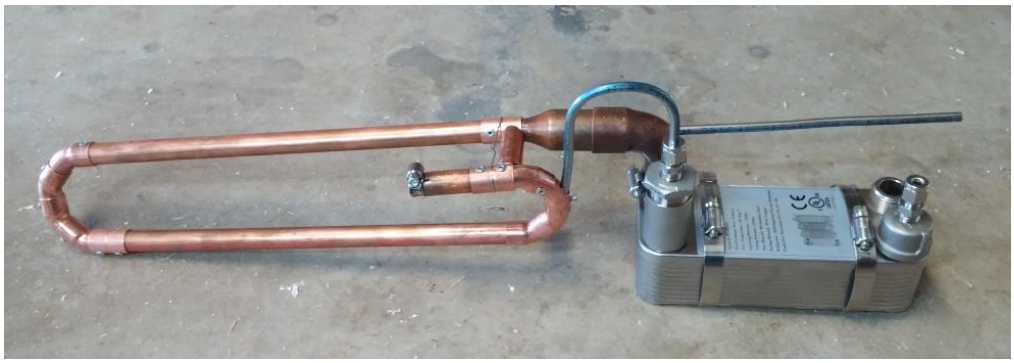

Figure 160 - Superheater after being coiled into proper position.

REFERENCES

[1] T. C. Hays, "High Energy Density Propulsion System Design and Testing for Small Unmanned Systems," 2012.

[2] Stewart, "Besler Steam Airplane," 2011. [Online]. Available: http://www.virtualsteamcarmuseum.org/.

[3] R. Mcconaghy, "An Improved Stirling Engine for Model Aircraft Propulsion," *AIAA: IECEC,* p. 1831, 1987.

[4] N. Clark, "TINY FDTD".

[5] J. Sprenger, "www.rcgroups.com," 11 may 2011. [Online]. Available: http://www.rcgroups.com/forums/showthread.php?t=296462&page=99#post18373923.

[6] "Model Aircraft Engines," Model Engineer, 1948.

[7] C. Mittelsteadt, "regenerative fuel cells for energy storage".

[8] R. McConaghy, "Flight Tests of a Stirling Powered Model Aircraft," in *Intersociety Energy Conversion Engineering Conference Proceedings (IECEC)*, 1986.

[9] d. haywood, "stirling cycle research group".

[10] R. Mcconaghy, "Flight Tests of a Stirling Powered Model Aircraft," *AIAA: IECEC,* p. 193.

[11] ". B", "learn thermo.com," [Online]. Available: http://www.learnthermo.com/. [Accessed 2014].

[12] AEC america, "aec-america," [Online]. Available: http://www.aec-america.com/images/pstnskrt.jpg. [Accessed 2014].

[13] T. A. Davidson, "Design and Analysis of a 1 KW Rankine Power Cycle Employing a Multi-Vane Expander, for Use With Low Temperature Solar Collector.," 1977.

[14] Mathias, "Experimental Testing of Gerotor and Scroll Expanders Used in, and Energetic and Exergetic Modeling of, an Organic Rankine Cycle.".

[15] V. Lemort, "Experimental Study if the Integration of a Scroll Expander into a Heat Recovery Rankine Cycle," University of Liege, 2006.

[16] M. Daif, "youtube - magnetic gear," 2015. [Online]. Available: https://www.youtube.com/watch?v=_qpHMZ9L4P8.

[17] magnetic gear turbines, "magnetic gear turbines," 2015. [Online]. Available: http://www.mgt.com.au/?pageId=6923.

[18] G. P. e. a. M. Pini, "Preliminary design of a centrifugal turbine for ORC applications," in *First International Seminar on ORC Power Systems*, 2011.

[19] M. Saarlas, Steam and Gas Turbines for Marine Propulsion, 1978.

[20] Borghese, "NARSA compact heat exchanger design presentation," 2012.

[21] unknown, "Early Aviator," [Online]. Available: http://www.earlyaviator.com/archive1.htm. [Accessed 2015].

[22] p. schreckengost, "Curtis RC3-2 Racer".

[23] F. W. Meredith, "Cooling of Aircraft Engines with special reference to Ethylene Glycol Radiators Enclosed in Ducts," *Reports and Memoranda No 1683: Director of Scientific Research, Air Ministy,* 1935.

[24] "super street online," [Online]. Available: http://www.superstreetonline.com/features/news/sccp-0808-p51-mustang-net-thrust-downforce/.

[25] "thermoelectrics," [Online]. Available: http://thermoelectrics.matsci.northwestern.edu/thermoelectrics/history.html.

[26] "chola turbo," [Online]. Available: http://www.cholaturbo.com/steam-turbines-salient-features.html.

[27] "Lehrstuhl für Elektrische Antriebe und Maschinen," [Online]. Available: http://www.eam.eei.uni-erlangen.de/Studien-Diplomarbeiten/Da550Ma.html.

[28] "3T RPD," [Online]. Available: http://www.3trpd.co.uk/design-museum-the-future-is-here/.

[29] G. Muller, Handbook of Engineering Acousics, springer, 2013.

[30] E. K. Z. Gnutek, "Application of Rotary Vane Expanders in Systems Utilizing the Waste Heat," *International Compressor Engineering Conference,* 1993.

[31] P. P. V. L. O. S. G. D. Yulia Glavatskaya, "Reciprocating Expander for and Exhaust Heat Recovery Rankine Cycle for a Passenger Car Application," *Energies ,* 2012.

[32] S. Yongkang, Heat Transfer - Introduction to Convection.

[33] H. Y. X.-J. Y. Xiao-Dong Niu, "Characteristics of a MHD Power Generator Using a Low Melting Point Gallium Alloy," *Electrical Engineering,* pp. 37-43, 2012.

[34] O. T. Wire, "H. H. Groves: The Legacy," *2014.*

[35] N. D. M. E. S. H. T. A. J. J. K. Wayne L. Staats, "Heat Transfer and Pressure Drop Performance of the Air Bearing Heat Exchanger," *ASHRAE.*

[36] S. Watanawanavet, "Optimization of a High-Efficiency Jet Ejector by Using Computational Fluid Dynamic Software," Texas A&M University.

[37] R. C. K. S. W. D. Bryce, "An Investigation of the Noise From a Scale Model of an Engine Exhaust System," *Journal of Sound and Vibration,* pp. 15-37, 1976.

[38] H. J. Visser, Array and Phased Array Antenna Basics, Netherlands: John Wiley and Sons, 2005.

[39] S. Q. C. C. J. L. Vincent Lemort, "Testing and Modeling a Scroll Expander Integrated Into an Organic Rankine Cycle," *Applied Thermal Engineering,* 2009.

[40] I. V. T. J. L. Vincent Lemort, "Experimental Study opf the Integration of a Scroll Expander into a Heat Recovery Rankine Cycle," *International Compressor Engineering Conference,* 2006.

[41] K. D. Viera, "Technical Study: Unmanned Aerial Systems, Engine Study," 2009.

[42] J. M. M. K. Vaclav VODICKA, "Scroll Expanders for Low-Power ORC," *ANNALS of Faculty Engineering Hunedoara - International Journal of Engineering,* vol. 12, 2014.

[43] R. L. M. V. V. Calmidi, "Forced Convection in High Porosity Metal Foams," *Journal of Heat Transfer,* 2000.

[44] S. Q. V. Lemort, "Designing Scroll Expanders for use in Heat Recovery Rankine Cycles," *ImechE,* 2009.

[45] UNEP, "Energy Efficiency Guide for Industry in Asia: Fuels and Combustion".

[46] R. H. Thurston, "The Graphics of the Efficiencies of the Steam Engine," *Journal of the Franklin Institute,* 1894.

[47] M. E. Talaat, "Magnetohydrodynamic Electric Power Generators," *Advanced Energy Conversion,* pp. 19-35, 1961.

[48] S. E. Systems, "Organic Rankine Cycle Silent Power Plant," 1980.

[49] G. P. Succi, "Design of Quiet Efficient Propellers," Massechusetts Institute of Technology.

[50] I. a. f. t. p. o. W. a. Steam, "The International Association for the Properties of Water and Steam," IAPWS, 2007.

[51] S. Q. V. L. Sebastien Declaye, "Development of a Waste Heat Recovery ORC Prototype Using an Oil-Free Scroll Expander," 2011.

[52] M. Sato, "Comparing three methods of free boundary implementation for analyzing elastodynamics using the finite-difference time-domain formulation," *Acoustical Science and Technology,* 2007.

[53] O. C. D. E. U. A. J. N. O. Samuel O. Mathew, "Magneto Hydrodynamics Power Generation Using Salt Water," *Asian Journal of Natural and Applied Sciences,* vol. 1, no. 4, 2012.

[54] A. H. S. W. Rienstra, "An Introduction to Acoustics," *Eindhoven University of Technology,* 2012.

[55] J. S. B.-S. C. S. Han, "Development of a 200KW ORC Radial Turbine for Waste Heat Recovery," *Journal of Mechanical Science and Technology.,* pp. 5231-5241, 2014.

[56] G. F. Robertson, "Experimental and Analytical Study of a Steam Vane Expander," *Technical Memorandum - Pennsylvania State University Applied Research Laboratory,* 1977.

[57] R. A. Renner, "The California Steam Bus Project," *International Research and Technology Corporation,* 1973.

[58] D. F. R. Zanelli, "Experimental Investigation of a Hermetic Scroll Expander-Generator," *International Compressor Engineering Conference,* 1994.

[59] A. G. S. B. E. T. Qijun Yu, "Carbon-Foam Finned Tunes in Air-Water Heat Exchangers," *Applied Thermal Engineering,* pp. 131-143, 2006.

[60] P. K. K. N. E. A. P Dutta, "Organic Brayton Cycles with solid sorption thermal compression," *Applied Thermal Engineering,* 2014.

[61] S. J. Orfanidis, Electromagnetic Waves and Antennas, 2010.

[62] L. D. Nichols, "Comparison of Brayton and Rankine Cycles Magnetogasdynamic Space-Power Generation Systems," *NASA,* 1969.

[63] A. B. Nagy, "Aeroacoustics Research in Europe: The CEAS-ASC Report on 2010 Highlights," 2010.

[64] N. Y. T. H. Musthafa b. Mohd.Tahir, "Efficiency of Compact Organic Rankine Cycle System with Rotary-Vane-Type Expander for Low-Temperature Waste Heat Recovery," 2010.

[65] G. A. Motors, "Air Motors/Gearmotors," GAST.

[66] S. J. Miley, "Review of Liquid-Cooled Aircraft Engine Installation Aerodynamics.," Texas A&M University, College Station Texas.

[67] A. W. Mike Todman, "Jet Age Steam Power for Marine Propulsion," *Ship Design and Operating for Environmental Sustainability.*

[68] X. Mengmeng, "Thermodynamic and Gas Dynamic Aspects of a BLEVE," Delft University of Technology, 2007.

[69] C. B. Meher-Homji, "The Historical Evolution of Turbomachinery," 29th Turbomachinery Symposium.

[70] R. McConaghy, "Flight Tests of A Stirling Powered Modelk Aircraft," *IC,* IECEC.

[71] R. Mcconaghy, "Design of a Stirling Engine for Model Aircraft Propulsion," *IECEC,* p. 490, 1986.

[72] R. Mcconaghy, "A Hot Aero Engine," *Model Engineer,* 14 February 1986.

[73] A. M. A. F. C. M. H. H. Matthew Orosz, "Comparison of Scroll and Piston Expanders for Small Scale ORC Applications," *STG International.*

[74] J. A. Mathias, "Experimental Testing of Gerotor and Scroll Expanders Used in, and Energetic and Exergetic Modeling of, and Organic Rankine Cycle," *Journal of Energy Resources Technology,* 2009.

[75] S. B. M. P. Masa Bukurov, "The Efficiency Rate of a Steam-Water Injector," University of Novi Sad, 2012.

[76] C. Lin, "Feasibility of Using Power Steering Pumps in Small-Scale Solar Thermal Electric Power Systems," *Massechusetts Institute of Technology,* 2008.

[77] O. G. E. A. Leonid Moroz, "Axial Turbine Flow Path Design for an Organic Rankine Cycle Using R-245FA," *ASME Turbo EXPO 2013: Turbine Technical Conference and Exposition,* 2013.

[78] Ledex, "Ledex Low Profile Linear Solenoids," Johnson Electric.

[79] B. Kolbrek, "Horn Theory: An Introduction," 2008.

[80] R. J. M. Klaus Brun, "The Power of Design: SwRI Engineers Develop a Low-Cost Centrifugal Gas Turbine," 2004.

[81] H. L. E. a. K.C. Leong, "Numerican and Experimental Study of Forced Convection in Graphite Foams," *Applied Thermal Engineering,* 2010.

[82] R. L. C. Jr., "Expansion Engines," Model Airplane News, 1948.

[83] J. Jopkinson, "How Good was the Steam Locomotive," Gloucestershire Society for Industrial Archaeology Journal for 1990, 1990.

[84] J. R. J. J. E. A. James A. Mathias, "Experimental Testing of Gerotor and Scroll Expanders Used in and Energetic and Exergetic Modeling of an Organic Rankine Cycle," *Journal of Energy Resources Technology,* 2009.

[85] J. R. Iwaszko, "History of Wireless Electromagnetic Powered Flight," AurumSolid Technologies, 28-11-2011.

[86] J. Y. E. A. Hyunjin Kim, "Design of a Scroll Expander for an ORC Applicible to a Passenger Car for Fuel Consumption Improvement".

[87] H. J. K. Y. C. K. Hyan Jin Kim, "A Steam Expander for a Waste Heat Recovery Cycle," *International Refrigeration and Air Conditioning Conference,* 2010.

[88] D. Y. G. Huijuan Chen, "A Review of Thermodynamic Cycles and Working Fluids for the Conversion of Low-Grade Heat," *Renewable and Sustainable Energy Reviews,* 2010.

[89] M. N. M. M. E. A. Hideki KUWABARA, "Micro Steam Energy Generator," *Kobelco Technology Review ,* 2010.

[90] M. K. E. A. Hideaki Nagata, "Development of a Scroll Expander for the CO2 Refrigeration Cycle," *International Compressor Engineering Conference,* 2010.

[91] G. P. Hatch, "Recent Developments in Permanent Magnet Gear Systems and Machines," *Magnetics 2010 Conference,* 2010.

[92] A. S. Hartmut Spliethoff, "The Organic Rankine Cycle - Power Production from Low Temperature Heat," *Electricity Generation - Combined Heat and Power,* 2006.

[93] K. J. Harada, "Development of a Small Scale Scroll Expander," *Oregon State University Thesis,* 2010.

[94] R. P. T. H. Hailei Wang, "Design Study of Configurations of System COP for a Combined ORC and VCC," *Energy,* pp. 4809-4820, 2011.

[95] R. B. P. T. H. H Wang, "Experimental Performance of a Compliant Scroll Expander for an Organic Rankine Cycle," *Power and Energy,* p. 863, 2009.

[96] H. H. Groves, "Celebrating 100 Years of Tethered Hydroplane Racing," *On The Wire,* 2014.

[97] B. Gothert, "The Drag of Airplane Radiators with Special Reference to Air Heating (Comparison of Theory and Experiment)," *Luftfahrtforshung,,* vol. 15, no. 9, 1938.

[98] K. P. Gnutek Zbingniew, "Experimental Studies on Low Power ORC's with Vane Expanders," *Wroclaw University of Technology, Institute of Power Engineering and Fluid Mechanics.*

[99] Y.-Z. L. J. L. J. J. Gang PEI, "Performance evaluation of a micro turbo-expander for application in low-temperature solar electricity generation," *Journal of Zhejiang University - Applied Physics and Engineering,* 2011.

[100] Y.-z. L. J. L. J. J. Gang PEI, "Performance Evaluation of a Micro Turbo-Expander for Application in Low-Temperature Solar Electricity Generatio," *Journal of Zhejiang University,* pp. 207-213, 2011.

[101] M. Gaia, "30 Years of Organic Rankine Cycle Development," *First International Seminar on ORC Power Systems.*

[102] T. Foale, "Engine Balance".

[103] K. S. B. F. Farassat, "The Acoustic Analogy and the Prediction of the Noise of Rotating Blades," *Theoretical and Computational Fluid Dynamics,* pp. 155-170, 1998.

[104] B. L. M. G. S. H. E. A. F. David Doty, "High-Efficiency Microturbine Technology," *IECEC,* pp. 436-442, 1991.

[105] D. G. ELLIOTT, "Magnetohydrodynamic Power Systems," *J. Spacecraft,* 1967.

[106] ECAT, "Foam Materials: Types, Properties, Applications," Perm, Russia.

[107] O. o. S. R. a. Development, Visibility Studies and Some Applications in the Field of Camouflage, Washington D. C., 1946.

[108] T. A. Davidson, "Design and Analysis of a 1 KW Rankine Power Cycle, Employing a multi-vane Expander, For use with a low temperature solar collector.," *Massachusetts Institute of Technology,* 1977.

[109] F. G. M. F. M. Daniele, "Thermo-Fluid Dynamics Preliminary Design of Turbo-Expanders for ORC Cycles," *Applied Energy,* pp. 601-608, 2012.

[110] I. V. E. A. Bruno Vanslambrouck, "Turn Waste Heat into Electricity by Using an Organic Rankine Cycle," *2nd European Conference on Polygeneration,* 2011.

[111] L. J. Brasz, "Ranking of Working Fluids for Organic Rankine Cycle Applications," *International Refrigeration and Air Conditioning Conference,* 2004.

[112] J. Branford, "On The Wire: Tethered Cars and Hydroplanes," *Flash Steam Tethered Hydroplane Engines,* 2014.

[113] L. L. Beranek, Acoustics, 1954.

[114] G. K. E. a. Bahaa Saleh, "Working Fluids for Low-Temperature Organic Rankine Cycles," *Energy,* 2006.

[115] A. Attarian, "Acoustic Wave Propagation," 25 may 2006.

[116] A. R. Arthur Williams, "The Performance of Centrifugal Pumps as Turbines and

] Influence of Pump Geometry," *University of Nottingham.*

[117] A. A. Adames, "Design Considerations of a 15KW Heat Exchanger for the CSPonD Project," *Massechusetts Institute of Technology,* 2010.

[118] Aalco, "Stainless Steel Pipe & Tube - Pressure Ratings".

[119] N. C. G. Q. Y. E. A. A. G. Straatman, "Forced Convection Heat Transfer and Hydraulic Losses in Graphitic Foam," *Journal of Heat Transfer,* p. 1237, 2007.

[120] G. L. B. A. D. Jones, "Determination of Two-Stroke Engine Exhaust Noise by the Method of Characteristics," *Journal of Sound and Vibration,* pp. 305-327, 1981.

[121] S. K. E. K. H. S. A Schuster, "Energetic and Economic Investigation of Organic Rankine Cycle Applications," *Applied Thermal Engineering,* pp. 1809-1817, 2009.

[122] "Heat Transfer From Condensing Vapours," 2015. [Online]. Available: http://www.nzifst.org.nz/unitoperations/httrtheory8.htm.

[123] "Heat Exchangers: Mechanical Equipment and Systems".

[124] "H. H. Groves - Model Aviation Pioneer," 2007. [Online]. Available: http://modelenginenews.org/sparey/hh_groves.html. [Accessed 2015].

[125] "Contrails! Aerodynamics of the Radiator," contrails.free.fr, 2015.

[126] "CNC Cookbook: Engine Projects: Steam Turbines," 2015. [Online]. Available: www.cnccookbook.com/CCSteamTurbines.htm.

[127] Y. S. P. Zuniga, "Design of an Axial Turbine and Thermodynamic Analysis and Testing of a K03 Turbocharger," Massachusetts Institute of Technology, 2011.

[128] Zanelli, "Experimental Investigation of a Hermetic Scroll Expander-Generator," 1994.

[129] E. Wonnacott, "Lower Exhaust Noise from Better Silencer Design Techniques," *Military Vehicles and Engineering Establishment,* 1974.

[130] L. H. WAP Hayward, "Pressure Generated by Syringes: Implications for Hydrodissection and Injection of Dense Connective Tissue Lesions," *Scandinavian Journal of Rheumatology,* pp. 379-382, 2011.

[131] H. J. Visser, "Array and Phased Array Antenna Basics".

[132] K. D. Viera, "Unmanned Aerial Systems Engine Study".

[133] S. D. e. a. V Lemort, "Experimental Characterization of a Hermetic Scroll Expander for use in a Micro-Scale Rankine cycle," 2011.

[134] M. A. Tussing, "Diesel Cylander Head Design Up To 250 Bar Peak Cylander Pressure," Southwest Research Institute, San Antonio, Texas, 2011.

[135] A. S. a. O. K. Tiow, "Introduction of the Revolving Vane Expander," *HVAC&R Research,* pp. 801-816, July 2009.

[136] Y. Teshome, "CFD Study on the Performance of Regeranative Flow Pump (RFP) with Aerodynamic Blade Geometry," Addis Ababa University, Addis Ababa, Ethiopia, 2007.

[137] M. A. Tarique, "Experimental Investigation of Scroll Based Organic Rankine Systems," University of Ontario Institute of Technology, Ontario, 2011.

[138] T. F. e. a. Takahisa Yamamotoa, "Design and testing of the Organic Rankine Cycle," pp. 239-251, 2001.

[139] M. V. D. B. e. a. Sylvain Quoilina, "Techno-economic survey of Organic Rankine Cycle (ORC) systems," *Renewable and Sustainable Energy Reviews,* pp. 168-186, 2013.

[140] G. P. Succi, "Design of Quiet Efficient Propellers".

[141] A. Stoll, "Design of Quiet UAV Propellers," Stanford University, 2012.

]

[142] W. B. a. R. Stevens, "An Investigation of the Noise from a Scale Model of an Engine Exhaust System," *National Gas Turbine Establishment,* 1975.

[143] D. o. D. D. C. Standard, "Noise Limits," *Military Standard 1974,* 1997.

[144] P. Z. S. Spakovszky, "Unified thermodynamics and propulsion," [Online]. Available: http://web.mit.edu/16.unified/www/FALL/thermodynamics/notes/node28.html.

[145] R. Shah, Compact Heat Exchangers for the Process Industries, New York: Begell House, 1997.

[146] P. Shah and D. P. Sekulic, Fundamentals of Heat Exchanger Design, New York: John Wiley, 2003.

[147] M. Sato, "Comparing Three Methods of Free Boundary Implementation for Analyzing Elastodynamics Using the Finite Difference Time Domain Formulation," *Acoustic Science and Technology,* 2007.

[148] A. Sanchez-Torres, Radioisotope Power Systems for Space Applications, InTech, 2011.

[149] T. W. S.J. Dudzinsky, "MHD Induction Generator," 1968.

[150] R. J. e. a. S. N.Y. Gerges, "Muffler Modeling by Transfer Matrix Method and Experimental Verification," pp. 132-140, 2005.

[151] C. S. S. Meir, "Highly-Efficient Thermoelectronic Conversion of Solar Energy and Heat into Electric Power," 2013.

[152] A. Ross, Making Stirling Engines, 1993.

[153] G. F. Robertson, "Experimental and Analytical Study of a Steam Expander," 1977.

[154] H. T. H. R. B. Peterson, "Performane of a small-scale Regenerative Rankine Power Cycle Employing a Scroll Expander".

[155] H. W. e. a. R B Peterson, "Performance of a Small-Scale Regenerative Rankine Power Cycle Employing a Scroll Expander," *Proceedings of the Institution of Mechanical Engineers, Part A: Journal of Power and Energy,* pp. 271-282, 2008.

[156] S. Quoilin, "Experimental Study and Modeling of a Low Temperature Rankine Cycle for Small Scale Cogeneration," University of Liege, 2007.

[157] S. B. Prasad, "Steam Engine Characteristics and Theoretical Performance," pp. 1323-1333, 1993.

[158] P. M. Piancastelli Luca, "The Bonus of Aircraft Piston Engines, an Update of the Meredith Effect".

[159] P. Peter, "Novel Steam Engine for Multi-Primary Energy Resources," in *First European Conference on Polygeneration*.

[160] F. J. Patel, "Component Matching for Ultra-Low Grade Thermal Energy Recovery Operating in Organic Rankine Cycle," San Diego State University, San Diego, California, 2013.

[161] C. A. Parsons, "The Steam Turbine," 2011.

[162] S. J. Orfanidis, "Electromagnetic Waves and Antennas".

[163] M. Ohadi, "Force-Fed Microchannels for High Flux Cooling Applications," in *Next Generation Microchannel Heat Exchangers*, 2013, pp. 33-34.

[164] K. E. Nichols, "How to Select Turbomachinery For Your Application".

[165] B. Nichols, "Specific Speed Expander Chart," 2014. [Online]. Available: http://www.barber-nichols.com/sites/default/files/wysiwyg/images/nsds_pump_chart.pdf.

[166] C. Newton, "A Concentrated Solar Thermal Energy System," Florida State University College of Engineering, 2007.

[167] N. Y. e. a. Musthafah b. Mohd.Tahir, "Efficiency of Compact Organic Rankine Cycle System with Rotary-Vane-Type Expander for Low-Temperature Waste Heat Recovery," *International Journal of Civil and Environmental Engineering,* pp. 11-16, 2011.

[168] R. G. A. a. J. E. Mullaney, "Effect of Back Pressure on Re-Entry Turbine Performance," Denver, Colorado, 1964.

[169] Mueller, "Aeroacoustic Measurements".

[170] C. C. Mowrey, "High Head-Low Flow Centrifugal Pumps," in *Fifth International Pump Users Symposium*, Arvada, Colorado.

[171] I. Micro Motors, "Miniature Air Motors and Drills for Exacting High Performance Applications".

[172] K. C. e. a. Michael Ohadi, "Next Generation Microchannel Heat Exchangers," *SPRINGER BRIEFS IN APPLIED SCIENCES AND TECHNOLOGY,* 2013.

[173] F. Meredith, "Cooling of Aircraft Engines with Special Reference to Ethylene Glycol Radiators Enclosed in Ducts".

[174] J. B. e. a. Marc C. Jacob, "A rod-airfoil experiment as benchmark for broadband noise modeling," *Theoretical and Computational Fluid Dynamics,* pp. 171-196, 2005.

[175] MacNaughton, "Elementary Steam Power Engineering".

[176] K. a. London, Compact Heat Exchangers, New York: McGraw-Hill, 1984.

[177] V. Lemort, "Experimental Charictarization of a Hermetic Scroll Expander for Use in Micro-Scale Rankine Cycle".

[178] J. Lamancusa, Outdoor Sound Propagation, 2009.

[179] N. P. Laboratory, "2.4.1 The Speed and Attenuation of Sound," 2014.

[180] W. Krase, "Ericsson Cylce Gas Turbine Powerplants," 1979.

[181] K. H. Kim, "Thermodyanimic Performance of Regenerative Organic Rankine Cycles," *World Academy of Science, Engineering, and Technology,* 2011.

[182] M. W. e. a. Kent Davey, "Magnetic Gears–An Essential Enabler for the Next Generation's Electromechanical Drives".

[183] Y. L. J. Jamin, "Enhanced Heat Transfer Using Porous Carbon Foam," University of Calgary, Calgary, Alberta, Canada, 2005.

[184] J. G. e. a. J. M. Corberan, "Modeling of Refrigeration Piston Compressors," in *International Compressor Engineering Conference*, Valencia, Spain, 2000.

[185] V. P. Ivanov, "Active Noise Control in a Waveguide," *Computational Mathematics and Mathematical Physics (Vol 51, No 11),* 2011.

[186] B. V. Ignace Vankeirsbilck, "Efficiency Comparison Between the Steam Cycle and the Organic Rankine Cycle for Small Scale Power Generation," Kortrijk, Belgium.

[187] N. S. e. a. Ian K Smith, "Power Recovery from Low Cost Two-Phase Expanders".

[188] H. E. e. a. Hisham El-Dessouky, "Evaluation of steam jet ejectors," *Chemical Engineering and Processing ,* pp. 551-561, 2001.

[189] D. Haywood, "An Introduction to Stirling-Cycle Machines".

[190] R. B. P. H Wang, "Experimental Performance of a Compliant Scroll Expander for an Organic Rankine Cycle," *Proceedings of the Institution of Mechanical Engineers, Part A:*

Journal of Power and Energy, pp. 863-872, 2009.

[191] F. K. &. L. Glassburn, "Low Flow/High Head Centrifugal Pump Options," in *Calgary Pump Symposium*, Calgary, Alberta, Canada, 2005.

[192] 1. M. B. a. A. Ghaffari, "On the Application of Steam-Driven Water Jets for Propulsion Purposes," *Journal of Research of the National Bureau of Standards,* pp. 137-141, 1958.

[193] J. Fridh, "Experimental Investigation of Performance, Flow Interactions and Rotor Forcing in Axial Partial Admission Turbines," Royal Institute of Technology, Stockholm, Sweden, 2012.

[194] N. M. a. L. Frechette, "Performance Analysis of Brayton and Rankine Cycle Microsystems for Portable Power Generation," in *ASME International Mechanical Engineering Congress & Exposition*, New Orleans, Louisiana, 2002.

[195] T. O. A. Frank T. Jørgensen, "The Cycloid Permanent Magnetic Gear," *IEEE TRANSACTIONS ON INDUSTRY APPLICATIONS,* pp. 1659-1665, 2008.

[196] H. Fitzgerald, "World's First Steam Driven Airplane," *Popular Science Monthly,* July 1933.

[197] A. T. F. Payri, "Application of MacCormack Schemes to I.C. Engine Exhaust Noise Prediction," 1995.

[198] e. a. Eric E. Ungar, "Guide for Predicting the Aural Detectability of Aircraft," *Air Force Flight Dynamics,* 1972.

[199] U. D. o. Energy, "Development of a High Efficiency Hot Gas Turbo-expander and Low Cost Heat Exchangers for Optimized CSP Supercritical CO2 Operation," *Sunshot,* 2013.

[200] M. A. T. e. a. E. Oralli, "A Study on Scroll Compressor Conversion into Expander for Rankine Cycles," *International Journal of Low-Carbon Technologies,* 2011.

[201] O. o. S. R. a. Development, "Visibility Studies and Some Applications in the Field of Camouflage," *National Defense Research Committee.*

[202] R. J. A. a. P. O. A. L. Davies, "The Radiation of Sound From an Engine Exhuast," *J. Sound*

] *Vib.,* pp. 389-408, 1970.

[203] T. A. Davidson, "Design and Analysis of a 1KW Rankine Power Cycle, Employing a Multi-Vane Expander, For Use With a Low Temperature Solar Collector," Massachusetts Institute of Technology, 1977.

[204] G. P. e. a. D. Manolakosa, "Experimental evaluation of an autonomous low-temperature solar Rankine cycle system for reverse osmosis desalination," in *Elsevier*, 2006.

[205] e. a. Christos N. Markides, "Reciprocating Piston Expanders for Small-Scale ORC Systems".

[206] D. M. e. a. Choon Seng Wong, "Selection and Conversion of Turbocharger as Turbo-Expander for Organic Rankine Cycle (ORC)," in *New Zealand Geothermal Workshop*, Rotorua, New Zealand, 2014.

[207] D. M. e. a. Choon Seng Wong, "Selection and Conversion of Turbocharger as Turbo-Expander for Organic Rankine Cycle (ORC)," in *35th New Zealand Geothermal Workshop*, Rotorua, New Zealand, 2013.

[208] C. E. Brennen, Hydrodynamics of Pumps, Pasadena, California: Concepts ETI, Inc. and Oxford University Press, 1994.

[209] J. Borghese, "Compact Heat Exchanger Designs, Characteristics, and Trends," in *NARSA Heavy Duty Heating and Cooling Conference*, Ann Arbor, Michigan, 2012.

[210] L. L. Beranek, "Acoustics," 1954/1993.

[211] M. Bahrami, "Vapor Power Cycles".

[212] A. B. e. a. A.J.. Torresgrosa, "Experimental Assessment of Emission Models used for IC Enginge Exhaust Noise Prediction," *Experimental Thermal and Fluid Science ,* 2005.

[213] G. B. A.D. Jones, "Determination of Two Stroke Engine Exhaust Noise by the Method of Characteristics".

[214] "Worlds First Steam Driven Airplane," *Popular Science,* 1933.

[215] "Turbine specific speed concepts".

[216] "Thunder Power," 2014. [Online]. Available: http://www.thunderpowerrc.com/Products/7700-mAh_2/TP7700-6SPF70.

[217] "The Radiation of Sound from an Engine Exhaust".

[218] "Steam turbine unit 1kW," Didatec.

[219] "Rotary Valve Steam Engine".

[220] "Nusselt Number Correlations".

[221] "Noise and Vibration Control," *Indian Institute of Technology Roorkee.*

[222] "Muffler Modeling by Transfer Matrix Method and Experimental Verification".

[223] "Magnetohydrodynamic (MHD) Power Generation," *MHD Power Generation,* pp. 214-230.

[224] "Diesel Cylinder Head Design Up To 250 Bar Peak Cylinder Pressure".

[225] "Brayton Cycle".

[226] *Model Airplane News,* p. 13, 1948.

[227 *Flight Global,* p. 473, 1943.
]

APPENDICES

ZZZ. Mathematical Progression of Key Closed Brayton Cycle Efficiency Calculation

The algebraic progression from:

$$\eta = 1 - \frac{T_1\left[\left(\frac{P_2}{P_1}\right)^{\frac{\gamma-1}{\gamma}} - 1\right]}{T_4\cdot\left[1 - \left(\frac{P_5}{P_4}\right)^{\frac{\gamma-1}{\gamma}}\right]}$$

To:

$$\eta = 1 - \frac{T_1}{T_4}\cdot\left(\frac{P_2}{P_1}\right)^{\frac{\gamma-1}{\gamma}}$$

Is not immediately apparent (at least to the author). So I chose to detail this path so others might avoid similar frustration and wasted time over basic algebra. (Note that P5=P1 and P4=P2 given the assumptions of closed Brayton cycles)

$$\frac{\left(\frac{P_2}{P_1}\right)^{\frac{\gamma-1}{\gamma}} - 1}{1 - \left(\frac{P_2}{P_1}\right)^{\frac{-\gamma+1}{\gamma}}}$$

The initial equation with P1 and P2 subbed in to unify high and low side pressures. Note also that the bottom ratio has been inverted (with accompanying change in exponent sign) to match that of the numerator.

$$\frac{\left(\frac{P_2}{P_1}\right)^{\frac{\gamma-1}{\gamma}} - 1}{\frac{\left(\frac{P_2}{P_1}\right)^{\frac{\gamma-1}{\gamma}} - 1}{\left(\frac{P_2}{P_1}\right)^{\frac{\gamma-1}{\gamma}}}}$$

The key transformation occurs by multiplying the denominator by unity in the form of:

$$\frac{\left(\frac{P_2}{P_1}\right)^{\frac{\gamma-1}{\gamma}}}{\left(\frac{P_2}{P_1}\right)^{\frac{\gamma-1}{\gamma}}}$$

So that the top cancels leaving only:

$$\eta = 1 - \frac{T_1}{T_4} \cdot \left(\frac{P_2}{P_1}\right)^{\frac{\gamma-1}{\gamma}}$$

Replacing the more complicated constants with variables to simplify, the process becomes more readily visible.

$$\frac{A^b - 1}{1 - A^{-b}} = \frac{A^b - 1}{\frac{A^b - 1}{A^b}} = A^b$$

Lastly, the key inversion is demonstrated in additional detail.

$$\left(\frac{P_1}{P_2}\right)^{\frac{\gamma-1}{\gamma}} = \left[\left(\frac{P_2}{P_1}\right)^{-1}\right]^{\frac{\gamma-1}{\gamma}} = \left(\frac{P_2}{P_1}\right)^{\frac{-\gamma+1}{\gamma}}$$

AAAA.Theoretical Acoustic Directionality

"If the dimensions of a source are much smaller than the wavelength of the sound being radiated, so that it is a simple source, then the details of the surface motion are not important and it will radiate exactly the same sounds as any other simple source with the same source strength." – Mueller

An understanding of three dimensional propagation characteristics from a two dimensional aperture can be gained by first solving for two dimensional propagation patterns from a continuous line source as shown in Figure 161. Following the method outlined by Mueller (1) if a line source is established in which each differential element can be considered a simple source of strength:

$$dQ = U_o 2\pi a \text{ dx}$$

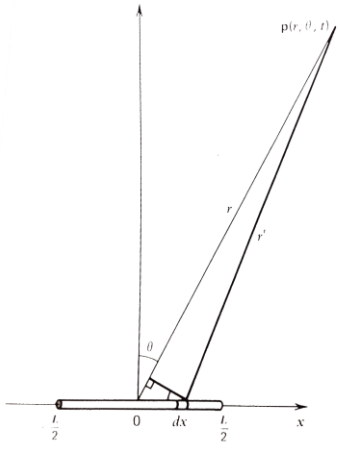

Figure 161 - Schematic showing integration of differential noise source elements across a line source. [29]

And generates a fluctuating pressure field identical to that of a simple source:

$$d\boldsymbol{p} = j\frac{\rho_o ck}{4\pi r'} U_o 2\pi a \, dx \, e^{j(\omega t - kr')} dx$$

Where r' is related to r by:

$$r' = r - x\sin\theta \qquad for\ r \gg L$$

The total pressure at a given location is found by integrating the pressure contributions of each source

$$\boldsymbol{p}(r,\theta,t) = j\frac{\rho_o c U_o k a}{2}\int_{-L/2}^{L/2}\frac{1}{r'}e^{j(\omega t - kr')}dx$$

Mueller (1) uses the simplification that r' in the denominator of the integral can be approximated as r, especially for cases when r>>L. This evaluates to (note the presence of a Bessel function as shown in Figure 162):

$$\boldsymbol{p}(r,\theta,t) = j\frac{\rho_o c U_o}{2}\frac{a}{r}kLe^{j(\omega t - kr)}\left[\frac{\sin(\frac{1}{2}kLsin\theta)}{\frac{1}{2}kL\,sin\theta}\right]$$

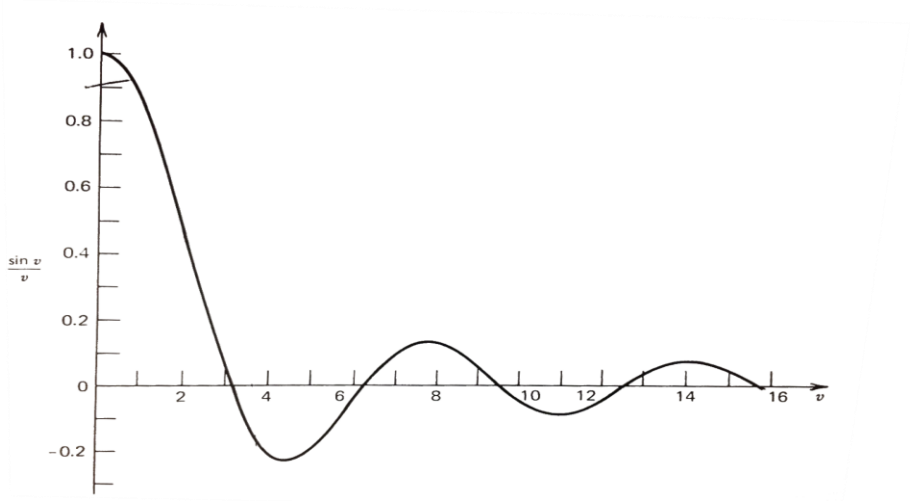

Figure 162 - Zeroth order spherical Bessel function, one can quickly see where the lobes in a typical antenna pattern arise from once the absolute value of this function is taken. [29]

Which is commonly written as:

$$P(r,\theta) = P_{ax}(r)H(\theta)$$

$$P_{ax}(r) = \frac{\rho_o c U_o}{2}\frac{a}{r}kL$$

$$H(\theta) = \left|\frac{\sin v}{v}\right| \text{ where } v = \frac{1}{2}kLsin(\theta)$$

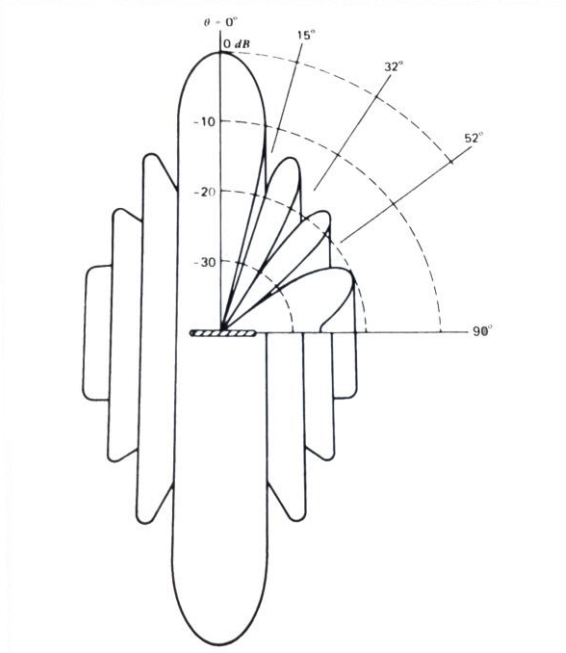

Figure 163 – The resulting 3D line source antenna pattern [29]

Where $H(\theta)$ is the zeroth order spherical Bessel function of the first kind and expresses pressures dependency on angle. $P_{ax}(r)$ is the factor that depends only on the distance away from the center of the line source. Figure 163 shows a typical volume of revolution produced by this line source.

One should note from this equation format that acoustic radiation patterns are the Fourier transform of the aperture function (2):

$$Fu(u) = \int_{-\infty}^{\infty} e_1(x) e^{-jkux} dx$$

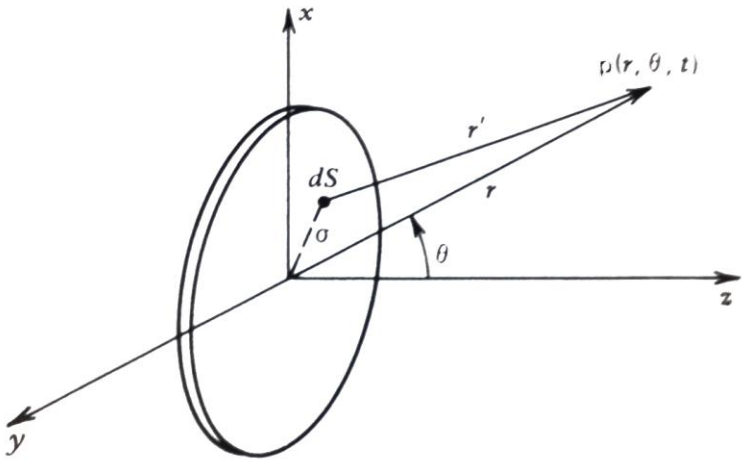

Figure 164 - Circular Radiating Aperture Element [29]

The same development method can be used to model a circular radiating aperture similar to the end of an exhaust pipe shown in Figure 164 with the resulting pattern shown in Figure 165. Instead of integrating across a line of simple radiators, one modifies the previous method to integrate over a disk of simple radiating elements. The directional gain $H(\theta)$ applied to the source field in the case of a circular radiating aperture is:

$$H(\theta) = \left|\frac{2J_1(v)}{v}\right| \text{ Where } v = ka\sin\theta$$

k is the wavenumber ($k = \frac{2\pi}{\lambda} = \frac{2\pi f}{c}$)

a is the radius of the aperture opening

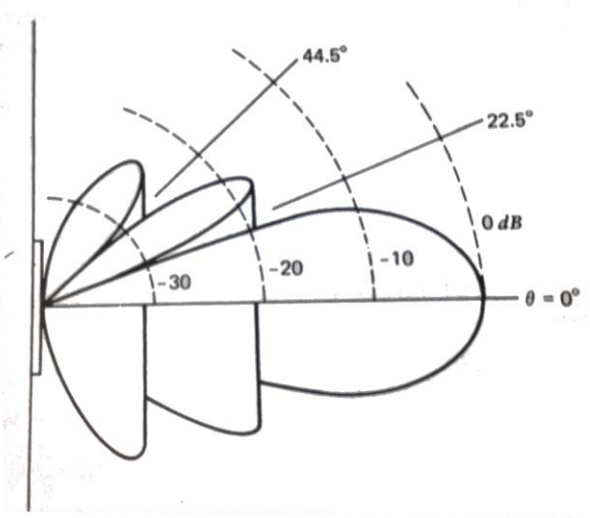

Figure 165 - Typical circular aperture beam and lobe antenna pattern. [29]

In the case of a 1 inch circular aperture, in an environment with a 1116 ft/s acoustic speed the relative transmission magnitude as a function of azimuth is shown in Figure 166 and Figure 167

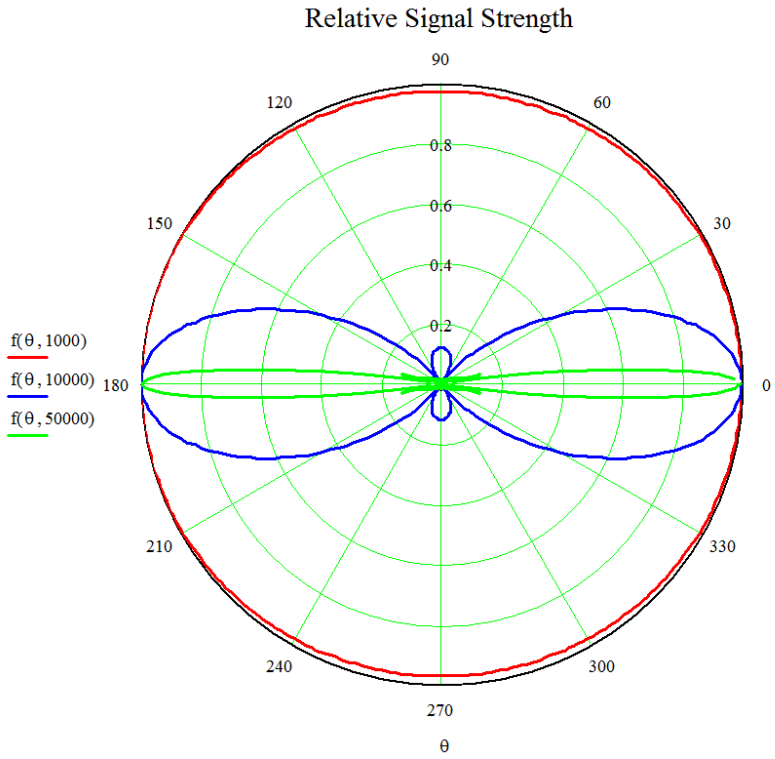

Figure 166 - Variation in Transmission Magnitudes with Direction

Unscaled Relative Signal Strength. Low frequencies (1000Hz - Red) exhibit omnidirectional propagation, while higher frequencies (50 KHz – Green) show extreme directionality from the 1 inch aperture.

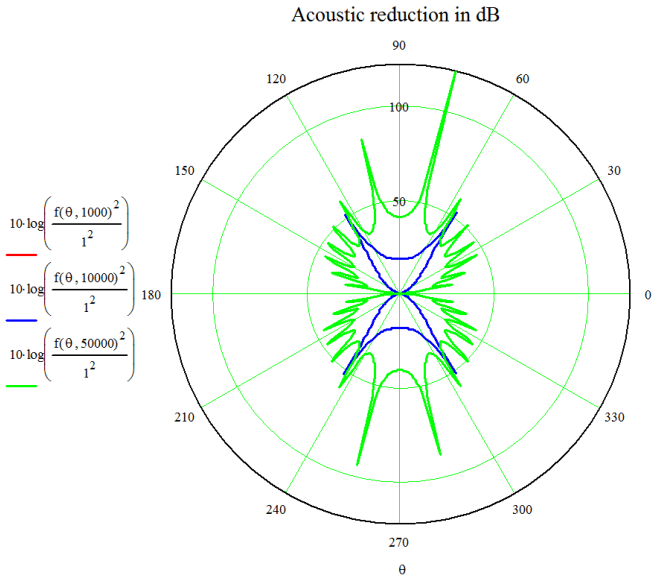

Figure 167 - Variation in Logarithmic SPL with Frequency

Identical dataset showing reduction in transmission in dB as a function of direction from a 1 inch diameter circular aperture. Note that the red curve at 1000Hz has nearly zero reduction.

If one records signal intensity 90 degrees from the axis of acoustic transmission, the chart below shows the predicted loss in dB as a function of frequency. This chart distinctively shows that low frequency noise propagation is entirely unaffected by a relatively small apertures.

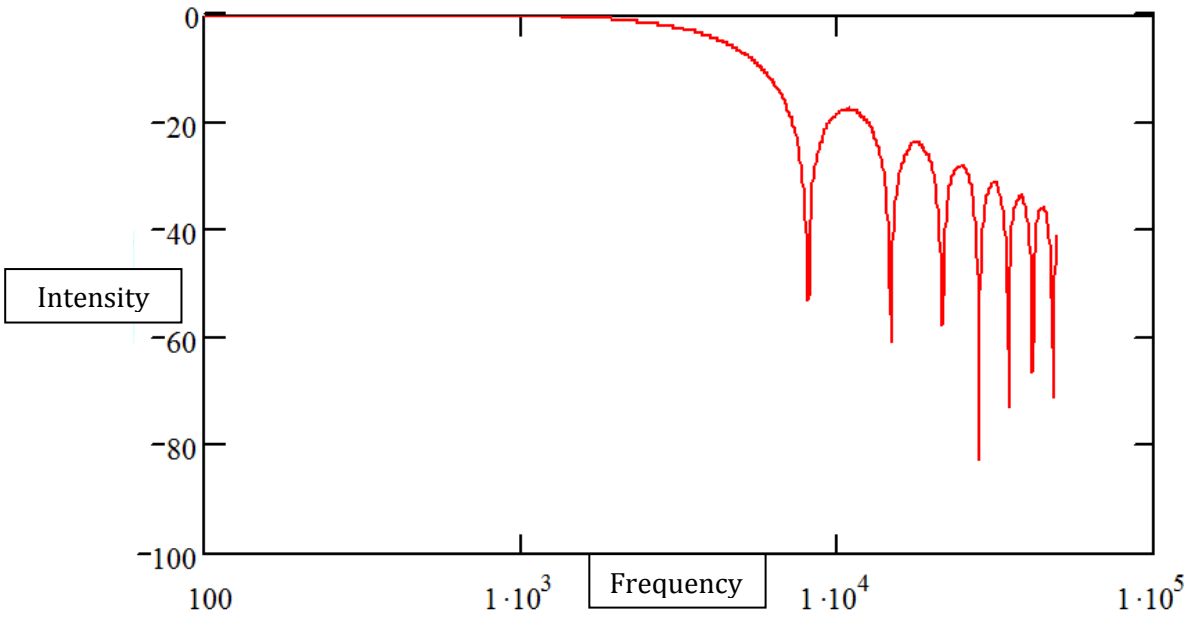

Figure 168 - Noise magnitude 90 degrees offset from transmission axis as a function of frequency.

One can follow a transmission strategy identical to low frequency radio antennas, and long range satellite communications dishes. If more directionality or higher gain is desired, size is the best way to improve performance. In the charts shown in Figure 168 through Figure 170, the previous study is repeated with a two foot diameter aperture at the same test frequencies. It is apparent that higher frequencies become more directional, but are still unaffected below the ~50 Hz fundamental frequency of many SUAV engines.

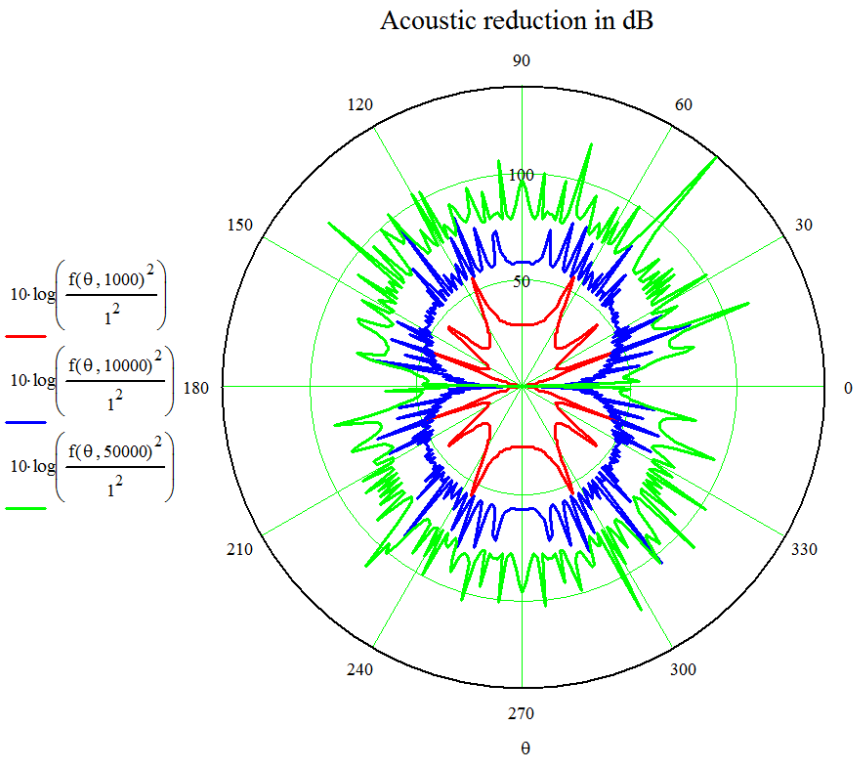

Figure 169 - Reduction in signal strength at 1K, 10K, and 50K Hz from a two foot uniformly vibrating aperture.

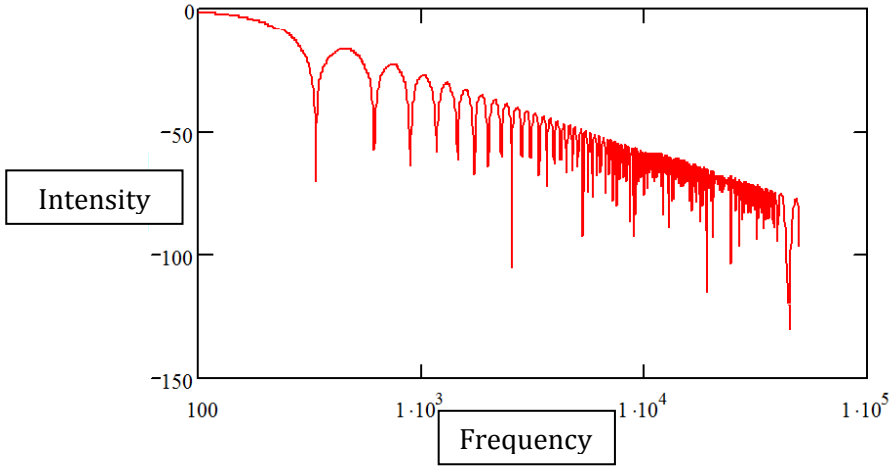

Figure 170 - Noise magnitude 90 degrees offset from transmission axis as a function of frequency

When compared to the previous 90 degree offset plot, one can see that signal losses from increased directionality begin at lower frequency, but are still negligible for the fundamental frequency of small UAV internal combustion engines.

The polar plots are symmetric fore and aft because the aperture is simple floating in space radiating energy just as effectively in one direction as the other. In a real implementation one should place the noise source in the middle of a perfectly reflective wall. The single point directionality equations cannot account for sound diffracting around the ends of the wall, and would erroneously show an infinite loss for all locations behind even a tiny surface.

The directionality solutions discussed thus far have been for a single source propagating in free space. Implementing any exhaust aperture larger than one or two inches into the upper surface of an airplane quickly becomes a governing design constraint, and does nothing to direct low frequency noise from the engine. Placing a horn of appreciable size to create a 24" acoustic aperture on even a 50 lb class UAV is infeasible. But again modern electromagnetic antennas have created a way to make conformal and highly directional antennas through the use of controlled phasing of small elements. Instead of creating physical surfaces to reflect a single signal source and maintain a coherent wave, Phased array antennas use precision delays between many radiating sources to create a similarly directional beam in the far field. This strategy facilitates conformal arrays of smaller emitters scattered across the upper reflecting surface of a smaller aircraft to act as a single antenna able to focus sound up and away from the airplane.

The most simple phased array antenna is the broadside array. In this structure a planar array is all synchronized to create a planar wave in the far field aligned with the array normal vector. Phasing of elements becomes more complicated as the beam is steered (assuming one has control of the signal phase at each element). Also if the array of elements is non-planar then the differences in distance must be accounted for if a coherent wave is desired. The mathematics are covered in detail in Mueller (1) and many other sources (3),(4) as well as being shown in Figure

171. The mathematics involved with phased arrays simply calculate the time delay required at each three dimensional noise generation point such that a pressure pulse would reach the intended focal point at the same time.

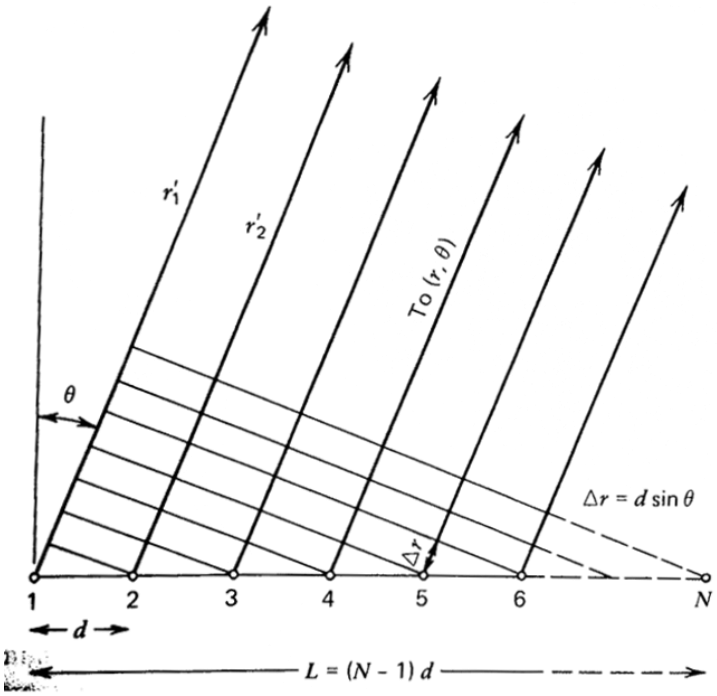

Figure 171 - Graphic from Mueller showing the relative phase delays required to steer a phased array antenna. [29]

BBBB. Prediction of Stored Energy for Studied Energy Conversion Methods

This study of closed cycle engines is meant to contrast the energy producing capability against the potential of other energy systems for use in propelling an aircraft. The most energy dense method of propelling small UAV's remains the un-muffled internal combustion engine as predicted in [1]. The chart below in Figure 172 shows the total amount of energy stored in a given type of propulsion system compared with the total weight associated with propulsion mechanisms and fuel. This eliminates the variation in effective energy density as the mass fraction of fuel in relation to the conversion mechanism changes. All engines in Figure 172 are sized to create 1 horsepower of shaft power. Both the regenerative closed Brayton cycle and internal combustion engine with silencing hardware

share the same approximate initial weight, and operate on the same set of fuels, but the RCBC has potential to be more efficient and can therefore provide more energy for the same weight. The efficiency of the RCBC and silenced internal combustion engine are uncertain, and presented as a range to represent possible variation in final system performance. Overall the closed cycle system is most promising in situations requiring quiet operation as it outperforms silenced internal combustion systems in acoustic performance and energy density. Because of the high power density potential of turbomachinery, higher power systems will further favor regenerative closed Brayton cycles over reciprocating internal combustion engines. The 1HP system weight shown for RCBC's below is governed by the maximum allowable turbine speed (which is most strongly sized by turbine diameter which in turn determines weight). Therefore turbine power can be significantly increased without additional weight. A 10 HP RCBC system may very well use the same turbine designed with higher admission percentage with different heating and cooling elements sized for the additional flux. Additionally because of the low pressure and moderate temperatures encountered by the turbine, a composite casing can be used for the turbine that will significantly reduce overall weight.

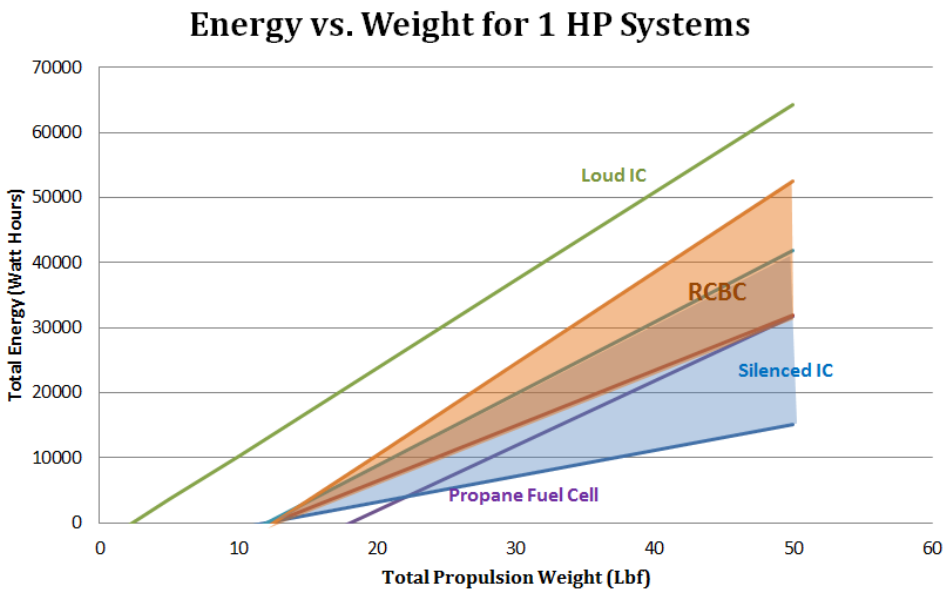

Figure 172 - Energy vs. Weight for 1 HP Systems

VITA

Thomas Chadwick Hays

Candidate for the Degree of

Doctor of Philosophy

Thesis: CLOSED CYCLE PROPULSION FOR SMALL UNMANNED AIRCRAFT

Major Field: Aerospace Engineering with UAS Option

Biographical:

Education:

Completed the requirements for the Doctor of Philosophy in Aerospace Engineering at Oklahoma State University, Stillwater, Oklahoma in July, 2015.

Completed the requirements for the Master of Science in Aerospace Engineering at Oklahoma State University, Stillwater, Oklahoma in July, 2009.

Completed the requirements for the Bachelor of Science in Aerospace Engineering at Oklahoma State University, Stillwater, Oklahoma in May, 2007.